THE EFFECT OF INTERFACIAL COMPOSITIONS ON THE DISPERSED PHASE-INDUCED GELATION AND CONTROLLED DIGESTION OF MONO AND BILAYER NANOEMULSIONS

A Thesis Submitted to the

College of Graduate and Postdoctoral Studies

in Partial Fulfillment of the Requirements for the

Degree of Doctor of Philosophy in the

Department of Food and Bioproduct Sciences

University of Saskatchewan

Saskatoon, Saskatchewan, Canada

By

Kunalkumar Kadiya

2021

PERMISSION TO USE

In presenting this thesis in partial fulfillment of the requirements for a Postgraduate degree from the University of Saskatchewan, I agree that the Libraries of this University may make it freely available for inspection. I further agree that permission for copying of this thesis/dissertation in any manner, in whole or in part, for scholarly purposes may be granted by the professor or professors who supervised my thesis work or, in their absence, by the Head of the Department or the Dean of the College in which my thesis work was done. It is understood that any copying or publication or use of this thesis or parts thereof for financial gain shall not be allowed without my written permission. It is also understood that due recognition shall be given to me and to the University of Saskatchewan in any scholarly use which may be made of any material in my thesis.

Requests for permission to copy or to make other uses of the materials in this thesis in whole or part should be addressed to:

Head of the Department,
Department of Food and Bioproduct Sciences,
University of Saskatchewan
Room 3E08, Agriculture Building, 51 Campus Drive,
Saskatoon, Saskatchewan, S7N 5A8 Canada

OR

Dean
College of Graduate and Postdoctoral Studies
University of Saskatchewan
116 Thorvaldson Building, 110 Science Place
Saskatoon, Saskatchewan, S7N 5C9 Canada

ABSTRACT

This thesis examines the role of the interfacial thickness (δ) in controlling the gelation and digestion behaviour of oil-in-water emulsions (oil volume fraction, ϕ = 0.2 to 0.4)-stabilized by food-grade emulsifiers and polysaccharides. Importance was given to addressing the increase in effective volume fraction (ϕ_{eff}) of oil droplets beyond maximum random jamming (ϕ_{MRJ}) by reducing droplet size, removing excess emulsifier and changing the interfacial composition.

In the first study, the gelation in 40 wt% canola oil-in-water nanoemulsions was investigated as a function of excess emulsifier Citrem (citric acid esters of mono and di-glycerides) removal from the aqueous phase. The removal of excess Citrem increased the viscosity, yield stress and storage moduli of nanoemulsions, more significantly at smaller droplet sizes. It was attributed to a change in inter-droplet interaction from non-DLVO oscillatory structural forces to DLVO dominated repulsive forces after removing excess Citrem. This also increased the δ and ϕ_{eff} beyond ϕ_{MRJ}, leading to a self-standing repulsively jammed nanoemulsion gel. Next, the droplet velocity and packing behaviour of Citrem-stabilized nanoemulsions were tracked using an analytical photo-centrifuge to predict their stability and shelf-life. The reduction of droplet size and removal of excess micelles improved the accelerated stability and shelf-life of the nanoemulsions. The droplets' packing density (ϕ_p) was decreased under the applied RCF after removing excess micelles, which we related to strong repulsive forces between nanodroplets.

To further increase the δ, a second layer of polysaccharide (chitosan and pectin) with different magnitude of charge was deposited on Citrem and whey protein isolate (WPI)-stabilized nanodroplets, respectively. Two different layer-by-layer (LbL) electrostatic deposition techniques, namely one-step versus two-step, were utilized for Citrem-chitosan and WPI-pectin systems, respectively. It was found that the rheology of bilayer emulsions was affected by the droplet size, presence and absence of excess emulsifier, polysaccharide concentration and charge, and the type of LbL method used. In the one-step LbL method, a liquid-like behaviour of Citrem-stabilized monolayer emulsions transformed into repulsive bilayer weak emulsions gel above a critical chitosan concentration, where electrostatic and steric repulsive forces had a significant contribution in elevating δ and ϕ_{eff}. However, the two-step LbL method and removal of excess emulsifier were more effective in creating well-distributed bilayer nanodroplets with increased interfacial thickness leading to an increase in gel strength compared to the monolayer emulsions

at a lower ϕ. The deposition of the second layer also controlled the lipase action during *in vitro* digestion leading to lowering of lipid digestibility. Overall, the study showed that the random jamming amongst the nanodroplets could be induced by increasing δ and ϕ_{eff} beyond ϕ_{MRJ} where emulsions behave like a viscoelastic gel. The fundamental knowledge developed from this research can be used to develop food-grade low-fat emulsion gels with controlled digestion.

ACKNOWLEDGEMENTS

First and foremost, I would like to express my sincere thanks and deepest gratitude to my Ph.D. advisor, Dr. Supratim Ghosh, for his support, guidance, encouragement, and positive critique in achieving the goal of this research project. His willingness to let me try different things and giving me open hands to explore different avenues in handling this project have helped me to build an independent research skill as well as broaden my experiences in the field. Thank you, Dr. Ghosh, for your perseverance and continuous trust in me and for encouraging me to further excel in whatever I am lacking. I want to thank him for providing me with many great opportunities and experiences of international travelling to present my research work.

I would like to thank the external examiner, Dr. Filip Van Bockstaele, for his time and valuable suggestions to improve my Ph.D. thesis. I want to thank my Ph.D. advisory committee members, Dr. Michael Nickerson, Dr. Yongfeng Ai, Dr. Richard Bowles, and my graduate chair, Dr. Xiao Qiu, for their guidance and support throughout my studies. They have always been accessible and offered their valuable input and advice to make this research project more interesting. Your time and contributions have been greatly appreciated. I am also obliged to many members of the Food Science department who have provided assistance, expertise, and/or the use of equipment that has made this work possible; Dr. Darren Korber, Dr. Takuji Tanaka, Dr. Phyllis Shand, Adrienne Woytowich, Yuanlong Cao. I would like to extend my thank to Ann Harley and Donna Selby for their help in administrative related work.

Special thanks to Dr. Ramaswami Sammynaiken and Dr. Neeraj from the Saskatchewan Structural Science Center for training me to use Langmuir trough apparatus in their facility. Thanks to Dr. Xi Xie from Dr. Xiao Qiu's lab for her time and for training me for GC analysis. I would like to thank Mr. Aakash Patel for demonstrating to me how to use homogenizer, rheometer, Mastersizer, and Zetasizer for emulsions preparation and characterization. I must thank summer research students Sacha Desprez and Emilien Campy (from AgroSup Dijon, France), for their outstanding research contribution in the preliminary work for the third objective of this research. I would also like to thank Manisha Sharma for her kind help in setting up and optimizing the digestion experiments. Thanks to Dr. Chi Diem for her help in analyzing the emulsion's microstructure using the cryo-SEM study. A special thanks to all my colleagues (from past and present) from the Food Nanotechnology lab (Vivek, Aakash, Maja, Athira, Ivan, Saakshi, Sacha, Emilien, Chi Diem, Neksha, YanRan, Maria, Fatemeh, Manisha, Madhurima, Femi, Shahrzad) for all their help, co-operation and for keeping the lively environment in the lab. Special thanks to Dr. Prashanth Pillai and Dr. Pravin Gadkari for always having a great scientific and career-oriented discussion at coffee time, which helped to enrich my knowledge. Financial assistant from Natural Sciences and Engineering Research Council (NSERC), Department of Food and Bioproduct Sciences Devolved Scholarship and Graduate Teaching Fellowship from the University of Saskatchewan is sincerely acknowledged.

Finally, I want to express my deepest thanks to my wife, Jinal Kadiya, and my parents, who believed in me. Without their continual love and unconditional support, this journey would never have been possible.

DEDICATION

This thesis is proudly dedicated to…..

My beloved wife and life partner, Jinal Kadiya

and

my lovely daughter, Trisha

Thank you for allowing me to pursue my passions and made this journey possible.

Appreciate your endless love, sacrifices, prayers and supports.

TABLE OF CONTENTS

LIST OF TABLES

LIST OF FIGURES

LIST OF ABBREVIATIONS AND SYMBOLS

A	Cross-sectional area of the rectangular LUMiSizer® cell
A_0	Mean molecular area
AFM	Atomic force microscopy
A_H	Hamaker constant
α_{FFA}	Degree of dissociation of the carboxylic group of FFA
ANOVA	Analysis of variance
A_{trough}	Effective area of the trough
C	Molar concentration of free ions
$C_{adsorbed}$	Adsorbed emulsifier concentration
C_e	Concentration of emulsifier
C_{excess}	Concentration of excess emulsifier
Citrem	Citric acid esters of mono- and diglyceride
CLSM	Confocal laser scanning microscope
cm	Centimetre
C_M	Number density of micelles in the continuous phase
CMC	Critical micelles concentration
CTAB	Cetyl trimethylammonium bromide
C_{total}	Total emulsifier concentration
d_{32}	Volume surface mean droplet diameter
d_{43}	Surface average droplet diameter
Datem	Diacetyl tartaric acid ester of mono- and diglycerides
DDA	Degree of deacetylation
DE	Degree of esterification
°C	Degree Celsius
δ	Electric double layer or shell-layer thickness
δ	Phase angle
Δ	Thickness of the steric layer

ΔA	Change in interfacial area
ΔG	Gibbs free energy
$\Delta\rho$	Density difference between the continuous and dispersed phase
ΔS	Change in entropy
D_{head}	Diameter of emulsifier head group
DI	De-ionized
DLS	Dynamic light scattering
DLVO	Derjaguin, Landau, Verwey and Overweek
d_m	Diameter of emulsifier micelle
DSL	Debye screening length
DWS	Diffusing wave spectroscopy
EDL	Electrical double layer
ε	Electric permittivity
η	Coefficient of viscosity
η_0	Zero-shear viscosity
η_C	Continuous phase viscosity
η_D	Dispersed continuous phase viscosity
f	Counterion dissociation factor
FAMEs	Fatty acid methyl esters
FFA	Free fatty acids
FG	Flaxseed gum
F_{max}	Maximum force
g	Gravitational acceleration
Γ	Gibbs surface excess
γ_c	Critical yield strain
γ	Shear strain
$\dot{\gamma}$	Shear rate
G''	Loss modulus
G^*	Complex shear modulus
G'	Storage modulus

GlcN	Glucosamine
GlcNAc	Glucosamine acetyl
$G'p$	Plateau storage moduli
GRAS	Generally recognized as safe
h	Interdroplet distance
HLB	Hydrophilic-lipophilic balance
HMP	High methoxy pectin
Hz	Hertz
i	Complex number
IUPAC	International Union of Pure and Applied Chemistry
J_E	Creep compliance
J_{max}	Maximum compliance
J_R	Recovery compliance
k	Consistency index
k_b	Boltzmann constant
k_H	Herschel – Bulkley consistency coefficient
κ^{-1}	Debye screening length
L	Wetted length of Wilhelmy plate
LAOS	Large amplitude oscillatory shear
LbL	Layer-by-layer
LMWE	Low-molecular-weight emulsifier
l_{tail}	Hydrocarbon tail length of emulsifier molecule
LVR	Linear viscoelastic region
m	Metre
M	Molar
MCT	Medium chain triglycerides
m_d	Weight (mass) of dispersed phase
µm	Micrometre
µL	Microlitre
µS	Micro siemens
mg	Milligram

min	Minute
mL	Millilitre
mm	Millimetre
mM	Millimoles
mN	Millinewton
MRJ	Maximal random jamming
mV	Millivolt
Mw	Molecular weight
n	Flow behaviour index
N	Normality
n_0	Number of emulsifier molecules
N_A	Avogadro number
N_{agg}	Micelle aggregation number
n_c	Carbon atoms in the surfactant tail
n_i	Number of droplets
nm	Nanometre
O/W	Oil-in-water
ω	Angular frequency
ω_c	Crossover frequency
OSF	Oscillatory structural force
p	Laplace pressure
Pa	Pascal
pI	Isoelectric point
P_o	Osmotic pressure created by micelles
psi	Pound force per square inch
ϕ	Oil volume fraction
ϕ_{core}	Actual oil volume fraction
ϕ_{eff}	Effective oil volume fraction
ϕ_m	Micellar volume fraction
$\phi_{m\text{-}eff}$	Effective volume fraction of emulsifier micelles

ϕ_{MRJ}	Dispersed phase volume fraction at maximal random jamming
ϕ_p	Packing density of droplets
ϕ_s	Shell-layer volume fraction
π_p	Plateau surface pressure
ψ_0	Surface potential
r	Droplet radius
rad	Radian
RCF	Relative centrifugation force
RCP	Random close packing
r_{eff}	Effective radius of droplet
r_f	Radius of film created between two droplets
R_g	Radius of gyration
RGE	Rabbit gastric extract
RGL	Rabbit gastric lipase
rpm	Revolution per minute
ρ_d	Density of dispersed phase
RT	Room temperature
s	Second
SANS	Small-angle neutron scattering
SAOS	Small amplitude oscillatory shear
SAXS	Small-angle X-ray scattering
SC	Sodium caseinate
SDS	sodium dodecyl sulphate
SEM	Scanning electron microscopy
SGF	Simulated gastric fluid
SIF	Simulated intestinal fluid
SLD	Scattering length density
SPSS	Soluble soybean polysaccharide
SSF	Simulated salivary fluid
SSL	Sodium stearoyl lactylate

STEP	Space- and Time-resolved Extinction Profiles
t	Time
T	Absolute temperature
tan δ	Loss tangent
TBARS	Thiobarbituric acid reactive substances
t_{relax}	Relaxation time
τ	Stress
τ_0	Yield stress
θ	Contact angle
v/v	Volume-per-volume
V_E	Volume of the continuous phase confined between droplets
v_{mic}	Emulsifier micelle volume
v_{tail}	Hydrocarbon tail volume
v	Velocity of the droplet
W/O	Water-in-oil
w/w	Weight-per-weight
W_{dep}	Depletion attraction forces
W_{ele}	Electrostatic repulsion forces
WOEP	Without excess protein
W_{OSF}	Oscillatory structural forces interaction energy
WPI	Whey protein isolate
wt%	Weight percentage
WTEP	With excess protein
W_{vdw}	van der Waals attraction forces
z_i	Valency of ion i
ζ	Zeta

1. INTRODUCTION

1.1 Overview

Emulsions are colloidal dispersions of oil and aqueous phases where one phase is well dispersed in the other. Emulsions form the general structure of many foods and related soft materials (McClements & Demetriades, 1998). Among the different emulsions, the metastable nanoemulsions with extremely small droplet size (r < 100 nm) were found to possess characteristics that have many advantages over conventional microscale emulsions (r > 100 nm to several micrometres) (Fryd & Mason, 2012). Advances in the formulation, emulsification, and characterization of nanoemulsions led to improved functionality and applications in the food system. Nanoemulsions have also been shown to transform into elastic gels at a dispersed phase volume fractions much lower than the microscale conventional emulsions (Wilking & Mason, 2007). As the droplet size (r) of nanoemulsion becomes smaller, the thickness of the interfacial layer (δ) surrounding the nanodroplets tends to a similar order of magnitude to the actual droplet size, which significantly increases the effective oil volume fraction (ϕ_{eff}) much beyond the actual oil volume fraction (ϕ_{core}) according to Equation 1.1 (Erramreddy & Ghosh, 2014; Mason et al., 2006).

$$\phi_{\text{eff}} = \phi_{\text{core}} \left(1 + \frac{\delta}{r}\right)^3 \tag{1.1}$$

This phenomenon may lead to the formation of a close-packed structure of the nanodroplets (even if the ϕ_{core} is much less) and self-supporting gel beyond the dispersed phase volume fraction at maximal random jamming (Weiss & McClements, 2000). Experimentally, translucent nanoemulsion gels have been prepared by strong electrostatic repulsion between the nanodroplets when the interfacial thickness of the electrical double layer (EDL) is closer to the order of the radius of the emulsion droplets (Kawada et al., 2010; Wilking & Mason, 2007). However, there is still concern about the stability of these close-packed nanoemulsions with respect to various environmental stresses. As a food component, these nanoemulsions should be able to function over a wide range of pH, ionic strength, processing temperature and storage time. However, often it is

difficult for a single layer of emulsifier to provide the requirements of complex nanoemulsion gel-based food formulations. An alternative strategy is to combine the functionality of different emulsifiers and biopolymers to create multiple interfacial layers on the nanodroplets using the so-called layer-by-layer (LbL) electrostatic deposition technique. In addition to stability, the thick versatile interfacial layers would also help to increase the δ or δ/r ratio in bilayer nanoemulsions according to Equation 1.1 which could lead to gelation in nanoemulsions at even much lower oil volume fraction (ϕ).

Different kinds of synthetic and natural emulsifiers, including low-molecular-weight emulsifiers (LMWEs) such as Citrem (Citric acid esters of mono- and diglyceride), Datem (diacetyl tartaric acid esters of mono- and diglycerides), SSL (sodium stearoyl lactylate), lecithin (phospholipid) and biopolymers, such as proteins (e.g., casein, whey proteins) and polysaccharides (e.g., gum Arabic, chitosan, pectin), are legally available for food emulsion preparation (Charalambous & Doxastakis, 1989; Krog & Sparso, 2004; Stauffer, 1999). Among them, LMWEs and proteins are usually more surface-active, reducing the droplet size to the nanoscale. However, as the polysaccharides are usually less surface-active and diffuse slowly towards the interface during emulsion formation, it is challenging to develop extremely small nanodroplets suitable for nanoemulsion gel production. On the other hand, polysaccharides have an excellent electrostatic property to deposit them as a second layer onto LMWE or protein-stabilized nanodroplets using the LbL technique. Two different kinds of LbL techniques, i.e., one-step (instant electrostatic complexation of oppositely charged polysaccharide at mixing step) or two-step (proper dispersion of similarly charged polysaccharide at mixing step followed by charge reversal in the next step for electrostatic complexation), can be used to deposit the second layer depending on the interfacial composition or pH condition (Guzey & McClements, 2006). As research on applying the LbL technique in the formation of food-grade concentrated nanoemulsion gel is still scarce, there is a need to improve the formation of bilayer-stabilized nanoemulsion gels.

Further, there remains virtually no knowledge on how factors like droplet size, excess emulsifiers in the continuous phase, type and charge of biopolymers and their interfacial interactions influence the formation, stability and rheology of bilayer nanoemulsion gel. To further improve their application, the lipid digestion or controlled release of bioactive from the nanoemulsion gels can be selectively manipulated by varying the properties and composition of the emulsifiers and biopolymers that form the interface (McClements, 2006). Therefore, this

research was envisaged with the overall goal to achieve gelation in nanoemulsion at a much lower oil volume fraction by reducing the droplet size (r) and increasing the interfacial thickness (δ) with various food-grade emulsifiers and biopolymers layers. The impact of the increase in interfacial thickness was also evaluated on the digestion properties of the bilayer emulsions.

1.2 Objectives

The following objectives were developed to address the overall goal of this research:

1. Study rheology and inter-droplet interaction as a function of the removal of excess emulsifier from the continuous phase of nanoemulsion
2. Study the stability mechanism and colloidal packing behaviour of nanoemulsion under the influence of excess micelles using analytical photo-centrifuge
3. Develop and investigate the mechanism of gelation in bilayer emulsion and nanoemulsion using food-grade emulsifiers and polysaccharides.
4. Investigate the effect of one-step versus two-steps layer-by-layer (LbL) deposition techniques in the formation of bilayer nanoemulsion
5. Investigate the effect of interfacial composition on the digestion behaviour of bilayer emulsions using *in vitro* study.

1.3 Hypotheses

The following hypotheses were tested to support the above objectives:

1. Liquid nanoemulsions will be transformed into viscoelastic gels with a reduction in droplet size (r) and removal of excess LMWEs from the continuous phase. The removal of excess emulsifier would enhance the repulsive barrier around the droplets, and therefore it will increase the effective volume fraction (ϕ_{eff}) of the droplets beyond random jamming (ϕ_{MRJ}).
2. Studying droplets packing behaviour under centrifugal compression will help us predict the colloidal forces responsible for the stability or instability mechanisms in the presence and absence of excess emulsifier micelles. The removal of excess micelles from the emulsions will decrease emulsion compressibility under the applied centrifugal force due to increased repulsive forces between droplets.

3. The bilayer (LMWE and polysaccharide-stabilized) nanoemulsion prepared using a one-step LbL method with a thick interfacial layer is expected to form a gel compared to a monolayer (LMWE-stabilized) nanoemulsion at the same oil volume fraction. The contribution of a thick interfacial shell layer will increase the effective oil volume fraction of bilayer nanoemulsion where the droplets can close-pack to create a gel-like structure.
4. The change in interfacial composition (from LMWE and polysaccharide-stabilized bilayer to protein and polysaccharide-stabilized bilayer) and LbL deposition method (from one-step mixing to two-step mixing) will create a gel-like emulsion structure at an even lower oil volume fraction. In the two-step LbL deposition method, proper dispersion of nanodroplets in polysaccharide solution will prevent coating of multiple nanodroplets, which will be more effective in elevating the effective oil volume fraction of nanoemulsion than the one-step mixing method.
5. The thick interfacial layer around the droplets would restrict access of gastric enzymes to the lipid droplets; hence it will reduce the lipid digestibility of the bilayer emulsions compared to monolayer emulsions.

1.4 Outline of the thesis

The whole thesis is divided into three major steps to achieve the overall goal of reducing the oil volume fraction required to get the dispersed phase-induced gelation in nanoemulsion: (i) reduction in droplet size (r) by preparing the nanoemulsion using a high-pressure homogenizer; (ii) removal of excess emulsifiers from the continuous phase of nanoemulsion and (iii) increase the interfacial shell-layer thickness by layer-by-layer (LbL) electrostatic deposition of the second layer of polysaccharide. Steps (i) and (ii) are envisioned with objectives 1 and 2 listed in section 1.2, whereas step (iii) is proposed with objectives 3, 4 and 5. The effect of steps (i) and (ii) on the rheological behaviour and stability of nanoemulsion is discussed in Chapters 3 and 4, respectively. Throughout the thesis, the objective of the gelation in nanoemulsion was characterized using rheological approaches. According to step (iii), the effect of the deposition of the second layer on the oil droplets on nanoemulsion rheology and stability is investigated in Chapter 5 and 6. Lipid digestibility of the mono versus bilayer nanoemulsions was also evaluated using *in vitro* digestion studies.

2. LITERATURE REVIEW

2.1 Definition and Classification of emulsions

Emulsions are defined as a structurally heterogeneous colloidal dispersion of two or more immiscible liquids, primarily oil and water, in which one of the liquids is dispersed in the other as small droplets. These droplets are enclosed by the interfacial layer of a surface-active agent called an emulsifier which plays an essential role in stabilizing emulsions by lowering the interfacial tension. There are two kinds of emulsions, oil-in-water (O/W) and water-in-oil (W/O), that exist in the food industry. An emulsion consisting of oil droplets dispersed in a continuous phase of water is called O/W emulsion, while in W/O emulsion, water droplets are dispersed in a continuous phase of oil. Milk, creams, salad dressings, mayonnaise, and soups are examples of O/W emulsions, whereas margarine and butter are W/O emulsions commonly found in our food (McClements, 2015). This thesis will consider the formation of O/W emulsions. The droplets size of emulsions has a crucial role in deciding their stability, applicability, optical properties, and rheology. According to Figure 2.1, emulsions can also be classified based on their droplets diameter into the conventional (macro) emulsion (0.1 µm – 100 µm), nanoemulsion (20 – 200 nm), and microemulsion (5 – 50 nm) (McClements, 2010).

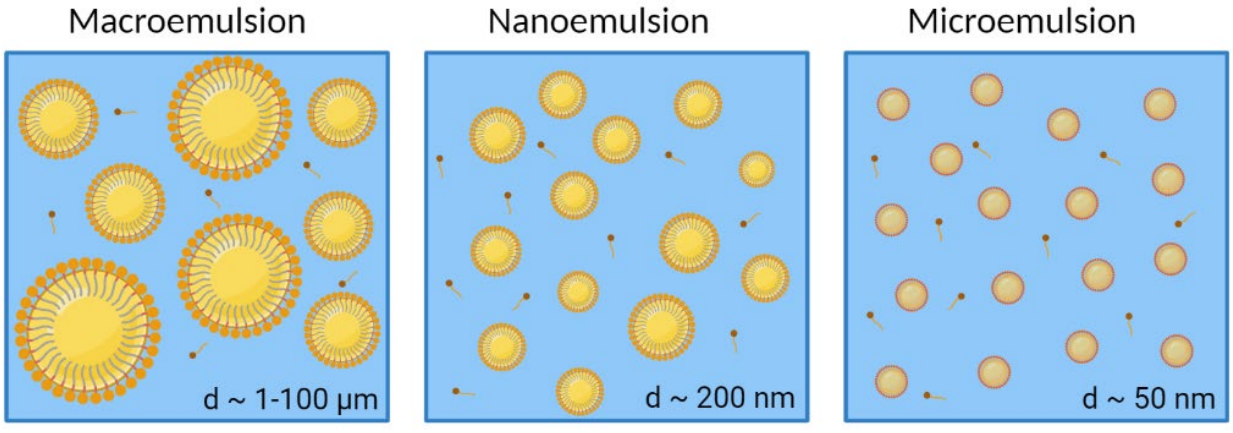

Figure 2.1 Schematic diagram of micro-scale to nano-scale oil-in-water emulsions. d stands for droplet diameter.

Amongst them, macro and nanoemulsions are thermodynamically unstable, while microemulsions are thermodynamically stable emulsions due to negative Gibbs free energy (further discussed in the section 2.2.1) (Rao & McClements, 2012). Extremely small droplets size of microemulsions makes them optically transparent, while conventional emulsions are turbid or opaque in nature (McClements, 2010). The visual appearance of nanoemulsions, on the other hand, ranges from translucent to opaque, depending on droplet size, volume fraction and presence of other ingredients. Although nanoemulsion and microemulsion have somewhat similar droplet size ranges, they are different from each other in their composition and method of preparation. Different aspects which make the nanoemulsion and microemulsions distinctive from each other are listed in Table 2.1 (McClements, 2012b).

Table 2.1 Differences in the properties of nanoemulsions and microemulsions (McClements, 2012b)

Nanoemulsion	**Microemulsion**
Named as 'nanoemulsion' in the 1990s	Mentioned in literature as early as the 1950s
High energy input required (high pressure or shearing action)	Low energy input required (stirring or temperature), spontaneous emulsion formation
The surfactant-to-dispersed phase ratio is low	The surfactant-to-dispersed phase ratio is high
Thermodynamically unstable, kinetically stable	Thermodynamically stable
Droplet diameter: < 200 nm	Droplet diameter: < 50 nm
Low interfacial tension	Very Low interfacial tension (10^{-5} mN/m)
Positive Gibbs free energy	Negative Gibbs free energy
The spherical shape of the dispersed phase (droplets)	Dispersed droplets can adopt spherical or non-spherical shape depending on the optimum curvature of the surfactant layer (Jönsson et al., 1998)
A range of emulsifiers can be used, i.e. low molecular weight emulsifiers, protein, surface active polysaccharides	Only low molecular weight emulsifiers can be used
Stability: height of energy barrier decide its stability against change in composition and environmental condition	Stability: unstable with change in composition or environmental condition

Nanoemulsions are formed utilizing much less emulsifiers compared to microemulsions. Nanoemulsions are made with both low molecular weight emulsifiers (LMWEs) and polymeric emulsifiers, while microemulsions can only be prepared using the former. Nanoemulsions can be prepared by the application of extreme shear and using high-energy approaches, while microemulsions are prepared by spontaneous emulsification (low-energy approaches) through self-assembly of emulsifiers (Deen et al., 2016). In the last 10-20 years, much attention has been given to nanoemulsions because of their versatile structure, higher stability, and extended shelf-life than conventional emulsions (Tadros et al., 2004).

2.2 Nanoemulsions

The term "nanoemulsion" had appeared as early as 1996 in the scientific literature (as shown in Figure 2.2); before that, any emulsion prepared with nanoscale droplet size was referred to as microemulsion in literature. Often, it is confusing to use nomenclature such as "microemulsion and nanoemulsion for nanoscale droplet size emulsions, and because of that, many definitions have been proposed for nanoemulsion in the scientific literature (McClements, 2012b). However, some researchers clarified that the nanoscale droplet size obtained using high shear methods should be termed as the 'nanoemulsion' whereas nanoscale droplet size obtained using spontaneous or phase inversion methods should be termed as the 'microemulsions'(Koroleva & Yurtov, 2012; McClements, 2012b; McClements & Rao, 2011).

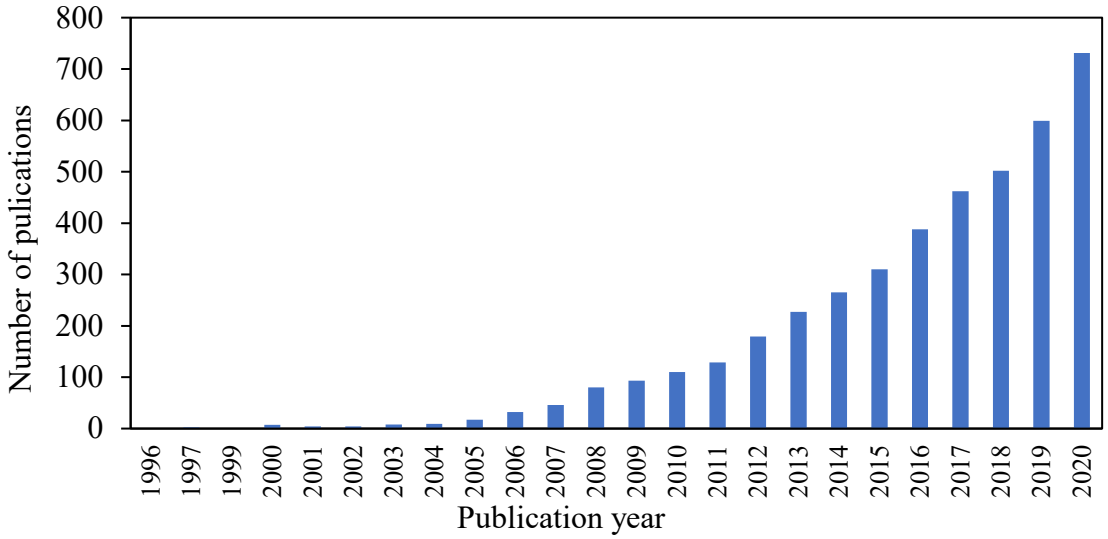

Figure 2.2 The first appearance of the 'nanoemulsion' word in published literature. The data for the number of publications per year on nanoemulsion was obtained from the web of science.

Different authors reported various ranges of droplets size for nanoemulsions and even considered the upper range of droplet diameter up to 500 nm (Fernandez et al., 2004; Gutierrez et al., 2008). Due to their smaller droplet size, nanoemulsions are kinetically more stable against gravitational separation and particle aggregation (Rao & McClements, 2012; Tadros et al., 2004). Typically, due to smaller droplets size (r < 100 nm) and high surface area, a relatively high emulsifier-to-oil ratio is required for the formation of nanoemulsion compared to conventional emulsions (McClements, 2012b). Depending on the droplets size (r) and droplet concentration (ϕ), nanoemulsions may have different optical properties. The relatively small droplets size (r) of around or below 50 nm showed a transparent appearance while the nanoemulsion with average droplets size ranging from 100 to 200 nm showed clear to a translucent system (McClements, 2010; Tadros et al., 2004). Nanoemulsions were also found to display a wide variety of unique rheological behaviour depending on the droplet size (r) and volume fraction (ϕ) (Erramreddy & Ghosh, 2014). Further, the reduced droplet size and higher interfacial area in nanoemulsion also increase the lipid digestibility and bioavailability of many nutrients compared to conventional emulsions (McClements & Xiao, 2012). Due to these advantages, nanoemulsions have shown increased interest in their application as an effective tool to deliver bioactive compounds and integral components in many food systems (Rao & McClements, 2012).

2.2.1 Formation of nanoemulsions

As shown in Figure 2.3, the emulsion formation is always thermodynamically unfavourable as it increases interfacial area after the emulsification process, indicating the free energy of nanoemulsion is always higher than the free energy of the separate phases (oil and water) (McClements, 2012b). The activation energy (ΔG) required to expand the interfacial area (ΔA) during the emulsification process is termed as interfacial energy ($\Delta A\gamma$), where γ is the interfacial tension (Equation 2.1). With numerous small droplets and the generation of high surface area, the activation energy to expand the interface ($\Delta A\gamma$) is also high and positive. The activation energy is also much higher in comparison to the entropic energy ($T\Delta S$) of the dispersion, because of which total free energy (ΔG) is also high and positive for the formation of emulsion (Figure 2.3) (McClements, 2012b).

$$\Delta G = \Delta A\gamma - T\Delta S \quad (2.1)$$

The formation of microemulsion is a spontaneous process (no external energy is required), because of negative Gibbs free energy (ΔG) contributed by the reduction in the surface tension (γ) of the system (due to very high surfactant concentration) and very low entropic energy (TΔS). Oppose to that the emulsification process for nanoemulsion is not a spontaneous but requires energy to produce droplets (Tadros et al., 2004). The energy requirement is much more significant in the case of nanoemulsions formation compared to the conventional emulsions because the formation of nanoscale droplets (r < 100 nm) with a large interfacial area requires a significant amount of energy (Equation 2.1).

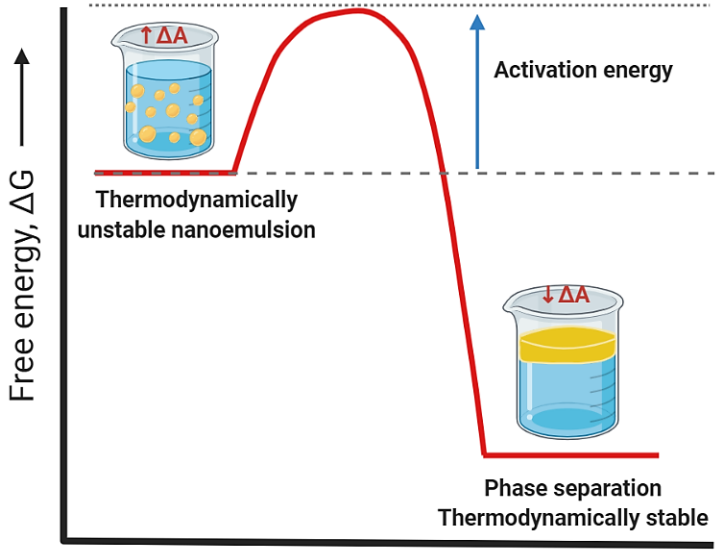

Figure 2.3 Gibbs free energy for the stable versus separated phases of nanoemulsion system. ΔA represents the change in interfacial area and activation or interfacial energy *(ΔAγ)* is a function of ΔA and interfacial tension (γ). Created with BioRender.com.

The high-energy requirement for nanoemulsion formation can also be understood from a consideration of the Laplace pressure (p), which is defined as the pressure difference between inside and outside of droplets across the interface. For a spherical droplet, Laplace pressure can be calculated by,

$$p = \frac{2\gamma}{r} \tag{2.2}$$

Where γ is the interfacial tension and *r* is the droplet radius (Tadros et al., 2004). This equation indicates that the pressure (*p*) difference across the interface increases as the interfacial tension increases or droplets size decreases. Therefore, in nanoemulsion, the high internal Laplace pressure of the smaller droplets must be overcome to further decrease the droplet size into the nanoscale range (McClements, 2011). Emulsifier plays a significant role in reducing Laplace pressure (Equation 2.2) and energy required to break up droplets by lowering the interfacial tension. The presence of an emulsifier at the oil droplet surface also prevents recoalescence between the newly formed droplets during emulsion formation (McClements, 2015).

2.2.2 Methods of preparation of nanoemulsions

To prepare nanoemulsion, oil, water, emulsifier, and energy are needed (Tadros et al., 2004). Emulsion formation is a dynamic process that includes droplet break-up by intense shear, adsorption of surfactants on the freshly created droplets and their further collision (Walstra, 1993). Nanoemulsions can be prepared by applying high energy input (Jin et al., 2016). High energy methods use specialized high-pressure equipment capable of generating the disruptive forces for intermixing two immiscible phases, e.g. high shear mixers, high-pressure valve homogenizers, microfluidizers, ultrasonicators (McClements, 2012a). The emulsion formation occurs through a simple mechanism to form small droplets by external shear to overcome interfacial and internal viscous forces to rupture bigger droplets into smaller ones (Fryd & Mason, 2012). The factors such as phase viscosity, interfacial tension, emulsifier type and concentration, and homogenization conditions influence the formation of nanodroplets using high-energy methods (Qian & McClements, 2011). The high-energy requirement for nanoemulsions formation is related to Equation 2.2, which shows that as the droplet's radius decreases, the internal Laplace pressure increases, and thus more energy is required to further disrupt the droplets into even smaller nanodroplets. The formation of nanoemulsions is usually a two-stage process where a primary coarse emulsion is prepared in a high-intensity blender (to disperse the droplets in the continuous phase) followed by homogenization using a high-pressure homogenizer or microfluidizer to further reduce the droplet size and their polydispersity. The final droplet size of freshly prepared nanoemulsions depends on the type of homogenization device and homogenization pressure, time and number of cycles (Lee & Norton, 2013; Qian & McClements, 2011). Qian and McClements (2011) showed that the droplet size reduced with an increase in homogenization pressure and the number of passes. However, the reduction in droplet size was limited above certain pressure and

number of passes due to an increase in droplet-droplet coalescence which is again depends on the concentration of oil and type and amount of emulsifier used for emulsion preparation (Qian & McClements, 2011). Newly formed droplets inside the homogenizer are thermodynamically unstable and tend to coalesce with surrounding droplets (Jafari et al., 2008). The low molecular weight emulsifiers (LMWEs) with their high diffusion rate rapidly equilibrate at the interface under a very small timescale during homogenization and are better in forming nanoscale droplets. Polymeric emulsifiers, on the other hand, are large and diffuse slowly to the droplet interface during homogenization, therefore they tend to create larger droplets and hence may not be suitable for the formation of nanoemulsions.

2.2.3 Destabilization in nanoemulsions

The formation of nanoemulsions is thermodynamically unfavourable, but they are kinetically more stable than conventional macroscale emulsions. There are four main physical destabilization mechanisms of the emulsion, e.g. gravitational separation, flocculation, coalescence and Ostwald ripening (Dickinson, 1992; McClements, 2015).

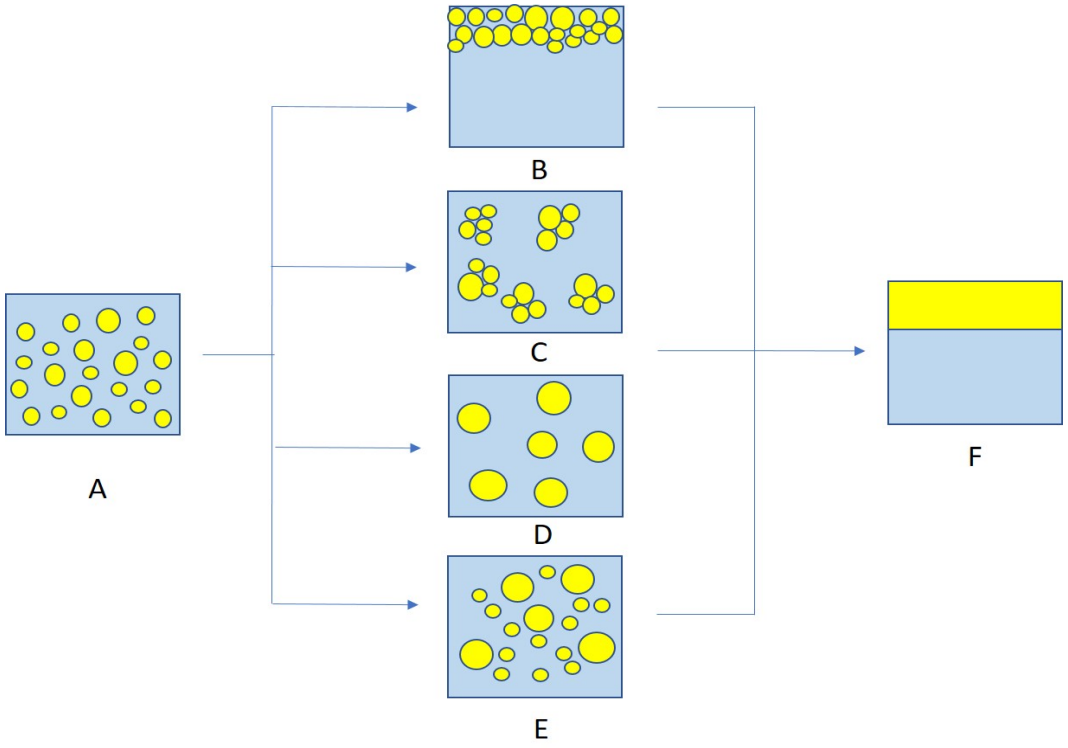

Figure 2.4 Nanoemulsion destabilization mechanisms. (A) stable nanoemulsion, (B) creaming, (C) flocculation, (D) coalescence, (E) Ostwald ripening, (F) phase separation.

The gravitational separation is a primary destabilization mechanism in emulsions, and it is due to the density difference between the two phases. The phase separation (Figure 2.4E) due to gravitational forces includes both forms of instability, i.e., creaming and sedimentation. The upward movement of oil droplets in O/W emulsion is due to their lower density than the surrounding continuous phase termed as creaming (Figure 2.4B), whereas sedimentation occurs due to the downward movement of water droplets in W/O emulsion when they have a higher density than the continuous phase (Gupta et al., 2016). The rate of creaming and sedimentation in a dilute emulsion can be calculated by Stokes' equation:

$$\nu = \frac{2g\Delta\rho r^2}{9\eta} \tag{2.3}$$

Where ν is the velocity of the droplet, $\Delta\rho$ is the density difference between the two phases, r is the droplet radius, η is the viscosity of the continuous phase, and g is the acceleration due to gravity. From Equation 2.3, droplets with a smaller radius (r) have relatively lower velocity and a lower creaming rate or sedimentation. Brownian motion, which is the random movement of small particles suspended in a fluid, becomes dominant at droplet size less than 100 nm, which would be sufficient to overcome the effect of gravitational separation (McClements, 2012b; Tadros et al., 2004).

Flocculation is the process of aggregation of emulsion droplets without affecting the individual identity of the droplets (Figure 2.4C), whereas coalescence is the process whereby two or more droplets merge to form a single larger droplet (Figure 2.4D). Flocculation occurs due to the net attractive force between the droplets (Gupta et al., 2016; McClements, 2015). Droplets may also encounter each other due to Brownian motion, and the balance of attractive and repulsive forces among the droplets would determine their stability against flocculation (Lin et al., 1990). The higher attractive force increases the flocculation rate, while increased Brownian motion reduces it. In general, nanoemulsions are more stable against flocculation and coalescence than conventional emulsions as the range of attractive interactions between the droplets decreased with the droplet size and concomitant increase in the Brownian motion (Rao & McClements, 2012; Tadros et al., 2004). Further, the smaller droplets (r < 0.5 μm) are difficult to deform during flocculation due to their higher Laplace pressure. Without droplet deformation, the drainage of

intervening film between droplets and thus coalescence would be delayed in nanoemulsion; however, this is further affected by the inter-droplet potential (Osorio & Urbina-Villalba, 2011). In nanoemulsions, the repulsive barrier or interfacial film thickness is often on the order of the radius of the droplets, which also makes them more stable to coalescence compared to conventional emulsions (Tadros et al., 2004).

Among the different destabilization mechanisms, Ostwald ripening is the key instability factor of nanoemulsions when an oil phase with partial solubility in the water phase is used (Anton & Vandamme, 2011; Solans et al., 2005). Ostwald ripening is a phenomenon in which the larger droplets grow larger at the expense of the smallest ones due to the mass transport of dispersed phase molecules from small droplets to larger droplets through the continuous phase (Figure 2.4E) (Gupta et al., 2016). This phenomenon leads to an increase in the average radius of the emulsion droplets with time (Taylor, 1998). The Laplace's Law (Equation 2.2), which states that pressure (p) difference across the interface increases as the interfacial tension increases or droplets size decreases, is one of the main physical basis of Ostwald ripening (Meinders & van Vliet, 2004). Extremely small droplets of nanoemulsions have higher internal Laplace pressure, which increases the dispersed phase solubility in the continuous phase and makes them more vulnerable to destabilization by Ostwald ripening (Chang et al., 2012). In many cases, Ostwald ripening is a major challenge in producing stable nanoemulsions for practical applications. Many factors like solute solubility, droplet size, droplet composition, interfacial diffusion, interfacial tension, and thickness significantly affect the occurrence of Ostwald ripening in emulsions (Kabalnov, 2001; Taylor, 1998). Certain dispersed phase (e.g., flavour oil, alkanes) with higher solubility in the continuous water phase shows faster Ostwald ripening rate. Hence, reducing dispersed phase solubility in the aqueous phase is the most effective method to delay or prevent Ostwald ripening in nanoemulsions (Saifullah et al., 2016). Food emulsions containing long-chain triacylglycerols (such as vegetable oil and fish oil) as the dispersed phase show negligible Ostwald ripening because of the extremely low solubility of these molecules in the aqueous phase essentially stopped diffusion from small to large droplets (Wooster et al., 2008). The stability of nanoemulsions against Ostwald ripening can also be improved by controlling the composition (e.g., oil and emulsifier type, aqueous phase) and microstructure (e.g., narrow particle size distribution) by incorporating additives such as ripening inhibitor. The ripening inhibitor is a highly hydrophobic material added to the oil droplets to slow down molecular diffusion and thus retard the Ostwald

ripening (Capek, 2004; McClements, 2010). As the molecular mass transport of droplets is dependent on their diffusion rate, it is possible to delay Ostwald ripening either by decreasing the diffusion coefficient of the dispersed phase in the interfacial layer or by increasing the thickness of the interfacial layer. The use of biopolymers for multilayer coating of oil droplets through electrostatic deposition has been shown to prevent Ostwald ripening by providing a mechanical barrier against molecular diffusion (Mun & McClements, 2006).

2.2.4 Properties and applications of liquid nanoemulsions

Nanoemulsions show unique physical and chemical attributes that can deliver substantial advantages over conventional emulsions (Fryd & Mason, 2012). The droplet size is one of the key features distinguishing nanoemulsions from conventional emulsions (Walstra, 2003). The characteristics of emulsion droplets, i.e. composition, concentration, size range, physical state, electrical charge, and interfacial properties, are key factors in controlling emulsion's major physicochemical properties and quality (McClements, 2015). Many properties of emulsions, such as textural and optical properties, can be significantly altered by reducing their droplet radii below 100 nm. The optical properties of nanoemulsions can be manipulated to yield appearance from nearly transparent to opaque, primarily by controlling the droplet size, oil volume fraction, and refractive indices of dispersed and continuous phases (Fryd & Mason, 2012). The optical properties (such as less turbid to translucent and transparent) of nanoemulsions explore their usefulness in many applications, for instance, flavour delivery in clear beverages (McClements & Rao, 2011; Walker et al., 2015). Many food products, such as soft drinks, juices, and jellies, need to be clear or slightly turbid, and other products, such as mayonnaise, sauces, creams, and yogurt, should be opaque. Thus, the optical properties of nanoemulsions are considered crucial to optimize their application in different food products (Goindi et al., 2016)

In a food system, nanoemulsions with various compositions and microstructure of droplets may exhibit a wide variety of rheological features ranging from viscous liquid to viscoelastic to elastic solids (Genovese et al., 2007; Walstra, 2003). Nanoemulsions, due to their relatively small droplet size, show considerably different rheological properties than conventional emulsions. The bulk rheology of nanoemulsions depends on droplet characteristics & volume fraction, which can be employed to modify the texture of food and other products. For products requiring low viscosity, such as beverages, the droplets should not increase the overall viscosity, so a meagre droplet volume fraction is used. The droplets also help in thickening a system by forming a gel

network or close packing for highly viscous or gel-like food products, such as salad dressings, spreads, and desserts (McClements & Rao, 2011). Finally, due to their small droplets size and large surface area, nanoemulsions were found to increase the bioavailability of active components, including oil-soluble vitamins, nutraceuticals, flavours, and antimicrobials (Acosta, 2009; Feng et al., 2016). Nanoemulsions got an enormous acceptance as delivery systems in the food, beverage, and pharmaceutical industries because of their high physical stability, the ability to increase bioavailability, as well as high optical clarity (McClements & Rao, 2011; Salvia-Trujillo et al., 2017; Walker et al., 2015).

2.3 Gelation in emulsions and nanoemulsions

2.3.1 Definition and types of gels

As per the International Union of Pure and Applied Chemistry (IUPAC), a gel is defined as a "nonfluid colloidal or polymer network that is expanded throughout its whole volume by a fluid" (Alemán et al., 2007). However, there is no exact definition that explains all the properties of a gel. The process of sol to gel transition is called gelation. Gelation in certain foods may be achieved by altering the temperature, pH, ionic strength, or solvent quality, or by adding enzymes, denaturants, or other cross-linking agents such as protein or polysaccharides (Chen et al., 2001). A gel is a transitional state between a liquid and solid possessing both viscous liquid-like and elastic solid-like characteristics and hence displays viscoelastic behaviour. The viscoelastic nature of a gel is greatly influenced by the properties of the dispersed and continuous phase (Geremias-Andrade et al., 2016; Van Vliet, 1988). Emulsion gels are complex colloidal soft matter with a network structure due to the presence of (i) crosslinked biopolymer molecules in the continuous phase or (ii) a network of aggregated droplets (Dickinson, 2013). Therefore, depending on the colloidal structuring, emulsion gels may exist in two distinct types of structural arrangements (Figure 2.5): (i) emulsion-filled biopolymeric gels (Figure 2.5A) and (ii) particulate gels (Figure 2.5B, 2.5C). This structural organization is mainly defined by the interactions among the emulsion droplets with the continuous gel matrix (Dickinson, 2012).

In the emulsion-filled gels, the emulsion droplets are randomly dispersed in a biopolymer matrix, and the network of these biopolymer molecules in a continuous phase leads to gelation of emulsions (Dickinson, 2013). It is a type of particle-filled gel, and its rheological behaviour is determined predominantly by the network properties of the spatially continuous matrix

(Dickinson, 2012). It is shown that if the emulsion droplets interact and are mechanically bound to the gel matrix, they are termed as the active filler particles (Figure 2.5Ai); if not, then as inactive filler particles (Figure 2.5Aii) (Van Vliet, 1988). These kinds of interactions are governed by the interfacial properties of emulsion droplets, and based on that, it can increase or decrease the strength of a gel (Chen & Dickinson, 1999). The active filler particles strengthen the gel matrix due to the strong interaction of interfacial emulsifier molecules with the macromolecules present in the gel matrix, whereas inactive filler particles weaken the gel due to their lower chemical and physical affinity toward macromolecules of the matrix (Sala et al., 2007; Van Vliet, 1988). For example, it was observed in the emulsions stabilized by non-ionic low molecular weight emulsifier (LMWE) such as Tween 20 that the droplets did not interact with the whey protein gel matrix (inactive particle fillers), but using whey proteins as an emulsifier showed strong interactions between the droplets and protein gel matrix (active particle fillers) (Dickinson & Chen, 1999).

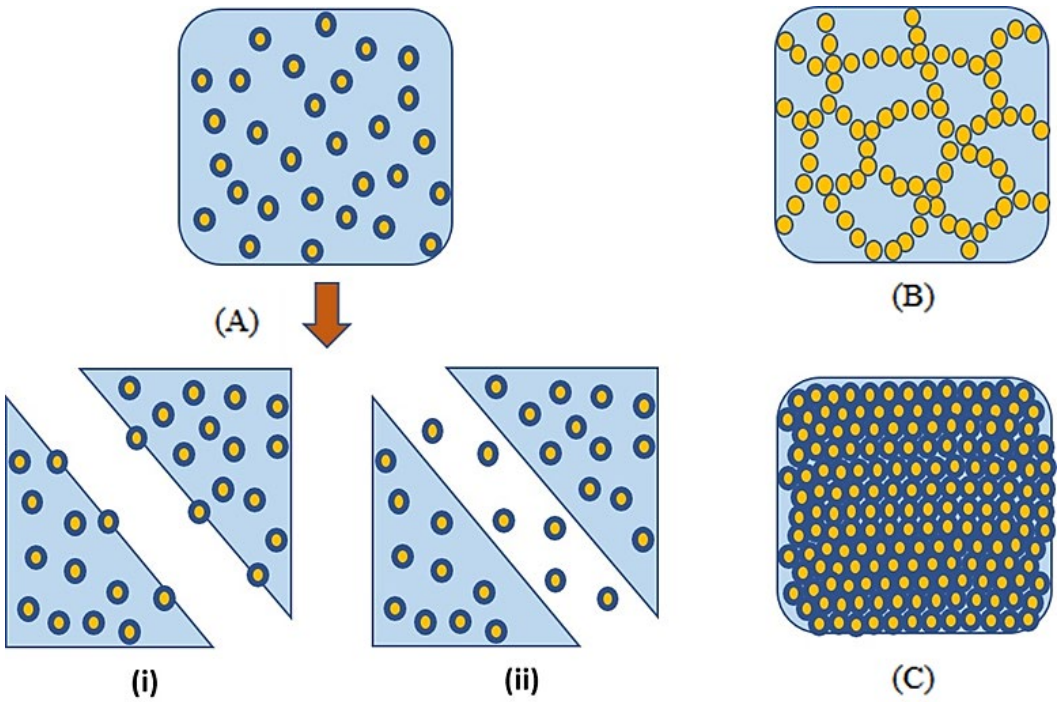

Figure 2.5 Schematic representation of types of gels: (A) emulsion filled gel: (i) active fillers: emulsion droplets strongly interact and are mechanically bound to the components of continuous gel matrix (ii) inactive fillers: lower affinity of emulsion droplets toward the components of continuous gel matrix; (B) attractive particulate gels: gel network structure is caused by the aggregation of emulsion droplets (C) repulsive gels: gel structure is caused by the close packing of emulsion droplets stabilized with the strong short-range repulsive forces.

In particulate gels, the three-dimensional network formed by the aggregation of attractive emulsions droplets leads to gelation (Figure 2.5B). The gelation of aggregated particles in biopolymer-based systems can be induced by enzymatic cross-linking of biopolymers at the interface and by changing the environmental conditions such as temperature, pH, and ionic strength (Chen et al., 2001). For example, it was shown that the gelation of β-lactoglobulin or casein stabilized emulsion could be induced by enzymatic cross-linking of these proteins using transglutaminase (Færgemand et al., 1997). The mechanical and rheological properties of the particulate gels are governed by the interactions between the emulsion droplets (Dickinson, 2012). If the interaction between the aggregated emulsion droplets is attractive, they are termed attractive gels.

On the other hand, ionic emulsifier-stabilized emulsion droplets with strong repulsive forces show close packing at high ϕ ($\phi_{MRJ} > 0.64$ for the monodisperse system) into a randomly jammed state which is referred to as the maximum random jamming (MRJ). At such a high ϕ, an emulsion attains a gel-like viscoelastic behaviour, also known as repulsive emulsion gel (Figure 2.5C) (Fryd & Mason, 2012). The concentration of emulsifier or biopolymer used as the interfacial layer around the droplets also has significant importance on the formation and stabilization of the attractive or repulsive gels. If the concentration is too low, biopolymer molecules adsorb onto the surface of more than one droplet leading to bridging flocculation (Dickinson, 2010). Oppositely, a high concentration of excess free biopolymer molecules in the continuous phase generates an attractive osmotic force when the biopolymer molecule escapes from a narrow region between two approaching droplets which may become strong enough to overcome the various repulsive forces and leads to depletion flocculation (Dickinson, 2010; Dickinson, 2013). Erramreddy and Ghosh (2014) showed that the sodium dodecyl sulphate (SDS)-stabilized 40 wt% canola O/W nanoemulsions transformed from a repulsive gel to an attractive gel with an SDS concentration from 0.5 – 2 times critical micelles concentration (CMC) to 5 – 15 times CMC. Authors attributed this change in gel structure of nanoemulsions to alteration in inter-droplet potential from repulsive to attractive dominated in the presence of excess SDS micelles in the aqueous phase. Therefore, without proper control of emulsifier selection and concentration, a repulsive emulsion gel may transfer into an attractive gel (Erramreddy & Ghosh, 2014).

2.3.2 Conventional emulsion gels versus nanoemulsion gels

Emulsions behave interestingly from the rheological and structural point of view when they are subjected to extreme shear or change in composition (Mason et al., 2006). A conventional emulsion can be transformed from viscous liquid to viscoelastic gel by increasing oil volume fraction (ϕ) or changing continuous phase composition. Mayonnaise is a classic example of an oil-in-water (O/W) type conventional emulsion gel stabilized by proteins and phospholipids from egg yolk. It has a typical viscoelastic property, which is achieved by slowly adding about 80% (v/v) oil with vigorous stirring into a 20% (v/v) aqueous mixture of vinegar and egg yolk helps in the breakdown of the oil phase into numerous microscale droplets. During this process, as the ϕ increased, oil droplets begin to jam pack so that the mayonnaise develops an elastic storage modulus (G′) and becomes a solid-like gel.

The gelation in nanoemulsions depends on the properties of the droplets, such as their size, packing, volume fraction (ϕ), and degree of deformation (Mason et al., 1996). At a very high ϕ where the droplets begin to deform due to close packing, the nanoemulsions' elastic storage modulus (G′) is proportional to the Laplace pressure (p) (Equation 2.2) of non-deformed droplets, thereby resulting in an increase in G′ with a decrease in droplet size. This indicates that large elastic moduli can be present in nanoemulsion, and hence close packing of the nanoscale droplets may behave like a strong elastic gel (Mason et al., 2006; Wilking et al., 2006). The gelation and viscoelastic behaviour of nanoemulsions are quite comparable to conventional emulsion gels or particulate gels made up of close-packed microscopic emulsion droplets (Dickinson, 2012; Dickinson, 2013). However, there is a critical need for high oil phase volume fractions ($\geq$ 64%) for conventional emulsion gels, while gelation of nanodroplets can be induced at much lower oil volume fractions, typically around 30 – 40% depending on nanodroplet size and their shell layer thickness (Mason et al., 2007). Therefore, nanoemulsions exhibit stronger elasticity compared to conventional emulsions at the same ϕ. This is a significant advantage of nanoemulsion gels compared to conventional emulsion gels that they can reach a close packing state at a much lower oil volume fraction, and this property of nanoemulsion gels can be used for fat reduction in bakery products and table spreads.

2.3.3 Mechanism of gelation in nanoemulsions

In conventional emulsions, the particle volume fraction is approximately equal to the actual volume fraction of the oil phase (ϕ_{core}), but in nanoemulsions, it is higher than the actual volume

fraction of the oil phase due to the increased effect of shell layer compared to the nanodroplet size. In this case, the effective droplet volume fractions (ϕ_{eff}) can be calculated from the actual volume fraction of droplets (ϕ_{core}) and effective radius (r_{eff}) of the nanodroplets. The effective radius ($r_{eff} = r + \delta$) is the sum of actual droplet radius (r) plus the shell layer thickness (δ) due to adsorbed emulsifier molecules and charge cloud around the droplets. The following equation can explain this calculation (Wilking & Mason, 2007):

$$\phi_{\text{eff}} = \phi_{\text{core}} \left(1 + \frac{\delta}{r}\right)^3 \tag{2.4}$$

In a nanoemulsion with an average droplet radius r and shell layer thickness δ, the ϕ_{eff} may be significantly higher than the ϕ_{core} (Weiss & McClements, 2000; Wilking & Mason, 2007). When ϕ_{eff} reaches a critical level where the droplet interacts hydrodynamically with each other, the nanoemulsions form an elastic gel structure. The critical droplet volume fraction for this to happen is commonly known as volume fraction for maximal random jamming (ϕ_{MRJ}) (Wilking & Mason, 2007). As the droplet size of nanoemulsion becomes smaller, the interfacial coatings (δ) surrounding the nanodroplets may appreciably contribute to the overall dispersed phase volume fraction (ϕ_{eff}), thereby inducing gelation at a lower ϕ_{core} than conventional emulsion (McClements & Rao, 2011; Wilking & Mason, 2007).

From Equation 2.4, manipulating two approaches in emulsion, such as reducing droplet size (r) and increasing shell layer thickness (δ), may result in a higher ϕ_{eff} compared to the ϕ_{core}. This equation is also plotted in Figure 2.6 to demonstrate the effect of droplet size (r) and three different shell layer thicknesses (δ) on ϕ_{eff}. From Figure 2.6, it can be seen that for a conventional emulsion ($r \geq 250$ nm), where ϕ_{core} is 0.4, the interfacial shell layer thickness (δ) has a negligible influence on ϕ_{eff}, but as the droplet size (r) decreased below 100 nm ϕ_{eff} rapidly increased, when δ increased from 1 nm to 10 nm. The nanoemulsions with 50 nm droplet radius and 10 nm shell layer thickness have much higher $\phi_{eff} = 0.7$ than with the shell layer thickness of 5 nm and 1 nm. Thus, a decrease in droplet size enhances the effect of shell layer thickness on $\phi_{eff,}$ which leads to close packing of nanodroplets and transforms liquid nanoemulsions into elastic gels at a much lower actual oil-phase volume fraction ($\phi = 0.4$) (Erramreddy & Ghosh, 2014).

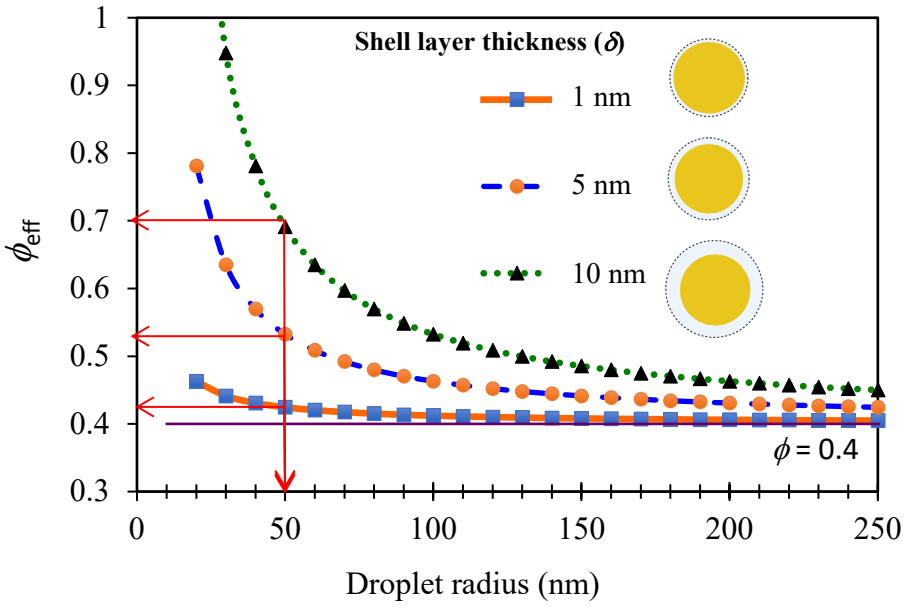

Figure 2.6 Influence of droplet radius (r) and shell layer thickness (δ) on effective droplet volume fraction (ϕ_{eff}) of proposed nanoemulsions gel model plotted from Equation 2.4.

The shell layer thickness (δ) of sterically stabilized emulsion droplets depends on the thickness of the absorbed surface-active molecules, whereas for electrostatically-stabilized emulsion, the shell layer thickness can be estimated from the thickness of the electrical double layer created by surface ions from the adsorbed emulsifier molecules and a layer of counterions that screen the surface charge. These oppositely charged counterions are electrostatically attached to the droplets, the thickness of which can be estimated from the Debye screening length (DSL, κ^{-1}) (Erramreddy & Ghosh, 2014; Wilking & Mason, 2007). Mondain-Monval et al. (1996) showed that the effect of this charge cloud felt 2.4 times DSL from droplet surface in SDS-stabilized emulsions. Wilking and Mason (2007) showed that nanoemulsion prepared using 20% silicon oil and stabilized by anionic emulsifier SDS shown to transform into an elastic gel when the droplet size falls below a critical value of 62 nm with a shell layer thickness of $\delta \sim 3$ nm. Similarly, it was found that SDS-stabilized nanoemulsion made up of 25% n-octadecane as dispersed phase transformed into a viscoelastic gel when the droplet radius was reduced below 80 nm (Weiss & McClements, 2000). Erramreddy and Ghosh (2015) transformed liquid 40 wt% canola oil-in-water nanoemulsions stabilized with 16.6 mM SDS into a viscoelastic gel by

reducing the droplet size to 156.5 nm. In another study, Patel, Mohanan, et al. (2019) demonstrated that 40 wt% canola O/W nanoemulsions stabilized by sodium caseinate (SC) exhibited strong elastic gel behaviour with the smallest droplet size (~160 nm) and higher interfacial thickness (δ ~18.9 nm) compared to liquid-like flowable behaviour of whey protein isolate (WPI)-stabilized nanoemulsions (~170 nm). At relatively similar droplet size, authors attributed this behaviour of SC-stabilized nanoemulsion gel to an increase in $\phi_{eff} = 0.79$ with a much higher contribution of steric barrier in increasing δ compared to whey protein (δ ~8.5 nm) (Patel, Mohanan, et al., 2019). In all these types of nanoemulsion gels, the nanodroplets with surface charge have strong electrostatic repulsions between them, and therefore, they are referred to as 'repulsive nanoemulsion gels' (Datta et al., 2011; Wilking & Mason, 2007).

A repulsive nanoemulsion gel can be transformed into an attractive gel in two ways: (1) increasing the depletion attraction through the addition of depletants such as emulsifier micelles or non-adsorbing biopolymer molecules or (2) screening the surface charge of the droplets through the addition of ionic salts (Dickinson, 2013; Fryd & Mason, 2012). For example, Datta et al. prepared repulsive gels from a sterically stabilized silicon oil-in-formamide nanoemulsion using lower than critical micelle concentration (CMC) of a non-ionic amphiphilic copolymer such as Pluronic P105, and they observed that at a higher concentration above CMC, the repulsive interactions between nanodroplets transformed into an attractive one due to micelle-induced depletion attraction (Datta et al., 2011). Erramreddy and Ghosh (2014) also showed that the repulsive nature of SDS-stabilized 40 wt% canola O/W nanoemulsions gel can be transformed into a strong, attractive gel by increasing the emulsifier concentration from 2 times CMC to 5 times CMC. Wilking et al. (2011) also developed attractive nanogels by adding sodium chloride solution (300 – 500 mM) to SDS-stabilized concentrated (ϕ > 12%) silicon oil nanoemulsion. Patel, Longmore, et al. (2019) demonstrated that the 5 wt% sodium caseinate (SC) and whey protein isolate (WPI)-stabilized repulsive nanoemulsion gels converted into attractive gels by changing the pH to isoelectric point (pI) and adding the salts (up to 1 M). The aggregation of droplets and formation of three-dimensional attractive gel-network was attributed to the charge neutralization and charge screening effect upon a change in pH and addition of salts, respectively (Patel, Longmore, et al., 2019).

2.3.4 Rheological characterization of emulsions and emulsion gel

An extremely important aspect of the emulsions and emulsions gels is their rheological behaviour. Rheological characterization of emulsions involved measuring flow and deformation as a function of applied force. The rheological behaviour of various emulsion-based foods, i.e., milk, cream, yogurt, salad dressing, mayonnaise, sauces, and soups, are characterized using different principles and techniques. All these food emulsions exhibit a wide range of different rheological behaviour, ranging from low viscosity liquid (milk) to viscoelastic gels (yogurt and salad dressing), to other solid-like viscoelastic emulsions (butter and margarine) (Zhu et al., 2020). Many factors involved in emulsions formulation, such as the composition of the dispersed and continuous phase (oil type and concentration, texture modifier, stabilizer), droplet size and droplet charge (influenced by the homogenization type and low molecular weight emulsifier versus biopolymer), and environment conditions (pH, ionic strength, and temperature) can affect their final rheological properties (McClements, 2015; Tadros, 1994; Zhu et al., 2020). More precisely, rheological measurements can help study the changes in the structural organization in emulsions resulting from the alteration of the bulk phase properties and the droplet characteristics such as droplet size, droplet charge droplet-droplet interactions. Accordingly, the changes in emulsions states from strongly electrostatically stabilization to a flocculated system or stabilization due to gelation of continuous phase can also be monitored by studying the rheological parameters such as viscosity and elastic modulus (Tadros, 2011).

There are different experimental techniques used to describe and quantify the rheological properties of the emulsions and emulsions gels. Further, a specific choice of rheological parameters is required to define the desired textural property of emulsions-based foods. For instance, liquid emulsions (milk) can be characterized by studying their flow behaviour (shear viscosity, η) from stress versus shear rate profiles. On the other hand, highly viscous (salad dressing) to viscoelastic solid-like food (mayonnaise) emulsions can be determined for viscoelastic moduli (G' and G") or creep-recovery parameters from stress versus strain profiles (Tadros, 2015). All these rheological behaviours can be characterized by considering a few simple models, the ideal liquid, the ideal plastic, and the ideal solid as well as by combining these simple models in the case of complex fluids (McClements, 2015).

2.3.4.1 Ideal and non-ideal liquids

The ideal liquid is the one where the relation between applied shear stress and the rate of strain is linear. Newton was the first who described this behaviour in liquid, so also referred to as the *Newtonian* liquid or shear-independent liquid. In Equation 2.5, applied stress (τ) is proportional to the change in displacement of the layers per unit time, also termed as the rate of strain ($\dot{\gamma}$) and the proportionality constant (η) is called the viscosity. Thus, the viscosity of the liquid is a measure of its resistance to flow; the higher the viscosity, the greater the resistance (McKenna & Lyng, 2003).

$$\tau = \eta\dot{\gamma} \tag{2.5}$$

Contrary to that, non-ideal liquid behaves differently and exhibits non-linear relation between applied stress (τ) and resultant rate of strain ($\dot{\gamma}$). In this case, the viscosity of liquid depends on the applied shear and/or the length of time and based on that; they are classified as the shear-rate dependent non-ideal liquids and time-dependent non-ideal fluids. The shear-rate-dependent nonideal liquids either exhibit an increase in viscosity (dilatant or shear-thickening) or decrease in viscosity (pseudoplastic or shear-thinning) as a function of shear rate (Figure 2.7A).

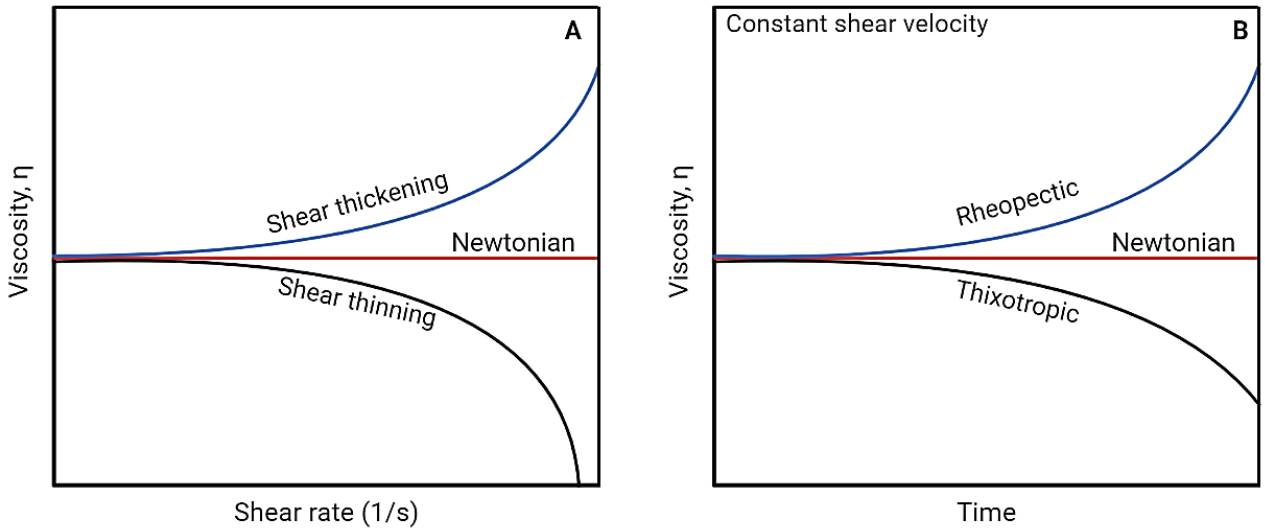

Figure 2.7 Non-Newtonian flow behaviour of liquid (A) shear dependent, (B) time-dependent viscosity of the fluid. Created with BioRender.com.

Similarly, the decrease in viscosity of time-dependent nonideal fluids at a constant shear rate is termed the thixotropic material, whereas the increase in viscosity is called the rheopectic materials (Figure 2.7B). In other terms, thixotropic and rheopectic materials exhibit time-dependent shear thinning and shear thickening behaviour, respectively. For the shear-rate-dependent nonideal liquids, the viscosity at a specific shear rate is referred to as the apparent viscosity (McClements, 2015; McKenna & Lyng, 2003).

Water, fruit juice, honey and pure vegetable oil are the example of ideal liquids, and they meet the criteria discussed above for the Newtonian fluid. The rheological behaviour of dilute emulsions (milk) can still be described by Equation 2.5. However, this relation does not work in the case of nonideal liquids where the change in dispersed phase composition (concentrated emulsions) or change in the aqueous phase composition (addition of biopolymer) and change in the droplet-droplet interactions (flocculated emulsions) greatly affect the viscosity of the emulsion system (McClements, 2015; Tadros, 2011). In the case of non-ideal behaviour, the viscosity of emulsions either increases or decreases as the shear rate is increased, rather than staying constant as the case with the Newtonian or ideal liquid (Figure 2.7). These changes in apparent viscosity can be described very well by the power-law model (Equation 2.6) (McKenna & Lyng, 2003).

$$\tau = k\dot{\gamma}^n \tag{2.6}$$

Where k is the consistency index, and n is the flow behaviour index. The power-law model can describe the Newtonian ($n = 0$), shear-thinning ($n < 0$), and shear thickening ($n > 0$) behaviours based on the value of the flow behaviour index (n) (McKenna & Lyng, 2003). Different rheological behaviours and their significance in describing the structural organization in emulsions are discussed in Table 2.2 (Genovese et al., 2007; Geremias-Andrade et al., 2016; McClements, 2015; Tadros, 1994; Tadros, 2011).

Among the different rheological behaviour, shear-thinning is a widely observed non-ideal behaviour in food emulsions, whereas shear-thickening is much less common. The emulsions continuously undergo microstructural rearrangement in the direction of applied shear because of the shear thinning. The deformation of droplets and its effect on the rheology of emulsions is determined by the balance of three main forces: Brownian diffusion, hydrodynamic interaction, and colloidal forces (repulsive or attractive). The droplet deformation and shear thinning behaviour

observed under applied shear field are quite interesting to understand the structure-function relationship in emulsions system (Tadros, 2011).

Table 2.2 Rheological behaviours in describing the structural organization in emulsions

Type of flow behaviour	Occurrence reasons
Newtonian	• Very dilute emulsions where droplet-droplet interaction is negligible. • Viscosity of the aqueous phase imparts the characteristic flow property to the emulsion
Non-Newtonian	• Changes in emulsion composition and hence structures
Shear thinning (most common behaviour in emulsions)	• Under applied shear field, there may be – • Droplet elongation and aligning with the flow • Alteration in the spatial distribution of repulsively stabilized droplets • Removal of solvent molecules bound to the droplet surface • Deformation and disruption of flocculated emulsions droplets
Shear thickening	• Shear-induced transition of droplets packing behaviour in concentrated emulsions • Shear-induced flocculation of droplets
Thixotropic	• Progressive (time-dependent) deformation and disruption of aggregated emulsions (usually containing crystal and biopolymers) structures associated with weak attractive forces • Structural relaxation in the emulsion system
Rheopectic	• Time-dependent rearrangement and interaction among the emulsions droplets leads to enhanced aggregation and hence viscosity in emulsion

Two different examples are explained in Figures 2.8A and 2.8B for the shear-induced structural breakdown in the colloidal system stabilized by the repulsive droplets and flocculated droplets, respectively. Interestingly, emulsions show a constant viscosity value (η_0) at very low shear rates called the zero-shear viscosity plateau. At such a low shear rate or stress, the rotational Brownian motion dominates among the randomly distributed repulsive droplets, and it is more pronounced where droplets are smaller (Figure 2.8A). The viscosity decreases with an increased shear rate or stress because the droplets start to rearrange or reorient themselves with the flow field. At a high shear rate, the hydrodynamic forces dominate and droplets start to elongate and

remain aligned with the shear plane, and therefore viscosity has a plateau value (McClements, 2015).

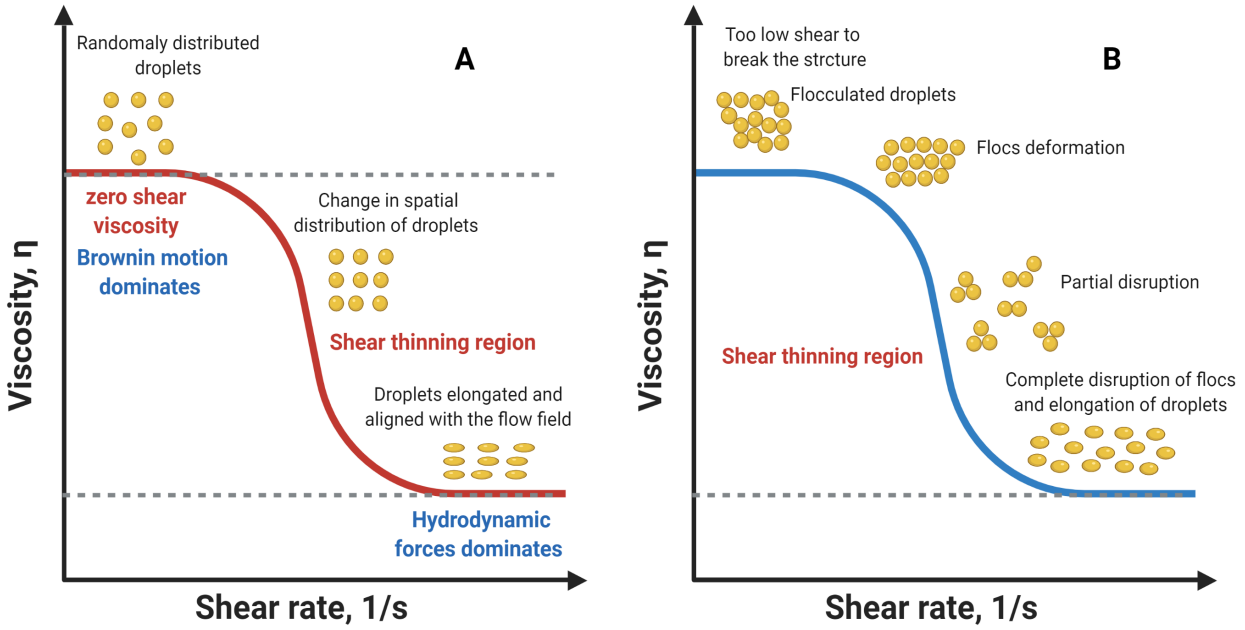

Figure 2.8 Shear thinning behaviour in two different emulsions structures (A) Repulsively stabilized non-flocculated colloidal system (B) flocculated colloidal system. Created with BioRender.com.

In a dilute flocculated emulsion, the attractive interactions between droplets dominate the repulsive forces. At low shear, these interdroplet interactions in flocculated emulsions overcome any hydrodynamic forces acting on the droplet; hence the viscosity remains constant (plateau region) (Figure 2.8B). At a higher shear rate, the applied stress becomes large enough to deform and rearrange the flocs into string-like overlapping layers indicated by the decrease in the viscosity. Further increase in shear rate leads to partial disruption of the flocs followed by complete disruption of the flocs into individual droplets (Tadros, 2011). At a high shear rate, the hydrodynamic forces dominate over the interdroplet (colloidal interactions), and there is n increase in the free space between dispersed droplets, which both contribute to a large reduction in the viscosity to a constant value at the end. The zero-shear viscosity plateau and starting of shear-thinning point in viscosity profiles of emulsions are mainly dependent on the droplet size, droplet

charge, droplet concentration, droplet-droplet interaction, and continuous phase composition (McClements, 2015).

2.3.4.2 Ideal and non-ideal plastic materials

Certain solid-like emulsions exhibit plasticity in their rheological behaviour, including mayonnaise, margarine, butter, and different fat spreads. These emulsions need an application of some critical stress to flow, called as yield stress (τ_0). Beyond this yield stress (Figure 2.9A), material either behave like a Newtonian fluid (called as ideal plastic) or non-Newtonian fluid (called as nonideal plastic) (McClements, 2015). The rheological properties of ideal plastic, which is also called as Bingham plastic, and nonideal plastic are shown in Figure 2.9A.

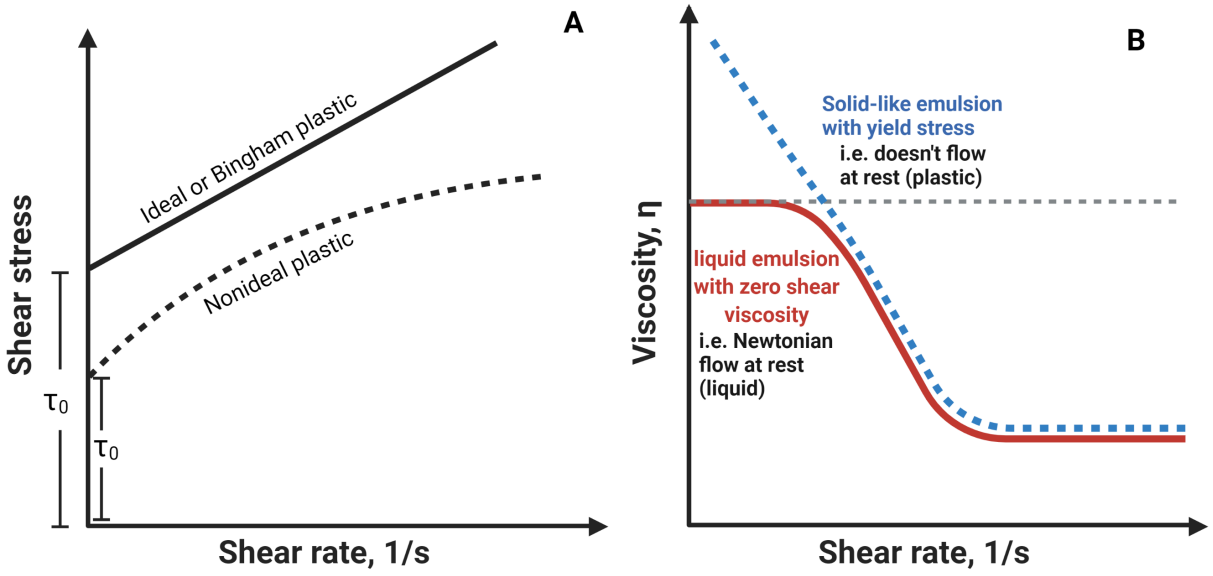

Figure 2.9 (A) Ideal and nonideal plastic behaviour (B) Emulsions with (solid-like) and without (liquid-like) yield stress behaviour. Created with BioRender.com.

After yielding, non-Newtonian behaviour, such as pseudoplastic behaviour, is quite common in many food emulsions. Food emulsions that exhibit such a plastic-like yielding behaviour comprise a network of aggregated droplets dispersed in a liquid matrix, such as oil-in-water concentrated emulsions containing a three-dimensional network of aggregated droplets (Weiss & McClements, 2000). Similar yielding behaviour is also observed in concentrated close-packed emulsions (mayonnaise), where jamming of dispersed phase leads to the requirement of

critical yield stress to flow (Pal, 1996b). In the case of yield stress material (Figure 2.9B), the viscosity is ever-increasing (without visible plateau) below some critical yield stress as shear rate approaches to zero and it does not allow material to flow, which is termed as "plastic flow" (McClements, 2015). Plastic flow behaviour is predominant in a system where the network of aggregated molecules or particles is dispersed in a liquid matrix. For example, butter and margarine where liquid oil phase is stabilized by the network of small ice crystals. Similar behaviour is also observed in O/W emulsions stabilized by the three-dimensional network of flocculated droplets (McClements, 2015). Below the yield stress, there is only a small deformation of the material as the interdroplet attraction is such strong that it does not allow the disruption of the droplet structure. Above yield stress, the material exhibits strong shear thinning behaviour as there is a gradual breakdown of the network structure of droplets over a range of applied stress. The rheology and the magnitude of yield stress depend on the strength of the attractive forces and the structural organization of the droplets (loosely or densely packed) (Marangoni, 2000; Pal, 1996b). The rheological behaviour of emulsions with yield stress (τ_0) can be described by the following two equations (McClements, 2015; Tadros, 2011):

Bigham (ideal) plastic: $$\tau - \tau_0 = \eta\dot{\gamma}^n \quad (2.7)$$

Nonideal plastic by Herschel – Bulkley model: $$\tau - \tau_0 = k_H\dot{\gamma}^n \quad (2.8)$$

where k_H is the consistency coefficient and n is the flow behaviour index.

2.3.4.3 Viscoelastic materials

Many soft materials show both the rheological properties, such as viscous and elastic behaviour simultaneously, instead of pure liquid (viscous) and pure solid (elastic) behaviour. Such material that exhibits both viscous and elastic properties under stress is called as viscoelastic material (McClements, 2015). In contrast to viscoelastic material, plastic materials dominate with elastic behaviour below certain critical yield stress and viscous behaviour above that critical stress value. For sure, the steady shear flow behaviour (viscosity) is helpful in characterizing all materials discussed in previous section 2.3.4.1, irrespective of they possess elastic property or not. However, viscosity alone is not sufficient sometimes to describe the many structural phenomena happening upon the deformation of the viscoelastic material. Because at the applied stress, either all the

mechanical energy is dissipated in the form of heat for pure viscous material or restored completely in the deformed bond for a purely elastic material. Oppositely, in a viscoelastic material, the applied mechanical energy is partly stored within the material and partly dissipated as heat due to friction (McClements, 2015; Tadros, 2011). The elastic behaviour exists in the viscoelastic material at only below some critical value of yield stress. The elasticity in a material is measured by complex shear modulus (G^*), which describes the entire viscoelastic behaviour of material (Equation 2.9) (Ahmed et al., 2016; McClements, 2015). It is measured by deforming (shear strain) material well below its yield stress and recording resultant stress. For that purpose, small deformation rheological techniques, such as *dynamic* and *transient* measurements, are widely used to study the rheological properties of the viscoelastic material (Ahmed et al., 2016).

$$G^* = \frac{\tau}{\gamma} \; ; when \; \tau < \tau_0 \tag{2.9}$$

2.3.4.3.1 Dynamic (oscillatory) tests

The viscoelastic materials are characterized by analyzing the dynamic or complex shear modulus (G^*), which is comprised of an elastic and a viscous contribution (Equation 2.10) (Norton et al., 2010; Zhu et al., 2020).

$$G^* = G' + iG" \tag{2.10}$$

where, $G' = {}^{\tau}/_{\gamma} \cos(\delta)$ is the storage modulus and $G" = {}^{\tau}/_{\gamma} \sin(\delta)$ is the loss modulus, and i is the complex number, and it is equal to $\sqrt{-1}$. G'represents the elastic component of the viscoelastic behaviour, which explains the solid-like behaviour of samples. $G"$ signifies the viscous component of the viscoelastic behaviour, which describes the liquid-like behaviour of samples. In dynamic measurements, G' and $G"$ is obtained by applying sinusoidal (oscillatory) stress or strain to viscoelastic material, and resultant sinusoidal strain or stress is measured with respect to time. The applied sinusoidal strain (γ) is characterized by its maximum amplitude, that is critical yield strain (γ_c), and angular frequency (ω). Similarly, the resultant sinusoidal stress (τ) is characterized by its maximum amplitude, that is yield stress (τ_0), at the same angular frequency (ω), but with different phase angles (δ) depending on the elastic and viscous contribution of the sample. For example, an ideal elastic material has a $\delta = 0°$ (no phase lag due to complete recovery), whereas the ideal viscous material has a $\delta = 90°$ (out of phase due to complete deformation), but in the case of

viscoelastic material there is always a phase lag ($0° < \delta < 90°$) between the applied stress (τ) and resulting strain (γ), or vice-versa (Tadros, 2011). Hence, the magnitude of applied sinusoidal shear strain (γ) and the resulting stress (τ) with phase angle (δ) as a function of time (t) can be given by the following equations (Norton et al., 2010):

$$\gamma = \gamma_0 \sin(\omega t) \tag{2.11}$$

$$\tau = \tau_0 \sin(\omega t + \delta) \tag{2.12}$$

There are usually two kinds of oscillatory tests are performed to characterize the viscoelastic material: (i) amplitude (strain or stress) sweep and (ii) frequency sweep (McClements, 2015; Tadros, 2011; Zhu et al., 2020).

2.3.4.3.1.1 Strain sweep analyzed viscoelasticity

Usually, strain sweep is the first step to characterize the viscoelastic behaviour of a material. In strain sweep measurement, the material is subjected to sufficiently small strain at a constant frequency (ω), where $\tau \propto \gamma$. The aim is to get the non-destructive range of strain which is called the linear viscoelastic region (LVR) (small amplitude oscillatory shear, SAOS) (Figure 2.10A) (Ahmed et al., 2016). This is followed by the Non–LVR region (large amplitude oscillatory shear, LAOS) with more deformation of material at higher strain or stress (Figure 2.10A) (Hyun et al., 2011). LVR is characterized by the plateau values of the $G'$and G'' which is independent of applied strain up to certain values. Within the LVR, G'values higher than G'' indicates more elastic or solid (gel)-like property of the material (Figure 2.10A), whereas higher G'' values than G' without proper LVR signifies the viscoelastic liquid-like behaviour of the material (Figure 2.10B) (Gunasekaran & Ak, 2000; Mrokowska & Krztoń-Maziopa, 2019). In general, G' values in the LVR region denotes the stiffness or gel strength of the material. Sometimes lack of LVR (although $G' > G''$) at a lower range of strain also implies the weak gel-like behaviour of material (not shown in Figure 2.10). For the gel-like material, G' dominates over G'' through the LVR, indicates only a few bonds are broken down in materials while the whole structure is still intact without much deformation. However, there is a sudden downturn into storage moduli curves at a certain point after LVR, which is called critical yield strain (γ_c) (Figure 2.10C) of the material above which structure starts to break down (Tadros, 2015). Here, the length (short or long) of the LVR helps understand the yielding behaviour of two different materials (for example, X and Y). For example,

material X in Figure 2.10C has a long LVR compared to material Y in Figure 2.10C. This signifies that the process of structural breakdown started earlier (at lower strain) in material Y than material X.

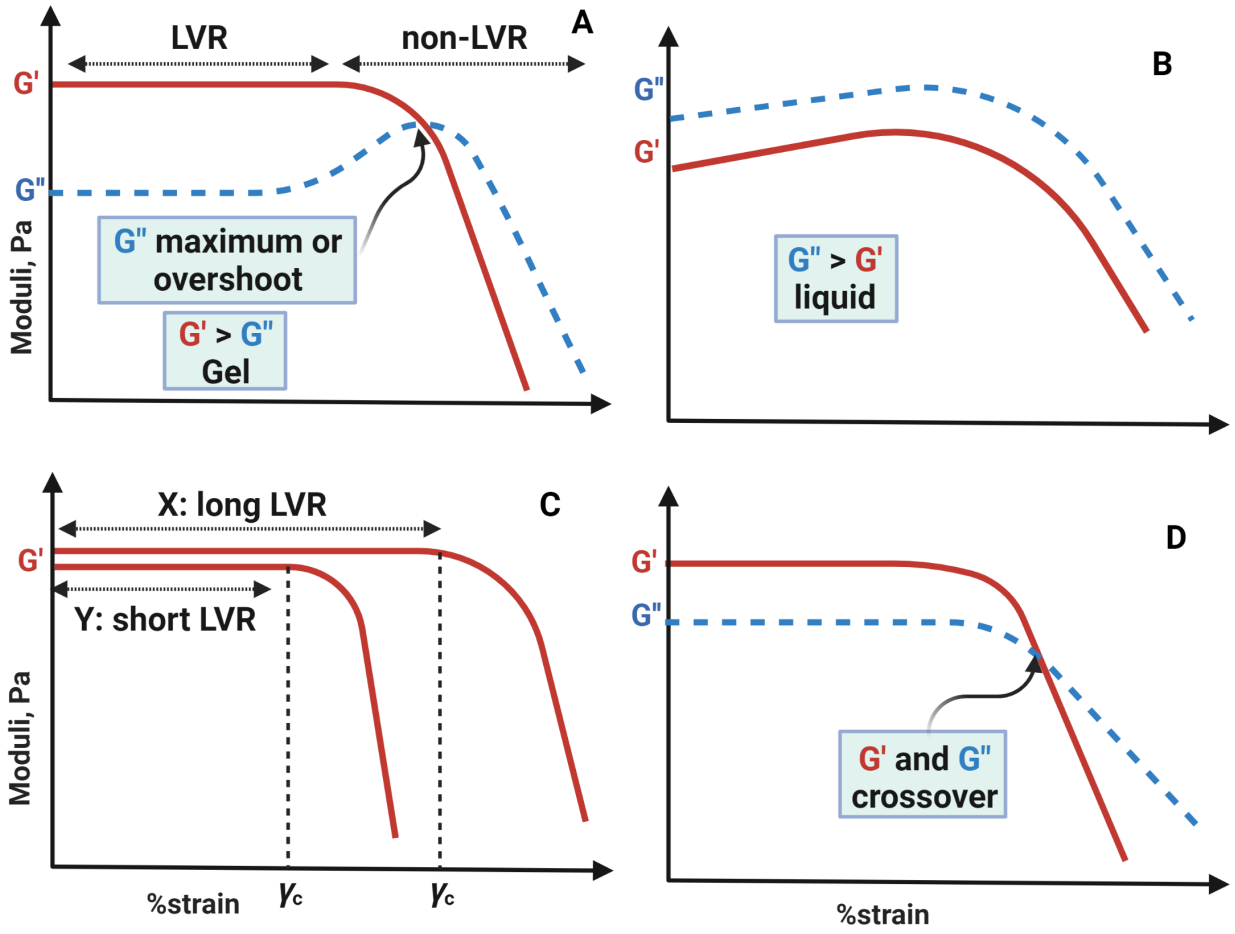

Figure 2.10 Various strain sweep profiles of viscoelastic materials (A) gel material with G″ maximum or overshoot (B) liquid material (C) material with a long and short linear viscoelastic region (LVR) (D) gel material with G′ and G″ crossover, but without G″ overshoot. Created with BioRender.com.

Beyond the yield point, $G'$and $G''$of the material become strain dependent with the application of large amplitude oscillatory shear (LAOS). Interestingly, the elastic component (G') of material still dominates over viscous component (G'') until the crossover point is reached, where $G' = G''$ (Figure 2.10D). Beyond the crossover point, the viscous portion (G'') will dominate, and

material starts to flow (Townsend & Wilson, 2018). According to Hyun et al. (2011), the shape of the $G'$and G''curves in LAOS (non-linear) region can be used to distinguish the behaviour of gel material (Hyun et al., 2011). In the LAOS region, many materials show the distinct maximum or overshoot in G'' which is typically very close to the crossover point (Figure 2.10A). This is classified as type III "weak strain overshoot" (G'decreasing and G''increasing followed by decreasing) LAOS behaviour and it is usually more pronounced in the soft glassy materials, such as concentrated emulsions and suspensions (Hyun et al., 2011). Similar overshoot in G''curve was also observed for the mayonnaise, and the author attributed this to the interactions between the oil droplets and loss of the stacking sequence of close-packed droplet structure at higher strain (Duvarci et al., 2017). Datta et al. (2011) observed the distinct peak in G″ for repulsively stabilized concentrated emulsions (ϕ = 0.7), and they attributed this behaviour to the structural relaxation process leading to gel network (structure) breakdown and followed by a flow of emulsions under applied amplitude.

On the other side, the kind of moduli curves observed in Figure 2.10D classified as type I "strain thinning" (G' and G'' decreasing) LAOS behaviour and it is more pronounced in the network kind of branched structure in polymer gel and emulsions with the aggregated structure, which will try to align in the direction of shear-field (Hyun et al., 2011; Li, Xu, et al., 2021). Oppositely, type II LAOS behaviour (not shown in the Figure 2.10) is termed as the "strain hardening," implying that both G' and G'' are increasing as amplitude is increased. For example, the interaction or cross-linking of biopolymer chains (fibrin and collagen) resists the deformation in material exhibits this kind of LAOS behaviour (Hyun et al., 2011; Townsend & Wilson, 2018). Thus, the analysis of the materials in LVR at lower strain and in non-LVR at higher strain can provide a better understanding of their structural changes.

2.3.4.3.1.2 Frequency sweep analyzed viscoelasticity

Frequency (ω) sweeps describe the time-dependent behaviour of material within the non-destructive deformation range. As the time is reciprocal of the frequency, the frequency can be used to describe the short-term and long-term relaxation behaviour of the sample (McClements, 2015). After determining the LVR through the preliminary strain sweep test, the dynamic shear modulus is determined as a function of frequency at constant strain value within LVR. Measurements of shear moduli as a function of frequency provide an essential insight into the

dynamic properties of the viscoelastic material. The G' and G'' values indicate whether the rheological properties of material are elastic ($G' > G''$) or viscous ($G'' > G'$) (Figure 2.11) (Ahmed et al., 2016). For example, a dilute solution shows the liquid-like behaviour with $G'' > G'$, where both moduli are frequency dependent (Figure 2.11A). Similarly, semi-dilute solution exhibits liquid-like ($G'' > G'$) behaviour at low frequency followed by G' and G'' crossover and finally transition into weak gel-like elastic ($G' > G''$) behaviour at high frequency (Figure 2.11B). If the moduli ($G' >> G''$) are independent of frequency and do not show any crossover, indicating strong gel behaviour depending on the applied range of frequency (Figure 2.11C). Oppositely, the frequency dependence of moduli ($G' > G''$) demonstrates a weak gel behaviour (Figure 2.11C) (Ahmed et al., 2016). Further, the crossover frequency (ω_c), where $G'= G''$, is an important parameter to correlate with the structural relaxation phenomenon in the sample (Figure 2.11B). It is inversely proportional to the relaxation time, i.e., $\omega_c \propto \frac{1}{t_{relax}}$ (Tadros, 2015; Zhu et al., 2020). The relaxation time (t_{relax}) is defined as the time at rest required for the material to relax against the applied stress (Norton et al., 2010). In low-frequency regime ($\omega < \omega_c$), the experiment time is long ($\omega \propto 1/\text{time}$); therefore, the system can dissipate the energy as viscous flow ($G'' > G'$). Oppositely, the system reduced the dissipation of energy, (less viscous or more elastic where $G' > G''$), in a short time experiment or at high frequency ($\omega > \omega_c$) (Figure 2.11B). Thus, depending on the kind of system (elastic versus viscous), the ω_c may shift towards lower frequency (more elastic) or higher frequency (more viscous), respectively (Tadros, 2015). In emulsions, the ω_c is determined by the droplet size (r), volume fraction of the droplets (ϕ) and kind of droplet-droplet interactions. For example, emulsions with smaller droplets and higher ϕ require more relaxation time, hence ω_c shifts to lower frequency (Tadros, 2015). However, in practice, all measurements are carried out at relatively high frequency as the low-frequency measurements (0.01 to 5 Hz) are time-consuming or due to the frequency limit of the instrument (Tadros, 2011). Therefore, the emulsions system, where droplet-droplet interaction is significant at higher ϕ, always exhibits frequency dependence of G' and G'' which is again dependent on the applied strain or stress and the elasticity of the sample (Tadros, 2015).

The delta (δ) is a phase angle between sinusoidal waves of applied stress and measured strain. Based on δ, another parameter which is widely used to describe the viscoelastic behaviour

is loss factor or tangent delta (tan δ). It is a ratio of G'' to G' and a dimensionless number (Tadros, 2015). In another term, tan δ is defined as the ratio of energy lost to the energy gained per cycle, and it can vary from zero to infinity ($0° < \delta < 90°$), depending on the elastic and viscous contribution from the viscoelastic material. Typically, when tan δ values ($G' > G''$) approach to zero indicates more elastic or solid-like behaviour in material, whereas at tan $\delta > 1$ ($G'' > G'$) correspond to more viscous or fluid-like behaviour in material (Lucey et al., 2003). Further, a lower tan δ is an indicator of the structural organization in a material (Létang et al., 1999).

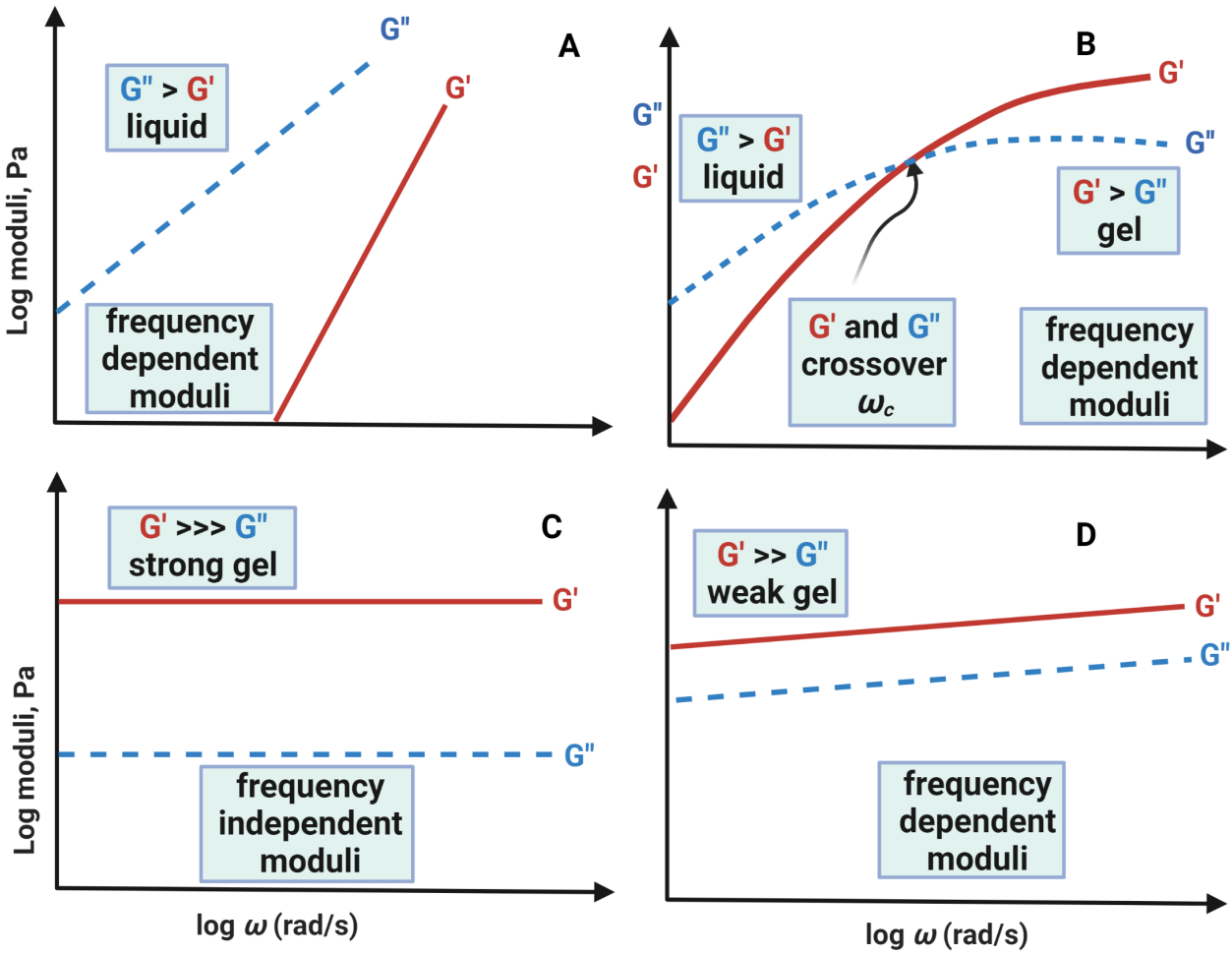

Figure 2.11 Various frequency sweep profiles of viscoelastic materials (A) very dilute liquid material (B) semi-dilute liquid material (liquid to weak gel transition) (C) strong gel material (D) weak gel material. Created with BioRender.com.

2.3.4.3.2 Transient test

Transient tests include *stress-relaxation* and creep measurements. A constant strain is applied to a material, and the resultant stress is measured over a time period. Oppositely, in creep tests**,** constant stress is applied to a material, and resultant deformation (strain) is measured as a function of time. When the time-dependent deformation is recovered after the removal of stress, it is called the recovery. The whole experiment is called the creep-recovery test, which results in a strain versus time profiles of the material (Tabilo-Munizaga & Barbosa-Cánovas, 2005). The creep-recovery data can be expressed in a better way with a parameter called compliance (*J)*, which is obtained by dividing the resultant strain by applied stress. The compliance is proportional to strain, but it is the reciprocal of the elastic modulus (Tadros, 2015). The creep test is performed by applying the stress within the LVR, so the resultant deformation (strain) also stays within LVR. Further, a creep test is the best suitable option for the frequency test for the viscoelastic material with longer time relaxation, as the low-frequency test is time-consuming discussed in the previous section (2.3.4.3.1) (Foegeding & Drake, 2007).

Typical compliance versus time curve for the pure elastic, pure viscous and viscoelastic material is shown in Figure 2.12A (Ahmed et al., 2016). For the ideal elastic material, the deformation and recovery are instantaneous upon application and removal of stress without any flow. Oppositely, ideal viscous material flows steadily under applied stress (follows Newton's law) and does not show any elastic deformation and recovery upon removal of stress. In the case of viscoelastic material, the instantaneous elastic deformation is followed by the non-steady flow under applied stress, which will recover partially when stress is removed (Ahmed et al., 2016; Tadros, 2011). Figure 2.12B shows the different components of the creep-recovery profiles relating to the viscoelastic material. The compliance (J_0) is related to the instantaneous elastic response of the material at time t_0, followed by a delayed viscous-retarded elastic response, and finally, a system reaches a steady-state flow (compliances increase linearly with a time) that is given by a viscous component (J_V). These two components (J_0 and J_V) are associated with creep compliance (J_E) (Tadros, 2015). The compliance at the time t_1 after creep test is called the maximum compliance (J_{max}). J_{max} value indicates an increase or decrease in the sample deformation, which can also be correlated with the modulus (G') or elasticity of the material (Norton et al., 2010; Tadros, 2011). In the recovery step, when stress is removed (Figure 2.12B), the stored elastic stress in the material start to relax and exhibits the instantaneous elastic recovery

followed by a creep recovery contributed mostly by any recovery from the retarded flow of the material, and they are associated with the recovery compliance (J_R). Finally, the viscous deformation is permanent without any recovery in the viscoelastic material. In the creep-recovery test, different mechanical models are used to describe the deformation behaviour of different materials (Figure 2.12B) (Norton et al., 2010).

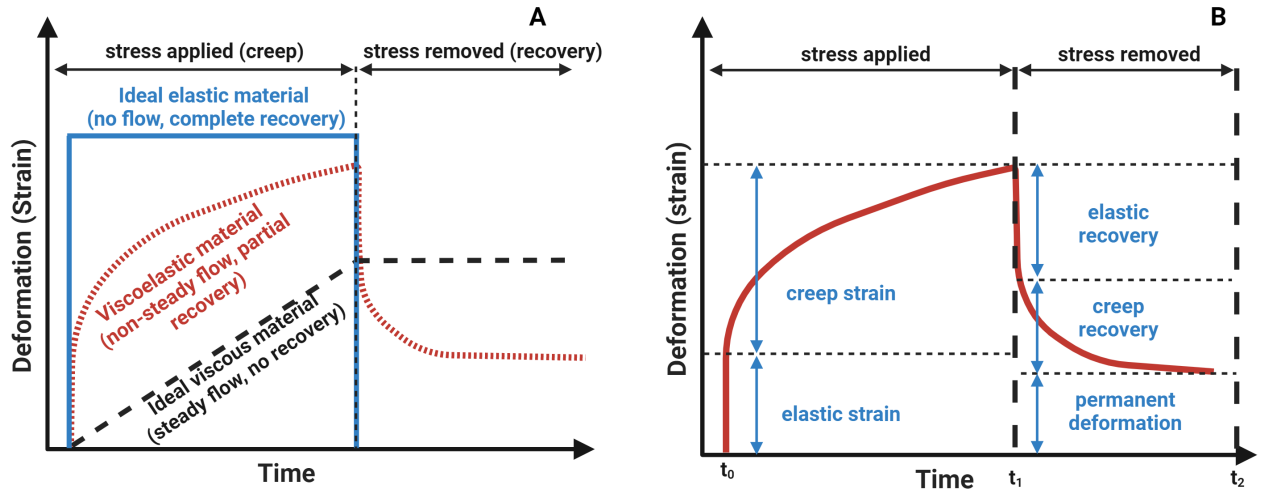

Figure 2.12 Stress relaxation (creep-recovery strain) profiles of different materials (A) creep-recovery profiles of viscous, elastic, and viscoelastic material (B) components of creep-recovery profiles. Created with BioRender.com.

2.3.5 Factors affecting the formation of gels from emulsions and nanoemulsions

The gelation in emulsions and nanoemulsions is influenced by droplet size, droplet charge, droplet-droplet interactions, droplet concentration and interfacial thickness (Helgeson, 2016; Zhang & McClements, 2018). These various parameters are discussed in detail under this section to understand how they control or affect the colloidal behaviour, particularly the rheology, of emulsions.

2.3.5.1 Droplet size

The droplet size in nanoemulsions is one of the most important characteristics since it influences its stability and rheological properties (McClements & Rao, 2011). The elasticity in nanoemulsions results from the energy dissipation by increasing the surface area due to droplet deformation. On the other hand, the deformation is dependent on the Laplace pressure of droplets,

and hence elasticity is inversely related to the droplet size (Pal, 1996a). As discussed in section 2.3.3, in electrostatically stabilized emulsions, a decrease in droplet size also results in an increase in $\phi_{eff,}$ which would further enhance the G' or gel strength of the emulsions (Fryd & Mason, 2012). The droplets size can be reduced by increasing the intensity (pressure) or duration (passes) of homogenization, by increasing the concentration of emulsifier used, or by controlling the viscosity ratio of the dispersed and continuous phase (η_D/η_C) (Qian & McClements, 2011). For example, Erramreddy and Ghosh (2015) reported that the droplet size of 16.6 mM SDS-stabilized emulsions reduced from 650 nm to 156 nm when the same emulsions were passed 8 times during homogenization. Further, it was observed in two separate studies that the droplet size of SDS-stabilized and protein-stabilized emulsions were decreased to the nanoscale with an increase in emulsifier concentrations while keeping the homogenization passes the same. The above studies showed an increase in viscosity and gel strength of emulsions with reduction in droplet size as a function of emulsifier concentration and homogenization passes, indicated by an increase in their ϕ_{eff} (Erramreddy & Ghosh, 2014; Patel, Mohanan, et al., 2019). The size can be further reduced by using the solvent evaporation method (Tan & Nakajima, 2005; Wooster et al., 2008). In this method, the immiscible organic solvent is added into the dispersed phase before the homogenization, and it is removed from the oil droplets by evaporation, which causes the droplets to shrink or reduce in size. The size of the droplets during the solvent evaporation method can be optimized by controlling parameters such as the particle size distribution of the initial emulsion, the amount of organic solvent present, and the water-solubility of the organic solvent (Chu et al., 2007; Lee & McClements, 2010).

2.3.5.2 Droplet charge

The charge or an electric potential on oil droplets is mainly due to the adsorption of ionic emulsifiers, mineral ions, or biopolymers (McClements, 2015). The change in droplet charge or zeta potential is a great indicator of colloidal stability or type of interaction between the droplets in response to change in the environmental conditions (pH and ionic strength) in emulsions (McClements, 2010). The electrical characteristics of nanoemulsion droplets can be controlled by careful selection of the types of emulsifiers. In principle, droplets stabilized by non-ionic emulsifiers (*e.g.*, Tweens and Spans) should have no charge. In contrast, droplets stabilized by anionic emulsifiers have a negative charge (*e.g.*, lecithin, citric acid esters of mono- and diglycerides (Citrem), sodium stearoyl lactylate (SSL), and diacetyl tartaric acid esters of mono-

and diglycerides (Datem)), whereas those stabilized by cationic emulsifiers have a positive charge (*e.g.*, lauric arginate and cetyl trimethyl ammonium bromide) (Kralova & Sjöblom, 2009; Mun et al., 2005). Biopolymer such as polysaccharide-based emulsifiers tend to stabilize the oil droplets with a net negative charge (*e.g.*, gum Arabic and modified starch) due to the presence of anionic groups (e.g., sulphate or carboxyl) on the polymer chains (Chanamai & McClements, 2002). On the other hand, protein (*e.g.*, whey protein, casein, soy proteins, egg proteins) stabilized droplets have a charge that depends on the pH of the medium in relation to the isoelectric point (pI) of the protein. Protein-coated droplets have a net positive charge for pH < pI, no net charge at pH = pI, and a negative charge at pH > pI. (Cooper et al., 2005; Gu et al., 2005). The charge on emulsifier-coated droplets has a significant impact on the stability, interfacial thickness and rheological properties of emulsions which can be altered by deposition of other charged molecules such as proteins and polysaccharides onto their surfaces or by the addition of mono or divalent salts in the continuous phase (Guzey & McClements, 2006; McClements & Rao, 2011). For example, Erramreddy and Ghosh (2014) reported that 40 wt% canola O/W nanoemulsions stabilized by non-ionic emulsifier (Tween 20, no charge) exhibited a flowable liquid-like behaviour compared to viscoelastic gel-like behaviour in the case of SDS-stabilized (highly negative charge) nanoemulsion. With the increased contribution of shell-layer from charged species (counterions) at the interface increased the ϕ_{eff} of SDS-stabilized nanoemulsions beyond ϕ_{MRJ} compared to Tween 20-stabilized nanoemulsions (Erramreddy & Ghosh, 2014). In another study, two oppositely charged protein-stabilized droplets (cationic lactoferrin versus anionic β-lactoglobulin at pH 6) were mixed in different ratios and sizes to induce the hetero-aggregation amongst the droplets. Authors reported that the hetero-aggregated mixture of oppositely charged small droplets was more effective in increasing the viscosity of the final suspension by forming a three-dimensional network that can entrap large amounts of aqueous phase (Mao & McClements, 2012).

2.3.5.3 Droplet-droplet interactions

The nature and magnitude of interactions between droplets is a critical factor in influencing the final rheological properties of emulsions. The kind of colloidal interactions decides whether emulsions droplets are in flocculated or non-flocculated states. In concentrated emulsion (high ϕ), the possibility of droplet-droplet interactions becomes significant compared to dilute

emulsions (low ϕ) (Tadros, 2011). The colloidal interactions between the droplets fall into two major categories (i) Repulsive forces (primarily electrostatic and steric) and (ii) attractive forces (includes van der Waals, hydrophobic, depletion forces). Generally, repulsively stabilized droplets stay apart as individual entities but tend to aggregate when attractive forces between them dominate (Wilking et al., 2006). For example, the strong electrostatic repulsive interactions between the droplets, particularly in the case of nanodroplets ($r < 0.2$ μm), there will be a few folds increase in viscosity due to an increase in the effective oil volume fraction of the droplets, as discussed in section 2.3.3. The increase in effective oil volume fraction of the droplets will be more pronounced in a concentrated emulsion, which is affected by the droplet size and degree of polydispersity. These two parameters (droplet size and polydispersity) have a significant influence on the droplet packing behaviour and hence on the emulsion's rheology. For example, Erramreddy and Ghosh (2014) demonstrated that the polydispersity of SDS-stabilized repulsive nanoemulsion gels was increased (from 0.18 to 0.23) with the decrease in SDS concentrations (from 2 times CMC to 0.5 times CMC). The increase in polydispersity significantly reduced the gel strength of nanoemulsions at similar $\phi = 0.4$. Authors also stated that the nanoemulsions with a higher polydispersity (0.23) would be jammed or gelled at higher ϕ_{MRJ} than at lower polydispersity (0.18) with similar ϕ_{eff} (0.75) (Erramreddy & Ghosh, 2014). Similarly, emulsion's viscosity and gel strength may increase when the droplet-droplet interaction is sufficiently attractive, which leads to an increase in effective oil volume fraction of the system by entrapping a large amount of aqueous phase in a fractal network of aggregated droplets (Berli et al., 2002; Datta et al., 2011). In contrast to repulsive emulsions, the attractive emulsions can form an elastic gel-like structure at $\phi < \phi_{MRJ}$ (Datta et al., 2011). As discussed in section 2.3.1, an attractive interaction between the droplets can be induced by depletant (micelles, smaller particles, non-absorbing polymer molecules) between the droplets, which cause depletion attraction or by changing the pH and ionic strength (addition of mono or divalent ions) of aqueous phase (Dickinson, 2013; Tuinier et al., 2003). For example, the viscosity of SDS-stabilized latex particles suspension was increased due to depletion attraction caused by the excess SDS micelles in the aqueous phase (Furusawa et al., 2002). Similarly, Patel, Longmore, et al. (2019) transformed the WPI-stabilized liquid nanoemulsions into attractive nanoemulsions gel by altering the inter-droplet interaction from repulsive to attractive as a function of change in the pH and ionic strength of nanoemulsions. The rheology of flocculated emulsions is very much dependent on the properties of the aggregates, such as size,

shape, porosity, and deformability, which is determined by the magnitude of attractive forces between droplets (Berli et al., 2002). Thus, it is possible to control the rheology of emulsions by manipulating the droplet-droplet interactions.

2.3.5.4 Droplet Concentration

The rheological properties of an emulsion are considerably dependent on the droplet concentration and its packing behaviour (Fryd & Mason, 2012; Mason et al., 2006; McClements & Rao, 2011). Depending on the dispersed phase volume fraction (ϕ), the rheological behaviour of emulsions transforms from liquids to viscoelastic gels. When the oil volume fraction of monodispersed droplets is higher than 64% (ϕ_{MRJ}), the random close packing of droplets occurs, and an emulsion exhibits gel-like viscoelastic characteristics (Mason et al., 2006; Quemada & Berli, 2002). For nanoemulsion, viscoelasticity develops at a much lower droplets concentration than that for conventional emulsions because of the increased effect of the interfacial layer on ϕ_{eff} as discussed in section 2.3.3 (Equation 2.4) (McClements, 2011).

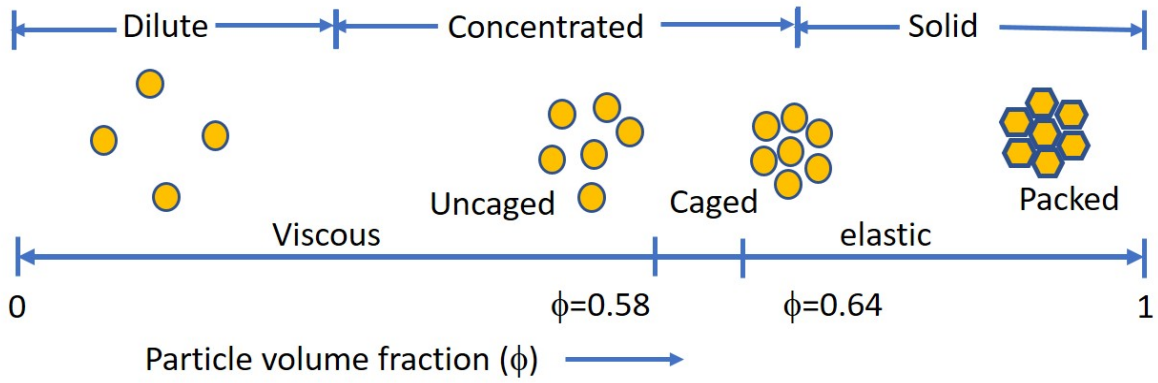

Figure 2.13 Structural transitions in monodispersed emulsion at different oil volume fractions

As shown in Figure 2.13, at a low oil volume fraction ($\phi < 0.05$), the droplet-droplet interaction is negligible but with some degree of Brownian motion. At this volume fraction, the emulsions behave like a Newtonian fluid with a viscosity very similar to the continuous phase. The concentrated monodispersed emulsions with ϕ between 0.49 to 0.58 show weak viscoelastic behaviour because of closer interaction of droplets, but at $\phi < 0.4$ it behaves like a viscous liquid.

At higher concentration ($0.58 < \phi < 0.64$), the motion of individual droplets is strongly constrained due to the presence of the neighbouring droplets in cage-like structures (Mason et al., 1995). Hence the droplets can oscillate in the cage surrounded by other droplets, and the system transformed into a glassy-state at $\phi = 0.58$. At ϕ above 0.58 and close to 0.64, a dramatic increase in viscosity and viscoelastic behaviour have been observed for monodispersed emulsions (Mason & Scheffold, 2014; Weiss & McClements, 2000). At $\phi = 0.64$, droplets are closely packed together, and they cannot easily flow past each other, and they become compressed and deformed when ϕ is higher than 0.64 for monodispersed system (Mason et al., 1995). This volume fraction is referred to as random close packing (RCP) or maximal random jamming (MRJ) (Wilking & Mason, 2007). Above this point, the compressed droplets' surface becomes so deformed that they exist as hexagonal packing as in a concentrated foam (Meleson et al., 2004). However, the above-discussed packing behaviour as a function of oil concentration is also affected by the polydispersity of droplet size distribution in emulsions, as discussed in the previous section 2.3.5.3. An emulsion with higher polydispersity would have a greater ϕ_{MRJ}, indicating higher ϕ (oil volume fraction) or ϕ_{eff} (effective oil volume fraction) is required for the close packing or jamming of droplets (Groot & Stoyanov, 2011). For example, Erramreddy and Ghosh (2014) stated that the polydispersity of SDS-stabilized repulsive nanoemulsion gels was decreased (from 0.23 to 0.18) with increase in SDS concentrations (from 0.5 times CMC to 2 times CMC) at similar $\phi = 0.4$ where the gel strength also decreased. This is indicating that the nanoemulsions with higher polydispersity would be jammed at higher ϕ_{MRJ} compared to nanoemulsions with lower polydispersity although their ϕ_{eff} were same (0.75).

2.3.5.5 Interfacial thickness

As discussed in section 2.3.3, the increase in shell layer thickness (δ) would significantly increase the effective droplet size ($r_{eff} = r + \delta$) and effective oil volume fraction (ϕ_{eff}) of the droplets according to Equation 2.4 (Mason et al., 2006). An increase in ϕ_{eff} with the increase in δ at constant r and ϕ will decide the physical state of nanoemulsions (glassy versus jamming). The interfacial thickness of nanoemulsion droplets can be controlled by a precise selection of emulsifier types such as low molecular weight emulsifiers (LMWEs), phospholipids, proteins or polysaccharides (Dickinson, 2003). As shown in Figure 2.14, the thickness of the layers formed by food-grade emulsifiers varies in the magnitude of typically, LMWEs (such as Tweens and Spans) <

globular proteins (such as egg, whey or soy proteins) < flexible proteins (such as casein or gelatin) < polysaccharides (gum Arabic) (Guzey & McClements, 2006). The thickness of the charge cloud or interface around the droplet can also be varied by changing the type of LMWEs (non-ionic versus anionic) (Figure 2.14). For example, the higher thickness (δ~18 to 36 nm depending on the emulsifier concentration) of charge cloud (electric double layer) around an anionic emulsifier (SDS) stabilized nanodroplets was able to induce the gelation in nanoemulsions at lower oil volume fraction ($\phi = 0.4$) compared to negligible or no thickness of non-ionic emulsifier (Tween 20) stabilized nanodroplets (Erramreddy & Ghosh, 2014). Similarly, the biopolymer is very good at the interface in providing the electrostatic (due to charge cloud) and steric barrier (flexible polymer chain) with the higher interfacial thickness (Figure 2.14). Patel, Mohanan, et al. (2019) showed that the flexible protein (sodium caseinate) at the interface provided higher interfacial thickness (δ ~ 18.9 nm) due to strong electrostatic and steric barrier compared to globular protein (whey protein, δ ~ 8.5 nm).

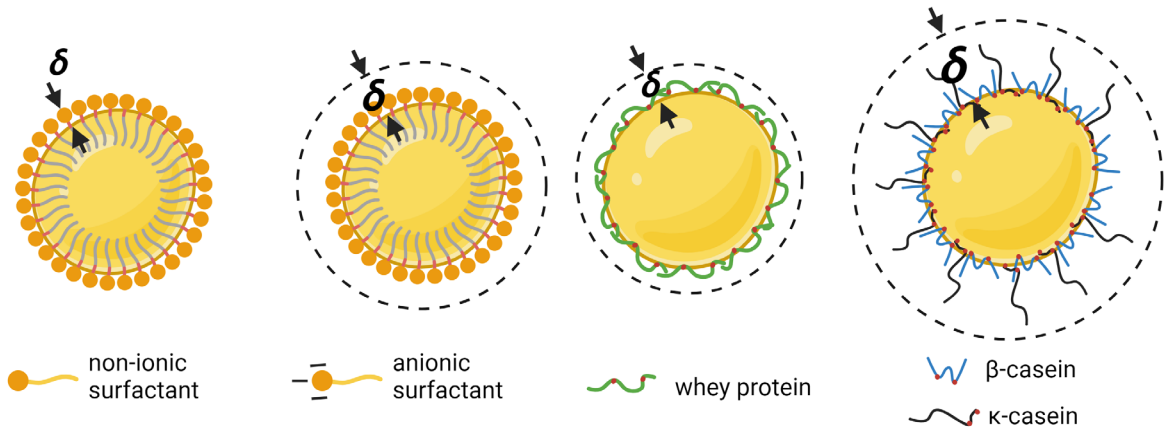

Figure 2.14 Interfacial thickness (δ) as a function of the type of emulsifier and its conformation arrangement at the interface. The dotted line in the anionic surfactant and protein-stabilized droplet shows the charge cloud (electric double layer) thickness. A similar charge cloud (not shown) around a steric layer of polysaccharide-stabilized droplet can also contribute to the interfacial thickness. Created with BioRender.com.

Such a significant contribution of shell layer around nanodroplets and associated increase in ϕ_{eff} beyond ϕ_{MRJ} led to gelation of sodium caseinate-stabilized nanoemulsions at $\phi = 0.42$ (Patel, Mohanan, et al., 2019). Similarly, the interfacial layer thickness can also be increased by layer-by-

layer (LbL) deposition of one or more oppositely charged layers of polysaccharides onto the emulsifier (LMWEs or protein)-coated oil droplets (Güzey & McClements, 2006). An ionic polysaccharide (anionic or cationic) molecules adsorbed as a second layer can provide the long-range (thick) electrostatic and steric repulsive layer around the droplets compared to only the short-range (thin) electrostatic barrier provided by the emulsifier-coated droplets (Dickinson, 2011; Wong et al., 2011).

2.3.6 Applications of nanoemulsion gels in food and soft materials

The nanoemulsion-based gels represent a potential new class of structural ingredients to improve the texture and stability of processed foods such as yogurt, cheese, mayonnaise. These types of processed foods are made from protein-based conventional emulsion gels (Dickinson, 2013). As the nanoemulsions can be structured into viscoelastic gels at much lower oil volume fraction with improved functionality and stability compared to conventional emulsion gels, this novel gel structure may open up new applications in many areas such as food, pharmaceuticals and cosmetics (Erramreddy & Ghosh, 2015; Kawada et al., 2010; Mason et al., 2006; Patel, Mohanan, et al., 2019; Wilking & Mason, 2007). The characteristics such as extremely small nano-scale droplet size and large surface area are also known to improve the bioavailability of active components, which can further extend the application of nanoemulsion gels in the field of functional food (McClements et al., 2007). Despite their advantages, not much research has been done on nanoemulsion gels. Hence, it is crucial to study the nanoemulsion gels for their structure-function relationships so that real food's texture and sensory properties can be improved. It is expected that this research will develop a novel gel-like structure at lower oil concentration which will explore its application in reducing heart-unhealthy saturated and trans fat in food formulations.

2.4 Multilayer emulsions: Formation, properties and advantages

2.4.1 Formation and properties of multilayer emulsions

Multilayer oil-in-water emulsions consist of dispersed oil droplets (the core) coated by nano-laminated layers (the shell) comprised of emulsifiers and biopolymer molecules (McClements & Li, 2010). The formation of multilayer emulsion is based on the layer by layer (LbL) electrostatic deposition technique, which principally involves the use of electrostatic attraction of oppositely charged emulsifiers and biopolymers to form a thick interfacial layer around the oil droplets (Bortnowska, 2015). Figure 2.15 shows the principle of the LbL electrostatic deposition technique.

In this technique, oppositely charged biopolymers are deposited sequentially to form a thick multilayer over the droplet. Initially, the primary emulsion is prepared by homogenizing a suitable concentration of oil in a mixture of water and emulsifier. The secondary layer consisting of an oppositely charged biopolymer is electrostatically adsorbed onto the surface of a primary emulsion droplet, and next, the third layer of another oppositely charged biopolymer can be added in an analogous way to stabilize the colloidal system with multilayer formation (Chen et al., 2011; Guzey & McClements, 2006). Depending on the number of interfacial layers surrounding the oil droplets, primary, secondary, or tertiary emulsions can be produced (Hu et al., 2011). Ideally, these steps can be repeated to create several layers around the oil droplets, but we will use the LbL deposition method to deposit only two layers at the droplet surface.

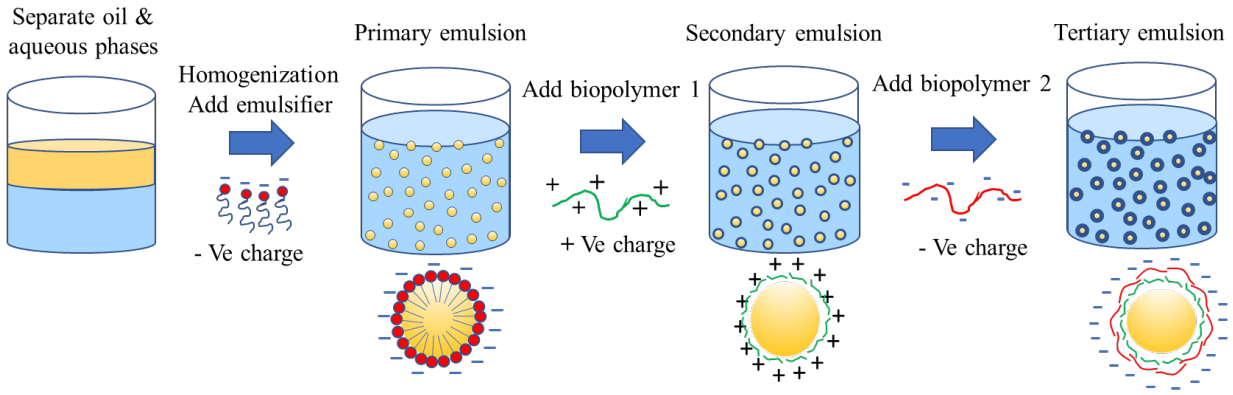

Figure 2.15 Formation of multilayer emulsion by LbL electrostatic deposition method

The multilayer interface can be designed by an effective deposition of biopolymer (protein/polysaccharide) around the oil droplet through the application of either a one-step or two-step mixing process depending on the charge – pH condition of the biopolymer used. Between each deposition step, a washing step is required to remove the excess emulsifier or biopolymer from the bulk phase (McClements et al., 2007). The removal of excess unadsorbed emulsifiers will ensure that added biopolymer goes to the interface instead of interacting with the polymer in the bulk phase. In the one-step process, the emulsion droplets coated by a protein at pH < pI with a positive charge are mixed with another biopolymer solution at the same pH but with a negative charge to make an electrostatic complex with the protein molecules at the droplet surface. Similarly, the negatively charged protein or LMWE-stabilized droplets is coated by positively

charged biopolymer using a one-step mixing method (Aoki et al., 2005; Guzey & McClements, 2006; Li et al., 2020). For example, Mun, Decker, and McClements (2006) used a one-step direct mixing method to deposit the positively charged chitosan onto the SDS-stabilized negatively charged droplets. In the two-step process, the emulsion and biopolymer solution is mixed at pH > pI of protein where biopolymer does not interact with the droplet surfaces because both are negatively charged at this pH. The pH is then reduced to less than pI, where the protein molecules become positively charged and react with the anionic biopolymer molecules present in the solution (Guzey & McClements, 2006; McClements, 2012a). Perrechil and Cunha (2013) used the two-step mixing method wherein they mixed the negatively charged sodium caseinate-stabilized emulsions and κ-carrageenan at neutral pH in the first step and changed the pH of the mixture to 3.5 in the next step for the charge reversal and electrostatic deposition of κ - carrageenan on sodium caseinate-stabilized droplets. The change of zeta (ζ) - potential during sequential deposition of biopolymer onto the primary emulsion can be used to confirm the adsorption of different interfacial layers and thus the stability of the emulsion. The measurement of ζ - potential is a useful indicator of surface charge of biopolymer stabilized emulsion droplet (McClements et al., 2007; Ye et al., 2011). Kartal et al. (2017) confirmed the adsorption of negatively charged pectin molecules onto the positively charged sodium caseinate-stabilized droplets by the charge (zeta potential) reversal from + 26.5 mV to – 11.2 mV. Also, the measurements of ζ-potential are widely used to monitor the effect on electric potential or charge of multilayer membranes in different pH and ionic environments (Hu et al., 2011; Lesmes et al., 2010). For instance, Ogawa et al. (2003a) reported that the negative charge of lecithin-stabilized primary emulsions was reduced while the positive charge of lecithin-chitosan-stabilized secondary emulsions remained the same with an increase in ionic strength (from 0 mM to 500 mM $CaCl_2$). Similarly, Hu et al. (2011) observed that the charge of sodium caseinate-pectin-stabilized droplets remained negative (-48 to -5 mV) from pH 7 to 3, whereas sodium-caseinate-stabilized droplets showed charged reversal from negative (-55 mV) to positive (+55) with neutral charge near to (pI) pH 4.5. Further, the adsorption kinetics of biopolymer and hence the formation of multilayer emulsions is much dependent on the concentration of the biopolymer (Pallandre et al., 2007). At a lower biopolymer concentration, it is not easy to coat the emulsion droplets with a huge surface area, leading to bridging flocculation. Oppositely, at higher concentrations, free polymer molecules can create an osmotic imbalance between droplets which will be responsible for the depletion flocculation. For example, Perrechil

and Cunha (2013) showed that the insufficient or low concentration of κ-carrageenan (< 0.2 wt%) in sodium caseinate-κ-carrageenan-stabilized droplets led to extensive aggregation due to bridging flocculated at pH 3.5. In addition to biopolymer concentration, there are other parameters, such as pH, ionic strength, type of biopolymer and molecular characteristics of biopolymer (molecular weight and charge distribution), needs to be considered in the formation of the multilayer emulsions.

2.4.2 Advantages of multilayer emulsions

The conventional emulsion with a monolayer of emulsifiers has several disadvantages, such as limited stability to pH, salt, heating, dehydration, and freezing. The most significant advantage of multilayer emulsion over monolayer emulsion is that the properties of interfacial layers, such as their composition, thickness, and charge, can be manipulated as per the final application (Li et al., 2020). Moreover, the stability of emulsions against environmental stresses can be improved by combining the properties of different emulsifiers and biopolymers in the form of multilayer at the oil-water interface. For example, protein at the interface imparts an excellent surface activity but is very susceptible to change in the pH and ionic environment due to a change in electric charge or the lack of a thick steric barrier, respectively. However, the protein-polysaccharide complexation either covalently and electrostatically has a good surface activity and stability against the different environmental stresses (Guzey & McClements, 2006). The deposition of polysaccharides to protein-stabilized droplets gives dual protection, i.e., electrostatic and long-range steric barrier, to the droplets against environmental stresses (pH, ionic strength, temperature (thermal processing and freeze-thaw cycle) compared to only protein-stabilized droplets. Chang and McClements (2015) reported that the contribution of electrostatic and steric repulsion from the fucoidan (sulphated polysaccharide from marine source)-deposition as a second layer increased the stability of caseinate-stabilized droplets against aggregation at different pH values (2 to 9) examined in fish oil-in-water emulsions. Likewise, it has been shown that the lecithin-chitosan coated bilayer emulsion was more stable to thermal processing (30 to 90°C for 30 min), freeze-thaw cycling (-10°C for 22h/30°C for 2h), and high ionic strength ($CaCl_2 \leq 500$ mM) (Ogawa et al., 2003a). Moreover, interfacial engineering through electrostatic deposition technique can lead to the formation of a versatile emulsion-based delivery system with better protection and control release of bioactive components (McClements & Li, 2010). For example, the incorporation of β-

carotene in WPI-pectin-stabilized oil-in-water bilayer emulsions improved the stability against the degradation and controlled delivery of β-carotene compared to only WPI-stabilized emulsions (Xu et al., 2012; Xu et al., 2014). The multiplayer nano-laminated coating on the droplets can also help to control lipid digestibility. The digestibility is controlled by the deposition of dense biopolymer layers around the oil droplet, which will modulate the diffusion process across the interface. Mun, Decker, Park, et al. (2006) reported that the lower amount of fatty acids released in the lecithin–chitosan-coated emulsions (38 ± 16 μmol ml^{-1}) than those emulsions coated by lecithin alone (250 ± 70 μmol ml^{-1}). Further from Equation 2.4, if we consider the core-shell structure in the formation of multilayer emulsions, then the thick interfacial shell layer (multilayer) on the nanoscale droplet can considerably contribute to the effective volume fraction of the droplet. As the shell layer thickness (δ) approaches to droplet radius (r) ($\delta \approx r$), there is an increase in the effective droplet volume fraction (ϕ_{eff}), and it could have a significant impact on the rheological behaviour of multilayer nanoemulsion. In this case, the viscosity and viscoelasticity of multilayer nanoemulsions may be substantially higher than that of a conventional microscale emulsion at the same oil content. In the proposed research, a similar approach will be considered in designing multilayer nanoemulsion gels.

2.4.3 Interfacial components for multilayer emulsions

2.4.3.1 Low-molecular-weight-emulsifier at the interface

Numerous different food-grade emulsifiers and biopolymers can be used to assemble nano-laminated coating around the oil droplets. The food-grade LMWEs, e.g. citric acid esters of mono- and diglycerides (Citrem), sodium stearoyl lactylate (SSL), diacetyl tartaric acid esters of mono- and diglycerides (Datem) and phospholipids (e.g. lecithin), are widely used in the formation of stable primary emulsion with negatively charged droplets (Klinkesorn & McClements, 2009). It has been shown that LMWEs-coated droplets remain highly negative and stable across a wide pH range (Hong & McClements, 2007). Lecithin is typically zwitterionic in nature, containing both positive and negative charges; however, it forms negatively charged emulsion droplets in acidic environments (McClements et al., 2007). These emulsifiers are generally more surface-active and can pack easily and efficiently than proteins at the oil-water interface. Further, they can diffuse to the interface at a much faster rate than proteins, leading to the formation of smaller droplets (Bortnowska, 2008; Dickinson, 2009).

2.4.3.2 Biopolymer: protein and polysaccharide at the interface

Proteins are biological polymers comprised of a polypeptides chain of 20 different amino acids linked through peptide bonds. The type, number and sequence of amino acids determine the molecular weight, conformation, hydrophobicity, electric charge, physical and chemical interaction of proteins (Jones & McClements, 2010). The proteins are often used as a food-grade emulsifier in emulsion preparation due to their amphiphilic nature and ability to adsorb to the surfaces of the oil droplets (Dickinson, 1994). Some protein films around the oil droplets are highly viscoelastic in nature which can help to prevent droplet coalescence under external stress (Wilde et al., 2004). They can also provide good emulsion stability against aggregation by generating electrostatic or steric repulsion between the droplets (Guzey et al., 2004). For example, the lactoferrin-stabilized droplets provide long-range steric repulsion in addition to strong droplet surface charge compared to β-lactoglobulin-stabilized droplets, which gives better stability to emulsions against droplet-aggregation induced by a change in pH or ionic strength (Dickinson, 2019; Schmelz et al., 2011). Protein stabilized emulsions, however, are sensitive to pH, ionic strength, and thermal treatment due to changes in the charge or conformation of the protein adsorbed around the oil droplets. As pH approaches the isoelectric point (pI), the net charge on the protein becomes zero, and they fail to remain in solution due to hydrophobic aggregation (Schmelz et al., 2011). Conformational changes in proteins also occur above their thermal denaturation temperatures and after interfacial adsorption, exposing non-polar and sulfhydryl groups and leading to extensive droplet aggregation (Cooper et al., 2005; Dalgleish, 1990). The protein stabilized emulsions are generally stabilized by short-range electrostatic and steric repulsive forces, which are not sufficient to overcome the long-range van der Waals or hydrophobic forces near the isoelectric point (Dickinson, 2019; Gashua et al., 2016). However, the deposition of polysaccharides on protein-stabilized droplets provides stability against those attractive forces by sufficiently increasing the steric and repulsive forces between droplets (Dickinson, 2009).

Compared to surface-active protein, many polysaccharides are much hydrophilic or less surface-active to stabilize the droplet surface, but they can make electrostatic complexation with protein-stabilized droplets. Polysaccharides are polymers of monosaccharides differing chemically from each other in type, number, sequence and bonding of the monosaccharides within the polymer chain. Due to these chemical differences, each type of polysaccharide has unique molecular characteristics such as molecular weight, electrical charge, branching, hydrophilicity,

hydrophilicity and conformational flexibility (Matalanis et al., 2011). Consequently, the different polysaccharide types exhibit different physicochemical properties, *e.g.*, thickness, charge, permeability, and environmental responsiveness at the interface, which in turn could lead to different emulsion functional properties such as stability, rheology, and delivery. Further, the electrical charge on the adsorbed polysaccharide molecules depends on the nature of ionic groups along with the chain background as well as solution conditions and accordingly, polysaccharides can be categorized as (i) neutral (e.g. starch, cellulose, dextran, galactomannans, agar), (ii) anionic (e.g., pectin, carrageenan, alginate, gum Arabic, xanthan gum, gellan), and (iii) cationic (chitosan) (Li et al., 2012; McClements, 2012a). At pH below pKa value, anionic polysaccharides tend to be neutral and negative above it, whereas cationic polysaccharides tend to be neutral at pH value sufficiently above their pKa value but positive below it (Matalanis et al., 2011). Thus, by selecting the type of polysaccharides and varying the solution pH, it is possible to "tune" the electrostatic deposition characteristics of the polyelectrolytes. When electrostatically adsorbed at the interface, these polysaccharides can provide long-term stability to protein-stabilized emulsions compared to protein alone due to the formation of a thick interfacial layer stabilized by the electrostatic and steric forces (Li et al., 2020). For example, the xanthan gum molecules with more linear charged density than pectin were able to make more complexes with wheat protein and were more effective in stabilizing protein-xanthan gum bilayer emulsions at higher ionic strength (Qiu et al., 2015). Oppositely, another study showed that the protein (rice glutelin)-pectin stabilized droplets were more stable to aggregation at low pH values than the protein-xanthan gum-stabilized droplets. This was explained by the pectin with long neutral (sugar) side chains protrudes more into the solution and enhance the steric repulsion between the droplets than xanthan gum with short side chains (trisaccharide) (Xu et al., 2017). Thus, selecting a suitable polysaccharide to form multilayer on emulsion droplets depends not only on their electrical characteristics but also on their responses to different environmental stresses.

2.4.4 Effect of environmental stresses on the stability of multilayer emulsions

The emulsions have versatile applications in various foods in which pH, temperature, and ionic strength of the medium being changed frequently. Many research studies have shown that the physical and chemical stability of multilayer emulsion-based systems can be improved by engineering their interfacial properties. For example, good stability to droplets aggregation over a wide range of pH, ionic strength, temperatures, and freeze-thaw stability has been reported by

Pallandre et al. (2007); Surh et al. (2005); Tokle et al. (2010); Zeeb et al. (2011). For example, Tokle et al. (2010) showed that the pH (3 to 7) and temperature (30 to 90°C) stability of the lactoferrin coated emulsion droplets could be improved by electrostatic deposition of the pectin and alginate molecules over them. In another study by Pallandre et al. (2007) showed that the controlled electrostatic deposition of alginate molecules over the caseinate-coated emulsion droplets had better stability at pH values near caseinate's isoelectric point (pH 4 and 5) and up to higher ionic strengths (< 300 mM NaCl). It has also been reported that palm oil-in-water multilayer emulsions (SDS-chitosan-pectin) were more stable to freeze-thaw cycles in terms of droplet coalescence and flocculation than primary (SDS) and secondary (SDS-chitosan) emulsions (Thanasukarn et al., 2006). The increase in physical stability of emulsion droplets to flocculation and coalescence can be explained by the formation of highly thick charged interfacial layers, which helps to decrease the attractive (van der Waals) forces and increase the repulsive (electrostatic or steric) forces between the multilayer-coated oil droplets (Guzey et al., 2004; McClements, 2012a; Zeeb et al., 2011). On the other hand, the high chemical or oxidative stability of multilayer-coated bioactive lipids can be due to the minimized interaction between encapsulated components and chemically reactive aqueous phase substances (McClements, 2012a). It has been shown that by increasing the positive charge over the lecithin-chitosan-coated thick interfacial layer, it was possible to prevent the close contact of positive transition metals (such as iron or copper) with the oxidative lipophilic components (Ogawa et al., 2003a). Gudipati et al. (2010) studied the oxidative stability of the fish oil-in-water multilayer emulsions by assessing their peroxide value, thiobarbituric acid reactive substances (TBARS), and headspace aldehydes at 20°C for 40 days. They found that positively charged Citrem-chitosan stabilized secondary emulsions were more stable to lipid oxidation compared to negatively charged Citrem and alginate stabilized primary and tertiary emulsions, respectively. Thus, the emulsions stabilized by the multilayer interfacial membranes comprised of two or more emulsifiers or biopolymers, rather than a single interfacial layer comprised of one type of emulsifier, may help develop food products with improved stability to environmental stresses.

2.4.5 Concentrated multilayer emulsions

The multilayer formation phenomenon at the oil droplet interface is widely used, focusing on improving the emulsions stability and controlled delivery of micronutrients. However, the final emulsions system with multiple interfacial layers was restricted to a lower dispersed phase

concentration (< 10 wt%). One of the major challenges in forming concentrated multilayer emulsions is to fully coat the oil droplets with different layers at higher oil concentrations. This is because either the emulsion tends to form the flocculated structure with an increase in oil volume fraction or the limitation of the LbL deposition technique and the type of biopolymer used in forming the multilayer emulsion. For example, Guzey and McClements (2006) shown through the stability map created for the multilayer system that the stable multilayer emulsions can only be formed within a certain limit of oil concentration ($\phi < 0.11$). At a higher concentration of oil, multilayer emulsions system would be unstable due to high particle-particle collision rate than polymer adsorption rate (Guzey & McClements, 2006). This challenge will be addressed in the present thesis research by developing concentrated multilayer O/W emulsion with nearly 40 wt% oil. Two different multilayer formation strategies (one-step and two-step mixing methods, discussed in 2.4.1) will be investigated using two different sets of interfacial materials for LbL deposition.

2.4.6 Applications of multilayer emulsions in delivery and controlled release

Multilayer emulsions, due to their improved stability and tailor-made interfacial properties, may have several potential applications in the food and pharmaceutical industry. For example, highly charged thick interfacial membranes can be useful in preventing droplet aggregation or lipid oxidation. Further, a multilayer around the droplets is very useful in many emulsion-based delivery systems to remain stable over a wide range of pH values or otherwise advantageous to a delivery system where breakdown (controlled release applications) at particular pH is necessary. The multilayer interfaces can respond to an environmental condition in a controlled fashion and change their properties accordingly for controlled and targeted delivery of bioactive ingredients (Guzey & McClements, 2006; McClements et al., 2007). There are several studies suggested that multilayer interfacial coating around the droplets can control the digestion of lipids under simulated gastrointestinal conditions. These properties of multilayer emulsions can be used to design delivery systems for lipophilic bioactive components that need to be encapsulated within foods but released at a target site in the human body (Hu et al., 2011; Klinkesorn & McClements, 2010; Li et al., 2010). It can also be utilized to restrict lipid digestibility and hence provide calorie restriction with induced satiety from the diet.

3. CONVERSION OF VISCOUS OIL-IN-WATER NANOEMULSIONS INTO VISCOELASTIC GELS UPON REMOVAL OF EXCESS IONIC EMULSIFIER[1]

3.1 Abstract

Viscous, flowable nanoemulsions stabilized with ionic emulsifier can be transformed into repulsively jammed elastic gels that do not flow under gravity by reducing the droplet size and increasing the interfacial repulsive shell layer thickness. However, a high concentration of emulsifier required to achieve nanodroplets could remain in the continuous phase and lead to oscillatory structural forces, thereby reducing repulsive interaction and forming flowable liquid systems. It was hypothesized that the removal of excess emulsifiers from nanoemulsion could lead to the formation of repulsive gels. Canola oil-in-water nanoemulsions containing 40wt% oil were prepared with a citric acid ester of monoglyceride (Citrem) using a high-pressure homogenizer. The excess emulsifier in the aqueous phase was removed by multiple ultracentrifugation cycles and the droplet size, rheology and stability of the nanoemulsions were investigated as a function of excess Citrem concentration. Nanoemulsions with an average droplet size of 222 and 150 nm were obtained with 3 and 5 wt% Citrem, respectively. Removal of excess Citrem did not change the droplet size significantly. However, viscosity, yield stress, and storage moduli increased significantly with the reduction of excess Citrem and decrease in droplet size, converting the flowable weak gel nanoemulsion into a strong viscoelastic gel. The calculated values of oscillatory structural forces decreased with the removal of excess emulsifier leading to an increase in repulsive interaction and thickness of the electric double layer. Such an increase in inter-droplet separation led to an increase in effective oil volume fraction beyond the maximum random jamming of oil droplets and the formation of viscoelastic nanoemulsion gel.

[1]Reprinted with permission from: Kadiya, K., & Ghosh, S. (2019). Conversion of Viscous Oil-in-Water Nanoemulsions to Viscoelastic Gels upon Removal of Excess Ionic Emulsifier. Langmuir, 35(52), 17061-17074. *Copyright © 2019, American Chemical society*. Kadiya, K. carried out the experiments and wrote the first draft. Ghosh, S. conceptualized, supervised, reviewed, and edited.

3.2 Introduction

Nanoemulsions are metastable emulsions with an average droplets diameter below 200 nm (McClements, 2012b). Different authors reported various ranges of droplet size for nanoemulsions and even considered the upper range of droplet diameter up to 500 nm (Fernandez et al., 2004; Gutierrez et al., 2008). Due to their smaller droplet size, nanoemulsions are kinetically more stable against gravitational separation and particle aggregation compared to their conventional counterpart (Rao & McClements, 2012; Tadros et al., 2004). Nanoemulsions are also found to display a wide variety of rheological behaviour depending on the droplet size, oil volume fraction, and emulsifier concentration. Nanoemulsion rheology also depends on the inter-droplet interactions governed by the DLVO (electrostatic and van der Waal), and non-DLVO (depletion and structural) forces. These forces are manifested by the ionic environment around the droplets, type of emulsifiers as well as through the excess emulsifier micelles concentration between the droplets (Erramreddy & Ghosh, 2014).

When an anionic emulsifier, such as sodium dodecyl sulphate (SDS), Citrem (Citric acid ester of mono- and diglyceride), and lecithin (a mixture of different phospholipids), stabilizes oil-in-water (O/W) nanoemulsions, it provides a negative charge to the nanodroplets, which are surrounded by a cloud of charged counter ions (Erramreddy & Ghosh, 2014; Hedegaard et al., 2013; Klinkesorn & McClements, 2009; Wilking & Mason, 2007). The charge cloud provides a nanoscale interfacial repulsive barrier against a close approach by another droplet. In high internal phase emulsions (e.g., mayonnaise), where droplets form a close-pack structure, the charge cloud essentially provides the inter-droplet separation and becomes largely responsible for emulsion stability. In such systems, flow behaviour becomes restricted, which imparts a viscoelastic gel-like structure to the system. Due to the electrostatic repulsive forces between the droplets, this kind of concentrated emulsion gel is often referred to as repulsive gel.

Apart from repulsive gelation, liquid emulsions can also be transformed into a gelled system by initiating attractive interactions among the dispersed droplets. There are many ways attractive interactions can be generated. For example, when the separation between two droplets become less than the diameter of the dispersed colloidal particles (e.g., emulsifier micelles, dispersed biopolymers etc.), a long-range attractive depletion forces generated due to the difference in the osmotic pressure between the inter-droplet region and the bulk continuous phase (Asakura & Oosawa, 1954). A similar kind of depletion forces with excess SDS micelles in the continuous

aqueous phase has been shown to transform a liquid 40 wt% canola oil nanoemulsion into an attractive nanoemulsion gel (Erramreddy & Ghosh, 2014). At an even higher emulsifier concentration, where the micelles became confined between two approaching droplets, the attractive depletion interaction significantly reduced (Erramreddy & Ghosh, 2014; Trokhymchuk et al., 2001; Wasan et al., 2004). In this case, excess emulsifiers in the aqueous phase formed structured layers of micelles between the inter-droplet region. As the droplets approach each other, the micelle layers squeezed out, leading to a stepwise thinning of inter-droplet films and fluctuating osmotic pressure acting on the droplets. Due to the resulting alternating repulsive and attractive forces operating on the droplets, the interactions are referred to as oscillatory structural forces (OSF) (Wasan et al., 2004). Many researchers showed the significance of these structural forces in the stabilization of colloidal systems, but not much knowledge is available on the effect of these forces on the rheological behaviour of concentrated emulsions (Bergeron et al., 1996; Ivanov & Kralchevsky, 1997; Marinova et al., 1998; Wasan et al., 2004). Recently, Erramreddy and Ghosh (2014) showed that increasing the amount of SDS concentration to 20 times its critical micelle concentration (CMC) in a 40 wt% O/W nanoemulsions led to the transformation of strongly attractive depletion force into OSF with a sharp reduction in gel strength from attractive gel into a viscous liquid.

In the present work, we aimed to develop repulsive O/W nanoemulsion gels using a food-grade anionic emulsifier Citrem with a hydrophilic-lipophilic balance (HLB) of 9 - 10. Although HLB is an empirical number, it plays an important role in the formation and stability of emulsions. For example, it has been shown that O/W emulsion with high stability can be prepared by using an emulsifier of HLB values ranging from 10 to 12 (McClements, 2015). Hence, we have chosen Citrem with a high HLB number for this study.

$$\phi_{\text{eff}} = \phi_{\text{core}} \left(1 + \frac{\delta}{r}\right)^3 \tag{3.1}$$

Based on Equation 3.1 (Erramreddy & Ghosh, 2015; Weiss & McClements, 2000; Wilking & Mason, 2007), we hypothesized that the reduction in droplet size to the nanoscale with a repulsive shell layer thickness (δ) approaching droplet radius (r) would help in increasing the effective radius ($r_{\text{eff}} = r + \delta$) of the droplet, and hence the effective volume fraction (ϕ_{eff}) of the

dispersed phase could become significantly higher than the original oil volume fraction (ϕ_{core}). Thus, by suitably reducing r and increasing δ it would be possible to reach beyond the maximum random jamming (ϕ_{MRJ}) at a lower ϕ_{core}, where the droplets along with their charge cloud would become closely packed, and the nanoemulsion would form a gelled structure. Due to smaller droplets size (r < 100 nm) and higher interfacial area, nanoemulsions are typically formed with a high emulsifier-to-oil ratio (McClements, 2012b). Similarly, we found that an excess emulsifier concentration is required to reduce the droplet size to the nanoscale, but with that excess emulsifier in micellar form, inter-droplet interaction fell into the OSF regime, which prevented the formation of repulsive as well as attractive nanoemulsion gels. We then hypothesized that the removal of excess emulsifiers from the aqueous phase of nanoemulsions should enhance the inter-droplet repulsion and may transform the viscous, flowable nanoemulsions into viscoelastic repulsive gels. Therefore, the present research aims to investigate how the removal of excess ionic emulsifier from the aqueous phase influence the stability and rheological behaviour of 40 wt% canola O/W nanoemulsions. The stable and strong viscoelastic nanoemulsion gel with lower fat content developed in this study could be used in many foods, cosmetics and pharmaceutical applications in the form of gel and paste and also for calorie reduction. To our knowledge, this is the first report of the transformation of food-grade liquid nanoemulsion into repulsive nanogels by removing excess emulsifiers from the aqueous phase.

3.3 Materials and methods

3.3.1 Materials

Canola oil (Great Value brand, Walmart Canada) was purchased from a local grocery store and stored at room temperature (RT, 25 ± 2°C) in the dark. De-ionized water (conductivity of 1.0 μS/cm) was used as the aqueous phase. Citric acid ester of mono and diglycerides (Citrem) with HLB 9 – 10 was donated by Palsgaard Inc. (Morris Plains, NJ, USA). All other chemicals, including the standard mixture of fatty acid methyl esters (FAMEs), were purchased from Sigma-Aldrich (St. Louise, MO, USA).

3.3.2 Interfacial tension analysis

Oil-water interfacial tension of the Citrem solutions was determined using Krüss K20 Tensiometer (KRÜSS GmbH, Germany) equipped with a Wilhelmy plate. An aliquot of 22 ml emulsifier solution was added in a 40 mm diameter glass sample cup, followed by immersion of

Wilhelmy plate and the addition of an upper layer of 44 mL canola oil. The maximum force exerted on to the plate due to interfacial tension of liquid was detected by the force sensor, and interfacial tension was calculated from the maximum force (F_{max}) using Equation 3.2. Three measurements were taken on each sample, and the average interfacial tension (σ, mN/m) was calculated from Equation 3.2:

$$\sigma = \frac{F_{max}}{L \cos \theta} \tag{3.2}$$

where L is the wetted length of the plate (40.2 mm), θ is the contact angle (equal to 0°, hence cos $\theta = 1$). We also measured the interfacial tension of Citrem solution at two different pH values (5.0 and 7.0), to confirm the role of pH and interfacial tension in reducing emulsion droplet size.

3.3.3 Emulsion preparation

Canola oil-in-water (O/W) emulsions stabilized by Citrem were prepared by pre-mixing 40 wt% canola oil (equivalent to $\phi = 0.42$) with aqueous phase containing different concentrations of Citrem (0.5 to 5 wt%) adjusted to pH 7 (using 1 N NaOH) in a rotor-stator mixer (Polytron, Brinkmann instruments, Ontario, Canada) for 60 s at 20,000 rpm. This was followed by high-pressure homogenization (EmulsiFlex-C3, Avestin Inc., Ottawa, ON, Canada) at 20,000 psi for 8 passes. Citrem has a melting point of 61 ºC (data not shown), so for comparison during preliminary research emulsification was performed at RT, where Citrem should be crystallized as well as at 65 ºC, where it would be in the liquid state. The final emulsions were stored in 120 mL glass bottles (VWR International, Edmonton, AB, Canada) for further analysis.

3.3.4 Droplet size distribution

Droplet size distribution of the emulsions was measured using a static laser diffraction particle size analyzer (Mastersizer 2000, Malvern Instruments, Montreal, QC, Canada) with a relative refractive index of the dispersed vs. continuous phases as 1.465. De-ionized water was used as a dispersant in the instrument, and the obscuration was brought up to ~12% by dropwise sample addition. Emulsions average droplet size was characterized by surface area mean diameter (d_{32}), calculated by using the Equation 3.3.

$$d_{32} = \frac{\sum n_i d_i^3}{\sum n_i d_i^2} \tag{3.3}$$

Where n_i is the number of droplets with a diameter of d_i.

3.3.5 Removal of excess Citrem from nanoemulsions

Excess Citrem from the nanoemulsions was removed by multiple cycles of ultra-centrifugation at 52,075 × g for 1.5 h. The emulsions were separated in two phases, a cream plug and an aqueous serum phase containing excess emulsifier molecules in micellar form. The aqueous phase was carefully removed by a syringe without disturbing the cream plug and collected for further analysis. The cream plug was then re-dispersed into the same amount of DI water that was removed after centrifugation and homogenized for two cycles at 20,000 psi so that the droplet size distribution remains unchanged. This process of centrifugation, cream plug separation, re-dispersion and re-homogenization was repeated two more times to ensure maximum removal of excess Citrem from the aqueous phase of the emulsions. Each centrifuged and homogenized emulsions were analyzed for their droplet size, viscosity, and viscoelasticity. Citrem concentration in the separated aqueous phases was quantified by gas chromatographic analysis and compared with the theoretically calculated excess Citrem concentration (more details discussed in results section).

3.3.6 Quantification of excess Citrem in the aqueous phase

The Citrem concentration of collected aqueous phases was determined by gas chromatography (GC) following the procedure adopted from Berton et al. (2011). Heptadecanoic acid (C17:0, purity ≥ 99.0%, Mw = 270.5 g/mol) and monoheptadecanoyl glycerol (purity ≥ 98.0%, Mw = 344.53 g/mol) were used as internal standards. The aqueous phase was passed through two surfactant-free cellulose acetate membrane filters (pore size 0.45 μm and 0.2 μm). The fatty acids present in Citrem were converted into fatty acid methyl esters (FAMEs) by transesterification in the presence of methanol and sulphuric acid. The aqueous phase containing Citrem (0.5 ml) was mixed with 100 μL of internal standard solution, 2 mL methanol and 400 μL sulphuric acid in a glass test tube and vortexed for 1 min at 3000 rpm. The tubes were hermetically sealed and incubated for 1 h at 100°C and quickly cooled down to room temperature using an ice bath. Next, 1 ml 0.9 wt% NaCl and 2 mL hexane was added to this reaction mixture and centrifuged at 1000×g for 5 min. The FAMEs were recovered from the upper organic phase into another test tube, and the solvent was evaporated under nitrogen flow. The recovered FAMEs were diluted with hexane (2 – 5 times) before separation in a GC using a polar chromatography column (DB-225, 30 m long, 0.320 mm internal diameter, 0.25 μm film thickness, Agilent J&W GC column,

Santa Clara, CA, USA). Hydrogen was used as a carrier gas at 2 ml min^{-1} flow and the time-temperature program used was 1 min at 50°C, 10°C min^{-1} until 180°C, 5°C min^{-1} until 220°C and finally 15 min isothermal. The eluted fatty acids were detected with a flame ionization detector set at 250°C and hydrogen and air flows set at 25 and 250 ml min^{-1}, respectively. The FAMEs were identified by comparison of their retention times with a standard mixture of FAMEs. The normalized ratios ($A_{fatty\ acid}$/ $A_{internal\ standard}$) of the C16 and C18 fatty acids ($A_{fatty\ acid}$) with respect to corresponding integrated peak areas of internal standards ($A_{internal\ standard}$) were converted into Citrem concentration using a calibration curve. To obtain the calibration curve, the same method was applied to known standard aqueous solutions of Citrem (0.02 to 0.1wt%), and the calibration curve was plotted as a function of Citrem concentration in the aqueous solution (Appendix A, Figure A1).

3.3.7 Debye screening length and droplet charge

The Debye screening length (DSL, κ^{-1}) was calculated from the molar concentration of free sodium ions present in Citrem solution. The conductivity of Citrem solutions (pH 7) was measured as a function of concentration using Orion Star™ A215 conductivity meter (Thermo Scientific, ON, Canada). Similarly, the conductivity of NaCl solutions was measured and plotted as a function of the molar concentration of sodium ions. From this standard curve, the equivalent molar concentration of sodium ions in Citrem solutions was calculated with known values of conductivity. DSL was calculated as a function of Citrem concentration from Equation 3.4 for 1:1 electrolyte at 25°C, where C is the is the bulk molar concentration of free ions in the aqueous medium (Israelachivili, 2011).

$$\kappa^{-1} = {}^{0.304}/_{\sqrt{C}} \tag{3.4}$$

Droplet charge was determined by a zeta potential analyzer (Zetasizer Nano-ZS90, Malvern Instruments, Westborough, MA, USA). To minimize the multiple scattering effects, the emulsion was diluted to a droplet concentration of approximately 0.01 wt% oil using deionized water before analysis.

3.3.8 Langmuir surface pressure isotherm

Langmuir monolayer was formed at RT using a Microtrough G2 Langmuir trough produced by Kibron Inc. (Helsinki, Finland), filled with DI water as the subphase. Compression of surfactant-free blank surface showed no significant change in the surface pressure. Different concentrations of Citrem stock solution (0.4 to 1 mg/mL) were prepared in chloroform. A 30 µL aliquot of Citrem solution was spread onto the aqueous phase surface, and the chloroform was evaporated for 10 min. Compression of the interfacial layer was carried out at a barrier speed of 10 mm min^{-1}. The surface pressure isotherm was obtained using FilmwareX 4.0, in two replicates and plotted against the mean molecular area (A_0). A_0 was calculated using Equation 3.5:

$$A_0 = {}^{A_{trough}}/_{n_0} \tag{3.5}$$

where A_{trough} is the effective area of the trough, which changed upon compression of the interface, while n_0 is the number of Citrem molecules spread, calculated by multiplying a number of moles with Avogadro number (N_A). The values of n_0 remained constant throughout the compression cycle. The diameter (D_{head}) of the Citrem head group was calculated from the values of A_0.

3.3.9 Nanoemulsion rheology

All rheological experiments were performed using an AR G2 rheometer (TA Instrument, New Castle, DE, USA) at RT. Emulsions were carefully transferred onto the lower stationary plate of the rheometer without disturbing the structure. Rotational or oscillatory force was applied on the emulsions using a 40 mm diameter stainless steel cross-hatched geometry plate to avoid any wall slip effect. The gap between the upper and lower plate was set to 1000 µm. The samples were equilibrated for 30 s before performing the measurements. The apparent viscosities of the emulsions were measured as a function of shear rate ranging from 0.01 to 1000 s^{-1}. Viscoelastic behaviour of the samples was determined by two different types of oscillatory measurements. First, strain sweep measurements were performed at 0.01–100 % strain and a constant frequency of 1 Hz (6.28 *rad*/s). From these experiments, a linear viscoelastic region (LVR) in which the storage (G') and loss (G'') moduli were independent of applied strain was identified. A constant strain amplitude of 0.1% strain was chosen within the LVR for subsequent series of frequency sweep measurements in the range from 0.01 to 100 *rad*/s. Visual observation of flow behaviour of the

nanoemulsions was also performed by placing an aliquot of 0.5 mL samples on a black cardboard surface held at 45º inclination and recording their flow behaviour with a digital camera.

3.3.10 Stability of nanoemulsions at accelerated gravitation

The accelerated stability of the nanoemulsions as a function of excess Citrem removal was evaluated using a photocentrifuge (LUMiSizer® 650.2 – 22, LUM America, Boulder, CO, USA) at 25°C, where the transmitted light at 865 nm is measured as a function of time and position over the sample length. An aliquot of 400 µL nanoemulsion was transferred into polycarbonate disposable cuvette with a 2 mm optical path length. Samples in duplicate were centrifuged at 2325×g relative centrifugation force (RCF) (4000 rpm), and the laser transmitted through the cuvettes were collected every 72 s till 1000 profiles. The change in the position of the cream layer (in mm) was plotted as a function of time, and the linear slope obtained from these curves was used as creaming velocity (in mm h^{-1}) of emulsion droplets at that RCF.

3.3.11 Statistics

All experiments were conducted with at least three replicates, and the samples from each replicate were analyzed at least twice. The results were reported as the mean ± standard deviation. The student's *t*-test was applied to determine the statistical significance, at 95% confidence level, for the independent samples. The statistical significance and correlation coefficient (*r*) were analyzed using Microsoft Excel 2016.

3.4 Results and discussion

3.4.1 Selection of Citrem concentration for nanoemulsion preparation

In preliminary research, emulsions were prepared with different concentration of Citrem, and the average droplet size decreased from 842 nm for 0.5 wt% to 151 nm for 5 wt% Citrem (Appendix A, Figure A2). Based on this result, further experiments were performed with 3 and 5 wt% Citrem with an average droplet size of 222.3 ± 12.7 nm and 151.0 ± 3.4 nm, respectively, thus forming nanoemulsions.

3.4.2 Quantification of unabsorbed excess Citrem

Excess Citrem concentration in the aqueous phase of nanoemulsions was theoretically calculated using the following equation.

$$C_{excess} = C_{total} - C_{adsorbed} \quad (3.6)$$

where C_{total} is the total Citrem concentration used to prepare the nanoemulsions, whereas the C_{excess} is the excess unabsorbed Citrem (in micellar form) dispersed in the aqueous phase of emulsions. $C_{adsorbed}$ is the concentration of Citrem required to saturate the O/W interfacial area (A_s), calculated by multiplying the Gibbs surface excess (Γ) of Citrem with $A_s = 6\phi/d_{32}$, Where ϕ is the oil volume fraction and d_{32} is surface average droplet diameter. The Gibbs surface excess (Γ) of Citrem was calculated from the linear slope of the interfacial tension vs. logarithmic concentration of Citrem (shown in Appendix A, Figure A3) (Kumar & Mandal, 2018a). The obtained value of surface excess at the oil-water interface was 3.29×10^{-6} moles/m^2. Therefore, Equation 3.6 can be rewritten as:

$$C_{excess} = C_{total} - {}^{6\Gamma\phi}/_{d_{32}} \quad (3.7)$$

Table 3.1 shows the calculated and experimental values of excess Citrem and their micellar volume fraction in the aqueous phase of nanoemulsions. Experimentally it was found that the nanoemulsions stabilized with 3 and 5 wt% Citrem contained a total amount of 1.43 and 1.58 wt% excess Citrem, respectively in the aqueous phase. The calculated values of excess Citrem were higher than the experimental values for both the nanoemulsions, which could be due to multilayer formation or irreversible adsorption of Citrem molecules at the droplet interface that could not be removed through centrifugal force. This difference between experimental and calculated values of excess Citrem was more in case of 5 wt% compared to 3 wt% Citrem nanoemulsions (Table 3.1). It was attributed to smaller droplet size or more surface area of the former, allowing more Citrem to form multilayer at the interface.

To confirm Citrem multilayer formation at the interface, Langmuir surface pressure isotherm was determined using different concentrations of Citrem at the air-water interface (Figure 3.1A). The plateau surface pressure beyond film collapse was obtained at different concentration of Citrem (Figure 3.1B) which evidenced that further compression of interface beyond the critical collapsible point forced the Citrem molecules to stack over monolayer and formed bilayer or multilayer interface (schematic diagram of formation of bilayer interface is shown in Figure 3.1A).

Table 3.1 Calculated and experimental values of excess Citrem concentration and their micellar volume fraction in the aqueous phase of nanoemulsions.

Emulsions	Citrem in emulsion	Concentration in the aqueous phase		Portion of surfactant in aqueous phase		Micellar volume fraction (ϕ_m) in the aqueous phase[#]	
		Calculated[*]	Experimental	Calculated	Experimental	Calculated	Experimental
	g / 100 mL	g / 100 mL	g / 100 mL	(%)	(%)		
3%Citrem	3.0	1.50 ± 0.22	1.43 ± 0.08	50.13 ± 7.43	47.86 ± 2.83	0.19	0.18
5%Citrem	5.0	2.41 ± 0.26	1.58 ± 0.03	48.38 ± 8.96	31.62 ± 1.23	0.32	0.20

[*]Calculated using Equation 3.7.
[#]Calculated based on the Citrem cmc = 0.15 wt%; micelle diameter d_m= 6 nm and micelle aggregation number N_{agg} = 104.
Data represent the average and standard deviation of duplicate measurements on at least 3 emulsions prepared independently.

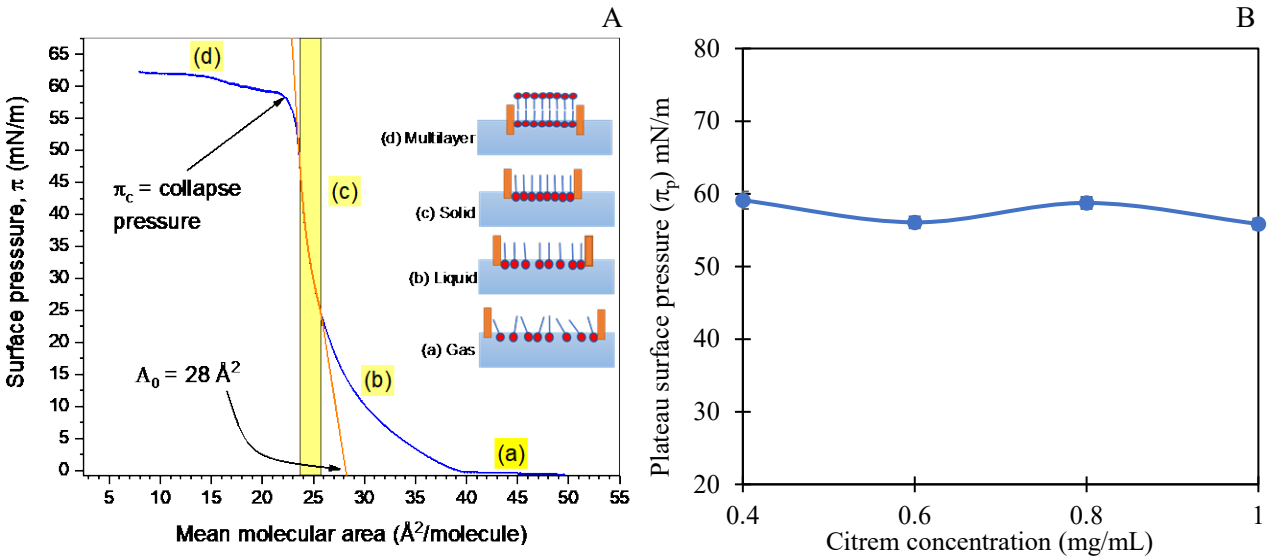

Figure 3.1 (A) Langmuir surface pressure isotherm of Citrem (1 mg/mL) at air-water interface. As the molecular area was decreased, surface pressure increased and Langmuir monolayer showed different phases: (a) gas (b) liquid, and (c) solid on the curve. Inset shows schematic diagram of Citrem molecule packing at air-water interface. The plateau surface pressure, beyond collapse pressure (π_c), indicates the multilayer formation by Citrem molecules at the interface. The linear fit of the solid phase (c), where Citrem molecules were close packed, was extrapolated to the x-axis to get the mean molecular area (A_0) occupied by one molecule of Citrem at air-water interface. (B) Plateau surface pressure (π_p) plotted as a function of Citrem concentration (mg/mL) beyond the collapse pressure where Citrem molecules could stack on each other on further compression of the monolayer.

For example, using similar Langmuir surface pressure isotherm, it has been demonstrated that stable phospholipid multilayers could be formed at the air-water interface by compression of the monolayer beyond collapse (Saccani et al., 2004). Furthermore, the plateau surface pressure beyond film collapse also indicates a stable, difficult to remove interfacial layer, which could promote the irreversible adsorption at the interface. This behaviour of Citrem is particularly interesting, as some of the more commonly used emulsifier, such as, SDS was unable to make compressible monolayer at air-water interface in Langmuir trough due to its high solubility in the aqueous phase (Coppock et al., 2009; Tah et al., 2011). Researchers also showed that SDS desorbed from air-water interface when its concentration in the aqueous phase become lower (Casandra et al., 2017). Thus, irreversible adsorption of Citrem at the interface was critical in preventing its desorption from the interface when the cream layer after centrifuge was re-dispersed into DI water.

3.4.3 Average size and charge of nanoemulsion droplets as a function of removal of excess Citrem

For both 3 and 5 wt% Citrem nanoemulsions, excess emulsifier in the aqueous phase decreased with number of centrifugation cycle (Figure 3.2A). To show the effect of multiple centrifugation cycles on emulsion stability, average droplet diameters (d_{32}) of 3 and 5 wt% nanoemulsions were plotted in Figure 3.2B against excess Citrem concentration. The excess Citrem concentration in the aqueous phase of freshly prepared emulsions was obtained from Figure 3.2A after 1st centrifugation. Therefore, for 3 wt% Citrem nanoemulsion, d_{32} = 222.3 nm was plotted against 1.43 wt%, while for 5 wt% Citrem d_{32} = 151 nm was plotted against 1.58 wt% excess Citrem. For the final nanoemulsions after three centrifugation cycles, it was assumed that negligible amount of excess emulsifier would be present in the aqueous phase. Hence the d_{32} was plotted against zero Citrem concentration in Figure 3.2B. Although, it may not be possible to have absolutely zero excess Citrem, as some emulsifier disruption from the droplet surface would eventually happen. However, it is safe to assume that the value would be less than what we obtained after the 3rd centrifugation (Figure 3.2A), which was 0.016 and 0.077 wt%, for 3 and 5 wt% Citrem nanoemulsions, respectively.

From Figure 3.2B, it can be seen that the droplet size of 3 wt% Citrem nanoemulsions increased from 222.3 ± 12.7 nm to 259.7 ± 40.0 nm ($p > 0.05$), when a total of 1.43 wt% excess Citrem was removed from the aqueous phase. On the other hand, 5 wt% Citrem nanoemulsions had an average droplet size 149.0 ± 3.3 nm upon the removal of 1.58 wt% excess Citrem and it did not show any significant change in droplet size as a function of excess Citrem removal. The droplet size distribution also did not change for 5 wt% Citrem nanoemulsions, while for 3 wt% Citrem nanoemulsions, it shifted slightly towards higher droplet size as a function of excess Citrem removal (Figure 3.2C). This shows that the 5 wt% Citrem nanoemulsions were more stable against droplet coalescence during multiple centrifugation cycles compared to 3 wt% Citrem nanoemulsions. As explained in the previous section, stronger multilayer formation as well as the irreversible adsorption of Citrem molecules at the oil droplet surface could be the reasons behind the higher stability of 5 wt% Citrem nanoemulsions against centrifugal force. The stability of the nanoemulsions after centrifugation could also be shown by zeta potential. The average droplet charge for 3 wt% and 5 wt% Citrem nanoemulsions varied from – 53.4 to – 54.0 mV and – 55.5 to – 56.5 mV, respectively and showed no significant change as the excess Citrem was removed

from the aqueous phase (Appendix A, Figure A4). Therefore, removal of excess Citrem did not have any significant effect on the emulsifier adsorbed on the droplet surface.

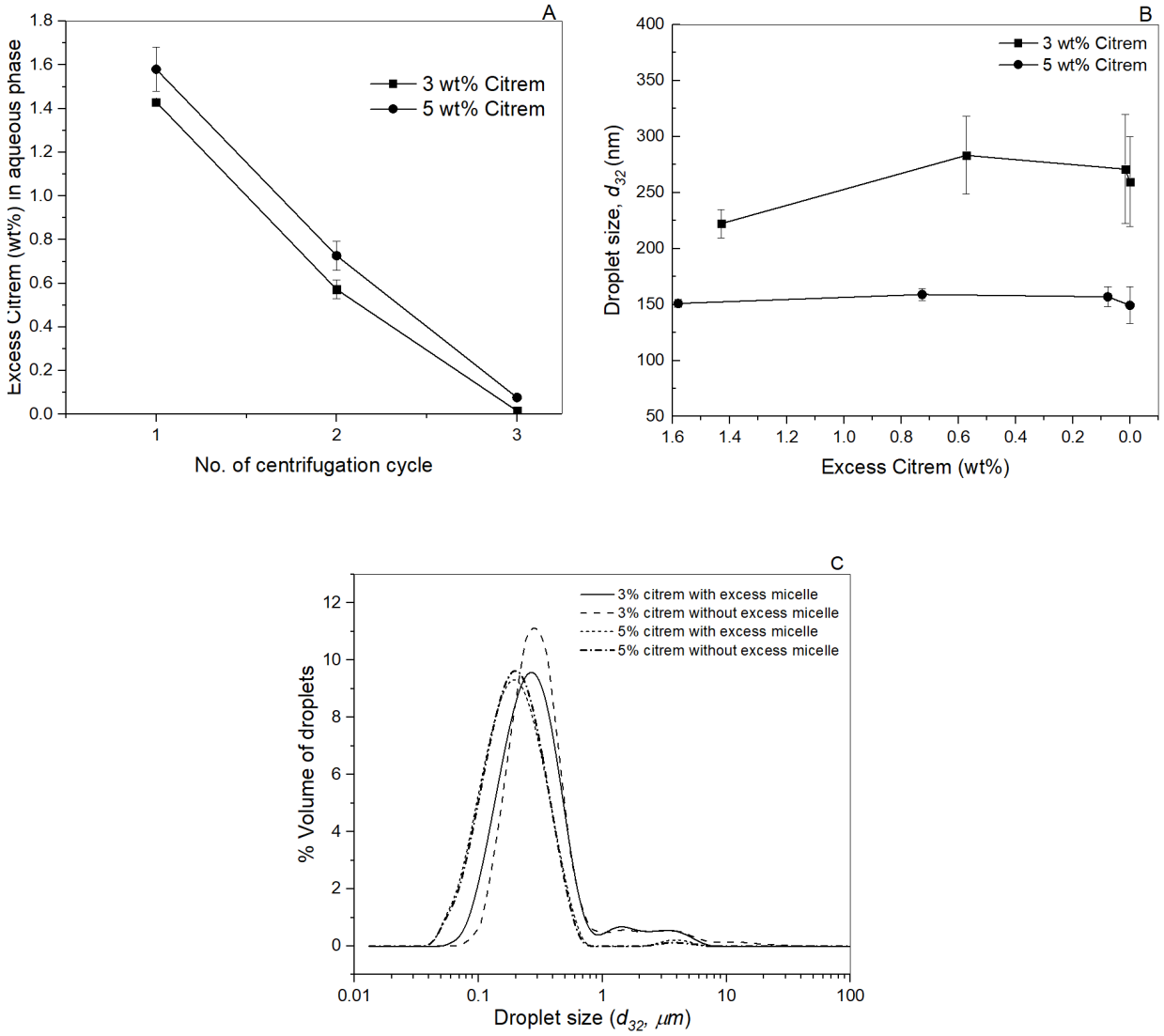

Figure 3.2 (A) The presence of excess emulsifier in the continuous phase of the nanoemulsions as a function of number of centrifugation cycles. The excess Citrem was quantified using gas chromatographic analysis. (B) Average droplet size (d_{32}), and (C) droplet size distribution of 3 wt% and 5 wt% Citrem nanoemulsions as a function of excess Citrem removal from the aqueous phase. Note, the x-axis is in reverse order in B. Error bars indicate ± standard deviation (n ≥ 3).

3.4.4 Flow behaviour of nanoemulsions as a function of excess Citrem

The average viscosities of 3 and 5 wt% Citrem nanoemulsions with and without excess Citrem in the aqueous phase was determined as a function of shear rate (from 0.01 to 100 s^{-1}) (Figure 3.3A).

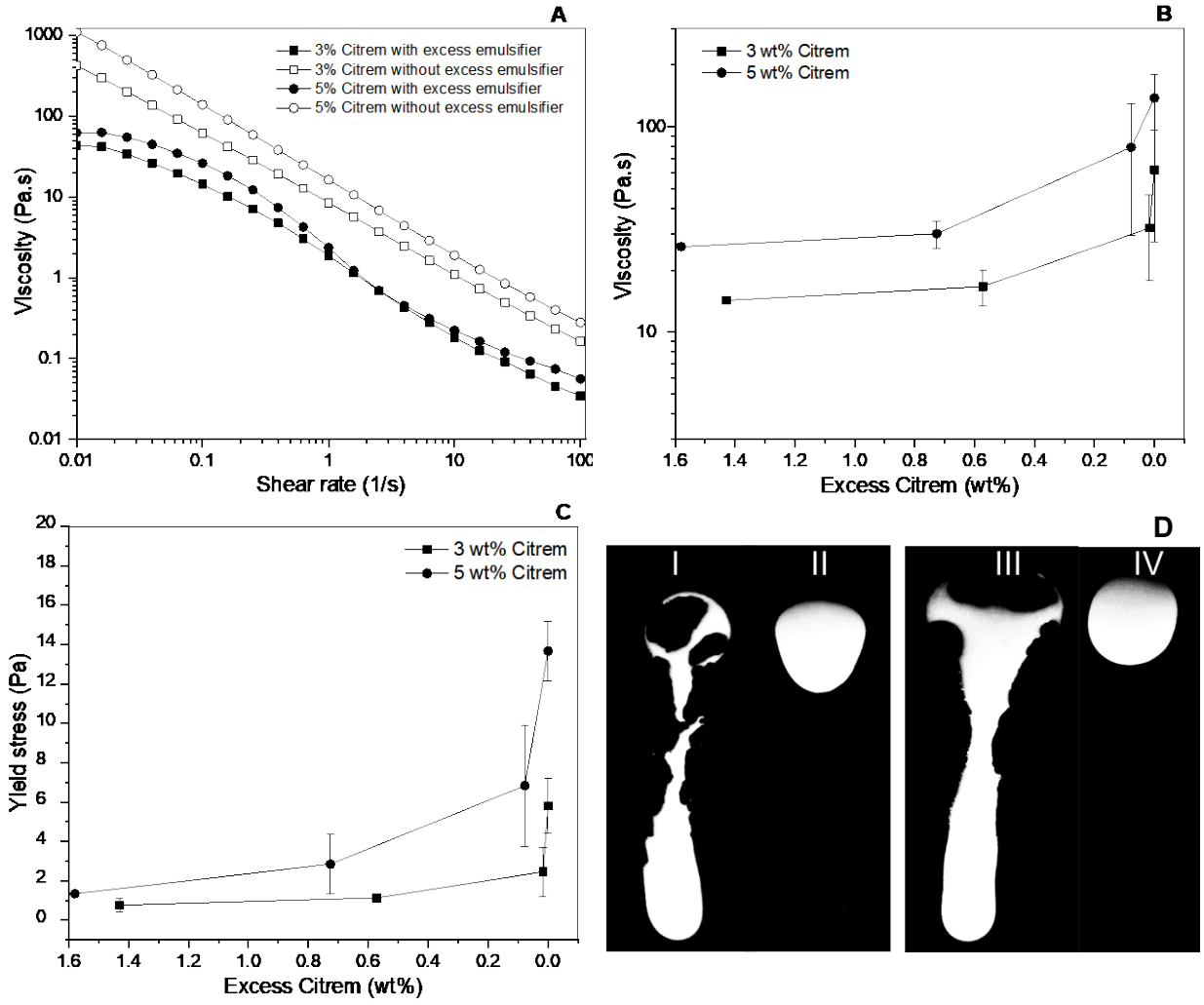

Figure 3.3 Effect of removal of excess emulsifier on the viscosity of nanoemulsions. Viscosities of 3% and 5% Citrem stabilized nanoemulsions were measured (A) as a function of shear rate with and without excess emulsifier in the aqueous phase. (B) Apparent viscosity at a constant shear rate (0.1 s^{-1}) as a function of excess Citrem concentration in the aqueous phase. (C) Values of yield stress (τ_0) calculated from (A) using the Herschel-Bulkley model. (D) Visual observation of flow behaviour of Citrem nanoemulsions at 45° inclination: 3wt% Citrem nanoemulsions (I) with and (II) without excess emulsifier; 5wt% Citrem nanoemulsions (III) with and (D) without excess emulsifier in the aqueous phase.

The viscosity of all nanoemulsions decreased with an increase in shear rate from 0.01 to 100 s^{-1}, indicating pseudoplastic behaviour of the nanoemulsions. The viscosities of both the nanoemulsions increased when excess emulsifier was removed from the aqueous phase. A low shear plateau in viscosity was observed for the nanoemulsions with excess Citrem, indicating Newtonian behaviour at a very low shear rate. The steep linear decrease in viscosity for the nanoemulsions without excess Citrem suggested that the inter-droplet packing in the nanoemulsions was much stronger when excess emulsifier was removed from the aqueous phase. To understand the role of excess emulsifier, the apparent viscosity was re-plotted at a constant shear rate (0.1 s^{-1}) as a function of excess Citrem in Figure 3.3B. When excess Citrem was removed, the viscosity increased from 14.3 ± 0.6 to 61.7 ± 34.2 Pa.s for 3 wt% Citrem and from 26.0 ± 0.8 to 138.2 ± 41.8 Pa.s for 5 wt% Citrem nanoemulsions. Almost 4 to 5 times increase in viscosity of both the nanoemulsions was observed as excess Citrem was removed from the aqueous phase. Moreover, a rapid increase in viscosity was observed when the last few layers of micelles around the droplet were removed. This behaviour suggests that the presence of excess emulsifier in micellar form between two approaching droplets has a significant effect on the flow behaviour of nanoemulsions. Next, we fitted the Herschel-Bulkley (HB) model to the viscosity of the nanoemulsions:

$$\tau = \tau_0 + K\dot{\gamma}^n \tag{3.8}$$

where shear stress (τ) is expressed as a function of shear rate ($\dot{\gamma}$) and yield stress (τ_0). The value of the shear rate is modified with flow behaviour index (n), consistency coefficient (K). Good fit to the model was obtained for all nanoemulsions with r^2 above 0.99. Figure 3.3C shows the yield stress values obtained by fitting the HB model to the viscosity data as a function of excess Citrem. Both the 3 and 5 wt% Citrem nanoemulsions with excess emulsifier showed very low yield stress values of 0.8 ± 0.3 Pa and 1.3 ± 0.1 Pa, respectively. However, for 5 wt% Citrem nanoemulsions, it increased gradually to 6.8 ± 3.1 Pa when about 0.1 wt% Citrem was present, and finally rapidly increased to 13.6 ± 1.5 Pa when negligible amount of excess Citrem was present. These trends are in accordance with our visual observations of nanoemulsions in the absence of excess emulsifier (Figure 3.3D, II & IV), where without excess emulsifier 5 wt% Citrem nanoemulsions with high yield stress did not flow at all (gel-like property), while 3 wt% Citrem nanoemulsions with lower yield stress showed some deformation upon tilting, compared to

immediate flow of both the nanoemulsions (Figure 3.3D, I & III) in the presence of excess emulsifier.

3.4.5 Viscoelastic behaviour of nanoemulsions as a function of excess Citrem

Figures 3.4A and 3.4B shows the strain-dependent storage (G') and loss (G'') moduli for 3 and 5 wt% Citrem nanoemulsions, respectively in the presence and absence of excess emulsifier.

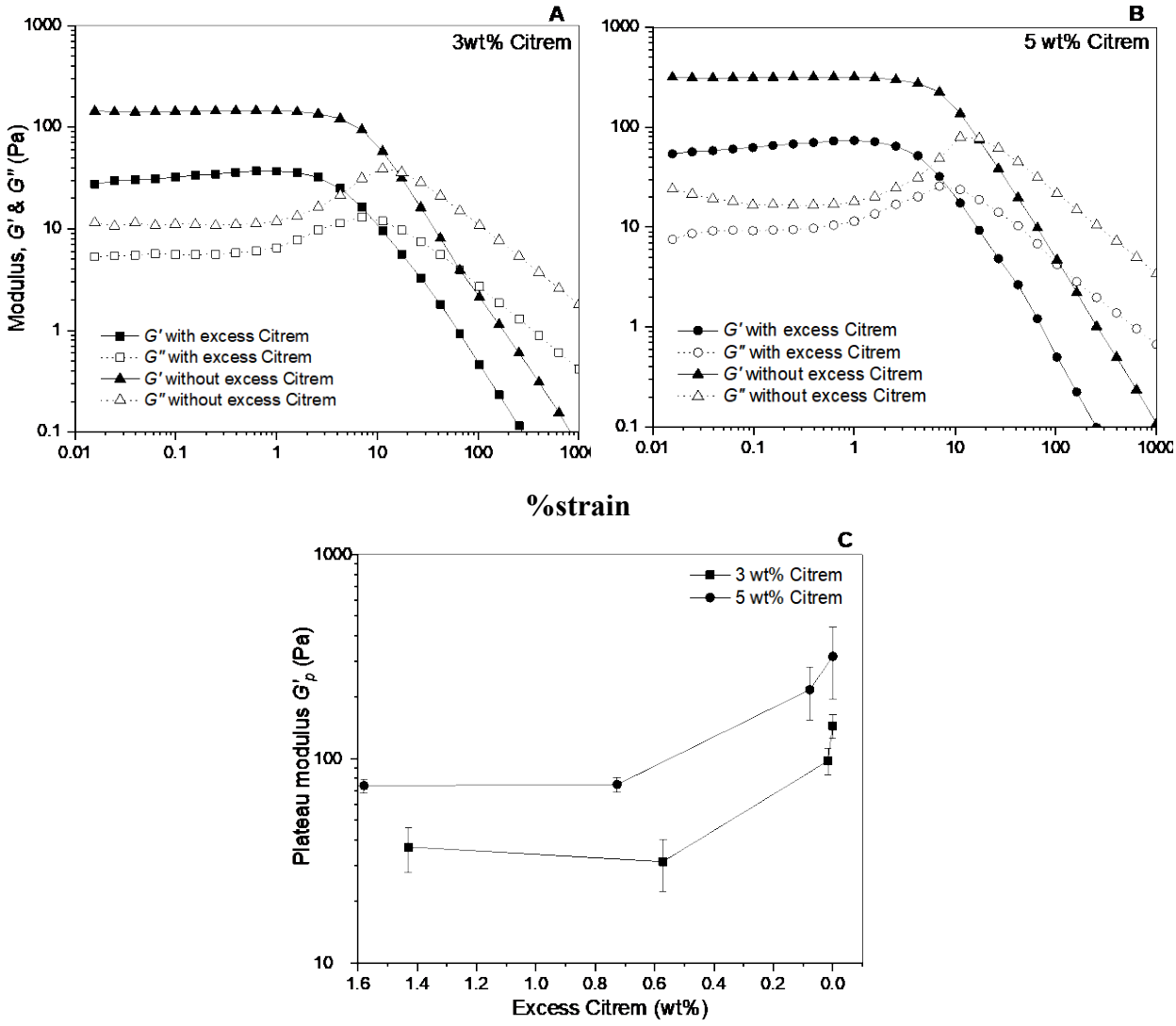

Figure 3.4 Gelation behaviour of nanoemulsions as a function of excess emulsifier using strain sweep analysis. Storage (G') and loss moduli (G'') of (A) 3 wt% and (B) 5 wt% Citrem nanoemulsions with and without excess emulsifier in the aqueous phase are plotted as a function of strain. (C) Values of plateau storage modulus (G'_p) at 1% strain is plotted as a function of excess emulsifier. Error bars indicate ± standard deviation (n ≥ 3).

All the nanoemulsions, without excess emulsifier in the aqueous phase, showed significantly higher storage moduli with a strong linear viscoelastic region (LVR) below 2% strain, compared to a lower and weaker viscoelastic region in the presence of excess Citrem. Both the nanoemulsions, without excess emulsifier, showed a significant increase in the G' compared to G'' within the LVR, demonstrating their transformation into the elastic gel-like structure. The viscoelasticity of 3 and 5 wt% Citrem nanoemulsions was compared by plotting the plateau storage modulus (G'_p) in the LVR at 1% strain as a function of the excess Citrem in the aqueous phase (Figure 3.4C). Initially, minor changes in G'_p were observed as a function of excess Citrem until 0.6 wt%. However, with further reduction in excess Citrem, the G'_p increased almost 4 to 5 times for both the nanoemulsions. For 3 wt% Citrem nanoemulsions, G'_p increased from 36.9 Pa to 144.8 Pa, while for 5 wt% Citrem nanoemulsions it increased from 73.7 Pa to 316.8 Pa, as excess Citrem was removed from the nanoemulsionsFrom Figure 3.4A, at a strain above 2%, G'' values began to rise, whereas G' values showed a drastic decrease, which was followed by a crossover of the moduli, after which G'' became dominant over G', and the gel-like nanoemulsions started to flow, behaving like a liquid, due to structural breakdown. Similar to storage moduli within the LVR, crossover strain for nanoemulsions were significantly higher when excess emulsifier was removed from the aqueous phase.

The frequency dependent viscoelastic behaviour of the nanoemulsions are shown in Figures 3.5A and 3.5B. For fresh nanoemulsions, an increase in storage modulus was observed with an increase in Citrem concentration, which could be due to reduction in droplet size. Similar increase in gel strength with an increase in emulsifier concertation was also observed by others (Erramreddy & Ghosh, 2014; Kumar & Mandal, 2018b). The storage and loss moduli increased with frequency from 0.1 to 100 rad/s when excess Citrem was present in the nanoemulsions. However, after the excess Citrem was removed, both nanoemulsions moduli showed plateau-like region through the entire frequency range studied. Even at a higher frequency, G' remained much higher than G'' which indicates the strong gel-like behaviour of Citrem nanoemulsions after removal of excess Citrem. To compare the frequency dependent viscoelastic behaviour, we plotted the storage modulus (G') at 10 rad/s frequency as a function of the excess Citrem in the aqueous phase (Figure 3.5C). Both Citrem nanoemulsions showed around 3 to 4 times increase in G' with a decrease in excess Citrem. For 3 wt% Citrem nanoemulsions, G' increased from 36.9 Pa to 98.8 Pa, while for 5 wt% Citrem nanoemulsions, G' increased from 71.1 Pa to 334.8 Pa as the excess

Citrem was removed from the aqueous phase. Similar to the strain sweep data in Figure 3.4, frequency sweep viscoelasticity also showed stronger gel formation for 5 wt% Citrem nanoemulsions compared to the other.

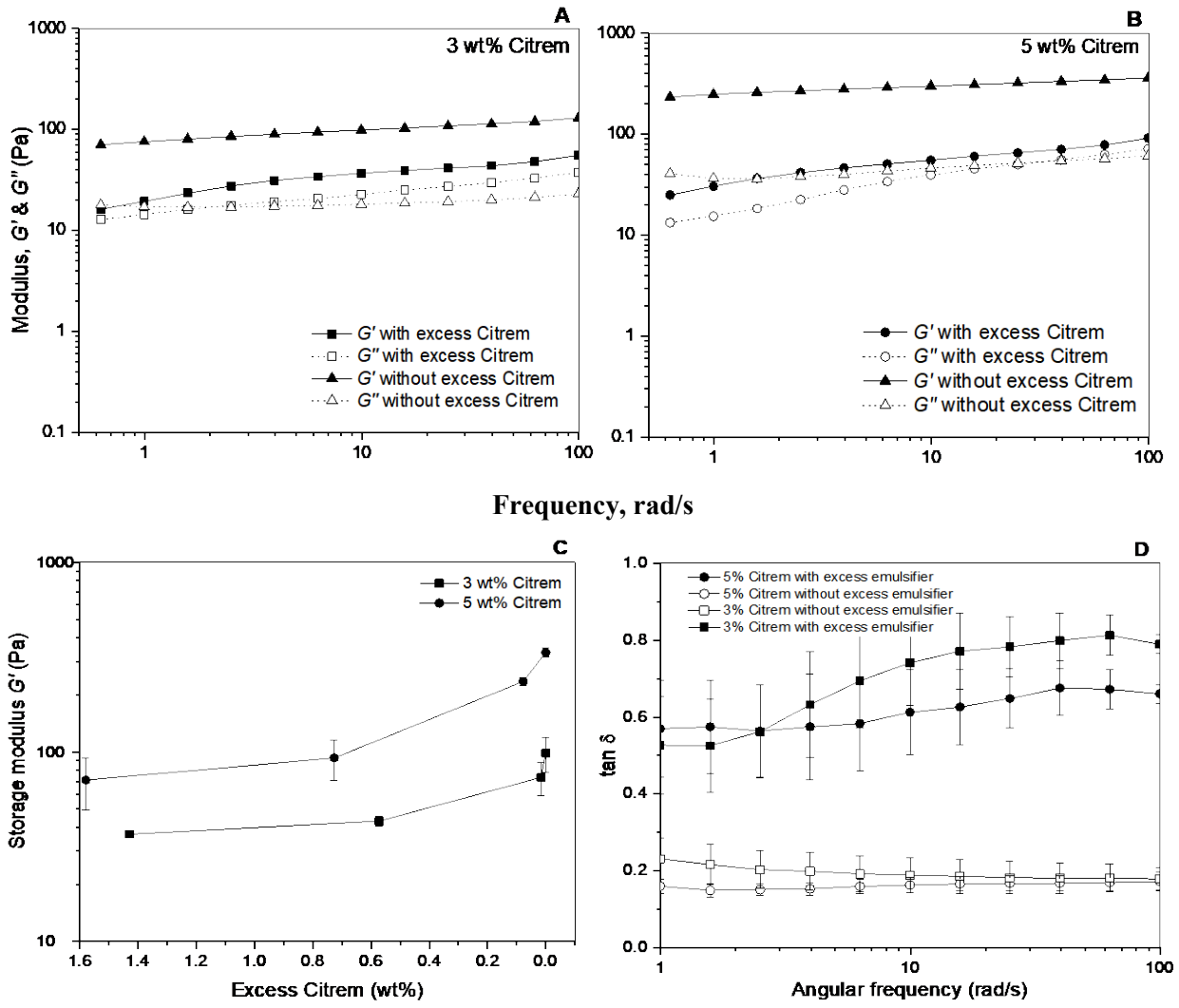

Figure 3.5 Gelation behaviour of nanoemulsions as a function of excess emulsifier using frequency sweep analysis. Storage (G') and loss modulus (G'') of (A) 3 wt% and (B) 5 wt% Citrem nanoemulsions with and without excess emulsifier in the aqueous phase. (C) Values of storage modulus (G') at 10 rad/s frequency as a function of excess emulsifier. (D) Values of tan δ calculated from frequency sweep data plotted with or without excess Citrem. Error bars indicate ± standard deviation (n ≥ 3).

The tan δ (ratio of G'' to G') is also an important factor to evaluate the viscoelastic behaviour of soft materials. Values of tan $\delta < 1$ indicates a weak to strong gel-like behaviour, whereas tan $\delta > 1$, indicates liquid-like behaviour of emulsions. The smaller is the value of tan δ, the stronger is the gel strength (Lapasin et al., 2001). Figure 3.5D shows the viscoelastic spectra of tan δ for different nanoemulsions with and without excess Citrem. It was observed that tan δ reached to around 0.2 as the excess Citrem removed from the nanoemulsions, while with excess Citrem tan δ remained in the range from 0.6 to 0.8. The tan δ values of nanoemulsions close to 1 in the presence of excess emulsifier showed that the viscous component was more prevalent, however with reduction in excess emulsifier, it reached close to zero and thus, showed more viscoelastic nature of the nanoemulsions. This behaviour suggests the transformation of a weak gel into a strong gel with the removal of excess Citrem from the nanoemulsions.

3.4.6 Creaming stability of nanoemulsions under accelerated gravitation

Studying creaming stability of extremely stable Citrem nanoemulsions was difficult at normal gravitational separation considering the experimental time frame. Nonetheless, accelerated creaming stability of the nanoemulsions was made possible with a photocentrifuge (LUMiSizer®). The creaming velocity of the nanoemulsions was calculated under an accelerated gravity (RCF 2325×g) and plotted as a function of excess Citrem removal (Figure 3.6).

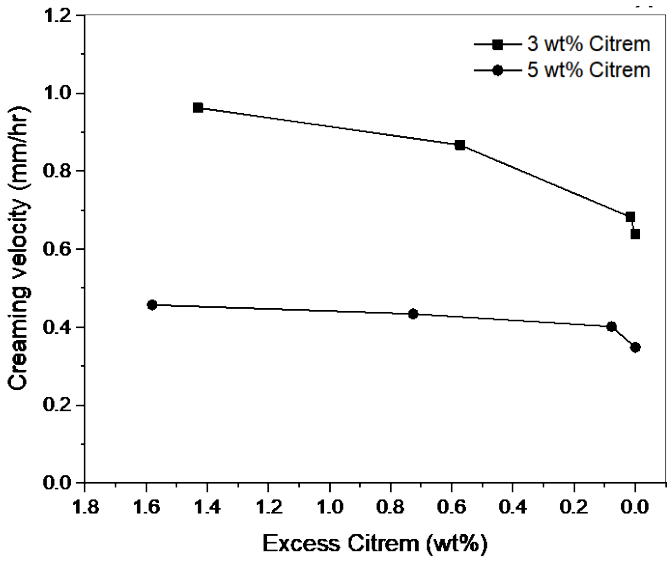

Figure 3.6 Accelerated stability, in terms of creaming velocity, of 3 and 5wt% Citrem-stabilized nanoemulsions as a function of excess emulsifier studied using a photocentrifuge at 2325×g RCF.

It was found that the creaming velocities were reduced and nanoemulsions became more stable to forced destabilization as excess Citrem was removed from the aqueous phase. It should be noted that the average droplet size of the nanoemulsions did not change significantly as excess Citrem was removed from the aqueous phase of the nanoemulsions. Therefore, the reduction in creaming velocity with the removal of excess Citrem at accelerated gravitation must be related to the increase in gel strength of the nanoemulsion as shown in Figure 3.4 and 3.5. On the other hand, higher creaming stability of 5 wt% Citrem nanoemulsions compared to 3 wt% at accelerated gravitation could be attributed to both the lower droplet size and higher gel strength of the former.

3.4.7 Mechanism of nanoemulsion gelation upon removal of excess emulsifier

In the present study, the transformation of rheological behaviour of flowable liquid nanoemulsions into strong gels, that does not flow under gravity, was observed as a function of removal of excess Citrem from the aqueous phase. We initially hypothesized that significant contribution of the repulsive electric double layer (EDL) formed around the nanodroplets by a layer of negatively charged Citrem would lead to a ϕ_{eff} beyond maximum random jamming (MRJ). To prove our hypothesis, we calculated ϕ_{eff} for the freshly prepared 3 and 5 wt% nanoemulsions using Equation 3.1. The DSL (κ^{-1}) obtained from Equation 3.4 was multiplied by a factor 2.4 to get the shell layer thickness (δ) in Equation 3.1 (Mondain-Monval et al., 1996). The calculated ϕ_{eff} was 0.556 and 0.559, well below ϕ_{MRJ}, for 3 and 5 wt% nanoemulsions, respectively. It should be noted that our nanoemulsions were polydisperse; therefore, it is expected that the critical volume fraction of random jamming of oil droplets would be even higher than ϕ_{MRJ} = 0.64 for monodisperse emulsions. This suggests that the physical state of the nanoemulsions was far away from random jamming, where the droplets would not move and a strong gel ($G' >> G''$) would be formed. This lack of gelation despite nanoscale droplet size was attributed to the required high concentration of Citrem for the preparation of nanoemulsions which would reduce the DSL due to the presence of excess ionic species in the aqueous phase. The excess Citrem remains in micellar form in the aqueous phase and may induce short-range attractive depletion interaction among the nanodroplets (Iracki et al., 2010; Mondain-Monval et al., 1996). However, at a very high micelle concentration, they form structured layers between two approaching droplets thereby providing depletion stabilization. This is more likely to occur in concentrated nanoemulsions where droplets are more closer with each other and micelles tend to become more ordered in the confining films

between droplets (Wasan et al., 2004). As the droplets approach each other, they face repulsive barrier from negatively charged micelles, and the inter-droplet potential reaches a repulsive maximum. On further approach, a micellar layer is squeezed out due to volume exclusion effect and the inter-droplet potential reaches an attractive minimum. This process continues with a reduction in the separation distance between the droplets till at least one layer of the micelle remained between the inter-droplet region, while rest of them are squeezed out (Basheva et al., 2007; Wasan et al., 2003). These structural forces, due to stepwise thinning of the inter-droplet film, oscillates from positive repulsive to negative attractive interaction between two approaching droplets, hence they are called oscillatory structural forces (OSF). The OSF is long range non-DLVO forces which operate up to 100 nm separation distance (Wasan et al., 2004). Based on this theory, we hypothesized that in the present case, the excess Citrem micelles generated long-range structural forces between two approaching droplets. The structural forces became so dominant that it resulted in liquid-like behaviour ($G'' > G'$) of the nanoemulsions, overcoming repulsive barrier from negatively charged Citrem-stabilized droplets and attractive depletion interaction (DLVO forces). Similar behaviour was also observed for SDS stabilized nanoemulsions, where increase in SDS concentration beyond 20 times CMC transformed physical state of the nanoemulsions from attractive gel-like structure to liquid like behaviour (Erramreddy & Ghosh, 2014). To understand the role of OSF on the rheological behaviour of the Citrem-stabilized nanoemulsions we calculated the resultant OSF and DLVO forces based on the removal of excess Citrem from the aqueous phase.

3.4.8 Calculation of non-DLVO structural forces

In this study, interaction energy (W_{OSF}) for OSF was calculated using Derjaguin's approximation modified by the Petsev and co-worker, between two approaching spheres (when inter-droplet distance $h > d_m$, the micelle diameter) (Petsev et al., 1995).

$$W_{OSF}(h,r) = \pi r_f^2 P_o \frac{d_m \exp\left(1-{}^{h}/_{d_m}\right)}{(4\pi^2+1)} \times \left[\cos\frac{2\pi h}{d_m} - 2\pi \sin\frac{2\pi h}{d_m}\right] -$$

$$\pi R P_o \frac{d_m^2 \exp\left(1-{}^{h}/_{d_m}\right)}{(4\pi^2+1)} \times \left[(4\pi^2+1)\cos\frac{2\pi h}{d_m} - 4\pi \sin\frac{2\pi h}{d_m}\right] \quad (3.9)$$

where r_f is the radius of the film created by closely approached deformed droplets and is taken as 0.045 times the radius of the droplets (Petsev et al., 1995). For anionic emulsifier, micelle diameter

d_m is taken as $d_{m\text{-}eff}$ (= $d_m + 2\kappa^{-1}$) (Danov et al., 2011). P_o is the osmotic pressure exerted by the excess micelles due to volume exclusion effect which was calculated from the Equation 3.10 (Petsev et al., 1995).

$$P_o = \xi C_M k_B T \tag{3.10}$$

where C_M is the number density of micelles in the aqueous phase, k_B is the Boltzmann constant, T is the temperature in (K). The value of ξ is calculated using Equation 3.11.

$$\xi = \left(1 + \phi_m + \phi_m^2 - \phi_m^3\right)/\left(1 - \phi_m\right)^3 \tag{3.11}$$

where ϕ_m is the micellar volume fraction in the aqueous phase. For anionic Citrem, we considered an effective micellar volume fraction ($\phi_{m\text{-}eff}$) due to the charge cloud around the micelles. Hence, ϕ_m in Equation 3.11 was replaced with $\phi_{m\text{-}eff}$ and calculated using Equation 3.12.

$$\phi_{m-eff} = \frac{4\pi}{3}\left(\frac{d_m}{2} + \kappa^{-1}\right)^3 C_M \tag{3.12}$$

The micelle number density (Gutierrez et al., 2008), was calculated from the experimentally determined values of excess Citrem concentration (C_{excess} in mol/L), see Table 3.1, based on the Citrem CMC = 0.15 wt%; micelle diameter d_m and micelle aggregation number N_{agg} (Briscoe, 2015).

$$C_M = C_{excess} \times N_A / N_{agg} \tag{3.13}$$

In Equation 3.13, N_A and N_{agg} are Avogadro number (6.023×10^{23} mol^{-1}) and micelle aggregation number, respectively. The Citrem micelle diameter was obtained by considering the double length of the Citrem molecule. Tanford has given an empirical formula to calculate the hydrocarbon tail length (l_{tail}) (Tanford, 1980), which was used to calculate the micelle diameter (d_m):

$$l_{tail} = 0.154 + 0.1265 n_c \tag{3.14}$$

$$d_m = 2\,(l_{tail} + D_{head}) \tag{3.15}$$

where n_c is the number of carbon atoms in the surfactant tail (for Citrem n_c = 18). D_{head} is the diameter of the surfactant head group (for Citrem D_{head} = 0.6 nm), calculated from the area (A_0) occupied by one molecule of Citrem at the air-water interface from the Langmuir surface-pressure

isotherm (shown in Figure 3.1). From the Citrem micellar volume (V_{mic}) and hydrocarbon tail volume (v_{tail}), N_{agg} was approximated (Nagarajan & Ruckenstein, 1991; van Stam et al., 1998):

$$N_{agg} = V_{mic}/v_{tail} \tag{3.16}$$

$$V_{mic} = \frac{4\pi l_{tail}^3}{3} \tag{3.17}$$

$$v_{tail} = v_{CH_3} + (n_c - 1)v_{CH_2} \tag{3.18}$$

where volume of a methyl (v_{CH_3}) and a methylene (v_{CH_2}) group can be approximated as 0.0546 nm^3 and 0.0269 nm^3, respectively (Nagarajan & Ruckenstein, 1991). Using Equations 3.14 to 3.18, the calculated values of Citrem d_m and N_{agg} were 6.06 nm and 104, respectively. Danov and co-worker also used the Tanford formula to calculate the SDS micelle size (4.54 nm), which was close to the experimentally measured values (4.6 – 4.8 nm) reported by many workers (Missel et al., 1980; Petsev et al., 1995). To test the accuracy of our method, we also calculated N_{agg} for SDS (~ 55) and cetyl trimethylammonium bromide (CTAB) (~ 93) using Equations 3.16 to 3.18, and they were quite comparable with the reported values of N_{agg}, 60 – 64 for SDS and 95 for CTAB micelles (Lianos & Zana, 1981; Mondain-Monval et al., 1996; Petsev et al., 1995; Quina et al., 1995).

Finally the oscillatory interaction energy for 3 and 5 wt% Citrem nanoemulsions with and without excess emulsifier in the aqueous phase was calculated using Equation 3.9 and plotted in Figure 3.7A and 3.7B, respectively. The period of oscillation is equal to the $d_{m\text{-}eff}$ of Citrem micelle. It was assumed that at a sufficiently high concentration, there would always be at least a layer of micelles present between the two approaching droplets when the distance between them approaches $d_{m\text{-}eff}$ (Erramreddy & Ghosh, 2014; James & Walz, 2014). It can be seen that the amplitude and length of oscillatory structural forces decreased significantly or almost disappeared upon removal of excess Citrem.

To understand the role of OSF in nanoemulsion gelling behaviour, in Figure 3.8A, we plotted the plateau storage moduli (G'_p) of the nanoemulsions as a function of droplet size (d_{32}) and the repulsive maxima of W_{OSF} when h approaches $d_{m\text{-}eff}$. There was a large reduction in W_{OSF} and about 4 to 5 increases in elastic moduli when excess emulsifier was removed (Figure 3.8A).

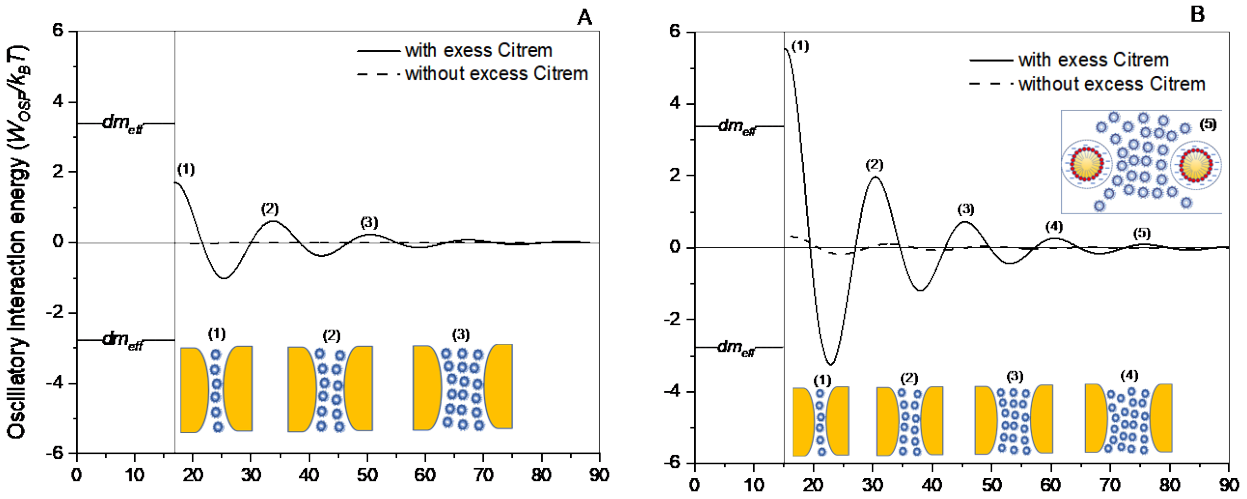

Figure 3.7 Oscillatory interaction energy between two approaching droplets calculated from Equation 3.9 for 40 wt% O/W nanoemulsions with (solid line) and without (dashed line) excess emulsifier micelles in the aqueous phase for (A) 3 wt% and (B) 5 wt% Citrem nanoemulsions. Inset shows schematic diagrams of two approaching droplets and their intervening micelle layers at the peak of each oscillation. The oscillation period is equal to the effective micelle diameter ($d_{m\text{-}eff}$) and it is assumed that when the separation distance approaches $d_{m\text{-}eff}$, the last layer of micelles stays between the droplets.

The 5 wt% Citrem nanoemulsions with lower droplet size showed more influence on gelling behaviour as a function of the reduction in OSF compared to 3 wt% Citrem nanoemulsion. Based on the theory of repulsive gelation, this suggests that the reduction in excess Citrem micelles led to the transformation of inter-droplet interaction energy from non-DLVO OSF dominated interactions to strong DLVO electrostatic repulsive interaction. Therefore, the DLVO interaction potential among the nanodroplets was calculated to understand the mechanism of repulsive gelation.

3.4.9 Calculation of DLVO forces

The overall DLVO interaction potential in the absence of excess Citrem micelles as a function of separation distance between two approaching droplets (R) was calculated by combining the electrostatic repulsive (W_{ele}) and van der Waals attractive (W_{vdw}) forces according to Equations 3.19 to 3.21 (Berli et al., 2002).

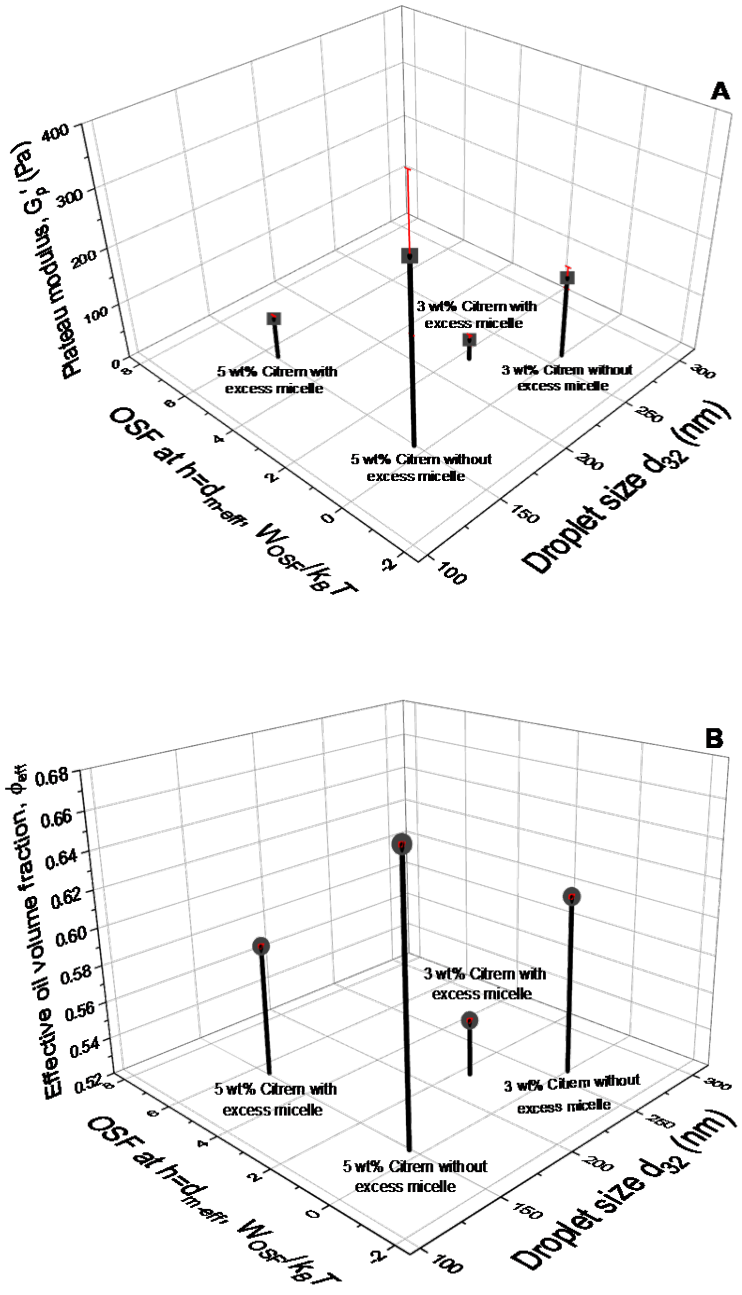

Figure 3.8. (A) Plateau storage modulus G_p', and (B) Effective oil volume fraction (ϕ_{eff}) as a function of droplet size and oscillatory interaction energy (W_{OSF}/k_BT) when separation between the droplets become equal to $d_{m\text{-}eff}$ for 3 and 5 wt% Citrem-stabilized nanoemulsions (ϕ_{core} = 0.42) with and without excess emulsifier micelles in the aqueous phase. Error bars indicate ± standard deviation (n ≥ 3).

The depletion forces were not considered for the calculation of overall interaction potential, as there was insignificant number of micelles (Figure 3.1A) in the aqueous phase after excess Citrem was removed through multiple cycles of ultracentrifugations.

$$W = W_{ele} + W_{vdw} \tag{3.19}$$

$$W_{ele} = 2\pi\varepsilon\psi_0^2 r\ ln\{1 + exp[-\kappa\ (R - 2r)]\} \tag{3.20}$$

$$W_{vdw} = -\frac{A_H}{6}\left[\frac{2r^2}{R^2-4r^2} + \frac{2r^2}{R^2} + ln\left(\frac{R^2-4r^2}{R^2}\right)\right] \tag{3.21}$$

In Equation 3.20, ε is the electric permittivity of the medium ($5.404 \times 10^{-10}\ C^2Nm^2$), κ is the inverse Debye screening length measured using Equation 3.4, r is the radius of the Citrem-stabilized oil droplet, and ψ_0 is the surface potential taken as measured zeta potential (-55 mV) (Berli et al., 2002). Equation 3.21 gives the van der Waals interactions between the droplets, where A_H is the Hamaker constant taken as 4×10^{-21} J for oil droplets dispersed in the aqueous phase (Israelachivili, 2011). The overall interaction potential was divided by k_BT to obtain the dimensionless energy parameter W/k_BT. The calculated overall interaction potential plotted in Figure 3.9 for 3 and 5 wt% nanoemulsions, respectively. From Figure 3.9, it can be seen that as the separation distance decreased between the two approaching droplets, the strength of the repulsive barrier increased. It was assumed that an overall repulsive interaction potential equal to 1 k_BT would be enough to prevent droplet flocculation. Other researchers have also taken similar approach, where the ϕ_{eff} for the silica nanoparticles was calculated through the assumption of interparticle distance based on the secondary minimum in the DLVO interaction potential (Antonopoulou et al., 2018). The inter-droplet distance at 1 k_BT (R) was calculated from Equation 3.19. Half of that value was taken as the repulsive shell layer thickness (δ) due to the presence of charge cloud around the negatively charged Citrem-stabilized droplet (see schematic diagram in Figure 3.9). The calculated values of δ from DLVO forces were 2.7 to 2.9 times DSL. It has also been proved by experiments and calculations that droplets stabilized with ionic surfactant showed significant repulsive interaction at a distance 2.1 to 2.4 times κ^{-1} from their surface (Mondain-Monval et al., 1996). The obtained

values of δ were used to calculate the ϕ_{eff} of nanoemulsions (Equation 3.1) in the absence of excess emulsifier.

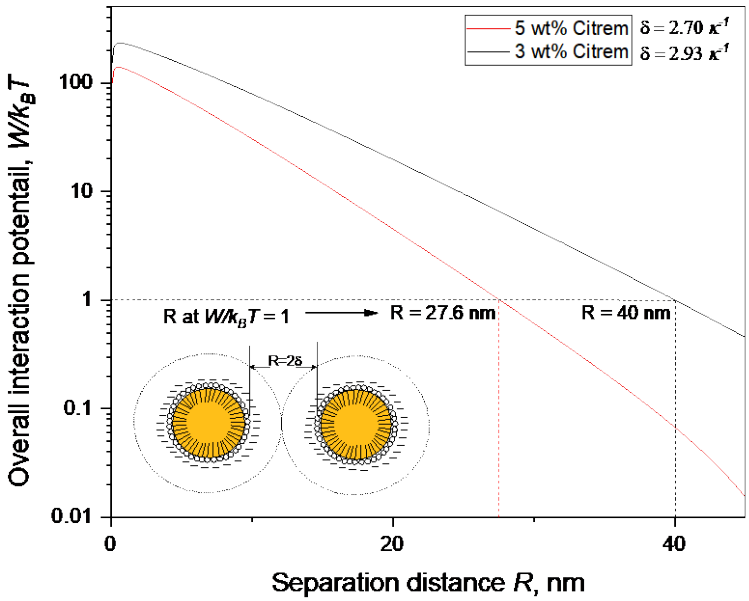

Figure 3.9 Overall interaction potential (W/k_BT) calculated using Equation 3.19 after removing excess emulsifier from the aqueous phase of 3 wt% and 5 wt% Citrem nanoemulsions as a function of inter-droplet separation distance (R). When interaction potential become equal to 1 k_BT, R was considered as two times the repulsive shell layer thickness (δ). Values for R at 1 k_BT are also shown for the two different nanoemulsions.

From Table 3.2, it can be seen that ϕ_{eff} for 3 wt% Citrem nanoemulsions without excess emulsifier was 0.614, still significantly below the ϕ_{MRJ}, where the nanodroplets can only have Brownian motion but cannot move past each other as they are caged by other nanodroplets. This state of emulsion system known as colloidal glassy phase (Mason & Scheffold, 2014). On the other hand, ϕ_{eff} for 5 wt% Citrem nanoemulsions without excess emulsifier was 0.665, which could be close to or above the ϕ_{MRJ}. It should be noted that the actual ϕ_{MRJ} for the polydisperse emulsion is unknown but should be greater than 0.64. The increase in ϕ_{eff} after removal of excess Citrem suggests that the electrostatic repulsive barrier became stronger between the two approaching droplets, which increased the effective size of the oil droplets, leading to a random jamming state and an increase in the gel strength of the nanoemulsions (Figure 3.4, 3.5 and 3.8A).

Table 3.2. Debye screening length (κ^{-1}), Interfacial shell layer thickness (δ) and effective oil volume fraction (ϕ_{eff}) for Citrem nanoemulsions after removal of excess emulsifier calculated from DLVO inter-droplet potential.

Oil volume fraction ϕ_{core}	Initial Citrem concentration in the nanoemulsion	Citrem concentration after removal of excess emulsifier	Counter ion concentration*	Debye screening length κ^{-1}**	Inter-droplet distance at 1 k_BT***	Shell layer thickness $\delta^{\#}$	Effective volume fraction of oil ϕ_{eff} §
	(wt%)	(wt%)	(mol/m^3)	(nm)	(nm)	(nm)	
0.42	3.0	1.56	1.94	6.82	40.00	20.00	0.614
	5.0	3.42	3.45	5.11	27.60	13.80	0.665

*Measured using the protocol mentioned in section 2.7.
** Calculated using Equation 3.4.
***Calculated as distance from droplet surface at 1 × k_BT using overall DLVO potential (Equation 3.19)
Half of total surface to surface inter-droplet distance at 1 × k_BT
§ Calculated using Equation 3.1.

To demonstrate why the transformation of inter-droplet interaction from OSF to strong electrostatic interactions influence gelation behaviour, in Figure 3.8B, we plotted ϕ_{eff} of the nanoemulsions as a function of a repulsive maxima of W_{OSF} (when h approaches $d_{m\text{-}eff}$) and average droplet diameter. When OSF disappeared and degenerated into DLVO dominated interaction energy, ϕ_{eff} became greater, perhaps more than the ϕ_{MRJ}, which explains strong gel behaviour of 5 wt% Citrem nanoemulsions. For 3 wt% Citrem nanoemulsion, a significant increase in ϕ_{eff} was observed after removal of excess Citrem, but it was lower than the 5 wt% Citrem nanoemulsion due to their larger average droplet size. Such a close packed structure due to removal of excess emulsifier, not only increased gel strength, but also improved overall emulsion stability by not allowing them to separate under accelerated gravitation.

3.5 Conclusion

In this study, transformation of weak gel nanoemulsions (ϕ_{core} = 0.42) into strong gels was investigated by removing excess emulsifier from the aqueous phase using multiple centrifugation cycles and reducing droplet size. The average droplet size and charge of 3 and 5 wt% Citrem-stabilized nanoemulsions did not change significantly when excess emulsifiers were removed, however a significant improvement in their creaming stability was observed. The calculated inter-droplet interaction dominated by OSF in the presence of excess Citrem micelles, whereas upon their removal, it was mainly governed by DLVO forces. This transformation of inter-droplet potential from non-DLVO to DLVO forces led to an increase in the DSL and the thickness of the charge cloud around the nanodroplets leading to an increase in ϕ_{eff}. For 3 wt% Citrem-stabilized nanoemulsions, a greater increase in charge cloud thickness was observed due to the removal of excess Citrem, but larger droplet size (~250 nm) led to an increase in ϕ_{eff} to 0.614, which was below the random jamming. Hence, for this nanoemulsion, although gel strength significantly increased upon removal of excess emulsifier, no self-supporting structure was formed, and they flowed under gravity. For 5 wt% Citrem-stabilized nanoemulsions, with a lower droplet size (~150 nm), ϕ_{eff} increased to 0.665, leading to a self-supporting gel which did not flow under gravity and exhibited a strong viscoelastic behaviour. Thus, we have shown that the reduction in the droplet size and removal of excess emulsifier from the continuous phase of nanoemulsion can lead to an increase in the repulsive inter-droplet interactions and a significant increase in their gel strength.

The food-grade Citrem-stabilized nanoemulsion gel prepared with the low oil volume fraction could be a novel way for calorie reduction in food formulations.

3.6 Connection to the next study

In this study, the mechanism responsible for the conversion of Citrem-stabilized viscous liquid oil-in-water nanoemulsions to viscoelastic gels upon removal of excess emulsifiers was investigated. The rheology of the nanoemulsions at two different Citrem concentrations with and without excess emulsifier in the continuous phase was compared. An excess emulsifier-induced OSF between the approaching nanodroplets was found to reduce the viscosity and viscoelasticity of the nanoemulsions. The removal of ionic emulsifier from continuous phase increased the electrostatic repulsive barrier between the nanodroplets, which led to increased viscoelasticity caused by a rise in ϕ_{eff} beyond the maximum random jamming volume fraction of the droplets. Thus, the gelation in nanoemulsions was achieved at $\phi = 0.42$ by reducing the droplet size and removing the excess emulsifier micelles. The increased gel strength of nanoemulsions after the removal of excess micelles also improved their stability against accelerated gravitation. Although the increase in the stability without excess emulsifier was attributed to the rheology of nanoemulsions, the kind of droplet-droplet interactions evolved in accelerated gravitation was unknown. In other words, the mechanism responsible for the stability or instability in nanoemulsions was required to be studied. Therefore, in the next study, to predict the colloidal interactions, the droplet packing behaviour under accelerated gravitation was investigated with and without excess micelles using an analytical photo-centrifuge. Additionally, the accelerated shelf-life of nanoemulsions was also studied using an RCF ramp, which further helped us compare the rheology data obtained in this first study.

4. ANALYTICAL PHOTO-CENTRIFUGE-BASED PREDICTION OF SHELF-LIFE AND DROPLET PACKING BEHAVIOUR OF NANOEMULSIONS UPON REMOVAL OF EXCESS MICELLES[2]

4.1 Abstract

An analytical photo-centrifuge was used to develop novel experimental methods to predict the shelf-life, rheology, and inter-droplet interactions in 40 wt% canola oil-in-water nanoemulsions stabilized by 3 and 5 wt% citric acid esters of monoglyceride (Citrem). The combined influence of micellar concentration and oil droplet size on the rheology, creaming stability, and compression behaviour was studied under a series of accelerated gravitations. Nanoemulsions without excess Citrem micelles were obtained by removing them from the continuous phase using multiple cycles of ultracentrifugation. Reduction in droplet size with an increase in Citrem concentration and the removal of excess micelles resulted in a significant increase in plateau storage moduli leading to a change in phase behaviour of the nanoemulsions from liquid to viscoelastic gels. Moreover, it also showed a simultaneous drastic decrease in nanodroplets creaming velocity under accelerated gravitation. The flow behaviour of the gels was well correlated with a critical relative centrifugal force required to initiate flow under accelerated gravitation. Additionally, the colloidal forces responsible for instability was satisfactorily explained by the packing behaviour of the nanodroplets studied under a series of compression and dilatational cycles of centrifugation. We showed that the strong electrostatic repulsive force between the nanodroplets without excess micelles led to a lower packing density during compaction that did not change significantly during successive dilatational cycles. The higher packing density or compaction in the presence of excess micelles was explained by the short-range attractive depletion forces leading to weak flocculation of nanodroplets. Overall, the presence and absence of excess micelles showed a significant

[2]Reprinted with permission from: Kadiya, K., & Ghosh, S. (2021). Analytical photo-centrifuge-based prediction of shelf-life and droplet packing behaviour of nanoemulsions upon removal of excess micelles. *Colloids and Surfaces A: Physicochemical and Engineering Aspects*, *612*, 125869. Kadiya, K. carried out the experiments and wrote the first draft. Ghosh, S. conceptualized, supervised, reviewed, and edited.

influence on the rheology and accelerated stability of nanoemulsions, which can be further described by the colloidal forces between the nanodroplets using the real-time advanced photo-centrifuge.

4.2 Introduction

Advances in the formulation, emulsification, and characterization of nanoemulsions led to their improved functionality and applications in the food system. When designing a nanoemulsion-based material for food application, its rheology and stability are essential elements that need to be considered (Kim & Mason, 2017). Rheological properties of emulsions and nanoemulsions are explained by various factors such as dispersed phase volume fraction (ϕ), physical and chemical properties of the aqueous phase, and the type and magnitude of the colloidal forces between the oil droplets (Mason et al., 1997; McClements, 2015). Concentrated nanoemulsions stabilized by ionic emulsifiers have been shown to transform into elastic gels at a dispersed phase volume fractions (ϕ_{core}) much lower than the microscale conventional emulsions (Wilking & Mason, 2007). An anionic emulsifier at the interface is responsible for the electrostatic stabilization of the droplets by providing a charge cloud of counterions from the continuous phase. As the droplet size of nanoemulsions becomes lower, beyond a critical size, the thickness of the charge cloud or repulsive shell-layer (δ) surrounding the nanodroplets tends to become similar order of magnitude to the actual droplet radius (r). This can significantly increase the effective droplet size ($r_{eff} = r + \delta$) of nanoemulsions and hence their effective volume fraction (ϕ_{eff}), calculated using Equation 4.1 (Erramreddy & Ghosh, 2014; Wilking & Mason, 2007).

$$\phi_{\text{eff}} = \phi_{\text{core}} \left(1 + \frac{\delta}{r}\right)^3 \tag{4.1}$$

When ϕ_{eff} is increased to 0.64 (for monodisperse droplets) or beyond the maximum random jamming (ϕ_{MRJ}), the nanodroplets eventually become deformed and arrange into a close-packed structure (Mason & Scheffold, 2014). At this stage, the nanoemulsion behaves like a repulsive viscoelastic gel even if the ϕ_{core} is much lower than ϕ_{MRJ} (Weiss & McClements, 2000). It has been shown that transparent nanoemulsion gels can be prepared by short-range electrostatic repulsion between nanodroplets when the interfacial thickness of the electrical double layer is closer to the order of the radius of the nanoemulsion droplets (Kawada et al., 2010). As nanoemulsions can be

structured into viscoelastic gels at significantly lower oil volume fractions, the novel gel structure with improved functionality and stability may open up new applications in food, pharmaceuticals and cosmetics (Kawada et al., 2010; Mason et al., 2006; Wilking & Mason, 2007).

Nanoemulsions are also important for their long-term stability-related applications in food, pharmaceuticals, and cosmetics. They are incredibly stable against physical destabilization via creaming and particle aggregation, due to their nanoscale droplet size, compared to the conventional emulsions (Rao & McClements, 2012; Tadros et al., 2004). Hence, studying the creaming rate to predict the shelf-life of nanoemulsions are difficult and time-consuming at normal gravitational separation condition. However, using accelerated gravitation in a photo-centrifuge (LUMiSizer®), it was possible to compare the stability of different nanoemulsions within a short timeframe. The instrument works based on the STEP (Space- and Time-resolved Extinction Profiles) technology, as shown in (Appendix B, Figure B1), in which the transmitted light at 865 nm wavelength is measured as a function of time and position over the sample length (Lerche, 2019). A great extent of research has been carried out to study the long-term creaming stability of nanoemulsions using the photo-centrifuge (Chen et al., 2016; Erramreddy et al., 2017; Ma et al., 2018; Primozic et al., 2017; Thompson et al., 2018; Yerramilli & Ghosh, 2017).

An essential aspect of nanoemulsion preparation is the use of a large amount of emulsifier under extremely high shear. However, the amount of emulsifier used in the formation of nanoemulsions has a profound effect on their inter-droplet interactions and rheological behaviour. For example, Erramreddy et al. showed that an increase in the sodium dodecyl sulphate (SDS) concentration from 0.5 to 25 times critical micelle concentration (CMC) led to a dramatic change in the rheology of a 40 wt% canola oil-in-water nanoemulsion (Erramreddy & Ghosh, 2014). At a low SDS (up to 2 CMC) concentration, the liquid nanoemulsion transformed into the repulsive gel and then at 5 CMC SDS into depletion interaction-induced attractive gel followed by re-transformation into liquid nanoemulsion beginning 20 CMC SDS due to the dominant oscillatory structural forces (OSF) generated from the excessive micellar concentration in the continuous phase of the nanoemulsion (Erramreddy & Ghosh, 2014). Recently, we have used a food-grade anionic emulsifier, Citrem (citric acid esters of mono-glyceride), at different concentrations for the preparation of 40 wt% canola oil-in-water nanoemulsions (Kadiya & Ghosh, 2019). It was found that at least 3 wt% Citrem was necessary to reduce the droplet size in the nanoscale; however, the excess Citrem micelles in the continuous phase induced OSF among the nanodroplets preventing

repulsive gelation. We then discovered that by removing the excess micelles from the continuous phase, it was possible to transform the liquid nanoemulsion into a repulsive viscoelastic gel (Kadiya & Ghosh, 2019). The gel strength of the nanoemulsions significantly increased as a function of the removal of excess micelles from the continuous phase.

As a consequence of increase in gel strength, the creaming velocity of the nanoemulsions under accelerated gravitation also significantly dropped as the excess micelles were removed (Kadiya & Ghosh, 2019). The creaming rate of the nanodroplets in such a viscoelastic system under accelerated gravitation depends on droplet hydrodynamics, the colloidal forces acting between them and their packing behaviour (Leal, 2004; Sjoblom, 2001). The packing behaviour of droplets can be expressed in terms of the packing density (ϕ_p), which is defined as the volume of droplets packed in a specific volume (Sarles & Leo, 2010; Sobisch & Lerche, 2002). A better understanding of droplet packing is expected to help in predicting the mechanism of stability of the nanoemulsions as the excess emulsifiers were removed from the aqueous phase. Therefore, an alternative method to characterize the stability in a viscoelastic colloidal system with a range of inter-particle interactions could come from the packing density (ϕ_p) of the nanodroplets at a given applied centrifugation force (Brujić et al., 2003; Krebs et al., 2013). As per our knowledge, no work has been done using an analytical photo-centrifuge to understand the droplet dynamics and packing behaviour responsible for nanoemulsion stability. We report a new experimental method to investigate the droplet compression behaviour and packing density at different centrifugal forces and its application in predicting the mechanism of nanoemulsion stability.

4.3 Materials and methods

4.3.1 Experimental materials

Canola oil, purchased from the local retail superstore, was used as the dispersed phase. Millipore® deionized pure water (conductivity of 1.0 μS/cm) was used as the nanoemulsion aqueous phase and for the preparation of chemicals and buffers used. The food-grade anionic emulsifier, citric acid esters of monoglyceride (Citrem) with the hydrophilic-lipophilic balance of (HLB) 9 – 10, was donated by Palsgaard Inc. (Morris Plains, NJ, USA). All other chemicals were purchased from Sigma-Aldrich (St. Louise, MO, USA).

4.3.2 Preparation of nanoemulsions with and without excess micelles

The aqueous phases, containing 3 and 5 wt% Citrem, were prepared by dissolving Citrem above its pre-determined melting point of 61°C (data not shown). An antibacterial agent, sodium azide, was added at 0.02 wt% of the aqueous phase to avoid any microbial growth during storage. Coarse O/W emulsion was prepared by pre-mixing 40 wt% canola oil with 60 wt% aqueous phases using a rotor-stator mixer (Polytron, Brinkmann Instruments, Ontario, Canada) for 60 s at 20,000 rpm. The coarse emulsion was adjusted to pH 7 (using 1 N NaOH) and subjected to eight cycles of high-pressure homogenization at 20,000 psi to prepare the nanoemulsion (EmulsiFlex-C3, Avestin Inc., Ottawa, ON, Canada). The nanoemulsion with excess micelles in their continuous phase was stored in a 120 mL glass bottles (VWR International, Edmonton, AB, Canada) at room temperature (25 ± 2 ºC) for further experiments.

For comparison, nanoemulsion without excess Citrem micelles was prepared by subjecting them to multiple cycles of ultra-centrifugation at 52,070×g force for 1.5 h following a method developed by Kadiya and Ghosh (2019). The ultracentrifugation force separated the nanoemulsion into a top cream layer of nanodroplets and a bottom aqueous serum layer containing excess Citrem micelles. The aqueous phase was carefully removed by a 5 mL Luer-lok™ syringe (BD #309646) attached with a reusable hypodermic needle (B-D YALE Luer-Lok™ 15 G x 1.5") and stored for the quantification of Citrem content. The cream layer was re-dispersed into an equal amount of deionized water, that was removed after ultracentrifugation and re-homogenized for two cycles at 20,000 psi so that the droplet size distribution remains unchanged. This process of ultracentrifugation, cream layer separation and re-homogenization was repeated two more times to ensure maximum removal of excess Citrem micelles from the aqueous phase of the nanoemulsion. The total excess Citrem removed by this process was quantified from the aqueous phase separated in each step using a gas chromatography according to (Kadiya & Ghosh, 2019). The nanoemulsions with and without excess micelles obtained by this way were analyzed for their droplet size, viscoelastic properties, accelerated shelf-life and stability, as well as for droplet packing density.

4.3.3 Droplet size measurement

The droplet size of the nanoemulsions with and without excess micelles was analyzed by a static light scattering technique, using the equipment Mastersizer 2000 (Malvern Instruments, Montreal, QC, Canada) with a relative refractive index of the dispersed vs. continuous phases as

1.465. Deionized water was used as a dispersant in the instrument, and the obscuration was brought up to ~12% by dropwise sample addition. The average droplet size of nanoemulsion was characterized by Sauter mean diameter (d_{32}), calculated by Equation 4.2.

$$d_{32} = \frac{\sum n_i d_i^3}{\sum n_i d_i^2} \tag{4.2}$$

Where n_i is the number of droplets with a diameter of d_i.

4.3.4 Viscoelastic properties of nanoemulsions

Viscoelastic properties of nanoemulsions with and without excess micelles were evaluated using an AR G2 rheometer (TA Instrument, New Castle, DE, USA) at 25°C. A definite quantity of nanoemulsions was carefully transferred onto the Peltier plate of the rheometer, and oscillatory strain or frequency was applied at 1000 μm gap using a 40 mm diameter cross-hatched geometry. The viscoelastic behaviour of the samples was determined by dynamic oscillatory strain sweep measurement. The strain sweep measurements were performed in the range of 0.01–100 % strain at a constant frequency of 1 Hz (6.28 *rad*/ s) to analyze the linear viscoelastic region (LVR) (data are not shown). From the obtained data the plateau modulus (G'_p) at 0.1% strain was plotted to compare the gel strength different nanoemulsions.

4.3.5 Stability and shelf-life study of nanoemulsions at accelerated gravitation

The accelerated stability and shelf-life of the nanoemulsions, in terms of droplet separation rate, in the presence and absence of excess micelles were evaluated using a photo-centrifuge LUMiSizer® (LUM GmbH, Berlin, Germany) at 25°C. 400 μL of nanoemulsion was transferred into a disposable polycarbonate cell with a 2 mm thick optical path length. Several samples were evaluated simultaneously at a desired relative centrifugal force (RCF) for accelerated gravitation, after temperature equilibration and normalization of transmission profile. The RCF was calculated using the following equation and expressed as times earth gravitation (Erramreddy et al., 2017).

$$\text{RCF} = 1.118 \left(\frac{RPM}{1000}\right)^2 r \tag{4.3}$$

Here, RPM is the centrifugation speed in revolution per min, and r is the distance of the droplets from the axis of rotation (130 mm).

For accelerated stability study, the nanoemulsions samples in duplicate with and without excess micelles were centrifuged at a maximum relative centrifugation force (RCF) of 2325×g. On the other hand, the predicted shelf-life at earth gravitation was evaluated by centrifugation of the samples at different relative centrifugation forces (RCF) from 145×g to 2325×g. The light transmitted through the transparent polycarbonate cell was collected at every 72 s till 1000 profiles were generated as a function of change in the position of the interface using the SEPView® software version 6.2 provided by the LUM GmbH with the instrument. The change in the position (in mm) of the cream layer throughout the optical path length in the cell at different RCF was plotted as a function of time. The linear slope obtained from these curves depicted the droplet separation velocity (in mm h^{-1}) of the nanoemulsions at that RCF. Next, the separation velocities were plotted as a function of RCF and extrapolated to one (1) RCF, equivalent to earth gravitation, to obtain the droplet separation rate of the nanoemulsions at normal room temperature storage condition.

4.3.6 Determination of packing density of oil droplets

The stability of nanoemulsions under applied centrifugal force is induced by the hydrodynamics of two approaching droplets, which in turn influenced by the colloidal forces acting on their interfaces. The presence of excess emulsifier micelles could significantly influence these colloidal forces, which can be well predicted by the packing behaviour of the droplets under the applied centrifugal force. Therefore, the average packing density (ϕ_p) in terms of the volume fraction and compression behaviour of the separating oil droplets was investigated as a function of excess Citrem micelles removal from the nanoemulsions. To obtain ϕ_p, experiments were performed under the influence of increased (compression) and decreased (dilatational/decompression) centrifugal force using the LUMiSizer® to establish the compression – dilatational curves for the nanoemulsions (Bharti et al., 2014; Sobisch & Lerche, 2002). The compression cycles of centrifugal force were carried out in three successive increases in RCF, every two hours, from 35×g to 325×g to 2325×g, whereas in dilatational (decompression) cycles, RCF was gradually reduced, every two hours, in two steps from 2325×g to 325×g to 35×g. The transmission profiles were collected at every 72 s till 100 profiles generated for each successive step in a compression – dilatational cycle. The change in the interfacial position (mm) of the cream layer was plotted with respect to time and as a function of the compression – dilatational cycle of

centrifugal force for the nanoemulsions with and without excess Citrem micelles in their aqueous phase. The ϕ_p was calculated according to Equation 4.4 (Bharti et al., 2014; Sobisch & Lerche, 2002) at the completion of each successive step in compression – dilatational cycle for the nanoemulsions with and without excess emulsifier in their aqueous phase.

$$\phi_p = \frac{m_d}{\rho_d h A} \tag{4.4}$$

where m_d and ρ_d are the mass and density of the dispersed phase respectively, whereas h is the height of the separated cream layer, and A is the cross-sectional area of the rectangular LUMiSizer® cell.

4.3.7 Statistical analysis

All experiments were conducted with at least three replicates, and results were reported as the mean ± standard deviation. The statistical significance was analyzed using Microsoft Excel 2016 (Microsoft Corp., Redmond, WA, USA), and power-law fittings were performed using OriginPro version 2020 software (OriginLab Corporation, Northampton, MA, USA).

4.4 Results and discussion

4.4.1 Micellar volume fraction in nanoemulsions

The nanoemulsions were subjected to multiple cycles of ultracentrifugation to remove the excess micelles from the continuous phase, as explained in section 2.2 and quantified using gas chromatography (Kadiya & Ghosh, 2019). In Equation 4.5, the micellar volume fraction (ϕ_m) was calculated from the amount of excess emulsifier removed through multiple cycles of centrifugation.

$$\phi_m = \frac{4\pi}{3}\left(\frac{d_m}{2}\right)^3 C_M \tag{4.5}$$

Where d_m is the diameter of Citrem micelle, which is 6.06 nm (Kadiya & Ghosh, 2019). C_M is the number density of Citrem micelle, calculated using Equation 4.6.

$$C_M = C_{excess} \times {N_A}/{N_{agg}} \tag{4.6}$$

Where C_{excess} (mol/L) is the excess Citrem removed through multiple cycles of ultracentrifugation; N_A is the Avogadro number (6.023×10^{23} mol^{-1}), and N_{agg} is the micelle aggregation number, which is 104 for Citrem (Kadiya & Ghosh, 2019). The calculated ϕ_m versus the number of centrifugation cycles (micelle separation steps) is plotted in Figure 4.1.

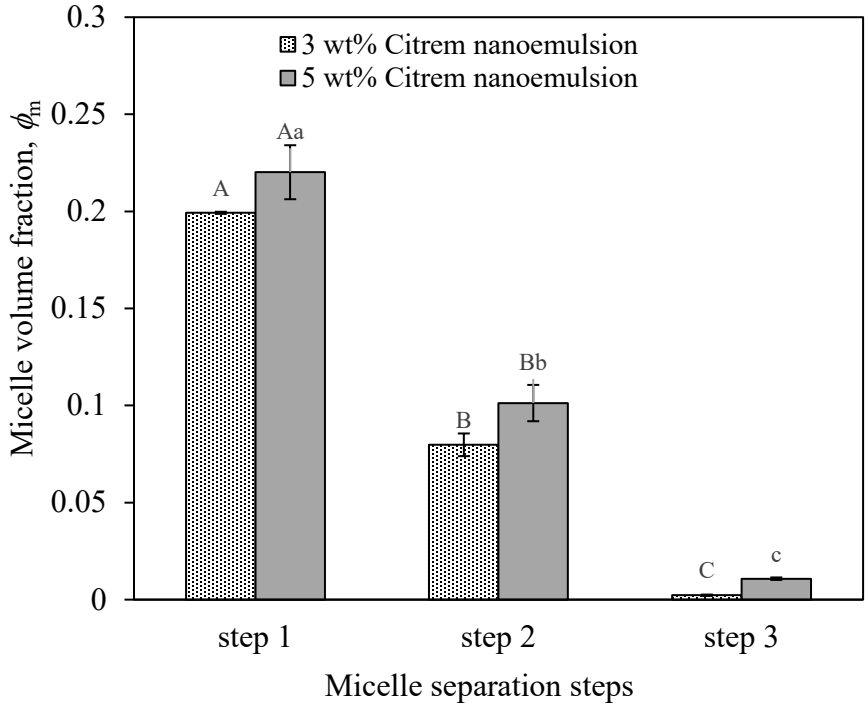

Figure 4.1 The micellar volume fraction (ϕ_m) of excess Citrem in the continuous phase of 3 and 5 wt% Citrem-stabilized nanoemulsions as a function of the micelle separation steps (number of ultracentrifugation cycles). Error bars indicate ± standard deviation (n ≥ 3). Different uppercase (for 3 wt% Citrrem) and lowercase (for 5 wt% Citrrem) letters denote the statistical significance (at 0.05 level) difference amongst the population means.

The ϕ_m was 0.199 and 0.220 during the first centrifugation cycle, which is equivalent to 9.5 and 10.5 times the CMC of Citrem for 3 wt% and 5 wt% nanoemulsions, respectively. The critical micelle concentration (CMC) of Citrem is 0.451 mol or 0.15 wt% (Kadiya & Ghosh, 2019). After three cycles of ultracentrifugation, ϕ_m was reduced to a negligible fraction 0.002 (0.1 times CMC) and 0.01 (0.5 times CMC) in the aqueous phase of 3 wt% and 5 wt% nanoemulsions, respectively. It should be mentioned that even if we were able to remove most of the excess Citrem emulsifier from the continuous phase, emulsifier adsorption and desorption is a dynamic process, and the re-

re-constructed nanoemulsions would have a different equilibrium than the original one, which could also influence emulsifier adsorption at the oil droplet surface. However, in the present case, such effect did not have any influence on droplet size. The excess micelles were removed with an aim to obtain nanoemulsions with different hydrodynamic forces between the droplets, which should have a significant impact on their physical properties and stability. Thus, Citrem-stabilized nanoemulsions obtained without excess micelles were characterized for rheology, storage stability and droplet packing or compression behaviour in comparison to the nanoemulsions with excess micelles in the continuous phase.

4.4.2 Droplet size and rheology of nanoemulsions with and without excess micelles

In Figure 4.2, the change in gel strength, effective oil volume fraction (ϕ_{eff}) and average droplet diameter (d_{32}) are compared for 3 and 5 wt% Citrem-stabilized nanoemulsions with and without excess micelles in their continuous phase. The average droplet size was 222.3 ± 12.7 nm and 151.0 ± 3.4 nm for 3 and 5 wt% Citrem nanoemulsions with excess micelles in their continuous phase, respectively. The increase in the emulsifier concentration led to a decrease in droplet size. When the excess micelles were removed from the continuous phase of the nanoemulsions, the droplet size was 259.7 ± 40.1 nm and 149.0 ± 16.4 nm for 3 and 5 wt% Citrem nanoemulsions and did not change significantly ($p > 0.05$) compared to the nanoemulsion with excess micelles. Similarly, we found that the droplet size distribution (data not shown) also did not change for any of the nanoemulsions after the removal of excess micelles. Therefore, by keeping the droplet size unchanged, we were able to study the effect of the presence and absence of excess micelles on rheology, accelerated stability and droplet packing behaviour of the nanoemulsions.

From Figure 4.2, it can also be seen that the plateau storage moduli (G'_p) of the nanoemulsions increased almost 2 times from 36.9 ± 1.7 to 71.1 ± 21.8 Pa with increase in Citrem concentration from 3 to 5 wt%. On the other hand, G'_p increased from 36.9 ± 1.7 to 98.8 ± 20.6 Pa and from 71.1 ± 21.8 to 334.8 ± 17.4 Pa, as the excess micelles were removed from the continuous phase of 3 and 5 wt% Citrem nanoemulsions, respectively. The removal of excess micelles showed almost 3 to 5 times increase in storage moduli of the nanoemulsions. The highest gel strength was observed for 5 wt% Citrem nanoemulsions in the absence of excess micelles. This could be attributed to their lower droplet size, compared to 3 wt% Citrem nanoemulsions. We have previously attributed this conversion from flowable liquid to viscoelastic nanoemulsion gel to the

stronger electrostatic repulsive forces between the droplets and corresponding increase in ϕ_{eff} beyond ϕ_{MRJ} (Equation 4.1) (Erramreddy & Ghosh, 2014; Kadiya & Ghosh, 2019). The calculation of ϕ_{eff} was shown in our previous work, where the repulsive shell-layer thickness (δ) was shown to be about 2.40 to 2.93 times than the measured values of Debye screening length (κ^{-1}) (Appendix B, Figure B2) (Kadiya & Ghosh, 2019).

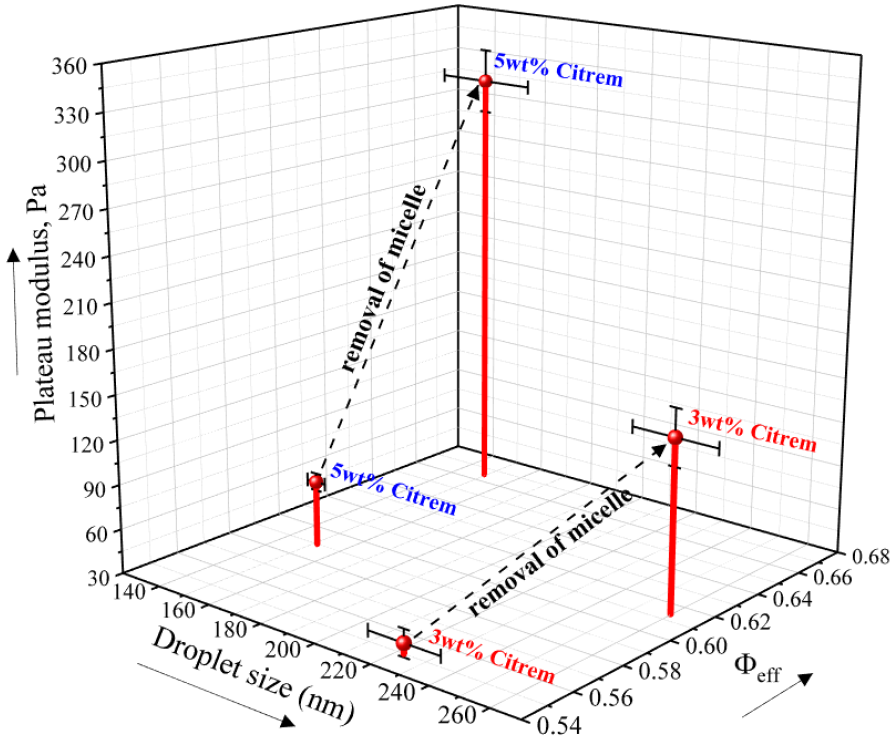

Figure 4.2 The effect of removal of excess micelles on the average droplet size and plateau storage modulus (G'_p) of 3 and 5 wt% Citrem-stabilized nanoemulsion with respect to their effective oil volume fraction (ϕ_{eff}). Error bars indicate ± standard deviation (n ≥ 3).

From Figure 4.2, it can also be seen that with excess micelles ϕ_{eff} increased from 0.55 to 0.59 due to a decrease in droplet size as the Citrem concentration raised from 3 to 5 wt%. With the removal of excess micelles from the continuous phase, ϕ_{eff} further increased to 0.61 and 0.67 for 3 and 5 wt% Citrem-stabilized nanoemulsions, respectively. The increases in ϕ_{eff} led to an appreciable increase in plateau modulus of the nanoemulsions, leading to a change in phase behaviour from viscous liquid to elastic gel when $\phi_{eff} > 0.64$. These findings also suggest that the

presence of excess emulsifier in the continuous phase plays a vital role in determining the colloidal forces between the droplets as well as the rheology of concentrated nanoemulsions.

4.4.3 Prediction of shelf-life and rheology via accelerated stability study of the nanoemulsions

The shelf-life of the nanoemulsions at earth gravitation (RCF = 1) could also be predicted using an analytical photo-centrifuge if the droplet separation velocity is known as a function of RCF by extrapolating to 1 RCF value. Therefore, multiple centrifugations of nanoemulsions in the presence and absence of excess micelles were performed at different RCF, and the droplet separation velocities were calculated from the transmission profiles, shown in the supplementary (Appendix B, Figures B3 and B4), for 3 and 5% Citrem nanoemulsions, respectively. The droplet separation velocity for the nanoemulsions with and without excess micelles under accelerated gravitation was plotted as a function of RCF in Figure 4.3A. Remarkably, only 3 wt% nanoemulsions with excess micelles showed an almost linear increase in creaming velocity with an increase in RCF, which can be extrapolated to RCF = 1. All other nanoemulsions showed a nonlinear trend and attained a zero-creaming velocity well before RCF = 1. In the case of 3 wt% nanoemulsions with excess micelles, extrapolating the liner fitting equation to RCF = 1, the calculated value of creaming velocity was 4×10^{-4} mm h^{-1} or 3.5 mm per year, which predicts an excellent shelf-life of these nanoemulsions at earth gravitation. In a similar work, nanoemulsions stabilized with 8 mM SDS was predicted with a creaming velocity of 5.3 mm per year at earth gravitation (Erramreddy et al., 2017). For the 5 wt% Citrem nanoemulsions, and with the removal of excess micelles from the continuous phase, our method predicts that the nanodroplets would cream only if a critical RCF was reached (Figure 4.3A).

Further, as shown in Figure 4.2, an increase in ϕ_{eff} created a close-packed structure of the droplets, which did not allow them to separate until the shear force reached sufficiently high, above the critical RCF. Similar behaviour of decrease in droplet creaming velocity due to an increase in ϕ_{eff} was also observed by others (McClements & Chanamai, 2002). In the present study, the suppression of creaming could also be related to the magnitude of centrifugal force (RCF) being lower than the extreme drag force created by the strong viscoelastic gel-like properties of the nanoemulsions. Therefore, a critical RCF was required to break the yield stress created by the nanodroplets in concentrated close-packed systems. Beyond this critical RCF, the droplets moved under accelerated gravitational force. This kind of behaviour was attributed to a gel-like structure

of the dispersion, and the critical RCF was correlated with the yield point of the gel system under centrifugal separation (Kuentz & Röthlisberger, 2003; Lerche & Sobisch, 2011).

To further explain this behaviour in terms of rheology, we described the non-linearity of the curve by power law. When the exponent n = 1.05 was higher than 1 for 3 wt% Citrem nanoemulsion with excess micelles, we observed a slight increase in the rate of change of creaming velocity due to an increase in RCF, indicating a shear-thinning behaviour (Figure 4.3A). With an increase in Citrem concentration from 3 to 5 wt%, the rate of change in creaming velocity as a function RCF decreased and hence the exponent was reduced to 0.86. Upon removal of excess micelles from both the nanoemulsions, the exponent further reduced to n = 0.42 – 0.44 due to increased packing of nanodroplets and their associated charge cloud, demonstrating pseudoplastic behaviour. Such change in flow behaviour of the nanoemulsions under accelerated gravity also follows their yield stress behaviour obtained from the viscosity data by applying the Herschel-Bulkley model (Appendix B, Figure B5). The yield stress value was found to increase with a reduction in droplet size and removal of excess micelles from the continuous phase of the nanoemulsions similar to a decrease in the exponent of change in creaming velocity as a function of RCF. Thus, a change in the rheological behaviour of the nanoemulsions as a function of excess micelles removal can also be predicted and correlated with the accelerated stability study. Well prediction of dynamic flow and viscoelastic behaviour of silica loaded hydrogel dispersions was assessed using accelerated stability technique (Hespeler et al., 2019). In another study, strong correlation was found between the various rheological parameters and sedimentation kinetics of bentonite and xanthan gum dispersion using analytical centrifuge (Kuentz & Röthlisberger, 2003). The authors established that the analytical centrifuge can be a great alternative for studying and creating the dispersion formulations with optimum sedimentation velocity and viscoelastic properties. Nevertheless, it should be noted that having a yield stress does not always mean a complete prevention of droplet movement under earth gravitation. A proof of this statement can be seen in the case of 3 wt% Citrem nanoemulsions with excess micelles, where, in spite of their finite yield stress as shown in Figure B5 (Appendix B), the nanodroplets had a predicted creaming velocity at earth gravitation. Similar observations were also noticed for particle sedimentation, where the yield point of the suspension was not able to completely stop the particle movement under gravitation (Kuentz & Rothlisberger, 2002).

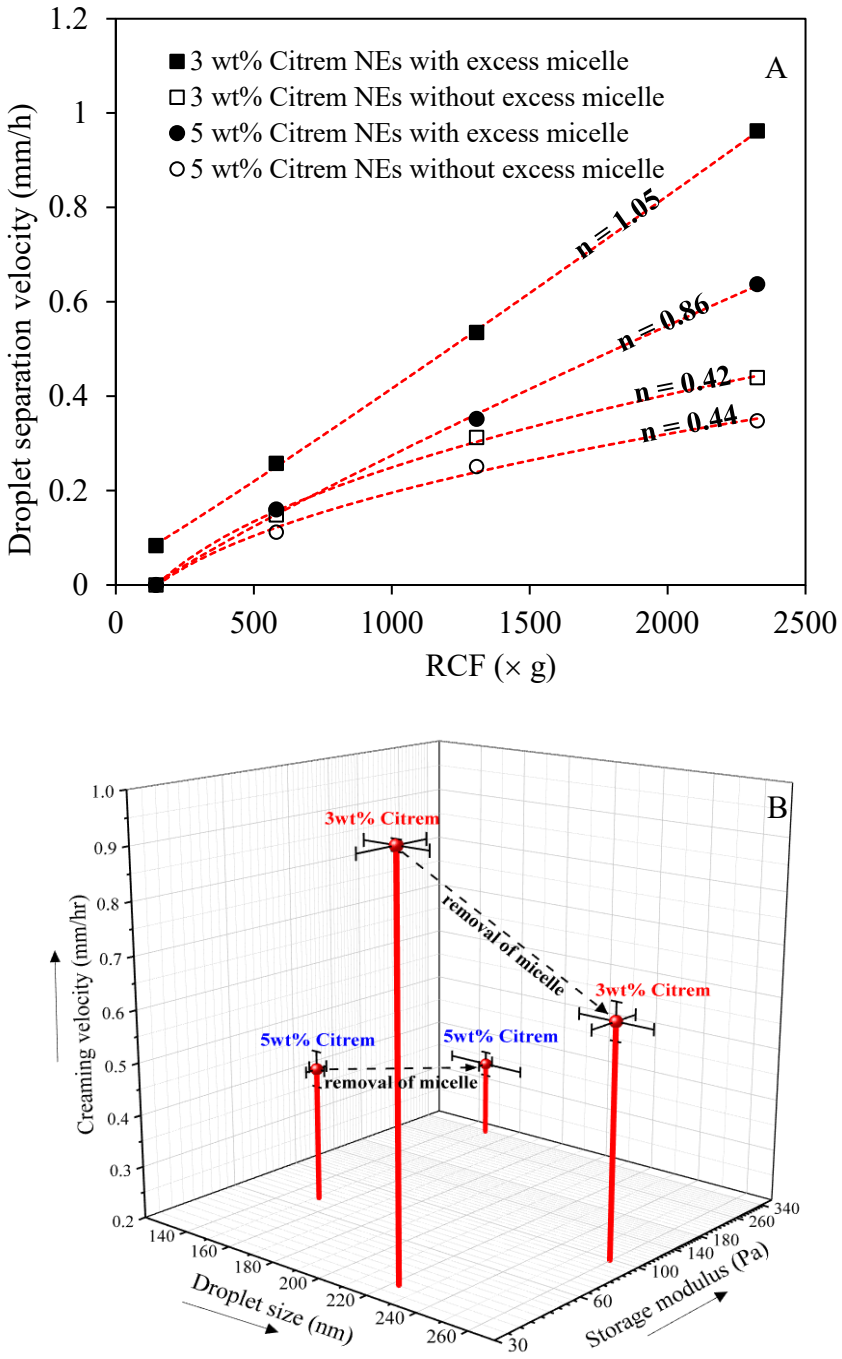

Figure 4.3 Photo-centrifuge-based accelerated stability study of 3 and 5 wt% Citrem-stabilized nanoemulsions (NEs) with and without excess micelles in the aqueous phase. (A) Shelf-life prediction at earth gravity (1×RCF) from the linearity of creaming velocity as a function of RCF from 145×g to 2325×g. Power law exponent (n) of the curves is also shown (B) Droplet separation velocity of nanoemulsions from Figure 4.3A at a relative centrifugation force (RCF) of 2325×g is plotted as a function of the average droplet size and gel strength of the nanoemulsions. Error bars indicate ± standard deviation (n ≥ 3).

Now, to further correlate the gel strength and droplet size of nanoemulsions (Figure 4.2) with their creaming velocity at maximum RCF (2325 × g) (Figure 4.3A) all three values were re-plotted in Figure 4.3B. The droplet separation velocity reduced from 0.96 to 0.46 mm h^{-1} with a reduction of droplet size (due to increase in Citrem concentration from 3 to 5 wt%). However, as the excess Citrem micelles were removed from the aqueous phase, it was further reduced from 0.96 to 0.64 for 3 wt% and from 0.46 to 0.35 mm h^{-1} for 5 wt% Citrem-stabilized nanoemulsions, which showed a significant increase in stability against forced destabilization ($p < 0.05$) (Figure 4.3B). Considering the droplet size and gel strength of the nanoemulsions, it can be seen that there was an almost 52% reduction in creaming velocity (from 0.96 to 0.46 mm h^{-1}) with a reduction in droplet size from ~220 nm to ~150 nm, while the gel strength increased about two times from 36.9 to 71 Pa for emulsions with excess micelles. On the other side, after removal of excess micelles, there was 33% and 24% reduction in creaming velocity (0.96 to 0.64 and 0.46 to 0.35 mm h^{-1}) when the droplet size remains unchanged, but the gel strength significantly ($p < 0.05$) increased to almost 3 to 10 times for 3 and 5wt% Citrem nanoemulsions, respectively. Therefore, between the droplet size and gel strength of nanoemulsions, droplet size was found to have a greater impact on the creaming velocity (52% reduction) compared to gel strength (33% and 24% reduction in creaming velocity). Between 5 and 3 wt% Citrem nanoemulsions without excess micelles, the higher stability of the former (creaming velocity 0.35 mm h^{-1}) compared to the latter (creaming velocity 0.64 mm h^{-1}) could be attributed to the combined effect of smaller droplet size and much higher gel strength (Figure 4.3B). This shows the substantial reduction in the creaming velocity of around 64% (from 0.96 to 0.35 mm h^{-1}) when contributions of both the factors, droplet size and gel strength, was considered in stabilizing the nanoemulsions.

4.4.4 Average packing density of nanodroplets

The droplet packing behaviour in a concentrated system can be used to understand the stability mechanisms responsible for such a drastic change in the shelf-life and droplet separation velocity observed in Figures 4.3A and 4.3B. The efficiency of droplets packing was studied using compression and expansion of nanoemulsion under different magnitudes of accelerated gravitational force, and the corresponding change in the height of the cream layer (h) was recorded as a function of excess micelles removal. Figure 4.4A shows the change in the interfacial position of the cream layer as a function of successive increase and decrease in RCF during compression

and dilatational cycles, respectively. At first, the dispersed nanodroplets without excess micelles did not show any compression at 35×g irrespective of their droplet size and the presence of excess micelles. At 325×g, only the 3 wt% Citrem nanoemulsion with excess micelles and larger droplet size showed a little compression of the cream layer, while the rest did not show any movement. These findings are supporting the critical RCF requirement to move the nanodroplets of some nanoemulsions with greater gel strength (Figure 4.3A). With further increase in RCF to 2325×g, the nanodroplets in the cream layer with excess micelles in the aqueous phase showed higher compression compared to the ones without excess micelles. This same trend was followed during the dilatational cycles. Remarkably, nanoemulsions without excess micelles were not further compressed during the dilatational cycle, and the height of the cream layer did not change significantly ($p > 0.05$), as shown in Figure 4.4A, after the end of the compression cycle.

Droplet packing density (ϕ_p) was calculated from the height of the cream layer (h), obtained from Figure 4.4A, using Equation 4.4. The change in ϕ_p in the presence and absence of excess micelles under compression and the dilatational cycle was plotted in Figure 4.4B. In accordance with the cream layer position, the average packing density also significantly increased for the nanoemulsions with excess micelles during compression as well as the dilatational cycle, while it did not change significantly for the nanoemulsions without excess micelles during the dilatational cycle ($p > 0.05$). In order to understand the impact of micellar concentration on the nanodroplet packing behaviour, the ϕ_p of the droplets under compressed state (at the end of the compression-dilatational cycles) was compared with the corresponding effective oil volume fraction (ϕ_{eff}) and gel strength of the nanoemulsions (Figure 4.5A). With the removal of excess micelles and reduction in droplet size (d_{32} from 259.7 to 149.0 nm) of nanoemulsions, ϕ_p was reduced from 0.55 to 0.47, whereas ϕ_{eff} and gel strength increased from 0.55 to 0.67, and 36.9 to 334.8 Pa, respectively. The droplet packing behaviour under the compressed state is inversely correlated to the effective oil volume fraction (ϕ_{eff}) and gel strength of the nanodroplets. This indicates that the nanodroplets, in the presence of excess micelles and with a lower contribution of an electric double layer (lower ϕ_{eff}) (Appendix B, Figure B2) were consolidating rapidly in the cream layer under the influence of the centrifugal force (Figure 4.5Ba), leading to a higher packing density.

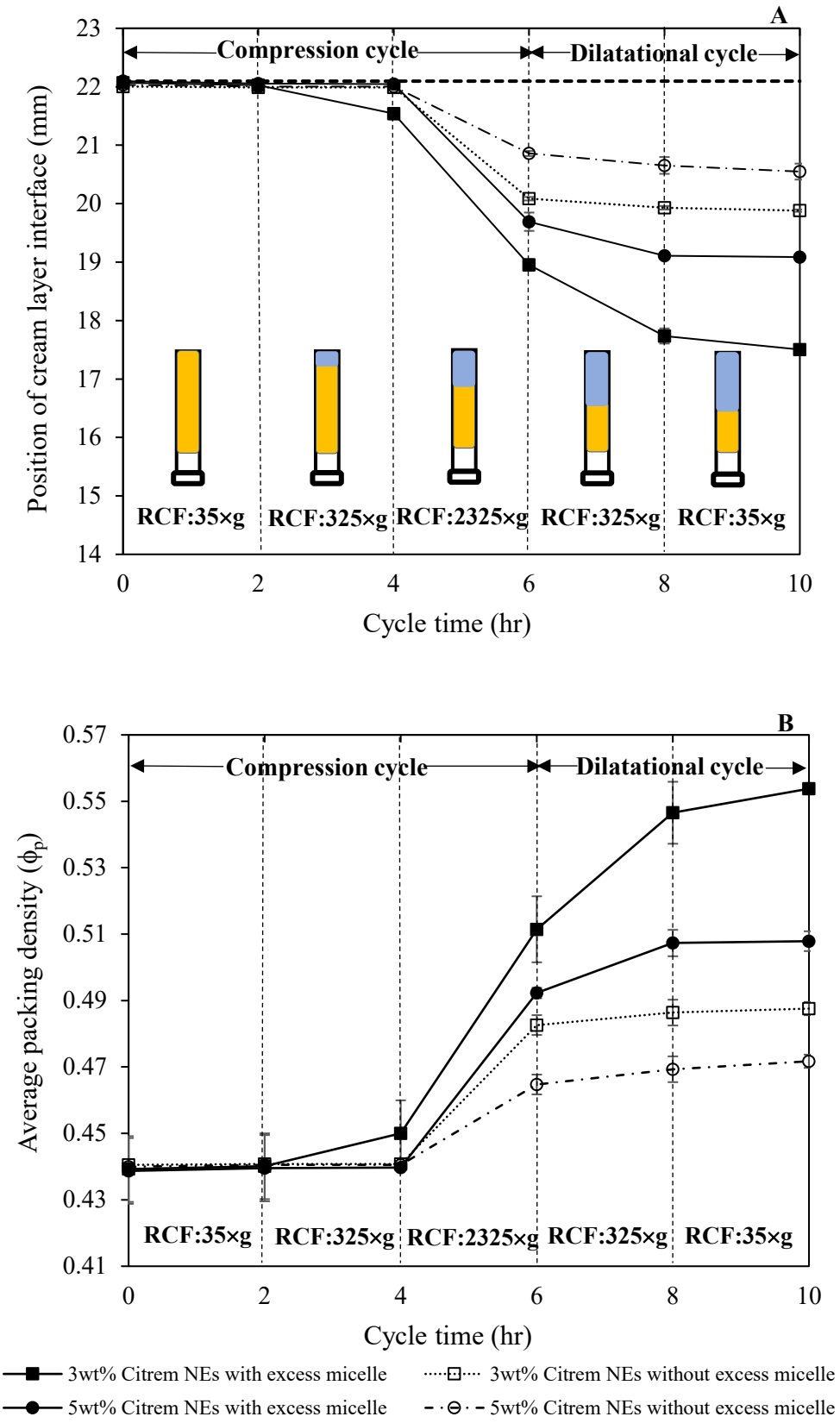
A
Compression cycle
Dilatational cycle
Position of cream layer interface (mm)
Cycle time (hr)
RCF:35×g
RCF:325×g
RCF:2325×g
RCF:325×g
RCF:35×g
B
Compression cycle
Dilatational cycle
Average packing density (ϕ_p)
Cycle time (hr)
RCF:35×g
RCF:325×g
RCF:2325×g
RCF:325×g
RCF:35×g
3wt% Citrem NEs with excess micelle
3wt% Citrem NEs without excess micelle
5wt% Citrem NEs with excess micelle
5wt% Citrem NEs without excess micelle

Figure 4.4 (A) Time course of the interfacial position of the cream layer, and (B) average packing density of nanodroplets calculated using Equation 4.4, under the compression – dilatational cycles of nanoemulsions with and without excess micelles in the aqueous phase. Relative changes in the height of the cream layer of 3 wt% Citrem nanoemulsion with excess micelles are schematically depicted by inverted centrifuge tubes in A, where yellow and blue colour indicates separated cream layer and the aqueous phase of nanoemulsion, respectively. The values of the successive relative centrifugation force (RCF) applied at an interval of 2 hrs are also shown in both the figures., Error bars indicate ± standard deviation ($n \geq 3$).

From this, it can be depicted that during the compression cycle, excess emulsifier micelles in the nanoemulsions led to an exclusion effect from the inter-droplet region due to increased osmotic pressure and hence attractive short-range depletion forces generated between the droplets, which were responsible for their weak flocculation (Figure 4.5Ba). Bharti et al. also showed that the packing density of silica nanoparticles-lysozyme hetero-aggregates increased as a function of ionic concentration, as the electrostatic repulsion among the protein stabilized nanoparticles were screened by the added salt leading to an increased attraction (Bharti et al., 2014). The network structure of flocculated droplets was further compressed on the dilatational cycle (Figure 4.5A and 4.5Ba) due to increased buoyancy pressure acting on them, leading to a structure collapse and a further increase in packing density (Krebs et al., 2013). It can also be said that the lower gel strength of the emulsions with excess micelles (Figure 4.5A) was not enough to retain their packing density intact during the dilatational cycle.

Opposite to that, lower packing density in the absence of excess micelles can be attributed to the strong electrostatic repulsive forces between the droplets, which did not allow them to pack in close proximity due to the thick electric double layer (Figure 4.5Bb). Therefore, the packing density remained lower than the nanoemulsions with excess micelles. Moreover, during the dilatational cycle, no significant change in packing density was observed as the close-packed structure has already reached equilibrium after the compression cycle and without the presence of any micelles, no change in interdroplet repulsive interaction was possible. The higher gel strength of the close-packed system (without excess micelles, Figure 4.5A) could also be responsible for retaining the packing density of the emulsions under the dilatational cycle.

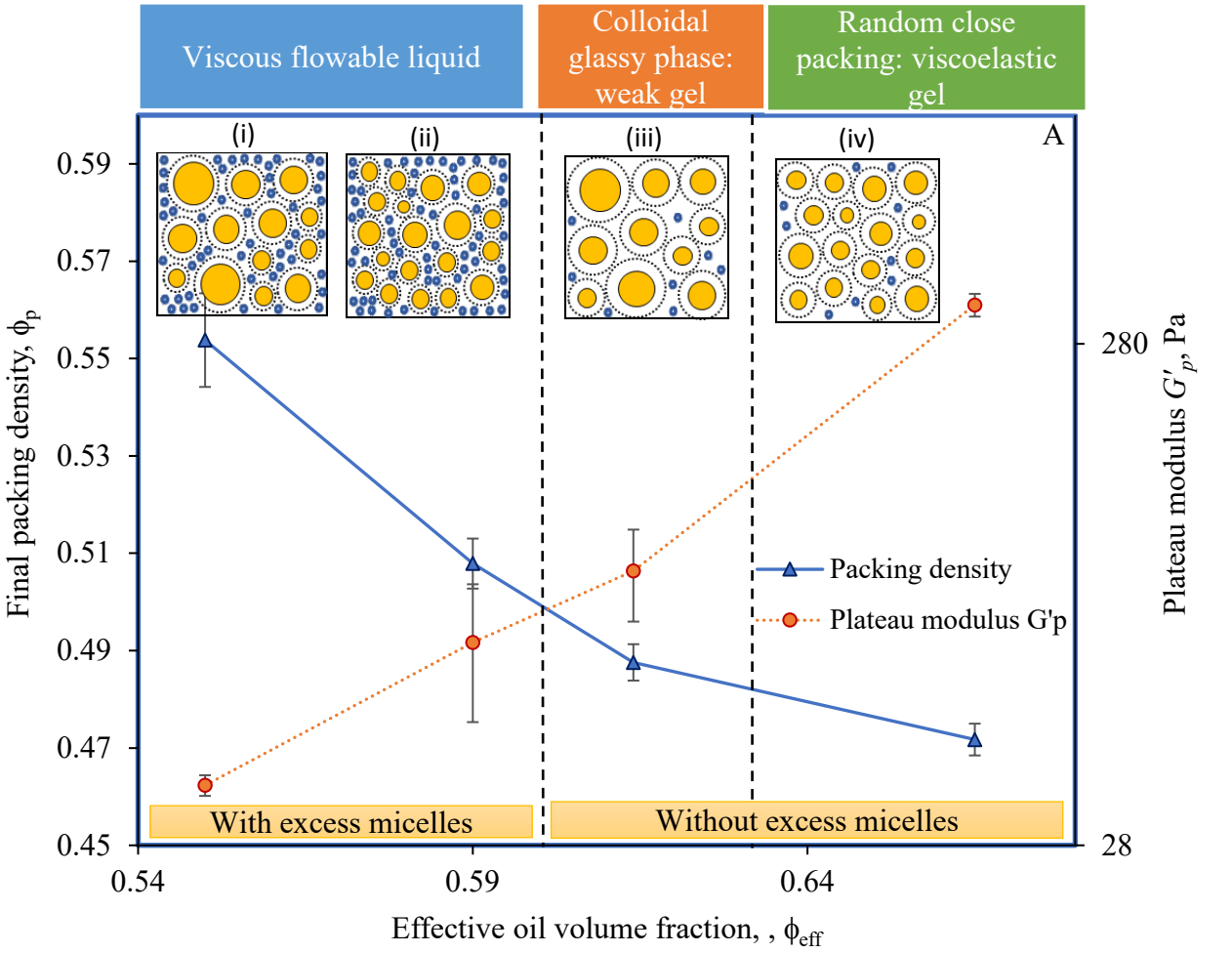
Viscous flowable liquid
Colloidal glassy phase: weak gel
Random close packing: viscoelastic gel
(i)
(ii)
(iii)
(iv)
A
Final packing density, ϕp
Plateau modulus G′p, Pa
0.59
0.57
0.55
0.53
0.51
0.49
0.47
0.45
280
28
Packing density
Plateau modulus G'p
With excess micelles
Without excess micelles
0.54
0.59
0.64
Effective oil volume fraction, , ϕeff

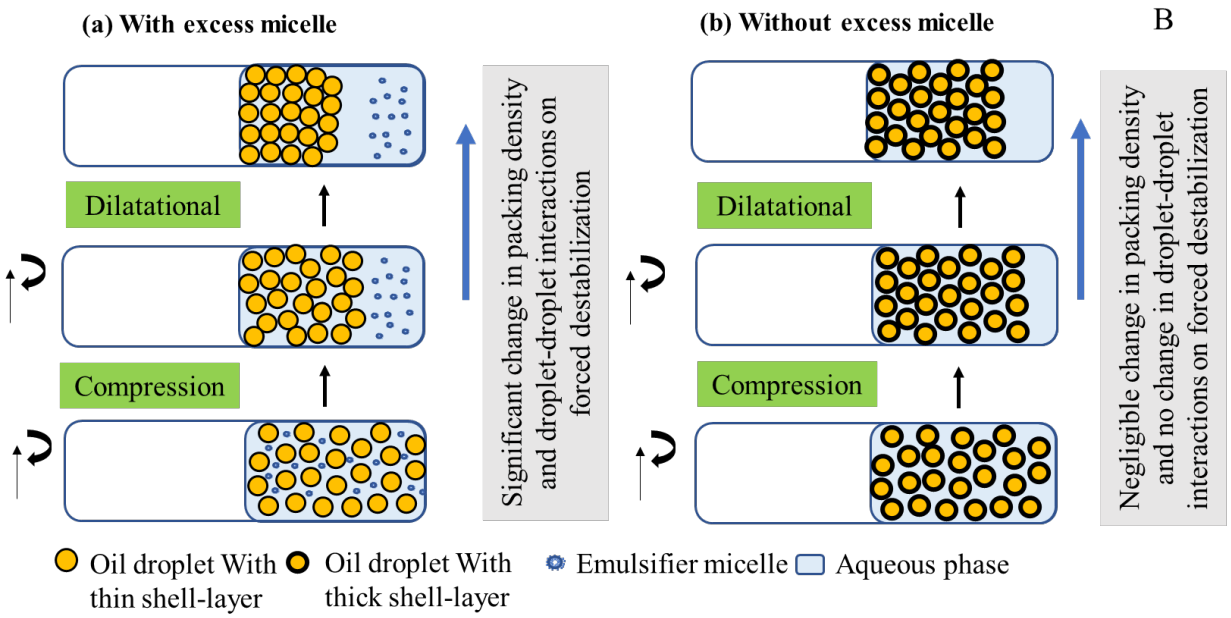
(a) With excess micelle
(b) Without excess micelle
B
Dilatational
Compression
Dilatational
Compression
Significant change in packing density and droplet-droplet interactions on forced destabilization
Negligible change in packing density and no change in droplet-droplet interactions on forced destabilization
Oil droplet With thin shell-layer
Oil droplet With thick shell-layer
Emulsifier micelle
Aqueous phase

Figure 4.5 (A) Relative changes in the final packing density (ϕ_p) of 3 wt% (i & iii) and 5 wt% (ii & iv) Citrem nanoemulsions obtained after the entire compression – dilatational cycles with respect to their effective volume fraction (ϕ_{eff}) and gel strength (G'_p) as a function of removal of excess micelles from the continuous phase. Error bars indicate ± standard deviation (n ≥ 3). (B) Schematic diagram of centrifuge tubes at accelerated gravitation showing the relation between packing density (ϕ_p) and effective volume fraction (ϕ_{eff}) of nanoemulsions (a) with and (b) without excess emulsifier micelles.

The packing density of droplets under compression is also governed by the rate of drainage of thin liquid film between the two approaching droplets. The rate of film drainage is a function of applied osmotic pressure (centrifugal force) as well as the surface or colloidal forces acting between the droplets (Bibette et al., 1992; Petsev & Bibette, 1995), which is expressed by the disjoining pressure (the force per unit area of a surface) (Stubenrauch & Von Klitzing, 2003). The disjoining pressure resist the rupture of the thin film between the droplets and prevent coalescence (Petsev et al., 1995; Sharma, 1978). However, the thin film between the two approaching droplets starts to rupture once the osmotic pressure acting on them reaches above a critical disjoining pressure (Bibette et al., 1992; Mason et al., 1997). The disjoining pressure starts to decrease with an increase in charge screening in the presence of excess ions from the anionic emulsifier micelles. Moreover, the excess emulsifier micelles can also raise the osmotic pressure to a level where it exceeds the critical disjoining pressure leading to rupture of thin film and droplets coalescence under compression. However, in our case, the applied osmotic pressure or centrifugal force (RCF) was always below the critical disjoining pressure which never allowed the droplets to coalesce (no change in droplet size even after multiple centrifugations to remove excess micelles, Figure 4.2). Apart from that the higher Laplace pressure of the nanodroplets would also be able to prevent deformation under the applied centrifugal force (Mason, 1999; Mason et al., 1997). However, the excess micelles-induced depletion interaction lowered the magnitude of overall repulsive forces leading to a decrease in disjoining pressure and increased film drainage rate and hence more ϕ_p was obtained under compression-dilatational cycles (Figure 4.5A).

Opposite to that, stronger electrostatic forces, i.e., higher disjoining pressure, in the absence of excess micelles helped to stabilize the thin liquid film between the droplets which allowed them to close pack at a higher separation distance with a lower ϕ_p (Figure 4.5A). Overall, the colloidal forces acting on the droplets has a major influence on the ϕ_p and rheology of the nanoemulsions.

Therefore, the application of analytical centrifuge in studying the packing behaviour of the nanodroplets under compression and dilatational cycles could be a novel way to predict the interdroplet interactions, long-term stability and gel strength of concentrated nanoemulsions. Such rapid tests could be extremely useful to understand the maximum forces a dispersion can withstand before breakdown, which could bring new insights into colloidal soft matters utilized in food, pharmaceuticals and cosmetics industry.

4.5 Conclusion

In this study, we have shown the usefulness of accelerated gravitation in a photo-centrifuge to predict the stabilization mechanism of nanoemulsions as a function of removal of excess micelles from the continuous phase. When the nanoemulsions with or without excess micelles were centrifuged at a range of RCF, only the flowable liquid nanoemulsions with 3 wt% Citrem and with excess micelles showed a linear relationship between creaming velocity and RCF that could be extrapolated to earth gravitation (RCF = 1). All other nanoemulsions showed a nonlinear trend with a critical RCF requirement to induce flow, indicating structure formation. The mechanisms of stability of the nanoemulsions in the presence and absence of excess micelles were also demonstrated by the change in the droplets packing behaviour under increasing (compression) and decreasing (expansion) RCF. The droplet packing density was found to decrease upon removal of excess micelles and with an increase in ϕ_{eff} and gel strength, and a decrease in average droplet size. It was proposed that during the compression cycle, excess emulsifier micelles led to attractive depletion force-induced aggregation among the nanodroplets. During the dilatational cycle, the aggregate structure collapsed, leading to a further increase in packing density. In contrast, the strong electrostatic repulsive force between the nanodroplets generated due to the removal of excess micelles led to the lowering of packing density, which did not change in the dilatational cycle as the close-packed structure was reached. Overall, studying the stability and packing density of droplets under accelerated gravity could be a viable and novel way to understand the inter-droplet interactions in a nano-colloidal system.

4.6 Connection to the next study

In this and the previous studies, the mechanism responsible for increasing the viscoelasticity and stability of nanoemulsions with and without excess emulsifier in the continuous phase was investigated. The reduction in droplet size and changes in the droplet-droplet interaction in the

presence and absence of excess emulsifier micelles were found to affect the rheology, stability, shelf-life and droplet packing behaviour. Especially, the packing density (ϕ_p) and the shape of RCF ramp curves obtained in this study were very useful to correlate with ϕ_{eff} and rheology data obtained for the nanoemulsions in the first study. Both the nanoemulsions (3 wt% and 5 wt%) showed improved stability upon removing excess micelles, but the increase in their gel strength was significantly different due to their droplet size differences. The 3 wt % Citrem nanoemulsions had a relatively larger droplet size and lower ϕ_{eff} compared to 5 wt % Citrem nanoemulsions, leading to a weak gel structure in the former. To further increase the ϕ_{eff} and gel strength at lower ϕ, in the next Chapter, we increased the interfacial thickness (δ) around the Citrem-stabilized nanodroplets by layer-by-layer (LbL) deposition of chitosan as a second layer using one-step mixing method described in Chapter 2.4.1.

5. EFFECT OF DEPOSITION OF CHITOSAN SECOND LAYER ON THE GELATION AND CONTROLLED DIGESTION OF CITREM-CHITOSAN BILAYER-STABILIZED EMULSION GELS[3]

5.1 Abstract

The influence of chitosan concentration (0-0.25 wt%) and degree of deacetylation (DDA 50% and 93%) on the formation, rheology and digestibility of Citrem-chitosan bilayer oil-in-water emulsions was studied. The bilayer emulsions were prepared by the electrostatic deposition of positively charged chitosan on Citrem-stabilized anionic oil droplets. The droplet size gradually increased from < 0.5 μm for the primary emulsion to 5 – 10 μm at an intermediate chitosan concentration (0.05-0.15 wt%) due to bridging flocculation. At higher concentrations of chitosan (0.2 and 0.25 wt%), droplets were smaller (1.7-3.6 μm) and repulsively stabilized due to complete coating with chitosan. The droplet charge changed from –48 mV to +41.4 and +54.5 mV after the surface saturation by DDA 50 and DDA 93 chitosan, respectively. The strain and frequency-dependent rheology indicated that with an increase in chitosan concentration, emulsions changed from viscoelastic liquid for monolayer emulsion to strong elastic gel due to bridging flocculation at an intermediate chitosan concentration and then to repulsive gel at the complete coverage, which was confirmed using visual observation of the emulsion gels and their confocal microstructure. The bilayer emulsions at surface saturation showed higher viscosity, gel strength, lower creep compliance, and higher structural recovery than the monolayer emulsion due to an increase in effective oil volume fraction towards close packing resulting from the expansion of interfacial steric barrier and charge cloud thickness. The rate of free fatty acid release and overall lipid digestibility during *in vitro* digestion of the primary emulsion was significantly increased when gastric lipase was introduced. The overall lipid digestibility was 25.7% for monolayer emulsion,

[3] Submitted to the journal Food and Function for peer-review: Kadiya, K., & Ghosh, S. (2021). Effect of chitosan concentration and degree of deacetylation on the gelation and controlled digestion of Citrem-chitosan bilayer-stabilized emulsion gels. *Food & Function. Manuscript# FO-ART-07-2021-002409.* Kadiya, K. carried out the experiments and wrote the first draft. Ghosh, S. conceptualized, supervised, reviewed, and edited.

which decreased with an increase in chitosan concentration and reached the lowest at surface saturation to 17.5%. The modification of interfacial composition, rheology and microstructure of emulsions stabilized with Citrem-chitosan bilayer shown to control lipid digestibility by delaying the action of gastric and pancreatic lipases, which was confirmed using confocal microscopy. Such bilayer emulsion gels can be utilized for fat reduction and controlled delivery of lipophilic components in food.

5.2 Introduction

Emulsions are an integral part of many industries such as food, cosmetics, personal care, and pharmaceuticals. A wide range of emulsions, from dilute to highly concentrated, with a variety of different appearance, stability, rheology, taste, and release behaviour of internal active components, are manufactured depending on the final application. In particular, in the food industry, concentrated emulsions with products such as creams, sauces, butter, margarine, salad dressings, mayonnaise, and spreads are of great importance in which the emulsion structure controls the overall properties of the final product (McClements, 2015). The food structure and the functionality of such products can be controlled by tuning the emulsion droplet size and volume fraction, interfacial composition, and inter-droplet interactions (Helgeson, 2016; Kim & Mason, 2017; McClements, 2015; McClements & Li, 2010; Nejatian & Abbasi, 2019).

Many researchers have shown that the conversion of conventional emulsions with repulsive inter-droplet interaction into nanoemulsions can significantly affect their rheology (Abbasian Chaleshtari et al., 2020; Erramreddy & Ghosh, 2015; Nejatian & Abbasi, 2019; Nejatian et al., 2018). Considering the core-shell structure of emulsion droplet, the repulsive gelation in concentrated nanoemulsion can be achieved at a significantly reduced oil volume fraction (ϕ_{oil}), according to Equation 5.1, compared to the conventional emulsion (Tadros et al., 2004; Weiss & McClements, 2000; Wilking & Mason, 2007).

$$\phi_{eff} = \phi_{oil}\left(1+\frac{\delta}{r}\right)^3 \tag{5.1}$$

Where ϕ_{eff} is the effective oil volume fraction, r is the droplet radius and δ is the droplet interfacial shell layer thickness. Wilking & Mason were the first to mention repulsive gelation in sodium dodecyl sulphate (SDS)-stabilized 40 wt% silicone oil-in-water (O/W) nanoemulsions with a significant increase in storage moduli (G′) when the droplet size was reduced below a

critical level (Wilking & Mason, 2007). The gelation in nanoemulsion was attributed to the increase in ϕ_{eff} of the droplets beyond maximum random jamming (MRJ) due to the reduction in r and increase in δ due to the presence of repulsive charge cloud at the interface. The droplets and their charge clouds are compressed due to close packing leading to a jamming transition and a drastic increase in nanoemulsions' viscoelasticity at an actual oil volume fraction far below the MRJ (Wilking & Mason, 2007). Subsequently, many research works have studied the impact of the type and concentration of emulsifiers on the rheology of nanoemulsions. For example, Erramreddy and Ghosh (2014) showed an increase in gel strength of 40 wt% canola O/W nanoemulsion stabilized by SDS compared to non-ionic Tween 20 due to an increase in the thickness of the repulsive charge cloud around the nanodroplets, which was absent in the case of Tween 20. In another study, Patel, Mohanan, et al. (2019) showed that sodium caseinate-stabilized O/W nanoemulsions were transformed into viscoelastic gels below a critical droplet size while whey protein stabilized-nanoemulsions remained liquid at the same droplet size, which was ascribed to the higher thickness of the random-coil casein steric barrier compared to globular whey proteins. In our previous study, we have also shown an increase in the gel strength of 3 wt% and 5 wt% Citrem (citric acid ester of mono and diglycerides)-stabilized 40 wt% O/W nanoemulsions upon removal of excess micelles from the continuous phase due to an increase in the thickness of repulsive barrier around the nanodroplets (Kadiya & Ghosh, 2019). Such improved elastic behaviour of nanoemulsion could make it an alternative structured material for various low-fat food applications.

Although we were able to achieve the repulsive gelation in 5 wt% Citrem-stabilized nanoemulsions at 40 wt% oil by reducing the droplet size (Kadiya & Ghosh, 2019), our focus for this study was to achieve gelation at a lower concentration of Citrem (3 wt%), hence with larger droplet size, and lower oil content (< 40 wt%) by further increasing the interfacial shell-layer thickness. One strategy to increase the interfacial shell-layer thickness is to employ a layer-by-layer (LbL) electrostatic deposition, which is based on the sequential adsorption of oppositely charged biopolymer to form the stable polyelectrolyte shell layer around the droplet (Chun et al., 2013; Guzey & McClements, 2006; Mundo et al., 2020). The main benefit of the LbL technique is that the composition, thickness, and charge of the interfacial layers can be modified for specific end applications by varying the polyelectrolytes (Li et al., 2020). Various charged polysaccharide molecules used for electrostatic deposition could impart both repulsive electrostatic and steric

barriers to the emulsion droplets (Dickinson, 2011; Guzey & McClements, 2006; Li et al., 2020). One critical aspect of this process is the removal of the excess non-adsorbed emulsifier present in the continuous phase of primary emulsion since the excess emulsifier would interfere with the subsequent coating by the second layer of oppositely charged biopolymer (Guzey & McClements, 2006; Li et al., 2020). Further, the amount and type of polysaccharide used to coat the primary emulsion droplets greatly influence the stability of the multilayer emulsions. Too little polysaccharide concentration between the droplets can promote bridging flocculation, whereas too high can lead to depletion flocculation (Huang et al., 2019; Li et al., 2019). Hence, it is a prerequisite to optimize the biopolymer concentration during the formation of multilayer emulsions without promoting droplet flocculation.

Chitosan is a natural linear cationic polysaccharide molecule derived from the alkaline deacetylation of chitin. Chitosan is widely used for multilayer emulsion formation because it is a unique cationic polysaccharide with generally recognized as safe (GRAS) status (Bouyer et al., 2012). The amino groups (pKa ~ 6.5) of chitin exposes upon deacetylation, which provides the positive charge to chitosan in acidic pH (Rinaudo, 2006; Shahidi et al., 1999). Chitosan with different degrees of deacetylation (DDA), i.e., with different magnitude of positive charge, can be obtained by varying the chitin extraction and treatment condition. So far, chitosan has been used to form the multilayer emulsion with an objective to improve the stability of dilute (oil concentration < 15 wt%) emulsions against environmental stresses such as a change in pH and ionic strength as well as to improve the stability against lipid oxidation, thermal treatment, freeze-thaw cycles, and drying (Aoki et al., 2005; Fang et al., 2019; Gudipati et al., 2010; Noshad et al., 2016; Noshad et al., 2015; Ogawa et al., 2003a, 2003b; Xiong et al., 2018; Xu et al., 2016; Zhang et al., 2015). Mun, Decker, and McClements (2006) have shown the effect of chitosan molecular weight and DDA on the droplet characteristics and stability of dilute emulsions (3 wt% oil) stabilized by SDS-chitosan or Tween 20-chitosan bilayer. Many researchers have also reported controlled digestibility and delivery of bioactives for dilute multilayer emulsions and attributed these results to the thick coating provided by chitosan and to the various phenomena involved during the digestion steps (Jo et al., 2019; Klinkesorn & McClements, 2010; Li et al., 2010; Mun, Decker, Park, et al., 2006; Zhang et al., 2015). For example, Gudipati et al. (2010) reported lower digestibility of fish oil due to chitosan secondary layer on Citrem-stabilized 0.5 and 5 wt% O/W primary emulsion. Kaasgaard and Keller (2010) demonstrated that coating Citrem-stabilized oil

droplets with 0.2 wt% chitosan improved flavour retention and redispersibility of the freeze-dried carvone emulsions. However, to our knowledge, the effect of LbL deposition of chitosan on the structure-functionality of concentrated bilayer emulsions has never been explored. Therefore, the objective of the present study was to examine the effect of chitosan deposition, with different concentrations and DDA, on the rheology and microstructure of the Citrem-chitosan-stabilized bilayer concentrated emulsion gels. It was hypothesized that the adsorbed chitosan molecules would form an improved steric barrier around the Citrem-stabilized droplets that would help to achieve gelation in emulsion at a lower oil volume fraction and larger droplet size than that was reported before (Kadiya & Ghosh, 2019). Further, we also studied the effect of deposition of chitosan second layer on the lipid digestibility. It was also hypothesized that the gastric stability of the thick chitosan layer would also help to control the lipid digestibility of the bilayer emulsions compared to the monolayer emulsion.

5.3 Materials and methods

5.3.1 Materials

Refined Canola oil was purchased from the local supermarket and stored away from the light at room temperature (RT, 25 ± 2°C). Ultrapure deionized water (conductivity 1.0 μS/cm) was used as the aqueous phase to prepare emulsions and any other chemicals. A food-grade anionic emulsifier, Citric acid esters of monoglycerides (Citrem) of HLB 9 to 10, was donated by Palsgaard Inc. (Morris Plains, NJ, USA). Chitosan (brand name ChitoClear®), a cationic polymer with a degree of deacetylation (DDA) of 93%, was purchased from the Primax ehf., Iceland. Digestive enzymes such as porcine pepsin (P7012), pancreatic lipase (L3126), bile extract (B8631), porcine pancreatin extract (8xUSP specifications, P7545), calcium chloride and any other chemicals used for the preparation of digestion fluids were purchased from Sigma-Aldrich (St. Louis, MO, USA). Lipase from Rabbit Gastric Extract (RGE-25) was purchased from Lipolytech® (Marseille, France) and used for gastric lipolysis. Sodium hydroxide pellets for preparing 1N NaOH and a standard solution of 1N HCl were purchased from VWR International (Edmonton, AB, Canada). All other chemicals were purchased from Sigma-Aldrich (St. Louis, MO, USA).

5.3.2 Preparation of Primary emulsion

The aqueous phases were prepared by dissolving 3 wt% of food-grade emulsifier Citrem at its pre-determined melting point of 61°C (data not shown). Canola oil (40 wt%) was added to the 60% aqueous phase at pH 7 to prepare coarse O/W emulsion using a rotor-stator mixer (Polytron, Brinkmann Instruments, ON, Canada) for 60 s at 20,000 rpm. The coarse emulsion was then subjected to eight cycles of high-pressure homogenization (EmulsiFlex-C3, Avestin Inc., Ottawa, ON, Canada) at 20,000 psi. Citrem-stabilized emulsions obtained this way were stored away from the light at room temperature (RT, 25 ± 2°C) in 120 mL glass bottles (VWR International, Edmonton, AB, Canada) for further experiments.

5.3.3 Preparation of bilayer secondary emulsions

To prepare the secondary emulsion with a Citrem-Chitosan bilayer, it is essential to remove the excess Citrem from the continuous phase of the primary emulsion. For this, Citrem emulsions were ultracentrifuged two times at 52,070 × g for 1.5 h following a method explained in (Appendix C, Figure C1) and developed by Kadiya and Ghosh (2019). The removal of excess Citrem did not show a change in the droplet size of re-dispersed and re-homogenized emulsion (data not shown). The Citrem stabilized emulsion obtained by this way was adjusted to pH 4 using 1N HCl, where the oil droplet carried a negative charge. The second layer of positively charged chitosan with different degrees of deacetylation (DDA 93% and 50%) was deposited by layer-by-layer electrostatic deposition technique at pH 4 according to Kaasgaard and Keller Kaasgaard and Keller (2010). The chitosan DDA 50% was prepared from DDA 93% according to Method C2 (Appendix C). The methods for determining actual DDA and their Raman spectra are also given in Appendix C (Method C2 and Figures C2 and C3). The 2.5 wt% stock solutions of DDA 50 and DDA 93 chitosan were prepared in 100 mM acetate buffer at pH 4 and used in different proportions for depositing a second layer on the Citrem-stabilized droplets. The formulation and amount of chitosan (DDA 93% and 50%) used to prepare bilayer emulsions are mentioned in Table C1 (Appendix C). For example, 20 g of 0.25 wt% Chitosan bilayer emulsion prepared by adding 18 g of Citrem emulsion dropwise, under continuous magnetic stirring, into a 60 mL glass bottle containing 2 g of 2.5 wt% Chitosan solution of either DDA 93% or DDA 50%. Similarly, 20 g of control emulsion with 0 wt% Chitosan was prepared by replacing the equal quantity of chitosan solution with the 100 mM pH 4 acetate buffer. Thus, bilayer emulsions, obtained with a range of

chitosan concentration from 0 wt% to 0.25 wt%, had a final oil concentration of 36% (Appendix C, Table C1). All the emulsions were stored overnight in the same glass bottle at room temperature (RT, 25 ± 2°C) for further analysis.

5.3.4 Droplet size and Droplet charge

Droplet or aggregate size in the emulsions was analyzed by a static laser diffraction technique, using the Mastersizer 2000 (Malvern Instruments, Montreal, QC, Canada) with a relative refractive index of the dispersed vs. continuous phases as 1.465. Distilled water was used as a dispersant in the instrument, and the obscuration was brought up to ~12% by dropwise sample addition. The average droplet size of emulsion was characterized by Sauter mean diameter (d_{32}).

The droplet charge as a function of chitosan concentration was determined using a zeta potential analyzer (Zetasizer Nano-ZS90, Malvern Instruments, Westborough, MA, USA). To minimize the multiple scattering effects during analysis, the emulsion was diluted in the same ionic environment using a 100 mM pH 4 acetate buffer to a final droplet concentration of approximately 0.01 wt% oil before analysis. Similarly, the chitosan solutions with DDA 50 and DDA 93 were also analyzed for their zeta potential to confirm the DDA effect on their magnitude of positive charge, which would have a considerable impact on the final characteristics of the bilayer emulsions.

5.3.5 Rheology of emulsions

The flow behaviour and viscoelasticity of emulsions as a function of chitosan concentration were evaluated using an AR G2 rheometer (TA Instrument, New Castle, DE, USA) at 25°C. A pre-determined quantity of emulsion was carefully transferred onto the Peltier plate of the rheometer using a spatula, and the flow behaviour or gel strength was measured at a 1000 μm gap using a 40 mm diameter cross-hatched geometry. Viscosity was measured by applying a shear rate in the range of 0.1 to 100 s^{-1}, whereas two different types of oscillatory measurements were used to characterize the viscoelastic behaviour of the samples. The strain sweep measurements were performed at 0.01–100 % strain and a constant frequency of 1 Hz (6.28 *rad*/s) to determine the linear viscoelastic region (LVR). A constant amplitude (0.1% strain) was chosen within the LVR to perform the frequency sweep measurements as a function of frequency ranging from 0.1 to 100 *rad*/s.

Creep-recovery tests were carried out to measure the compliance for liquid and gelled emulsions as a function of chitosan concentration. During creep compliance measurement, constant stress was applied to the samples instantly and maintained for 300 s. After removing stress, recovery compliance was recorded for the following 300 s. The constant stress pre-determined from LVR (from strain sweep) was 0.25, 5, and 50 Pa for liquid, weak gel and strong gel emulsions, respectively. The compliance versus time was plotted as a function of chitosan concentration, and from that, %Recovery (γ_{RE}) from deformation was determined by using peak compliance (J_{max}) and recovery compliance (J_{RE}), as shown in Equation 5.2.

$$\%Recovery = \left[\frac{(J_{max} - J_{RE})}{J_{max}}\right] \times 100 \quad (5.2)$$

5.3.6 *In vitro* lipid digestion of emulsions

Digestion assembly and set up: Static *in vitro* lipid digestion of mono- and bilayer Citrem-chitosan emulsions were performed in a 100 mL double-wall jacketed reaction vessel connected to a water bath maintained at 37°C. The whole set was mounted on the pH-STAT assembly (907 Titrando, Metrohm, Switzerland) to monitor lipid digestibility at different stages of digestion (Appendix C, Figure C4A). Activities of all the enzymes were analyzed and used as a reference to calculate the appropriate amount necessary for each digestion step, according to the INFOGEST protocol (Brodkorb et al., 2019).

Specific considerations: The gastric and intestinal digestion protocol was used according to Brodkorb et al. (2019) with some specific modifications for pH-STAT setting as follows: (1) The electrolyte formulation for the digestive fluids changed to NaCl instead of $NaHCO_3$, because the latter was responsible for the abrupt change in pH when using pH-STAT settings (Mat et al., 2016); (2) gastric lipolysis was performed for 2 h (Appendix C, Figure C4B), using rabbit gastric lipase (RGL), which was divided into upper gastric phase at pH 5.5 for 1 hr (by considering the 50% gastric emptying rate of food in a real digestive system), and lower gastric phase at pH 3 for 1 hr (Sams et al., 2016); (3) use of optimized mass ratio of colipase to lipase (1:2 w/w) for maximum activity of pancreatin lipase (Salhi et al., 2020); (4) consideration of degree of dissociation (α_{FFA} = 0.54) of carboxylic groups of free fatty acids (FFA) liberated during the intestinal digestion at pH 7, because at this pH, depending on the pKa, fatty acids are not fully ionized (Chatzidaki et al., 2016; Mat et al., 2016).

Digestion protocol: Briefly, 5 g of emulsions was weighed in a 100 mL reaction vessel followed by the addition of 5 mL of simulated salivary fluid (SSF) in the absence of α-amylase because no starch was present in the emulsion. The purpose of adding SSF was to maintain proper electrolyte concentration and proper dilution for gel or liquid emulsions. To attain 37°C temperature, the digestion mixture was stirred for two minutes using three propeller stirrers mounted on pH-state assembly. To begin with upper gastric digestion, a 10 mL mixture of simulated gastric fluid (SGF) and gastric enzymes were added to the system, and then the pH was adjusted to 5.5 using 1N HCl. The gastric enzymes, pepsin and rabbit gastric lipase (RGL) were added to achieve the final enzyme activities of 2000 U and 120 U per mL of gastric digestion mixture, respectively. The upper gastric phase was run for 1 h, and then for the next 1 h of lower gastric phase digestion, the pH was reduced to 3 using 1N HCl. After 2 h of total gastric digestion, 20 mL mixture consisted of simulated intestinal fluid (SIF), bile extract solution (10 mM bile salts in the final mixture), pancreatin extract with pancreatin lipase (100 U/mL trypsin and 2000 U/mL lipase activity) were added and the pH was adjusted to 7 using 1N NaOH in the final digestion mixture. The intestinal digestion phase was also run for 2 h. The release of FFA due to the action of gastric and pancreatin lipase on the emulsion led to a decrease in the pH due to the generation of H^+, which was monitored using an automatic titration unit (907 Titrando, Metrohm, Switzerland) with pH-STAT programming maintained at static a pH necessary for the digestion step with 0.1 N NaOH. Titration blank for the digesta was performed in the absence of enzymes, and the volume of NaOH used was deducted from the respective titration volume of the sample. The digestion curves were obtained for three replicates with a data acquisition frequency of 2 per s. From the data obtained, in terms of NaOH volume (0.1 N), the kinetics of reaction that occurred at different stages of digestion were converted into percentage FFA released using Equation 5.3.

$$\%\, FFA\ release = \frac{V_{NaOH} \times M_{NaOH} \times Mw}{\alpha_{FFA} \times m \times 2 \times 1000} \times 100 \qquad (5.3)$$

Where V_{NaOH} and M_{NaOH} are the volume and molarity of titrant NaOH respectively, Mw is the molecular weight of the triglyceride in canola oil (877 g/mol) (Guo et al., 2017), m is the mass of oil in emulsions (g), and α_{FFA} is the degree of dissociation of the carboxylic group of FFA at pH 7 (0.54 in this study) (Mat et al., 2016), and 2 in the denominator indicates every triglyceride molecule liberates two FFA.

5.3.7 Microstructure of emulsions

Emulsions microstructure for different chitosan concentrations (0%, 0.075%, 0.15% and 0.25%) for chitosan DDA 50 and DDA 93 were evaluated using a Nikon C2 confocal laser scanning microscope (CLSM) (Nikon Inc., Mississauga, ON, Canada). The oil phase was stained using 0.01 wt% of Nile red before emulsification. A 543 nm laser was used to excite the Nile red, and emission spectra were collected in the range of 573-613 nm. During digestion, mono- and bi-layer emulsion samples were taken before and after gastric and intestinal digestion and evaluated for microstructure using CLSM. Chitosan in the emulsion was also stained by adding 0.01 wt% fast green in the continuous phase and detected with a 633 nm laser for excitation, and the emission spectra were collected using a 650 nm long-pass filter. All microstructure images were captured using a 60 × Plan Apo VC (numerical aperture 1.4) oil immersion objective lens and 2.5× digital zoom.

5.3.8 Statistical analysis

All experiments were conducted with at least three replicates, and results were reported as the mean ± standard deviation. The statistical significance and analysis of variance (ANOVA) were performed with a 95% confidence level ($p < 0.05$) using OriginPro version 2020 software (OriginLab Corporation, Northampton, MA, USA).

5.4 Results and discussion

5.4.1 Characteristics of chitosan polymer

Chitosan with a lower DDA was prepared by introducing acetyl groups onto the amino groups of the original chitosan with higher DDA according to the method explained in Appendix C (Method C2). Figure 5.1 shows the changes in %DDA of chitosan upon reacetylation and its effect on the positive charge at pH 4. The original commercial sample of chitosan had an average DDA of 92.1 ± 1.7%. After reacetylation, chitosan with a lower DDA of 51.9 ± 2.9% was obtained. The two different chitosan samples, in the context of their expected DDA, were designated as DDA 93 and DDA 50, respectively. A chemical modification such as reacetylation of chitosan also resulted in a change in the Raman spectra (Appendix C, Figure C3). Chitosan is a linear polymer molecule made up of repetitive units of Glucosamine (GlcN) and Glucosamine acetyl (GlcNAc). The amount of acetyl groups attached to glucosamine molecules decides the degree of

deacetylation or the magnitude of the positive charge of chitosan polymer (Ma et al., 2009). The changes in the intensity of the two functional groups, amide II (NH) at 1591 cm^{-1} and carbonyl (CO) at 1658 cm^{-1}, are associated with the content of GlcN and GlcNAc units in chitosan, respectively (Zając et al., 2015). The lower intensity of amide II (1591 cm^{-1}) and higher intensity of CO (1658 cm^{-1}) was observed in the chitosan DDA 50, compared to chitosan DDA 93, indicating increase of GlcNAc units in Chitosan DDA 50 upon reacetylation. On the other side, the higher intensity of amide II (1591 cm^{-1}) in the chitosan DDA 93 was related to the higher content of GlcN. A similar increase in the intensity of amide II (1591 cm^{-1}) was reported upon deconvolution of the Raman contours of chitosan samples with DDA ranging from 70% to 95% (Zając et al., 2015). At low pH, the glucosamine (GlcN) groups are protonated and positively charged. Decreasing the free amino groups reduced the positive charge of DDA 50 chitosan. Hence, the charge density along the polymer chain of chitosan can be reduced by decreasing the degree of deacetylation. From Figure 5.1, it can be seen that the positive charge of chitosan reduced from + 92.6 ± 5.4 mV to + 65.9 ± 1.6 mV upon reacetylation (reduction of DDA from 92.1% to 51.9%).

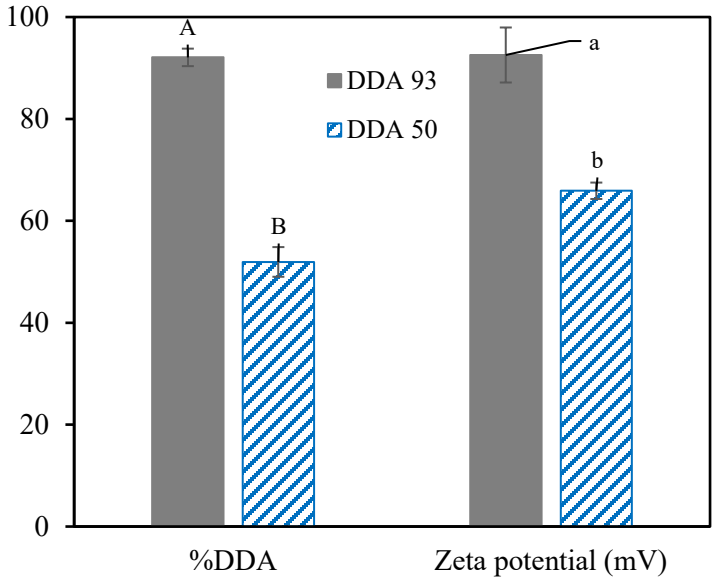

Figure 5.1 Changes in DDA and zeta potential (at pH 4) of chitosan DDA 93 upon reacetylation. DDA for both the chitosan DDA 50 and DDA 93 was calculated using Equation S4. Note that chitosan with 92.1% and 51.9% DDA is indicated by DDA 93 and DDA 50, respectively. Error bars indicate ± standard deviation (n ≥ 3). Different uppercase (for %DDA) and lowercase (for zeta potential) letters denote the statistical significance (at 0.05 level) difference amongst the population means.

5.4.2 Droplet size and zeta potential of emulsions

Figures 5.2A and 5.2B show the effects of chitosan type and concentration on the droplet or aggregate size and zeta potential of the Citrem-chitosan-stabilized bilayer emulsions, respectively. The average droplet size (d_{32}) and charge of monolayer emulsion were 0.42 ± 0.14 μm and – 48 ± 2.6 mV in the absence of chitosan, respectively. With the addition of either DDA 50 or DDA 93 chitosan as a second layer, at a lower concentration (0.05 wt% to 0.075 wt%), the average size was increased to 1.98 ± 0.82 μm and 1.28 ± 0.21 μm in the case of DDA 50 and DDA 93 chitosan, respectively. From Figure 5.2B, it can also be seen that the addition of positively charged chitosan neutralized the negative charge of Citrem-stabilized droplets, thereby decreasing the charge and reaching an almost zero value for the whole system at 0.075%wt chitosan, irrespective of their DDA. This could be the reason for the initial increase in the average aggregate size of emulsions at a lower concentration of chitosan where the opposite charge of chitosan polymer chains seeks to make the electrostatic complexes between the positively charged amino groups of D-glucosamine molecules of chitosan with the negatively charged citric acid residues of Citrem at pH 4 (Bruinsmann et al., 2019). This favours the interactions of chitosan polymer with multiple Citrem-stabilized droplets leading to bridging flocculation.

At an intermediate chitosan concentration (0.1 wt%), the average size of the aggregate reached a maximum, 5.75 ± 1.06 μm and 10.34 ± 1.86 μm for DDA 50 and DDA 93 chitosan, respectively. The bilayer droplet charge became positive at this chitosan concentration and reached +24.88 ± 0.87 mV and +41.92 ± 5.68 mV for DDA 50 and DDA 93 chitosan, respectively. At this concentration, the droplet surfaces were partially covered with chitosan molecules, which promoted inter-droplet attraction between the positive patches on the surface of one droplet and negative patches on another (Liu et al., 2019). It is possible that such inter-droplet attraction led to a weak network throughout the emulsion leading to a significant increase in aggregate size detected by the particle size analyzer (Dickinson & Pawlowsky, 1997). A similar increase in droplet or aggregate size was also overserved at lower concentrations (0.05 to 0.1%) of chitosan due to bridging flocculation of the WPI-Flaxseed gum stabilized droplets (Xu et al., 2016).

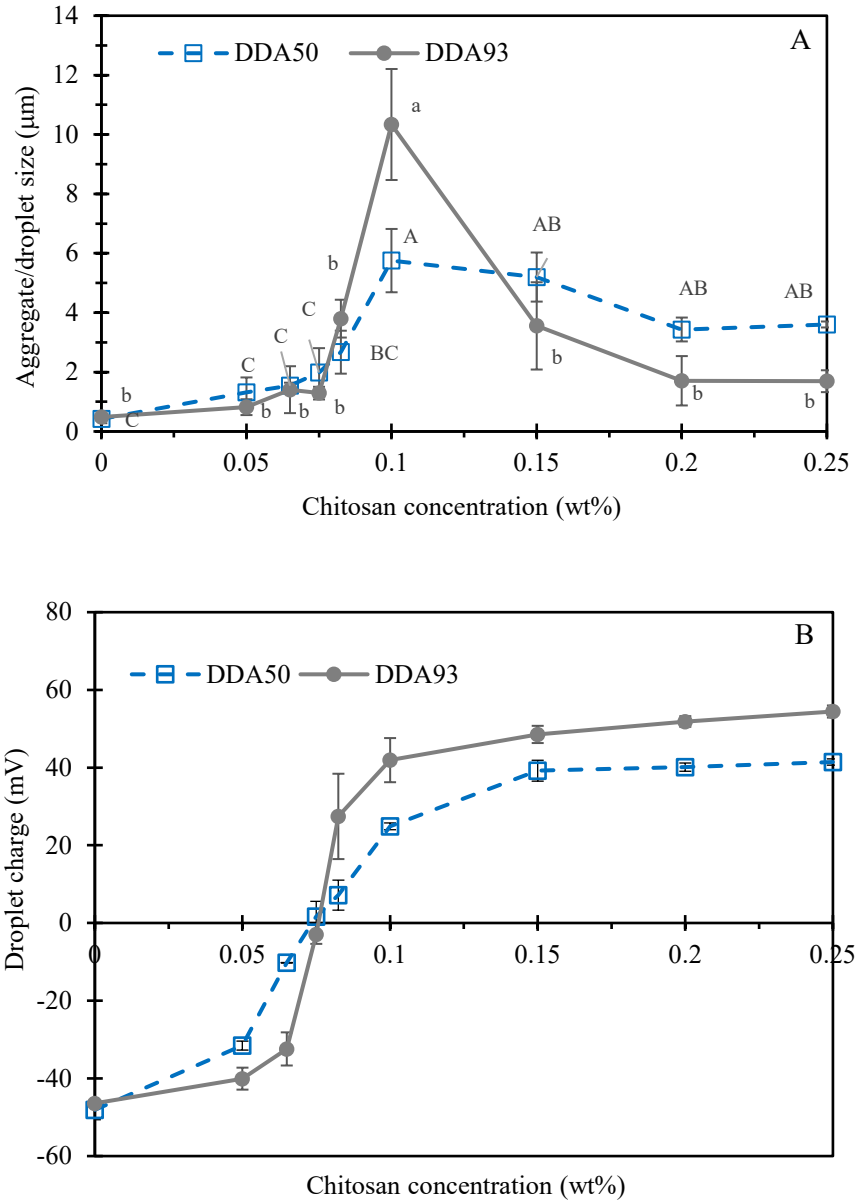

Figure 5.2 Changes in (A) Droplet or aggregate size (B) Droplet charge of emulsions as a function of chitosan concentration and degree of deacetylation (%DDA). Error bars indicate ± standard deviation (n ≥ 3). Different uppercase (for DDA 50) and lowercase (for DDA 93) letters denote the statistical significance (at 0.05 level) difference amongst the population means.

With the further addition of chitosan (0.15 wt%), the average size of the aggregates reduced to 5.20 ± 0.82 µm and 3.55 ± 1.46 µm, for DDA 50 and DDA 93 chitosan, respectively. However, the charge of the bilayer droplets reached almost plateau at +39.20 ± 2.68 mV and +48.53 ± 2.21

mV, for DDA 50 and DDA 93 chitosan, respectively. At this point, we have enough chitosan to reach the surface saturation of some of the Citrem stabilized droplets. Therefore, bridging flocculation is replaced by combined electrostatic and steric repulsion between the Citrem-chitosan-coated droplets leading to a significant reduction in a droplet or aggregate size. A similar phenomenon of re-stabilization of the emulsion was also observed by Dickinson and Pawlowsky (1997) in the case of bovine serum albumin (BSA)–*i*-carrageenan coated droplets.

At an even higher concentration of chitosan (0.2 wt%), the smallest droplet size of 3.43 ± 0.1 μm and 1.71 ± 0.36 μm was observed for DDA 50 and DDA 93 chitosan, respectively. At 0.25 wt% chitosan, droplet size remained unchanged, indicating no sign of aggregation. At 0.2 wt%, zeta potential reached +40.12 ± 1.06 mV and +51.87 ± x1.36 mV, for DDA 50 and DDA 93 chitosan, respectively, which increased insignificantly when chitosan concentration was increased further to 0.25 wt%, suggesting that the Citrem-stabilized droplets have been saturated with chitosan. Such an increase in the zeta potential (positive charge) with an increase in the chitosan concentration and reaching to surface saturation was also reported in other studies where the primary emulsion was stabilized by the Citrem (Gudipati et al., 2010; Kaasgaard & Keller, 2010). Most droplets are coated with chitosan at this saturation point and appeared as single droplets along with droplet aggregates due to some open patches of negatively charged Citrem primary later. A similar drop in droplet size at a high concentration of polysaccharide was also observed by Dickinson and Pawlowsky (1997) for their BSA–*i*-carrageenan coated droplets and by Xu et al. (2016) for chitosan interaction with whey protein isolate (WPI)–flaxseed gum (FG)-stabilized droplets.

Interestingly, even with a higher magnitude of positive charge (Figure 5.1) in the case of DDA 93 chitosan compared to DDA 50 chitosan, no early bridging flocculation of droplets was observed (no significant difference in aggregate size from 0.05 to 0.075 wt% chitosan). This observation is in contrast with Mun et al. who reported that the differences in charge density of 40% and 92% DDA chitosan had a significant effect on the tendency of bridging flocculation of SDS (sodium dodecyl sulphate) stabilized primary emulsions (Mun, Decker, & McClements, 2006). Interestingly, although DDA 50 chitosan had a less positive charge, it lowered the negative zeta potential more at a lower concentration (0.05 and 0.065 wt%) than DDA 93 chitosan, which could be due to more interaction of low charge-density chitosan with the droplets. The high charge of extensive GlcN groups of DDA 93 chitosan is distributed throughout the polymer chain;

however, for DDA 50, it is possible that that the reacetylation happened heterogeneously, leading to the formation of a region of charged GlcN groups (block copolymers) (Franca et al., 2011; Gatto et al., 2019), which could lead to a more preferential interaction of DDA 50 with oil droplets.

At 0.075 wt% chitosan concentration, however, the charge of the droplets became almost zero for both chitosan molecules, indicating a lower amount of high-charge DDA 93 chitosan is actually attached to the droplets. Beyond this charge neutralization, DDA 93 chitosan-coated droplets always showed a higher positive charge compared to DDA 50 chitosan-coated droplets. At 0.1 wt%, the maximum aggregate size was significantly higher for DDA 93 than DDA 50, which could be due to greater inter-droplet attraction due to the higher charge of DDA 93 chitosan. At a higher concentration of chitosan at the surface saturation, aggregate size for DDA 93 became significantly smaller than aggregates size of DDA 50 coated droplets, which could be attributed to higher electrostatic repulsion in the case of the former as the zeta potential of the droplets was significantly higher for DDA 93 compared to DDA 50. Mun, Decker, and McClements (2006) also demonstrated that the positive ζ-potential of the droplets increased as the charge density of the chitosan molecules increased. Overall, the increase in chitosan concentration and charge density helps to stabilize bilayer emulsions through increased steric and electrostatic repulsions.

5.4.3 Rheological behaviour of bilayer emulsions

5.4.3.1 Flow behaviour of bilayer emulsions

All emulsions with different chitosan types and concentrations showed a decrease in viscosity with an increase in shear rate (Figures 5.3A and 5.3B), indicating shear thinning behaviour. However, while strong shear thinning behaviour was observed for DDA 50 chitosan, shear-thinning of DDA 93-stabilized emulsions was reduced at the highest concentration (0.25 wt%) compared to all other concentrations (0.05 to 0.15 wt%). Shear-thinning behaviour in bilayer emulsions has been well-reported in the previous literature (Anvari & Joyner, 2017a; Hou et al., 2010; Klongdee et al., 2012). Interestingly, a low shear plateau in viscosity was observed at minimum (0 wt%) and maximum (0.25 wt%) concentrations of DDA 50 and DDA 93 chitosan, which can be ascribed to Newtonian behaviour of the emulsions. For all other intermediate concentrations (0.05 to 0.15 wt%), there was a steep linear decrease in the viscosity since the beginning of 0.01 s^{-1} shear, indicating the presence of droplet's network, which broke down under the application of even a very low shear (McClements, 2015).

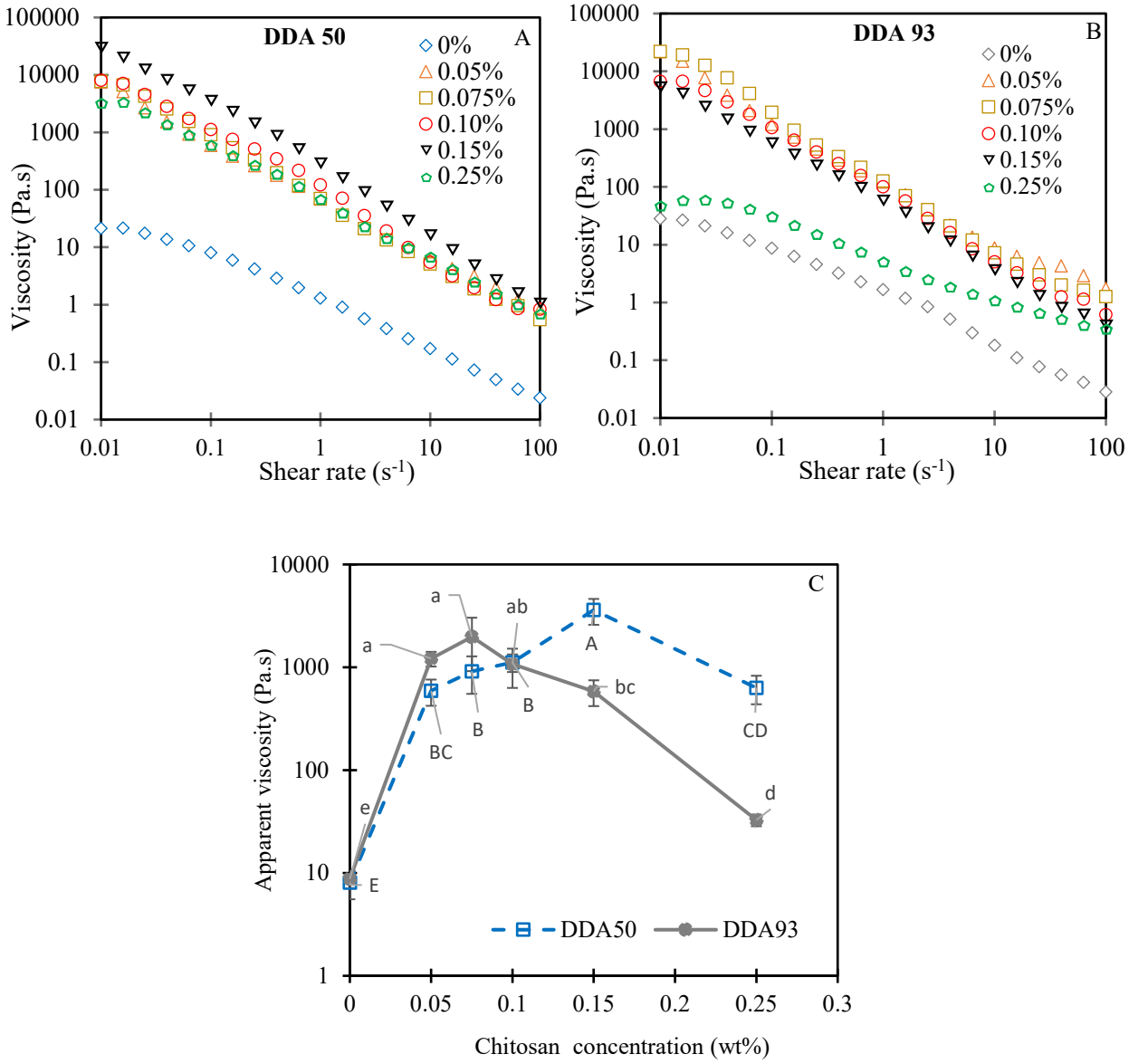

Figure 5.3 Effect of Chitosan concentration and DDA on the apparent viscosity of emulsions. Viscosities of (A) DDA 50 and (B) DDA 93 emulsions were measured as a function of shear rate (C) Apparent viscosity at a constant shear rate (0.1 s^{-1}) as a function of chitosan concentration and DDA. Error bars indicate ± standard deviation (n ≥ 3). Different uppercase (for DDA 50) and lowercase (for DDA 93) letters denote the statistical significance (at 0.05 level) difference amongst the population means.

In order to directly compare the viscosity of emulsions, the apparent viscosity at 0.1 s^{-1} is plotted in Figure 5.3C as a function of chitosan concentration and charge (DDA). The addition of chitosan increased the viscosity of emulsions from 8.8 Pa.s at 0% chitosan to 591 Pa.s and 1216

Pa.s at 0.05 wt% for DDA 50 and DDA 93, respectively. With a further increase in chitosan concentration, the apparent viscosity increased to a maximum 1978 ± 105.89 Pa.s at 0.075 wt% DDA 93, while for DDA 50, the maxima in viscosity (3608 ± 101.7 Pa.s) was reached at 0.15 wt% DDA 50. Higher viscosity for DDA 93 added emulsion at a lower concentration could be attributed to larger droplet aggregates, as observed in Figure 5.2A. At 0.15 wt% DDA 93 chitosan, some droplets started becoming saturated with chitosan, leading to a greater electrostatic repulsion (higher zeta potential, Figure 5.2B) and breakdown of droplet aggregates, leading to a significant drop in viscosity. However, for DDA 50 chitosan, due to the lower magnitude of positive charge compared to DDA 93 (Figure 5.1), a higher amount of the former would be required to saturate the droplet surface and to increase the electrostatic repulsion between the droplets. Therefore, the aggregate size remained higher for 0.15% DDA 50 chitosan, leading to increased viscosity to a maximum value. At an even higher concentration of 0.25 wt%, the apparent viscosity started reducing and reached 632 Pa.s and 33 Pa.s for DDA 50 and DDA 93, respectively. At this time, droplets are saturated with chitosan and the increased electrostatic and steric repulsion between the droplets minimized the droplet aggregation, which is evident from the reduction in aggregate size (Figure 5.2A) leading to a decrease in viscosity. Similar observations have been reported previously where the viscosity of lecithin-stabilized emulsions increased and then decreased with an increase in chitosan concentration (Klongdee et al., 2012). The bilayer emulsion with 0.25 wt% DDA 50 showed much higher viscosity than DDA 93 chitosan, which could be attributed to the heterogeneous distribution of charge on DDA 50 as discussed before, leading to more extended hydrophobic patches on the polymer and hence more droplet aggregation (Franca et al., 2011; Gatto et al., 2019).

Although the viscosity of Citrem-chitosan-stabilized bilayer emulsions at 0.25 wt% chitosan showed the lowest viscosity of all chitosan-added emulsions, their viscosity was significantly higher compared to Citrem-stabilized monolayer emulsions (0 wt% chitosan), which could be attributed to the higher electrostatic and steric repulsion around the droplets leading to an increased effective volume fraction of the dispersed phase. This phenomenon is further discussed in section 3.6. It should be noted that any free chitosan molecules in the bulk phase have a negligible contribution in increasing the viscosity of emulsions. A stock solution of 2.5 wt% chitosan showed apparent viscosity (at 0.1 s^{-1}) of only 2.36 and 0.79 Pa.s for DDA 50 and DDA 93 chitosans,

respectively, which is more than an order of magnitude lower than the bilayer emulsion with 0.25 wt% chitosan (data not shown).

5.4.3.2 Viscoelastic behaviour of emulsions

The change in viscoelastic behaviour of Citrem-chitosan bilayer emulsions was studied by analyzing the strain and frequency-dependent storage (G′) and loss (G″) moduli. Figures 5.4A and 5.4B show the change in strain-dependent G′ and G″ of Citrem-chitosan emulsions as a function of chitosan concentration for DDA 50 and DDA 93, respectively. All the emulsions exhibited predominantly elastic behaviour, where G′ was higher than G″ within the strong linear viscoelastic region (LVR) irrespective of the chitosan concertation and charge. Moreover, the addition of chitosan initially increased the moduli of the bilayer emulsions up to a certain concentration and reduced after that until a critical concentration of chitosan was added to reach surface saturation. This can also be seen in Figure 5.4C, where the plateau moduli (G'_p) taken at 0.1% strain was plotted as a function of chitosan concentration and type. At 0 wt% chitosan, where the negatively charged Citrem stabilized the droplets, G'_p was very low, 25 Pa for DDA 50 and 36 Pa for DDA 93, which was increased to 6912 Pa and 7726.5 Pa at 0.05 wt% for DDA 50 and DDA 93 chitosan, respectively. Further addition of chitosan up to 0.15 wt% showed a slightly different effect for the two different DDA. For DDA 50, gel strength slightly decreased at 0.075 wt% chitosan, followed by an increase to maximum gel strength (8064.5 Pa) at 0.15 wt%. For DDA 93, gel strength decreased gradually to (3097.1 Pa) till 0.15 wt%. Beyond 0.15 wt%, the gel strength dropped rapidly to 849.1 Pa and 522.9 Pa for DDA 50 and DDA 93 chitosan, respectively.

To understand the force required for gel breakdown, the crossover strain of G′ and G″ was also calculated (Figure 5.4D). In the absence of chitosan, crossover strain was very low (7%), indicating viscous component of the emulsions became dominant at such a low strain value. With the addition of 0.05 to 0.10 wt% of chitosan, the crossover strain increased rapidly and reached almost seven (~ 48%) to ten-fold (~76%) for both chitosans, indicating the dominance of the elastic component at a high range of strain. This was followed by a rapid drop in crossover strain to ~20% at 0.15 wt% for DDA 50, while for DDA 93, crossover strain remained relatively high (~ 48%) till 0.15 wt%, followed by a drop to ~28% at 0.25 wt% chitosan. Lower crossover strain for DDA 50 chitosan at surface saturation could mean brittleness in the gel structure, which could be due to the larger aggregate size of the former compared to DDA 93.

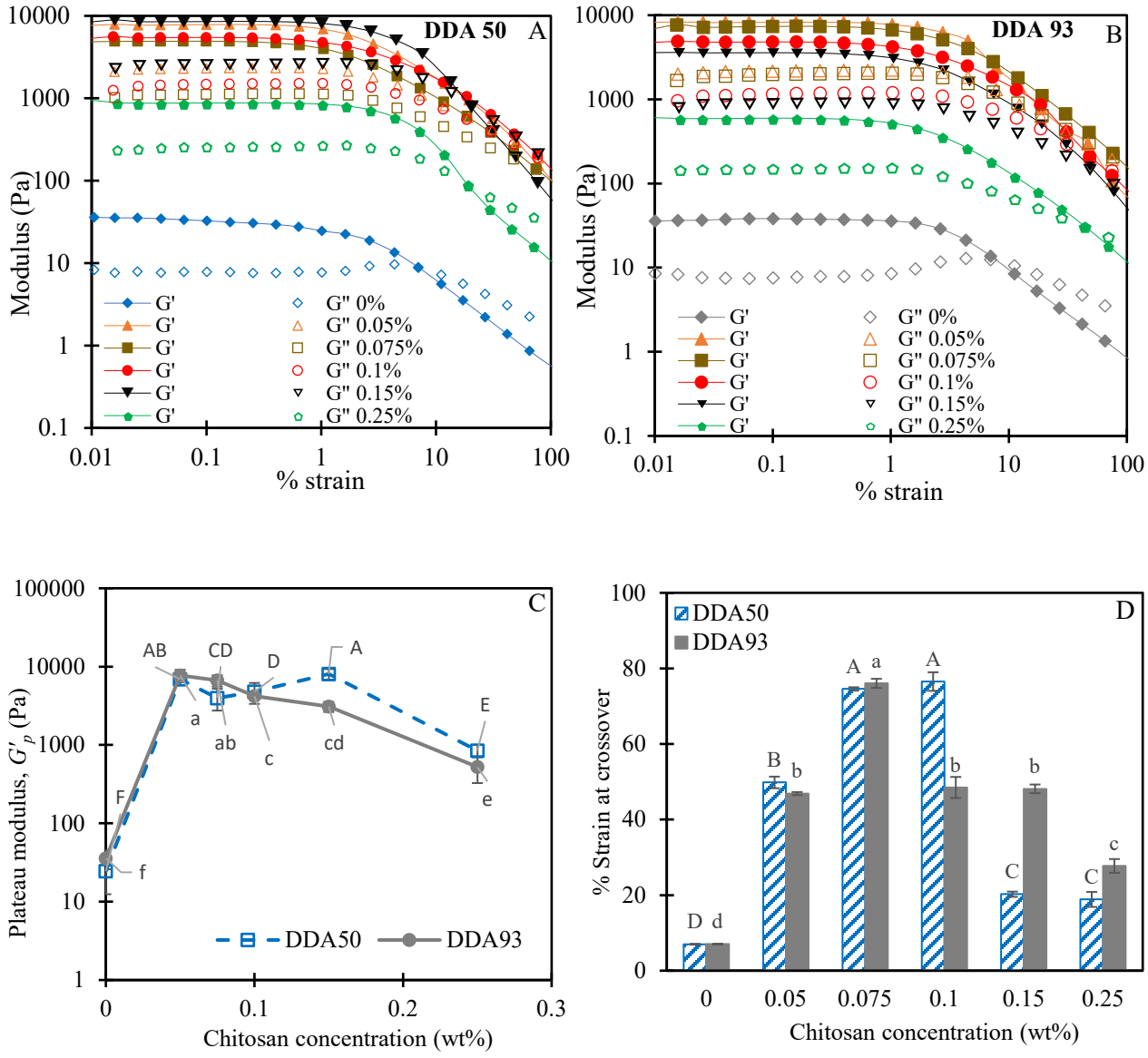

Figure 5.4 Effect of chitosan concentration and DDA on the gelation behaviour of emulsions. Strain dependent storage (*G′*) and loss (*G″*) moduli of (A) DDA 50 and (B) DDA 93 emulsions were recorded as a function of chitosan concentration (C) Values of plateau storage modulus (G'_p) at 0.1% strain, and (D) %Strain at *G′* and *G″* crossover were plotted as a function of chitosan concentration and DDA. Error bars indicate ± standard deviation (n ≥ 3). Different uppercase (for DDA 50) and lowercase (for DDA 93) letters denote the statistical significance (at 0.05 level) difference amongst the population means.

We have also studied the change in the frequency-dependent moduli of emulsions as a function of chitosan concentration and charge (Figures 5.5A and 5.5B for DDA 50 and DDA 93,

respectively). All the emulsions showed G′ higher than G″ with some degree of frequency dependency. For better comparison, changes in G′ of emulsions at 10 rad/s as a function of chitosan concentration and the charge was plotted in Figure 5.5C. Frequency-dependent G′ also showed a very similar trend as in strain-dependent G'_p (Figure 5.4C). The addition of chitosan DDA 50 and DDA 93 to Citrem emulsions at 0.05 wt% to 0.15 wt% showed a drastic increase in G′ to many folds compared to the primary emulsions attributed to strong bridging flocculation when sufficient concentration of chitosan was not available to coat the droplets. On the other side, the higher gel strength of DDA 93 emulsions compared to DDA 50 emulsions at 0.05 to 0.1 wt% chitosan could be explained by their higher magnitude of positive charge, which could have bridged many droplets strongly. At 0.15 wt% chitosan, the gel strength of the DDA 50 emulsion became higher than the DDA 93 emulsion, which was similar to strain-dependent viscoelastic behaviour (Figure 5.4C). As discussed above, this could be due to the larger aggregate size for the emulsions with DDA 50 chitosan. At the highest chitosan concentration (0.25 wt%), the gel strength of both emulsions decreased drastically, and both the DDA 50 and DDA 93 emulsions showed an almost similar value of G′, but still 10 times higher than primary emulsions. Such higher gel strength at surface saturation could be mainly due to the increased steric repulsion by the chitosan layer around the Citrem-chitosan stabilized droplets (see section 3.6 for further discussion). It has been indicated that if electrostatically stabilized droplets in emulsions have a sufficiently long-range steric repulsion, the increased ϕ_{eff} of the droplets could slow down their movement, and the emulsions would behave like a viscoelastic gel (Patel, Mohanan, et al., 2019). Therefore, by increasing chitosan concentration, the rheology of monolayer emulsion was transformed from a flowable liquid-like material to a self-supporting elastic gel due to droplet aggregation at 0.1 wt% and finally into a repulsive bilayer viscoelastic gel at 0.25 wt%. In a similar work, Hou et al. (2010) observed that the addition of chitosan up to 1.0 wt% in soluble soybean polysaccharide (SSPS)-stabilized 10 wt% MCT (medium-chain triglycerides) O/W emulsions promoted the formation of the viscoelastic structure due to extensive droplet flocculation. However, the authors did not observe a decrease in aggregate size and lower gel strength at higher chitosan concentrations. The excess SPSS in the continuous phase probably formed a complex with chitosan, leading to droplet aggregation and increased viscosity and gel strength. In contrast, in the present case, excess Citrem was removed from the aqueous phase of emulsion before chitosan addition; hence the biopolymer only interacted with the Citrem-stabilized oil droplets.

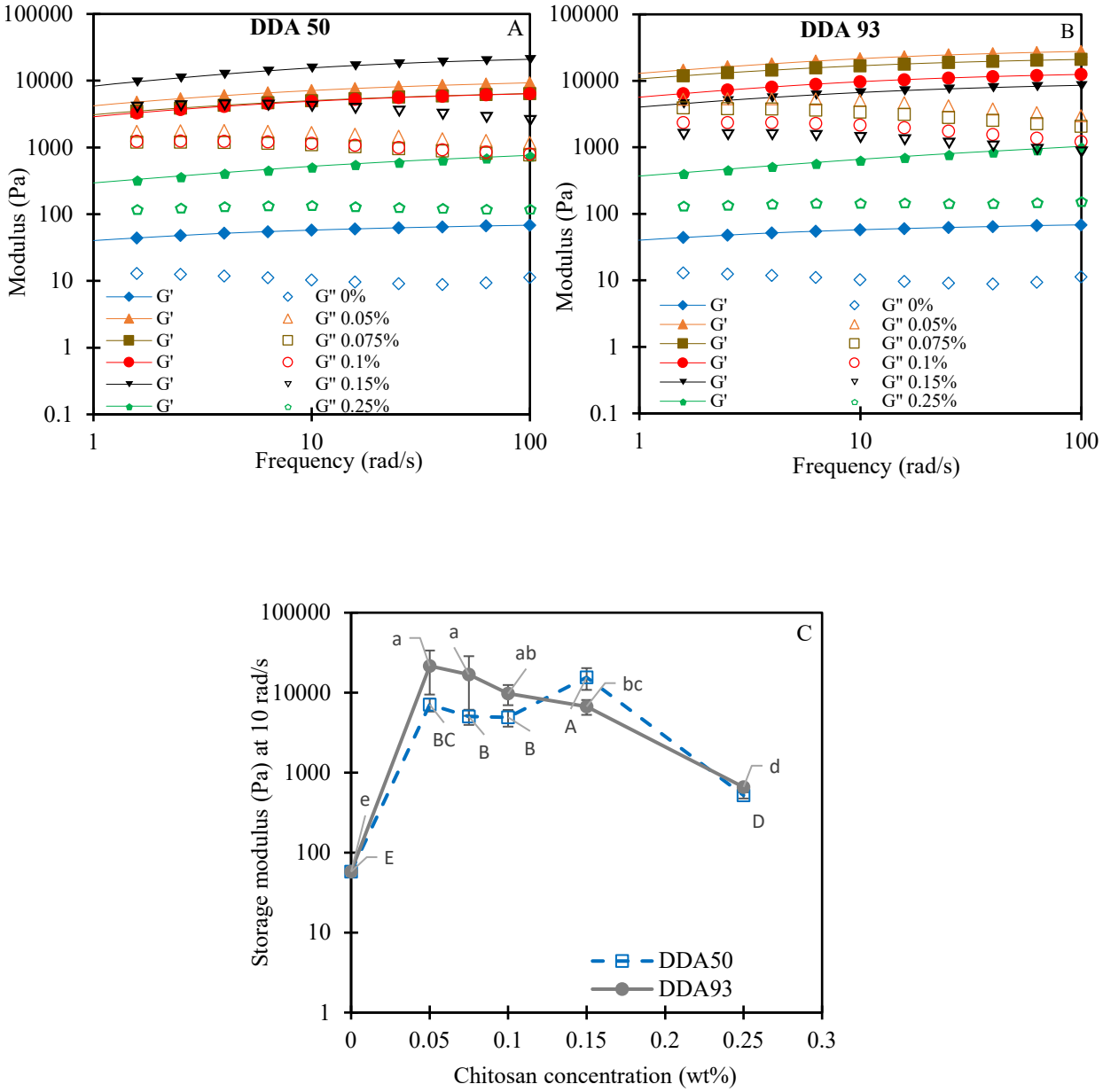

Figure 5.5 Effect of chitosan concentration and DDA on the gelation behaviour of emulsions. Frequency-dependent storage (*G′*) and loss moduli (*G″*) of (A) DDA 50 and (B) DDA 93 emulsions were recorded as a function of chitosan concentration (C) Values of storage modulus (*G′*) at 10 rad/s was plotted as a function of chitosan concentration and DDA. Error bars indicate ± standard deviation (n ≥ 3). Different uppercase (for DDA 50) and lowercase (for DDA 93) letters denote the statistical significance (at 0.05 level) difference amongst the population means.

5.4.3.3 Creep and recovery compliance of emulsions

To better understand the behaviour of emulsion gel under applied stress, creep-recovery analysis was carried out within the linear viscoelastic region. The creep compliance (J_E), deformation per unit stress, is a useful parameter for studying structural or phase-behaviour changes in the colloidal system. It signifies the softness of material under the applied stress as a function of time. Higher J_E is an indicator of more deformation, therefore weaker or softer material structure and vice versa (Sozer, 2009). The recovery in the structure as a function of time can be explained by regaining strain when the applied stress is released. The more the recovery of strain, the better is the material's elastic properties (Huang et al., 2016). Creep-recovery curves of the emulsions with DDA 50 and DDA 93 chitosan at different concentrations are shown in Figures 5.6A and 5.6B, respectively. The creep compliance (J_E) was noticeably higher for the monolayer emulsions (0 wt% chitosan). However, J_E decreased to a large extent as DDA 50 or DDA 93 concentration increased to 0.05 wt% to 0.15 wt% chitosan, suggesting the formation of stiffer material that does not deform much under applied stress. Further addition of DDA 50 and DDA 93 chitosan (0.25 wt%) again increased the creep compliance, suggesting more deformation and softer material. Figure 5.6C shows the peak compliance (J_{max}) plotted as a function of chitosan concentration and charge. The chitosan concentration had a significant ($p < 0.05$) effect on the J_{max}, whereas the chitosan charge did not show any significant effect on the J_{max} ($p > 0.05$). At 0 wt% chitosan, J_{max} was 38 Pa^{-1}, which was reduced to < 0.1 Pa^{-1} with the increase in chitosan concentration up to 0.15 wt% but increased again to ~ 1 Pa^{-1} at 0.25 wt% chitosan concentration.

After releasing the applied stress on emulsions, the recovery of the structure in terms of the %recoverable strain (γ_{RE}) was plotted in Figure 5.6D. The higher recoverable strain (γ_{RE}) is indicative of more elasticity in the emulsion structure. The recoverable strain (%γ_{RE}) was also affected significantly ($p < 0.05$) as a function of chitosan concentration, but not on the DDA values ($p > 0.05$). In the absence of chitosan, 0 wt% chitosan, γ_{RE} was < 10%, which was increased to 60% to 70% with the addition of both DDA 50 and DDA 93 chitosan up to 0.15 wt%, which again reduced to 40% to 50% at 0.25 wt% chitosan. Overall, higher deformation with less structure recovery in the absence of chitosan could be due to the liquid-like behaviour of monolayer emulsions. In contrast, lower deformation and higher structure recovery at intermediate chitosan concentration (0.05 to 0.15 wt%) could be explained by the increased elasticity of the chitosan-mediated bridged droplet network. It is important to note that the bilayer emulsions with droplets

completely coated at 0.25 wt% chitosan showed relatively less deformation and increased structural recovery compared to monolayer emulsion, which can be attributed to an increase in the electrostatic repulsion and steric barrier between the Citrem-chitosan-stabilized bilayer droplets (see section 5.4.6 for further discussion).

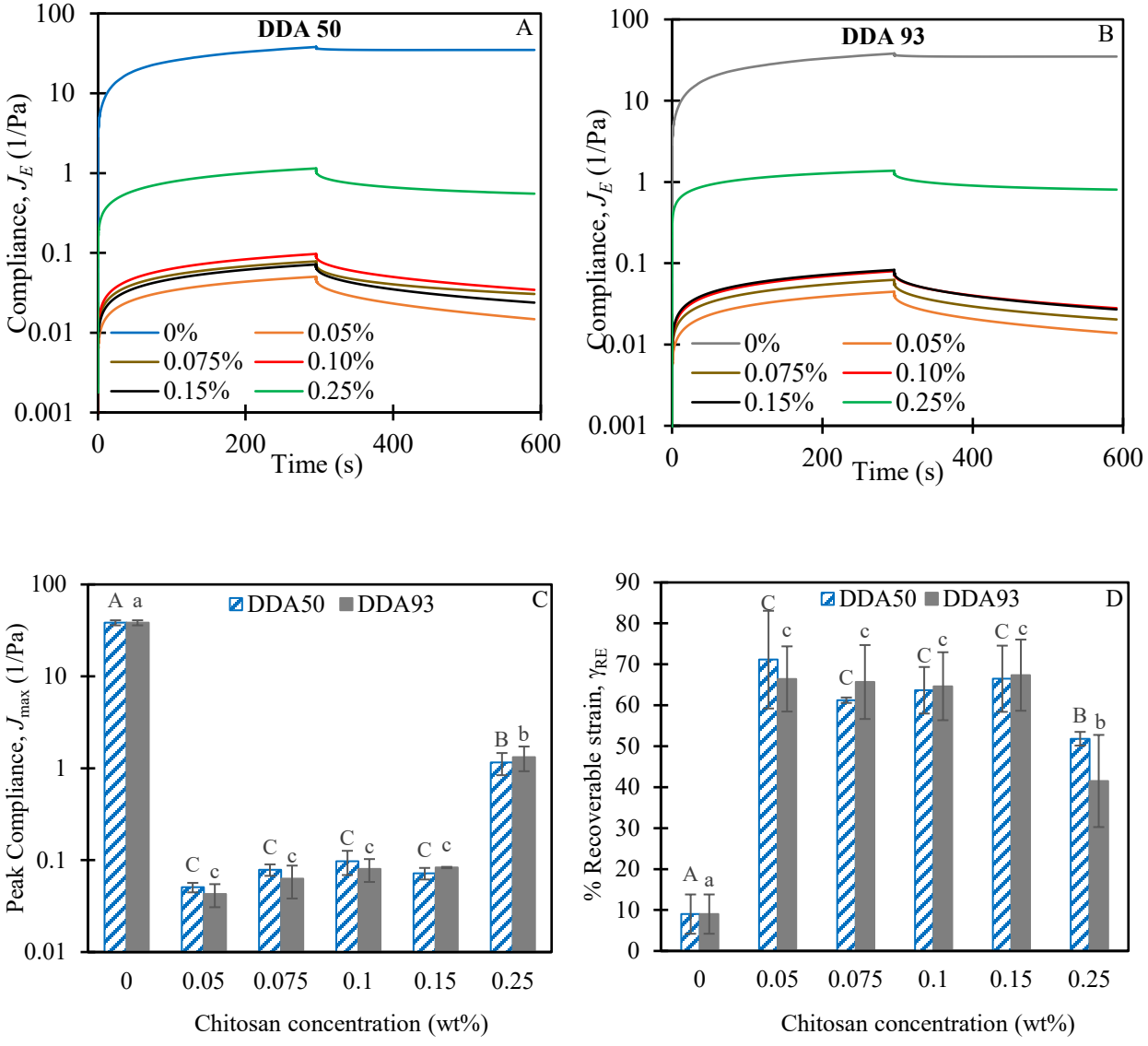

Figure 5.6 Creep-recovery curves of (A) DDA 50 and (B) DDA 93 emulsions were recorded as a function of chitosan concentration by applying the constant stress within the LVR limit. (C) Peak compliance (J_{max}) and (D) %Recoverable strain (γ_{RE}) was calculated using Equation 5.2 and plotted as a function of chitosan concentration and DDA. Error bars indicate ± standard deviation (n ≥ 3). Different uppercase (for DDA 50) and lowercase (for DDA 93) letters denote the statistical significance (at 0.05 level) difference amongst the population means.

5.4.4 Visual observation of emulsions

A range of viscoelastic behaviour of the bilayer emulsions can also be seen from their visual observation (Figure 5.7). In the absence of chitosan, the monolayer emulsions were flowable liquids (Figures 5.7A, B i) without any visual sign of aggregates. However, the addition of 0.075 and 0.15 wt% chitosan transformed them into elastic gels (Figures 5.7A, B ii & iii) with clearly visible large aggregates. Further addition of chitosan at 0.25 wt% (Figure 5.7AB iv) exhibited a different viscoelastic gel structure for DDA 50 and DDA 93 emulsions. Some aggregates were still visible with the former, and the emulsion could provide evidence of gelled structure. However, emulsions with 0.25 wt% DDA 93 chitosan showed a much weaker gel structure. Such difference in emulsion structure at 0.25 wt% was evident in their viscosity data (Figure 5.3C) and could be related to the formation of larger aggregates and the heterogeneous distribution of charged groups on the DDA 50 chitosan polymer chain, as explained before.

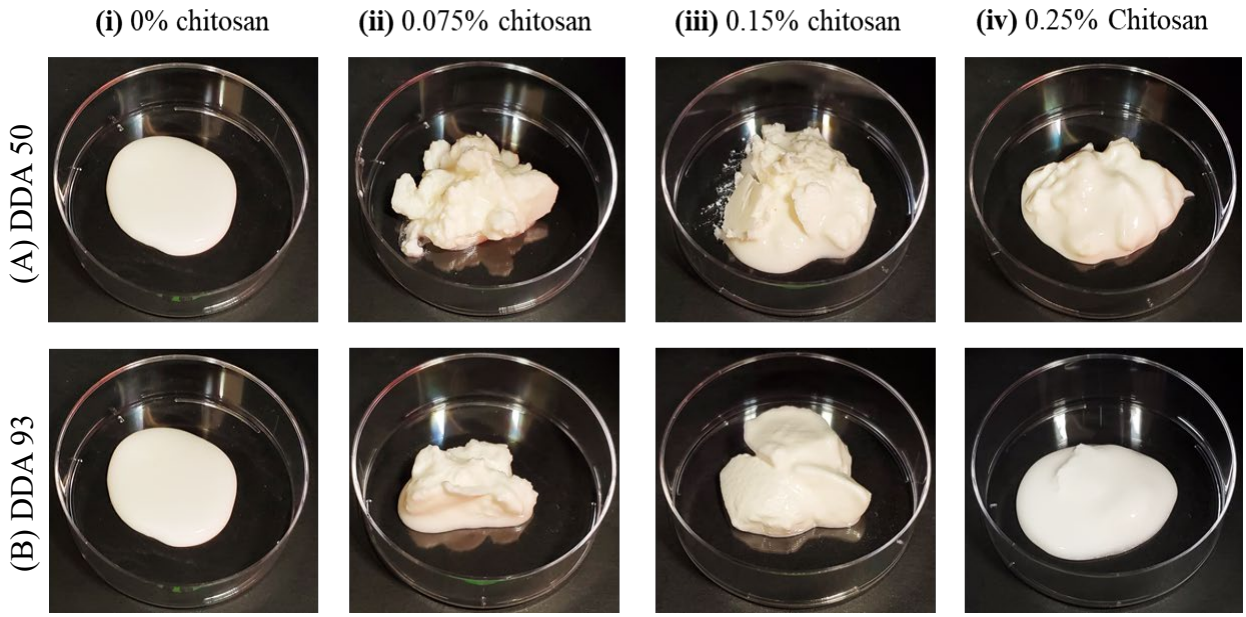

Figure 5.7 Change in visual observations of Citrem-chitosan emulsions at different concentrations of (A) DDA 50 and (B) DDA 93 chitosan.

5.4.5 Microstructure analysis of emulsions

To further investigate the role of chitosan concentration and charge in the rheology and visual observation of the bilayer emulsions, their microstructure was captured using a CLSM

(Figure 5.8). At 0 wt% chitosan (Figures 5.8Ai and 5.8Bi), the droplets were smaller and homogeneously distributed in the primary emulsions where the highly negative charge of Citrem repulsively stabilized them. The secondary emulsions coated with Citrem-chitosan exhibited different microscopic structures depending on the chitosan concentration and charge (DDA). For example, with the addition of 0.075 wt% chitosan (Figures 5.8Aii and 5.8Bii), the microstructure showed larger droplets aggregates which started to reduce when more chitosan (0.15 wt%) was available to cover the Citrem-stabilized droplets (Figures 5.8Aiii and 5.8Biii). At 0.075 wt%, the appearance of larger aggregates could be due to the charge neutralization of the system (Figure 5.2B) and bridging flocculation where one polymer chain of chitosan-coated multiple Citrem-stabilized droplets. Klongdee et al. (2012) also exhibited that droplets were highly aggregated at lower concentration of chitosan (0.05 wt%) in the lecithin-chitosan stabilized bilayer emulsions due to bridging flocculation. At 0.15 wt% chitosan, larger aggregates were still observed, but many droplets appeared free from aggregation, which was previously explained (Figure 5.2A) by saturated surface coverage for these droplets with chitosan leading to increased electrostatic and steric repulsion. Nevertheless, the reason behind the smaller apparent size of the aggregates at 0.075 wt% chitosan compared to 0.15 wt% chitosan reported in Figure 5.2A (opposite to the microstructure observation) could be due to the break-up of weekly bound aggregates at 0.075 wt% under intense stirring and mixing in the particle size analyzer, a phenomenon also indicated by Dickinson and Pawlowsky Dickinson and Pawlowsky (1997).

Further addition of chitosan (0.25 wt%) was much more effective in preventing the aggregation of positively charged droplets (Figures 5.8Aiv and 5.8Biv). Here droplet surfaces were fully covered by chitosan, and the repulsive interaction increased due to stronger electrostatic and steric repulsion. The microstructure of the emulsions is also in agreement with the aggregate size, where a significant reduction was observed at 0.25 wt% compared to 0.15 wt% chitosan (Figure 5.2A). The size of droplet aggregates and hence microstructure was also affected by the magnitude of the positive charge of chitosan polymer. DDA 50 chitosan with a lower magnitude of positive charge showed larger aggregates (Figure 5.2A and Figure 5.8iv) compared to DDA 93, which was attributed to higher electrostatic repulsion for the latter (Figure 5.2B). Similarly, a reduction in aggregate size or degree of flocculation was also noticed in the microstructure of multilayer emulsions with an increase in biopolymer (sodium alginate and chitosan) concentration (Fioramonti et al., 2015; Xu et al., 2016).

The differences in confocal microstructures of the Citrem-chitosan emulsions were also well in agreement with their visual observation, flow and viscoelastic behaviours (Figures 5.7, 5.3 and 5.5, respectively). Larger droplet aggregates observed at 0.075 wt% and 0.15 wt% chitosan led to increased viscosity and viscoelastic gel strength of the emulsions (Figure 5.3 and 5.4). Their visual observation also clearly indicated stronger gels at these chitosan concentrations (Figure 5.7). However, at higher concentration (0.25 wt% chitosan), smaller aggregates with stronger repulsion between them led to a significant drop in viscosity and gel strength and more flow of materials in visual observation. Thus, differences in chitosan concentration and charge could also reflect the differences in the microstructure and rheology due to the kind of biopolymer interactions involved in the formation of bilayer emulsions.

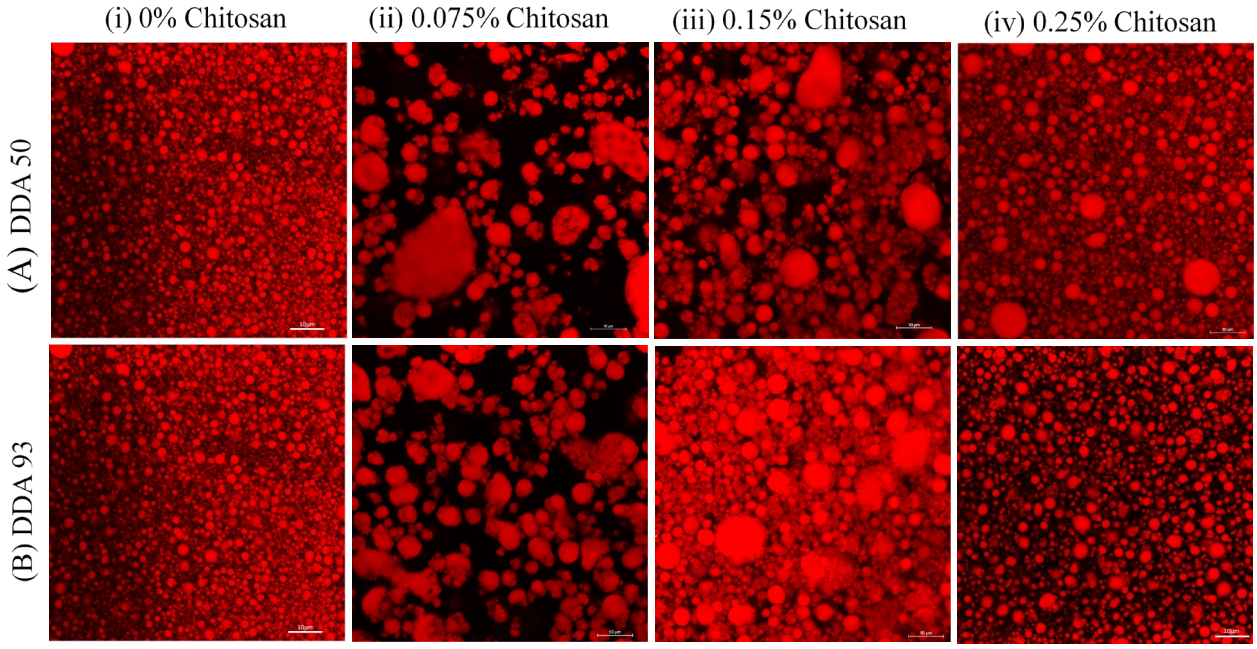

Figure 5.8 Microstructural changes in Citrem-chitosan emulsions as a function of chitosan concentration (i to iv) and DDA (A & B). The oil droplets were stained with Nile red and marked in red. The scale bar is 10 µm.

5.4.6 Mechanism of gelation in bilayer emulsion at surface saturation

In rheology analysis, we have seen that at the highest chitosan concentration (0.25 wt%), when the droplet surfaces were fully covered, the viscosity and gel strength of both the DDA 50

and DDA 93 bilayer emulsions were almost 10 - 20 times higher than the primary emulsions. We proposed that it could be mainly due to the increased repulsive electrostatic charge cloud and steric layer around the Citrem-chitosan-stabilized droplets. Previously, it has been shown that an increased shell layer around the nanodroplets led to an increase in the ϕ_{eff} towards close packing leading to a large increase in emulsion viscosity and elasticity (Kadiya & Ghosh, 2019; Patel, Mohanan, et al., 2019). Patel, Mohanan, et al. (2019) explained the elastic nature of 5 wt% sodium caseinate-stabilized nanoemulsion (ϕ_{oil} = 0.42) by calculating the shell layer thickness from the steric layer of casein plus the charge cloud around the oil droplets (from Debye length), which gave a ϕ_{eff} of 0.79, sufficiently high to create a close-packed structure. In the present case, we have also calculated the shell layer thickness (steric + charge cloud) by first measuring the chitosan layer thickness from the hydrodynamic droplet diameter (Appendix C, Method C7) and then calculating the charge cloud thickness from the Debye screening length (DSL) of the oil droplets in the bilayer emulsions (Appendix C, Method C8). Details of the method are given in Appendix C. In table C3 (Appendix C), these values were used to calculate the ϕ_{eff} of the mono- and bilayer emulsions. The actual oil volume fraction (ϕ_{oil}) of the emulsions was 0.38. From that, the ϕ_{eff} of monolayer emulsion was estimated as 0.47. However, the ϕ_{eff} of the bilayer emulsions was 0.53 and 0.66 for chitosan DDA 50 and DDA 93, respectively. Higher ϕ_{eff} of the DDA 93 chitosan-coated droplets could be responsible for their higher viscosity and visual observation of gelled structure compared to the DDA 50-coated bilayer emulsion. It should be noted that the droplet size used in the calculation is actually the size of the droplet aggregate obtained in the static light scattering measurement. Such a large droplet size of the bilayer emulsion could be due to the coating of multiple droplets by chitosan, which can also be seen in the cryo-SEM image shown in Figure C6 (Appendix C). As discussed before, the heterogeneous charge distribution in the chitosan DDA 50 could be responsible for more droplet aggregation and larger size compared to DDA 93 chitosan with a more homogeneous charge distribution. Due to the unknown nature of the aggregate structure, it is not possible to estimate the effective volume of droplet aggregate, which would further add to the overall effective volume of the dispersed phase. Nevertheless, our estimation showed that the increased volume fraction of the interfacial shell layer (ϕ_s) could be responsible for the increased viscosity and elasticity of the bilayer emulsions compared to the monolayer emulsion.

5.4.7 *In vitro* lipid digestibility and its influence on emulsion microstructure

Lipid digestion of emulsified oil droplets is an interfacial phenomenon that is mainly controlled by pancreatic lipase action in the presence of colipase and bile salts. However, the contribution of gastric lipase in the stomach to the overall lipid digestion is significant, although mostly ignored in most *in-vitro* digestions studies. In this study, we have considered the importance of gastric digestion of lipid by using RGL in the *in-vitro* digestion of emulsion according to INFOGEST (Brodkorb et al., 2019). At first, we have studied the effectiveness of incorporating RGL in the lipid digestion of Citrem-stabilized primary emulsion. During gastric digestion, the fatty acid release profiles of the primary emulsions (0 wt% chitosan) with and without RGL are shown in Figure 5.9A. Interestingly, the expected contribution of RGL, in terms of FFA released during the gastric phase of lipid digestion, was not observed. This could be attributed to the lower rate of lipid digestion by RGL and non-ionization of released FFA at the pH of gastric digestion (pH 5.5 or pH 3), which practically makes them unsuitable for pH-titration (Chatzidaki et al., 2016). RGL also has specificity for the short-chain fatty acids (FAs) compared to long-chain fatty acids, which could limit the hydrolysis of lipids (such as canola oil) with long-chain FAs in the stomach (Sassene et al., 2016). However, pre-digested lipid in the stomach significantly contributes to triggering the pancreas lipase mediated lipolysis in the small intestine (Gargouri et al., 1986; Sassene et al., 2016). In the present case, it was evidenced through a significant difference ($p < 0.05$) in the FFA released profiles during the intestinal digestion of the primary emulsions with and without RGL (Figure 5.9A). Noticeably, intestinal FFA released profiles with and without RGL remained the same for the initial 25 min but significantly decreased afterwards for the digestion without RGL. The overall percentage of lipid digestibility of Citrem-stabilized primary emulsions was 18.8 ± 1.6%, in the absence of RGL, which increased to 25.7 ± 1.1% in the presence of RGL (Figure 5.9B). Such a significant change (26.8% increase) in lipid digestibility of Citrem-stabilized primary emulsions can be attributed to RGL action on lipolysis during gastric digestion but was not detected by the pH-STAT. Gastric lipolysis is known to contribute 10 to 25% to the overall lipid digestion (Brodkorb et al., 2019; Sams et al., 2016). Roy et al. (1979) demonstrated that the principal role of gastric lipolysis is to facilitate intestinal lipolysis by increasing the contact of pancreatic lipase with the oil droplet interface, leading to an overall increase in the lipid digestibility of emulsions in the presence of RGL. Given the importance of gastric lipase in the human digestive system, we have included the gastric digestion

step to better mimic the in-vitro digestion model. Here, we analyzed the impact of the emulsion gel structure and interfacial thickness on the overall lipid digestibility of the bilayer emulsions.

Figure 5.9A also shows the extent of lipid digestion as FFA release profiles at the different stages of digestion of the three different bilayer emulsions stabilized by different concentrations of DDA 93 chitosan. Only the DDA 93 chitosan was considered for *in vitro* digestion study. None of the emulsions showed a release of FFA during gastric digestion in the presence of RGL, which could be due to the above-mentioned reasons. During the intestinal digestion, all the emulsions showed similar FFA released profiles with 4.5% of lipolysis in the initial 12 min of digestion (total time 120 min in Figure 5.9A). With progress in time, the primary emulsion (0% chitosan) showed rapid lipolysis, with ~19.5% of total FFA released in the initial 1 h and the remaining FFA released gradually in the next hour leading to a total release of 25.7% of FFA (Figure 5.9B). The flocculated emulsion gel obtained at 0.075 wt% chitosan showed a significant ($p < 0.05$) decrease in the FFA release profile, with ~18% lipid hydrolyzed by the pancreatic lipase within the first 1 h of *in-vitro* intestinal digestion (total 3 hr including gastric digestion). FFAs released profile was further decreased at 0.15 wt% of chitosan and only 14.5% of total lipid digested in the first 1 h of intestinal digestion due to more coverage of the droplet interface by the second layer of chitosan. At 0.25 wt% chitosan, lipolysis was further reduced to 12% after 1 h intestinal digestion. In Figure 5.9B overall lipid digestibility of the emulsions after 4 h of digestion (2 h gastric phase + 2 h intestinal phase) is plotted as a function of chitosan concentration. The overall lipid digestibility was significantly ($p < 0.05$) higher for the monolayer emulsion in the absence of the chitosan. The overall lipid digestion in terms of FFA release was in the order 0 wt% > 0.075 wt% > 0.15 wt% > 0.25 wt% chitosan, from 25.7% for primary emulsion to 17.5% for the 0.25% chitosan-added bilayer emulsion with complete droplet coverage. As the chitosan concentration increased, the droplet surface coverage was also increased, which could be responsible for the decrease in lipid digestion. A similar reduction in lipid digestibility, from 28% to 20.7%, was observed when whey protein-stabilized 40% oil-in-water monolayer emulsions were transformed into whey protein-CMC (carboxymethyl cellulose) stabilized bilayer emulsions (Malinauskytė et al., 2018). In another *in-vitro* digestion study, it has also been shown that coating protein-stabilized oil droplets with chitosan delayed lipid digestion (Zhang et al., 2015).

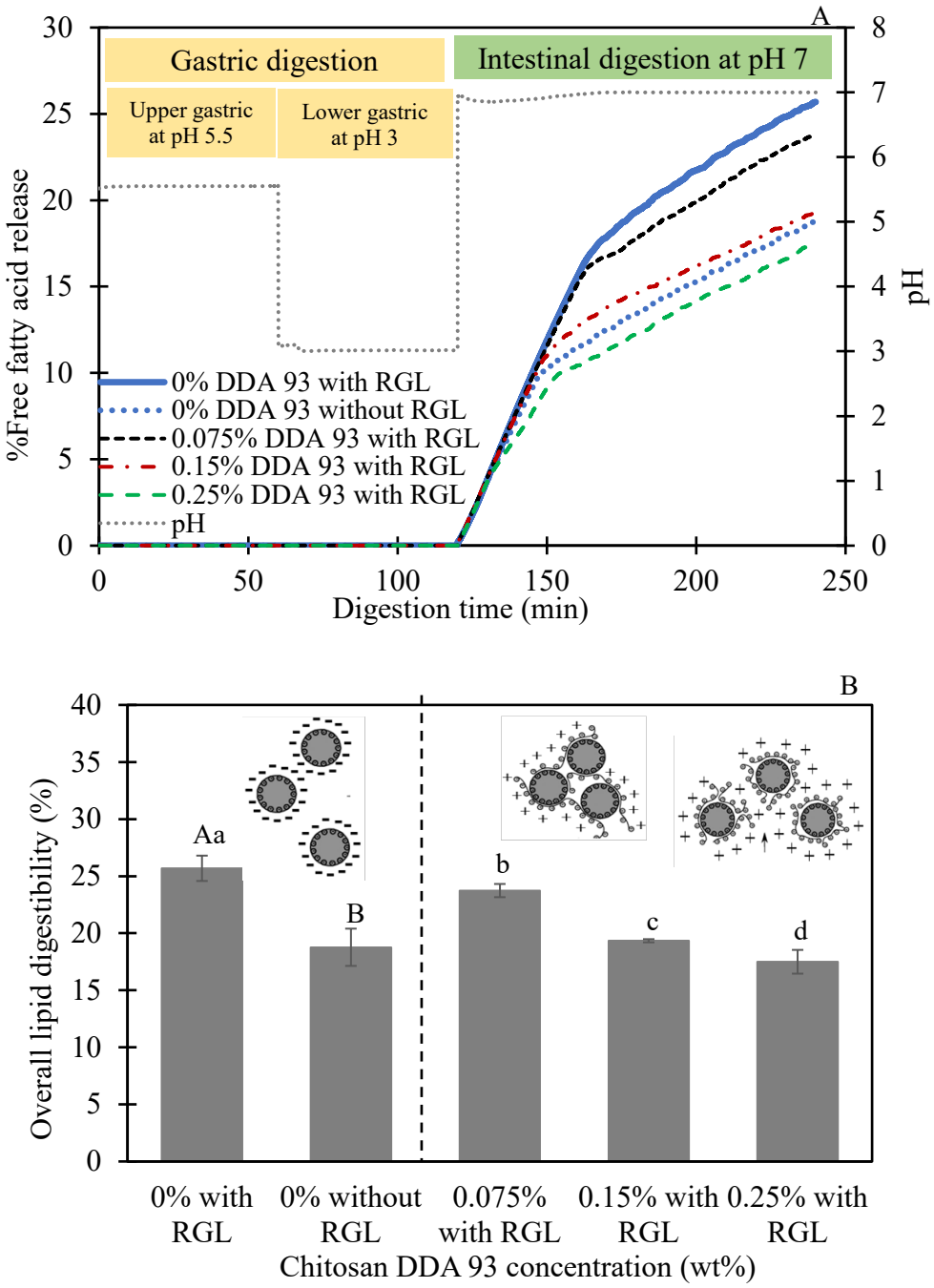

Figure 5.9 Effect of DDA 93 chitosan concentration on the digestion kinetics of bilayer emulsions. (A) Free fatty acid release profiles for mono- and bilayer emulsions, (B) Overall lipid digestibility percentage as a function of DDA 93 chitosan concentration. The effect of RGL (rabbit gastric lipase) on free fatty acid release profiles (9A) and overall lipid digestibility (9B) of Citrem-stabilized emulsions (0% DDA 93) is also shown here. Error bars indicate ± standard deviation (n ≥ 3). Different uppercase (for the effect of RGL) and lowercase (for various chitosan concentration) letters denote the statistical significance (at 0.05 level) difference amongst the population means.

Such a difference in digestibility of monolayer and bilayer emulsions can be explained by several physicochemical phenomena happening during *in-vitro* digestion. Smaller droplets of the primary emulsions are only stabilized by a single layer of anionic emulsifier, Citrem, which promotes faster hydrolysis of lipid due to the easy access of the gastric and pancreatin lipase to the core upon displacement of Citrem molecules by the bile salts. On the other hand, lower digestibility of bilayer emulsions compared to monolayer emulsion could be attributed to the improvement in the interfacial barrier and thickness in the presence of chitosan as a second layer, which delayed the action of lipase on either Citrem molecules or triglycerides molecules of oil droplets. The slower or controlled lipolysis of bilayer emulsions could also be attributed to the tendency of chitosan to bind bile salts, making them unavailable from their action to emulsify the oil droplets or to solubilize the lipid digestion products (Gudipati et al., 2010). Moreover, the chitosan polymer chain at the interface loses its positive charge at the neutral pH of the intestine because the positively charged amino groups on glucosamine residues (NH_3^+) have a pKa value of ~ 6.5 (Shahidi et al., 1999). Loss of positive charge could induce aggregation of chitosan polymer at the interface, and hence the pancreatin lipase could not get easy access to the lipid core (Corstens et al., 2017; Shah et al., 2016). Interestingly, the bilayer emulsion with 0.075 and 0.15 wt% chitosan with significantly higher gel strength (Figures 5.4C and 5.5C) showed higher lipid digestibility than the emulsion with 0.25 wt% chitosan. It can be said that the emulsion gel strength had less influence on lipid digestion compared to the surface coverage by chitosan, which could be due to the breakdown of gel structure upon mixing the emulsion with SGF.

The microstructure of monolayer and bilayer emulsions during *in vitro* digestion was also evaluated by withdrawing samples at different stages of digestion (Figure 5.10). For Citrem-stabilized (0 wt% chitosan) monolayer emulsion (Figure 5.10A i), well-dispersed oil droplets were observed, which became flocculated after mixing with SGF before starting the gastric digestion (Figure 5.10A ii). However, in the presence of RGL, extensive droplet flocculation with some degree of coalescence was observed after gastric digestion (Figure 5.10A iii). This was an indication of the action of RGL, which was undetectable using pH – STAT titration (Figure 5.9A). In another study, it has also been shown that the integrity of the Citrem-stabilized droplets in infant formula was disrupted, and their spherical shape was partially lost after 60 min of gastric digestion by RGL (Sassene et al., 2016). After 2 h of gastric digestion in the presence of RGL, when bile salts were added to the digesta at pH 7, the oil droplets were again finely dispersed (Figure 5.10A

iv). A few larger droplets were also visible, which could be attributed to coalescence due to the limited lipolysis that occurred during the gastric phase of digestion. Severe oil droplet coalescence was observed after 2 h of intestinal digestion in the presence of pancreatin lipase (Figure 5.10A v). This could have resulted from a series of events such as displacement of Citrem by bile salts from the oil-water interface followed by the complete hydrolysis of Citrem, and then lipolysis of triglyceride molecules leading to the high degree of coalescence. The significant change in the droplet morphology before and after intestinal digestion indicated the most lipolysis of the emulsion happened during the intestinal phase. Other digestion products such as fatty acids and monoacylglycerols liberated during digestion were emulsified in the micelles formed by the excess bile salts present in the digesta. However, they were not detectable during microstructure analysis of digesta using CLSM due to their smaller size.

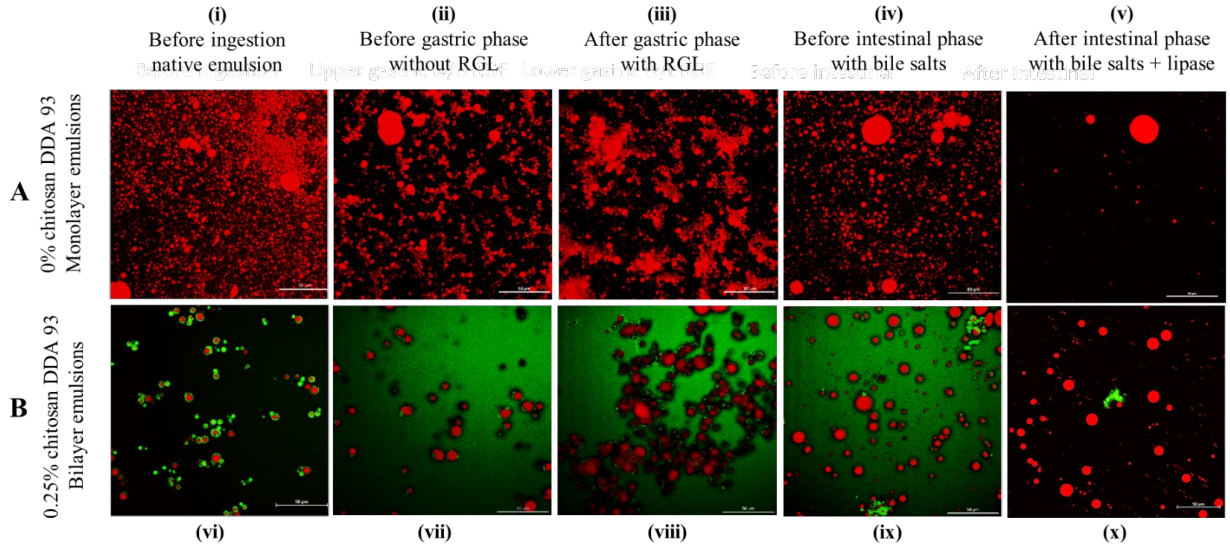

Figure 5.10 Structural changes in (A) mono- and (B) bi-layer emulsion digesta at different stages of *in vitro* digestion. The confocal images were collected using Nile red for monolayer Citrem emulsions, representing oil droplets, and using Nile red and fast green dyes for Citrem-chitosan bilayer emulsions, representing oil droplets and chitosan, respectively. The scale bar is 50 µm.

Bilayer emulsion with 0.25 wt% chitosan (complete surface coverage) was also analyzed for its microstructure during digestion (Figure 5.10B). The presence of the second layer showed a significant influence on the droplet morphology during different stages of digestion. Before digestion, stable oil droplets with a coat of chitosan can be observed (Figure 5.10B vi). Droplets

in digesta were intact and covered by the chitosan after mixing with SGF (Figure 5.10B vii). After the gastric digestion, bilayer emulsion droplets appeared less flocculated compared to the monolayer emulsion (Figure 5.10B viii). Subsequent addition of intestinal fluid with bile salts did not show any sign of coalescence, and the droplets were no longer flocculated (Figure 5.10B ix). Possible reasons for this could be the detachment of chitosan (indicated by green aggregates in Figures 5.10B ix and x) from the interface due to the loss of positive charge at neutral pH of intestinal fluid, followed by the displacement of Citrem by the bile salts at the interface. Unlike monolayer emulsions, the presence of a more significant number of smaller droplets in the bilayer emulsions (Figure 5.10B x) after 2 h of intestinal digestion indicates limited lipid hydrolysis due to restricted lipase action during gastric or intestinal digestion. Thus, the interfacial composition played an important role in deciding the action of lipase during the gastric and intestinal phases of digestion.

5.5 Conclusion

This study has shown that the electrostatic deposition of chitosan with different DDA on Citrem-stabilized emulsion droplets affected their characteristics, rheological properties, and lipid digestibility. Lower concentration of chitosan induced polymer bridging between multiple droplets, followed by complete surface saturation and the repulsive stabilization droplets at higher concentration. Chitosan with lower DDA and charge led to larger aggregates, lower zeta potential and higher viscosity at surface saturation which could be due to the heterogeneous charge distribution for the low-DDA chitosan, leading to more hydrophobic interaction among them. Aggregation of droplets at lower concentrations of chitosan led to the transformation of liquid monolayer emulsion into a strong elastic gel, evidenced by many folds increase in viscosity and the storage moduli of the emulsions. At surface saturation, Citrem-chitosan stabilized bilayer emulsions behaved like a repulsive viscoelastic gel with higher gel strength, lower creep compliance, and higher structural recovery than the monolayer emulsion, which was ascribed to the increase in the thickness of the interfacial shell layer due to the steric barrier and charge cloud leading to an increase in the effective volume of droplets. Monolayer emulsions in the absence of chitosan coating showed the highest lipid digestibility, which decreased as the chitosan concentration increased. Chitosan coating around the oil droplets restricted lipase action on Citrem and triglycerides during gastric and intestinal digestion. These results have an important implication in designing structured bilayer emulsions gel with controlled gel strength and lipid

digestion, which can also be used for fat-reduction and controlled delivery of bio-active components.

5.6 Connection to the next study

In this study, the interfacial thickness was increased by LbL deposition of positively charged chitosan molecules on negatively charged Citrem-stabilized droplets using a one-step mixing method. The effect of chitosan concentration and chitosan charge (%DDA) on rheology and digestibility of bilayer emulsions was studied. It was found that the strong electrostatic and steric forces between bilayer-stabilized droplets at higher chitosan concentrations increased the gel strength of bilayer emulsions than primary emulsions. This was attributed to increased shell–layer volume fraction (ϕ_s) and higher ϕ_{eff} of the bilateral emulsions compared to the monolayer emulsion. We could have increased the ϕ_{eff} much beyond 0.66 by keeping the chitosan-coated droplets to the nanoscale. Although Citrem-stabilized droplets were much smaller in size, we observed a larger size of the bilayer droplets due to the coating of multiple droplets by chitosan molecules using the one-step method. In the one-step method, the electrostatic adsorption of the second layer is so instantaneous that the polymer adsorbed to multiple droplets at the mixing pH before the droplets could distribute uniformly in the chitosan solution. Oppositely, in the two-step LbL deposition method, the same surface charge of emulsion droplets and polysaccharides of interest at the mixing pH will allow a uniform distribution of the droplets. We hypothesized that the uniform distribution of the droplets in a polysaccharide solution would help them coat individually upon change in pH or charge reversal. Therefore, in the next study, we used the two-step LbL deposition method using pectin to coat whey protein-stabilized droplets. Using a protein to stabilize the primary emulsion was essential to ensure charge reversal upon lowering of pH. Based on the above discussion, we hypothesized that the increase in interfacial thickness (δ) of whey protein isolate-pectin stabilized bilayer nanodroplet would further enhance the gel strength or ϕ_{eff} at an even lower actual oil volume fraction than that required for the Citrem-chitosan bilayer emulsions.

6. EFFECT OF PECTIN CHARGE ON THE RHEOLOGY AND DIGESTION BEHAVIOUR OF WHEY PROTEIN ISOLATE-PECTIN-STABILIZED BILAYER OIL-IN-WATER NANOEMULSIONS[4]

6.1 Abstract

The influence of pectin charge (degree of esterification (DE) 33% and 73%) on the rheology and digestion properties of mono- and bilayer stabilized 20 wt% canola oil-in-water emulsions was studied. The primary 4 wt% WPI-stabilized monolayer emulsions at pH 7 prepared with excess protein (WTEP) and without excess protein (WOEP) in the continuous phase at pH 7. To prepare the secondary emulsion with 1 wt% pectin, primary emulsion WTEP and WOEP was mixed with the pectin stock solution of different charges (DE33% and DE73%) at pH 7. The addition of pectin (DE33 and DE73) increased the droplet size (d_{43}) of primary emulsions (WTEP and WOEP) from 0.40 – 0.42 μm to 0.47 – 0.50 μm, while droplet charge reduced from – 59 to – 50 mV due to the formation of soluble complexes between WPI and pectin at pH 7. The viscosity of secondary emulsions increased almost two orders of magnitude than primary emulsions at pH 7, but emulsions were still flowable. Oppositely, the droplet characteristics and rheology of the secondary bilayer emulsions were significantly changed than primary emulsions when pH was changed to 3. At pH 3, droplet size (d_{43}) considerably increased from 0.40 – 0.42 μm to 2.34 – 2.53 μm WTEP in secondary emulsions due to charge neutralization, whereas there was a smaller increase in droplet size (0.69 – 0.70 μm) WOEP due to complete saturation of droplet surface by the second layer of pectin. The secondary emulsions pH 3 showed higher viscosity, higher viscoelasticity, higher structural recovery, and lower creep than the secondary emulsions at pH 7 or primary monolayer emulsions. Remarkably, the higher pectin charge (DE33) and excess protein (WTEP) were very helpful in increasing the gel strength of bilayer emulsions compared to the lower pectin charge (DE73), confirmed from the visual observation and confocal microstructure. The emulsion's gel strength increased WTEP due to aggregation of droplets attributed to the lack

[4] Kadiya, K. carried out the experiments and wrote the first draft. Ghosh, S. conceptualized, supervised, reviewed, and edited. This manuscript is under preparation for submission to a journal.

of surface saturation by the pectin, where excess protein favours more protein-pectin complexation in the continuous phase. Removing excess protein from the continuous phase promoted the maximum complexation of pectin at the interface, evident from the close-packed droplet structure obtained without any sign of aggregation in bilayer emulsions due to increased steric barrier and charge cloud thickness. Thus, the addition of pectin transformed the liquid monolayer emulsions into viscoelastic gel due to gelation of continuous phase WTEP or gelation manifested by the close packing of the droplets WOEP in the continuous phase. The monolayer emulsions showed 37.2% lipid digestibility which further reduced to 24.0% and 16.1% for the bilayer emulsions with an increase in the pectin charge due to the restricted action of digestive enzymes on lipid molecules. This study established that gelation in emulsions can be achieved at a lower oil volume fraction (20 wt%) as a function of pectin charge and by manipulating the protein-pectin interaction either at the interface or in the continuous phase. Such novel findings can be used to better understand and alter the emulsion's rheological and digestion properties for application in the food and pharmaceutical industries.

6.2 Introduction

Structured emulsions gels are an integral part of many food products used every day, such as yogurt, cheese, salad dressings and mayonnaise (Dickinson, 1994). Emulsion gels can be structured in different ways by increasing the viscosity of the continuous phase or changing the inter-droplet interactions (Dickinson, 2012). For example, the viscous contribution from the biopolymer or protein present in the continuous phase of emulsions could be responsible for gelling a dilute emulsion, although the oil-volume fraction remains too low. Conversely, dilute emulsions can also behave like a viscoelastic gel when the droplets form a network structure due to a net inter-droplet attractive interaction (Dickinson, 1994, 2012). Finally, the close-packed structure of repulsively stabilized droplets may also result in the structuring of concentrated emulsions (Knudsen et al., 2008). At a high volume of the dispersed phase, the closely packed oil droplets provided a structural framework that held the emulsion together with the resultant formation of a self-standing elastic gel-like structure (Wilking & Mason, 2007). Therefore, in food products containing a dispersed phase, the microstructure of the oil droplets and their inter-droplet interactions play an essential role in deciding the final product rheology. It is well known that the formation of gel structure and the rheological properties of concentrated emulsions are strongly influenced by droplet size (r) and oil volume fraction (ϕ) (Welch et al., 2006). However, an

additional factor, such as interfacial thickness (δ), has not been studied extensively, which may also play a significant role in structuring emulsions gel. In our previous studies, we have shown that by reducing the droplet size to nanoscale, anionic emulsifiers (sodium dodecyl sulphate (SDS) or citric acid esters of mono- and diglycerides (Citrem))-stabilized 40% canola oil-in-water emulsions can be transformed into repulsive viscoelastic gels (Erramreddy & Ghosh, 2014; Kadiya & Ghosh, 2019). We attributed this gel formation in emulsions, at much lower oil concentration than conventional emulsions, to an increase in effective volume fraction (ϕ_{eff}) of the oil droplets leading to a close-packing structure of the nanodroplets and associated charge clouds around them (Wilking & Mason, 2007). A similar increase in interfacial shell-layer thickness was also utilized for protein-stabilized nanodroplets forming a repulsive emulsion gel at lower oil volume fraction ($\phi = 0.4$) (Patel et al., 2017; Patel, Mohanan, et al., 2019). Patel, Mohanan, et al. (2019) showed that at the same emulsifier-to-oil ratio, sodium caseinate (SC)-stabilized nanoemulsions formed a viscoelastic gel whereas whey protein isolate (WPI)-stabilized emulsion did not, although the droplet size of both the emulsions was very similar. The authors attributed the difference in the rheology of the emulsions to the distinct conformational arrangement of protein at the interface, which was responsible for the nanoscale difference in their interfacial thickness, leading to a significant change in ϕ_{eff} (Li Zhai et al., 2013; Patel, Mohanan, et al., 2019). Notably, the WPI-stabilized emulsions showed a lack of close-packed droplets (liquid-like behaviour) due to a much lower interfacial thickness of WPI (~ 2 nm interfacial steric barrier) compared to SC-stabilized emulsions (gel-like structure) due to a higher interfacial thickness of SC (10-12 nm interfacial steric barrier) (Patel, Mohanan, et al., 2019). In the present work, we hypothesized that by increasing the shell-layer thickness by forming multiple interfacial layers, we could transform the liquid-like WPI-stabilized repulsive emulsions into a viscoelastic emulsion gel.

The interfacial thickness of protein-stabilized droplets can be increased by non-covalent or electrostatic interactions between protein and polysaccharide at the interface (Guzey & McClements, 2006; Liu et al., 2018). These interactions are the result of sequential (layer-by-layer) adsorption of the negatively charged biopolymer groups onto the positively charged another biopolymer group. The layer-by-layer (LbL) deposition of polysaccharide molecules onto the protein-stabilized droplet is a widely used interfacial structuring phenomenon (Guzey & McClements, 2006; Li et al., 2020). Electrostatic interactions of different biopolymers at the droplet surface can alter the structural organization, rheology, thickness and charge of interfacial

layers (Ettelaie & Akinshina, 2014; Li et al., 2020). Many researchers used the LbL technique with an objective to improve the stability of emulsions against the various environmental factors, and that has been performed on relatively dilute emulsions ($\phi < 0.2$) (Berendsen et al., 2014; Bouyer et al., 2011; Gharsallaoui, Saurel, et al., 2010; Roudsari et al., 2006; Wei & Gao, 2016). However, to our knowledge, there is a lack of knowledge on using the LbL technique in the fabrication of concentrated emulsions with a focus on the interfacial contribution in their rheological properties. In this study, we want to use the two-step LbL method for second layer deposition in comparison to the one-step LbL method used in Chapter 5 for chitosan deposition on the Citrems-stabilized droplets. We hypothesized that the two-step LbL method would help to disperse the protein-stabilized droplets uniformly into polysaccharide solution of similar charge at mixing pH in the first step. In the second step, the charge reversal at acidic pH would favour the polysaccharide adsorption on invidual droplets by electrostatic complexation. This led us to the aim of the present study, to explore the two-step LbL technique in the formation of thick interfacial layers around the whey protein-coated nanodroplets using pectin as a second layer. Our overall goal was to develop food-grade emulsion gels at a much lower oil volume fraction than conventional monolayer emulsions.

To achieve our goal, we prepared the primary monolayer emulsions using whey protein isolate. It has been shown that to produce nanoscale droplets in a concentrated emulsion, a high amount of emulsifier is required to stabilize the huge interfacial area generated. However, this process also increases the amount of unabsorbed protein in the continuous phase of emulsions which, often become detrimental to emulsion stability (Patel, Mohanan, et al., 2019). Guzey and McClements (2006) highlighted the critical effect of the excess unabsorbed emulsifier/biopolymer molecules in forming multilayer emulsions using an LbL approach. They identified that the excess unabsorbed biopolymer molecules in the continuous phase of emulsion could impede the electrostatic deposition of the second layer (Guzey & McClements, 2006). To overcome this problem, we removed the excess unabsorbed protein from the continuous phase of emulsions by multiple cycles of ultracentrifugation. Emulsions obtained without excess protein (WOEP) in the continuous phase were then used to prepare the WPI-pectin coated bilayer emulsions. As a control, emulsions with excess protein (WTEP) in the continuous phase were also used to prepare bilayer emulsions.

Pectin is an anionic biopolymer composed of a backbone of partially esterified galacturonic acid residues with protruding hairy regions containing rhamnose, galactose, arabinose, xylose and glucose (Stephen, 1995). The stabilization of oil-in-water (O/W) emulsions by complexation of proteins and polysaccharides have long been used to improve the stability of the emulsion (Neirynck et al., 2007; Salminen & Weiss, 2014; Schmidt et al., 2016; Wijaya et al., 2017; Xu et al., 2012). Notably, in the case of pectin, hairy regions provide the steric barrier, and the ionization of carboxylic groups (-COOH) provides a negative charge to the droplet surface for improved stabilization of the emulsions (Ngouémazong et al., 2015). Moreover, the composition of the adsorbed films, their thickness, and configuration are strongly influenced by the total charge and charge distribution pattern along the pectin molecule, which is ultimately affected by their degree of esterification (DE) (Ettelaie & Akinshina, 2014; Ettelaie et al., 2012; Lutz et al., 2009; Verkempinck et al., 2018; Warnakulasuriya et al., 2018). Therefore, in the present study, we also used pectin with two different DE or charge densities to coat the whey protein stabilized droplets in the presence (WTEP) and absence (WOEP) of excess protein in the continuous phase of the emulsions. We hypothesized that the strength of electro-steric repulsions between the two approaching droplets and their interfacial thickness could be increased by increasing the charge density of pectin at the interface, leading to improved rheological properties of emulsions. Finally, the effect of the interfacial composition on the microstructure and *in vitro* digestibility of the multilayer emulsions was also studied as a function of biopolymer charge density.

6.3 Materials and methods

6.3.1 Materials

Whey protein isolate (WPI) was provided by the Fonterra (USA) Inc., IL, USA. It was composed of 89.7 ± 3 wt% protein, 6 wt% moisture, 4 wt% ash, 2 wt% fat and 1 wt% lactose. Citrus pectin with different degrees of esterification (DE) was donated by the Herbstreith & Fox KG (Neuenbürg, Germany). Two different types of pectin used in this study had a 33% DE and 73% DE. Canola oil was purchased from a local retail store. Deionized water was used for preparing all samples, buffers, and chemicals. For *in vitro* digestion, all the enzymes and chemicals such as porcine pepsin (P7012), pancreatin lipase (L3126), bile extract (B8631), porcine pancreatin extract (8 × USP specifications, P7545), and calcium chloride purchased from Sigma-Aldrich (St. Louis, MO, USA). Rabbit Gastric Extract (RGE-15) (a source of gastric lipase) was procured

from the Lipolytech® (Marseille, France). All other reagents and chemicals were analytical grade and purchased from Sigma-Aldrich (St. Louis, MO, USA).

6.3.2 Preparation of biopolymer solutions

An emulsifier solution containing 4 wt% WPI was prepared by dispersing WPI powder into 10 mM phosphate buffer (pH 7) at room temperature (25 ± 2°C) and stirred at 400 rpm overnight for complete solubilization. Pectin stock solution (3 wt%) of DE 33% (DE33) and 73% (DE73) were prepared by dissolving powdered pectin in 10 mM phosphate buffer (pH 7) at room temperature. For complete dissolution of pectin biopolymer, prepared suspensions were stirred at 600 rpm until free from any suspended particle. An antimicrobial agent, sodium azide (0.02 wt%), was added to WPI and pectin solutions to restrict any microbial growth during sample preparation and storage.

6.3.3 Preparation of primary emulsion

Preliminary experiments were conducted to optimize the amount of WPI required to get stable emulsions with monomodal droplet size distribution. Based on that, the primary emulsions were prepared by adding the 30 wt% canola oil to 70 wt% aqueous phase containing 4 wt% WPI. This dispersion was then processed into an oil-in-water (O/W) coarse emulsion using a rotor-stator mixer (Polytron, Brinkmann Instruments, Ontario, Canada) for 60 s at 20,000 rpm. The coarse emulsion was subsequently homogenized using a high-pressure homogenization (EmulsiFlex-C3, Avestin Inc., Ottawa, ON, Canada) at 20,000 psi for 8 cycles. During the homogenization process, the emulsion was cooled down to room temperature (25 ± 2°C) at the homogenizer outlet using a cooling coil submerged into cold water (~ 5°C). Whey protein stabilized primary emulsions obtained after 8 cycles were collected and stored in 120 mL glass bottles (VWR International, Edmonton, AB, Canada) at room temperature for further experiments.

6.3.4 Removal of excess whey protein

To prepare the secondary bilayer emulsions, our aim was to deposit negatively charged pectin onto the positively charged whey protein-stabilized droplets at pH 3. However, the presence of positively charged excess protein into the continuous phase can interfere with the electrostatic interaction of negatively charged pectin with the protein at the oil droplet surface (Perrechil & Cunha, 2013). McClements et al. (2007) also suggested that a washing step is required between

each LbL deposition step to remove any excess biopolymer remaining in the bulk phase of emulsions. Researchers also advocated that the excess biopolymer can be easily removed by centrifugation or filtration technique (McClements et al., 2007). Hence, the excess protein was removed from the primary whey protein-stabilized emulsion by ultracentrifugation (Sorvall discovery 90, Kendro Laboratory Products, Sorvall Ltd., UK) at 52,070 × g (20,000 rpm, rotor no. AH-629) following the method developed by Kadiya and Ghosh (2019). After ultracentrifugation, the separated aqueous phase was removed by a 5 mL Luer-lok™ syringe (BD #309646) attached with a reusable hypodermic needle (B-D YALE Luer-Lok™ 15 G x 1.5″) without disturbing the cream layer. Next, an equal amount of deionized water was added to redisperse the cream layer using a rotor-stator mixer (Polytron, Brinkmann Instruments, Ontario, Canada) for 60 s at 20,000 rpm. The prepared dispersion was then subjected to two cycles of high-pressure homogenization (EmulsiFlex-C3, Avestin Inc., Ottawa, ON, Canada) at 20,000 psi pressure. This process of excess unabsorbed protein removal was repeated one more time to ensure maximum protein removal from the continuous phase of the emulsion. The experimental protocol to analyze the excess protein and excess whey protein in the aqueous phase of emulsions is mentioned in a similar work published by Patel, Mohanan, et al. (2019). Both the emulsions with excess protein (WTEP) and without excess protein (WOEP) in the continuous phase were used to prepare the secondary bilayer emulsions.

6.3.5 Preparation of bilayer secondary emulsions

Formulation and the protocol to prepare the secondary emulsions were explained schematically in Figure D1 (Appendix D). Secondary bilayer emulsions with 20 wt% canola oil were prepared using a the two-step LbL electrostatic deposition method. Here, in the first step, each of the two different 2.5 wt% pectin stock solutions with different charges (DE33 and DE73) were mixed with the primary emulsions (30 wt% canola oil) at pH 7 in 60 mL glass bottles. In the second step, the pH of the mixture was changed to pH 3 while stirring using 1M HCl so that the protein and pectin carry an opposite charge for the electrostatic interactions. The amount of pectin required to coat the whey protein stabilized nanodroplets was optimized by conducting series of preliminary experiments using 0 to 1 wt% pectin. It was found that the 1wt% pectin (DE33 and DE73) was sufficient in the secondary emulsions to saturate the surface of the individual oil droplets. Droplet charge reached a negative at about 1 wt% pectin concentration (Appendix D, Figure D2). Further, the stock solution of pectin used to attain the 1wt% pectin in secondary

emulsions was very difficult to dissolve when concentration exceeded 2.5 wt%, especially for the pectin with higher DE73 due to its higher viscosity (Appendix D, Figure D3B). Hence, for the rest of the research 1 wt% pectin (DE33 and DE73) was used in the secondary emulsions. We hypothesized that an oppositely charged pectin and protein at pH 3 could interact electrostatically only at the oil droplet surface for the emulsion WOEP or in the bulk phase as well as at the droplet surface for the emulsion WTEP (Appendix D, Figure D1). Therefore, to understand the effect of excess protein on the bilayer emulsion characteristics, both the primary emulsions WTEP and WOEP were investigated. For better comparison and to understand how pectin can interact with the protein and affect the emulsion characteristics, a part of all secondary emulsions was also kept at pH 7. Finally, WPI-pectin bilayer emulsions obtained with 20 wt% oil concentrations were evaluated for their droplet size, droplet charge, microstructure, rheological properties, and *in vitro* lipid digestibility.

6.3.6 Droplet size and Droplet charge

The droplet size of the primary and secondary emulsions was analyzed by a static light diffraction technique, using the Mastersizer 3000 (Malvern Instruments, Montreal, QC, Canada) with a relative refractive index of the dispersed vs. continuous phases as 1.465. Distilled water was used as a dispersant in the instrument and adjusted to appropriate pH (pH 3 and 7) using either 1M HCL or 1M NaOH before measurement. The obscuration was brought up to ~8% by dropwise sample addition. The average droplet size of emulsion was characterized by Sauter mean diameter (d_{32}). The zeta potential or droplet charge of all primary and secondary emulsions at two different pH values (pH 3 and 7) was determined using a zeta potential analyzer (Zetasizer Nano-ZS90, Malvern Instruments, Westborough, MA, USA). To minimize the multiple scattering effects, the emulsion was diluted before analysis in the same ionic environment using a 100 mM pH 3 citrate buffer or pH 7 phosphate buffer to a final droplet concentration of approximately 0.01 wt%. Similarly, the DE33 and DE73 pectin stock solutions were also analyzed for their zeta potential to confirm that DE of commercial pectin samples has a significant effect on their magnitude of a negative charge, and hence can make a considerable impact on the final characteristics of the bilayer emulsions.

6.3.7 Rheology of emulsions

The flow behaviour and viscoelasticity of primary and secondary emulsions as a function of pectin charge with and without excess protein in the continuous phase were evaluated using an AR G2 rheometer (TA Instrument, New Castle, DE, USA) at 25°C. For each measurement, a predetermined quantity of emulsion was carefully placed onto the Peltier plate of the rheometer, and the flow behaviour or gel strength was measured at a 1000 μm gap using a 40 mm diameter stainless steel cross-hatched geometry. Viscosity was measured for primary and secondary emulsions by applying a shear rate in the range of 0.1 to 1000 $s^{-1,}$ and the viscoelastic behaviour of the samples was determined by two different types of oscillatory measurements. The strain sweep measurements were performed at 0.01–1000 % strain and a constant frequency of 1 Hz (6.28 *rad*/ s) to analyze the linear viscoelastic region (LVR). From this data, the plateau modulus (G'_p) at a certain strain of oscillation was plotted for better comparison. A constant strain amplitude of 0.01% strain was chosen within the LVR for subsequent series of frequency sweep measurements in which the G′ and G″ of emulsions were determined as a function of frequency ranging from 0.01 to 100 *rad*/s. The obtained data were used to plot the storage modulus at a certain frequency of oscillation from these experiments.

Creep-recovery tests were carried out to measure the compliance for liquid and gelled emulsions as a function of pectin charge with and without excess protein in the continuous phase. During creep compliance measurement, constant stress was applied to the samples instantly and maintained for 300 s. After removing the stress, recovery compliance was recorded for the next 300 s. The constant stress predetermined from LVR was 0.02 Pa for liquid samples, whereas it was 0.1 and 0.5 Pa for weak and strong-gelled emulsions, respectively. The compliance versus time was plotted for the emulsions as a function of pectin charge with and without excess protein, and from that, %Recovery (γ_{RE}) of deformation was determined by using the peak compliance (J_{max}) and recovery compliance (J_{RE}), according to Equation 6.1.

$$\%Recovery = \left[\frac{(Jmax - J_{RE})}{Jmax}\right] \times 100 \tag{6.1}$$

6.3.8 Confocal microstructure of emulsions

The microstructure of all the primary and secondary emulsions was evaluated using a Nikon C2 confocal laser scanning microscope (CLSM) (Nikon Inc., Mississauga, ON, Canada). Oil

droplets in emulsions were stained using 0.01 wt% of Nile red before emulsification. A 543 nm laser was used to excite the oil phase, and the emission spectra were collected in the range of 573-613 nm. The whey protein or whey protein-pectin complexes were stained by adding 0.01 wt% fast green in the continuous phase after emulsification. A 633 nm laser was used for excitation, and the emission spectra were collected using a 650 nm long-pass filter. All microstructure images were captured using a 60 × Plan Apo VC (numerical aperture 1.4) oil immersion objective lens and a 2.5× digital zoom.

6.3.9 *In vitro* lipid digestion of emulsions

Digestion assembly and set up: Static *in vitro* lipid digestion of mono- and bi-layer WPI-pectin emulsions were performed in a 100 mL double-wall jacketed reaction connected with a water bath maintained at 37°C. The whole set was mounted on a pH-STAT assembly (907 Titrando, Metrohm, Switzerland) for monitoring lipid digestibility at different stages of digestion. Activities of all the enzymes were analyzed and used as a reference to calculate the right amount necessary for each digestion step, as mentioned in the INFOGEST protocol (Brodkorb et al., 2019).

***Digestion protocol*:** The gastric and intestinal digestion protocol followed the recommendations given by Brodkorb et al. (2019) with some specific modifications for the pH-STAT setting. Briefly, 5 g of emulsions was weighed in a 100 mL reaction vessel followed by the addition of 5 mL of simulated salivary fluid (SSF) and the *in vitro* oral phase was performed for 2 min in the absence of α-amylase, because no starch was present in the emulsion formulation. The purpose of adding SSF was only to maintain proper electrolyte concentration or to carry out proper dilution for solid gel or liquid matrices of the emulsions. To attain 37°C temperature, the digestion mixture (bolus) was stirred for two minutes using a three-propeller stirrer mounted on the pH-state assembly. To begin the upper gastric digestion, a 10 mL mixture consisted of simulated gastric fluid (SGF) and gastric enzymes such as pepsin and gastric lipase (RGE) were added in the bolus to achieve the final enzyme activity of 2000 U and 120 U, respectively per mL of gastric digestion mixture (chyme). Next, the pH was adjusted to 5.5 using 1N HCl. The upper gastric phase was kept running for 1 h, and then for the next 1 h of lower gastric phase digestion, the pH was again reduced to 3 using 1N HCl. After 2 h of gastric digestion, 20 mL mixture consisted of simulated intestinal fluid (SIF), bile extract solution (10 mM bile salts in the final mixture), pancreatin extract with pancreatin lipase (100 U/mL trypsin and 2000 U/mL lipase activity) were added to the gastric

chyme. The pH was adjusted to pH 7 with 1N NaOH in the final digestion mixture. The intestinal digestion phase was also kept running for 2 h. The release of free fatty acids (FFA) upon the action of gastric or pancreatin lipase on the emulsion leads to a decrease in pH due to the generation of H^+, which was monitored using the automatic titration unit with pH-stat programming maintained at a static value of pH (pH 5.5 and pH 3 for upper gastric and lower gastric phase, respectively and pH 7 for intestinal phase). All the digestion curves were obtained for the three replicates with a data acquisition frequency of 2 s. The kinetics of lipolysis at different stages of digestion was monitored in terms of volume of NaOH (0.1 N) used, and it was converted into percentage FFA released using Equation 6.2.

$$\%\ FFA\ release = \frac{V_{NaOH} \times M_{NaOH} \times Mw}{\alpha_{FFA} \times m \times 2 \times 1000} \times 100 \quad (6.2)$$

Where V_{NaOH} and M_{NaOH} are the volume and molarity of titrant NaOH respectively, Mw is the average molecular weight of the triglyceride in canola oil (877 g/mol) (Guo et al., 2017), m is the mass of oil in emulsions (g), and α_{FFA} is the degree of dissociation of the carboxylic group of FFA at pH 7 (taken as 0.54) (Mat et al., 2016). The value 2 indicates that every triglyceride molecule liberates two FFA and a monoglyceride during lipid digestion.

6.3.10 Statistical analysis

All experiments were conducted with at least three replicates, and the results were reported as the mean ± standard deviation. The results were analyzed for statistical significance using analysis of variance (ANOVA) with a 95% confidence level ($p < 0.05$). The statistical analysis was performed using Microsoft Excel 2016 and OriginPro version 2020 software (OriginLab Corporation, Northampton, MA, USA).

6.4 Results and discussion

6.4.1 Droplet size distribution and average droplet size of emulsions

Figure 6.1 shows the changes in the average droplet size (d_{32}) and droplet size distribution of 4 wt% WPI-stabilized 30 wt% canola oil-in-water primary emulsions before and after removing the excess protein from the continuous phase. The surface-weighted mean diameter (d_{32}) of primary emulsions was 0.34 μm with excess protein (WTEP) in the continuous phase (inset Figure

6.1). After removal of excess protein (WOEP), d_{32} was non-significantly reduced to 0.32 µm. Further, the droplet size distribution did not change significantly upon removing excess protein from the continuous phase (Figure 6.1). This is following our previous findings where we used the same protocol to remove the excess emulsifier from the continuous phase of Citrem-stabilized 40 wt% oil-in-water nanoemulsions. We observed that the removal of excess emulsifiers did not affect the average droplet size and droplet size distribution (Kadiya & Ghosh, 2019). In another study, it was analyzed that 4 wt% WPI-stabilized 40 wt% canola oil-in-water contained about 1.21 wt% excess protein in the continuous phase of emulsions (Patel, Mohanan, et al., 2019). Hence, in this study, the excess whey protein from the bulk phase was removed to facilitate the electrostatic deposition of pectin on the WPI-stabilized droplets during the formation of secondary emulsions (Bertsch et al., 2019; Guzey & McClements, 2006; Li, Wu, et al., 2021; McClements et al., 2007; Xiang et al., 2016).

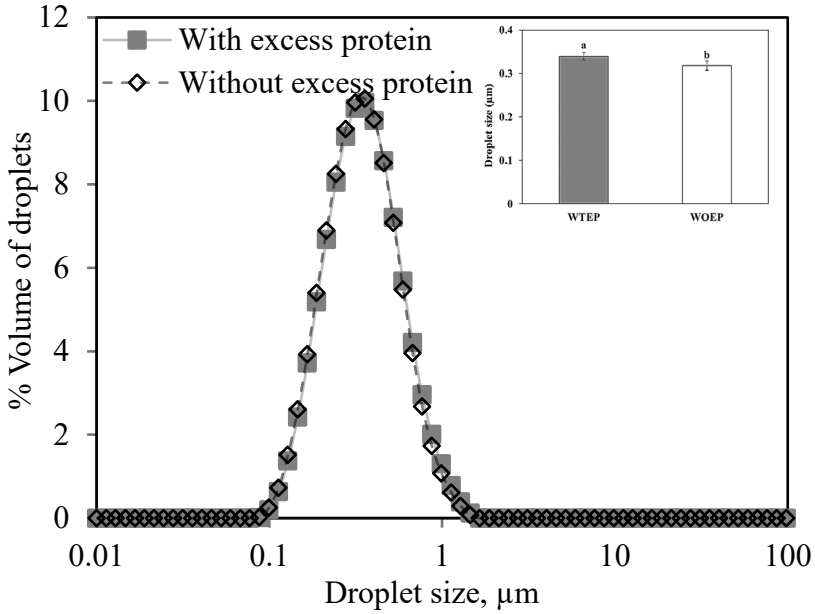

Figure 6.1 Changes in the droplet size distribution of WPI-stabilized primary emulsions upon removal of the excess protein from the continuous phase. Inset shows the average droplet size (d_{32}) of emulsions with (WTEP) and without (WOEP) excess protein in the continuous phase. Error bars indicate ± standard deviation (n ≥ 3). Different lowercase letters on the bars are used to denote the statistical significance (at 0.05 level) amongst the population means.

Figure 6.2 shows the effect of pectin type (DE33 and DE73) on the average droplet size and droplet size distribution of primary and secondary emulsions at pH 3 and PH 7 with and without excess

protein in the continuous phase. In Figure 6.2A, the d_{32} and d_{43} of primary WPI-stabilized emulsions were increased from 0.32 to 0.33 μm and from 0.40 to 0.42 μm, respectively with a change in pH from pH 7 to pH 3 in the absence of excess protein (WOEP) in the continuous phase, although this increase was not significant ($p > 0.05$). Similarly, in Figures 6.2B and 6.2C, the droplet size distribution of primary emulsions (no pectin) did not change significantly without excess protein (WOEP) at pH 3 and pH 7. Further, the addition of pectin (DE33 and DE73) at pH 7 did not affect the droplet size (Figure 6.2A) and droplet size distribution (Figure 6.2B) of the secondary emulsions. At pH 7, both the biopolymer whey protein and pectin were negatively charged (Figure 6.3), and hence the repulsive forces between them did not favour the protein – pectin electrostatic interaction, causing no change in droplet size distribution. Although unabsorbed biopolymer in the continuous phase of emulsions is known to promote depletion flocculation (Dickinson, 2003; McClements, 2000), we did not see any increase in droplet or aggregate size in the presence of non-adsorbed pectin (Dickinson et al., 1998). This could be due to the dilution of the emulsion during the droplet size measurement, which reduced the concentration of free biopolymer and hence any possible effect of depletion flocculation (Qiu et al., 2015). Gancz et al. (2006) have measured the droplet size of emulsions in the non-diluted system using the in-situ Diffusing Wave Spectroscopy (DWS) technique. The authors reported that the addition of 0.1 wt% high methoxy pectin (HMP) did not affect the size distribution of droplets in WPI-stabilized emulsions maintained at pH 7. Therefore, the droplets were covered by only whey proteins, not by protein-pectin bilayer, at pH 7, indicating the secondary emulsions still possessed a single layer at this stage.

Interestingly, when the pH of the secondary emulsions changed from pH 7 to pH 3, significant ($p < 0.05$) increase in the droplet size (d_{43}), from 0.49 to 2.53 μm for DE33 and from 0.48 to 2.34 μm for DE73 coated droplets, was observed in the presence of excess protein in the continuous phase. With excess protein (WTEP), the droplet size distribution of secondary emulsions (at pH 3) also showed bimodal with a smaller second peak in the range of 2 to 6 μm (Figure 6.2C). It showed that the excess protein in the continuous phase favoured the electrostatic interaction with pectin at pH 3, which reduced the available pectin to cover the WPI-stabilized oil droplets completely and hence led to the aggregation of droplets. Perrechil and Cunha (2013) advocated the similar effect of free sodium caseinate in the solution, which would first complex with carrageenan in the continuous phase at pH 3.5 rather than the protein at the interface complex

with carrageenan to create the multilayer oil droplets. They also demonstrated that there were insufficient biopolymer molecules to completely cover the caseinate-stabilized droplets due to lower κ-carrageenan concentration, which resulted in droplets aggregation (Perrechil & Cunha, 2013).

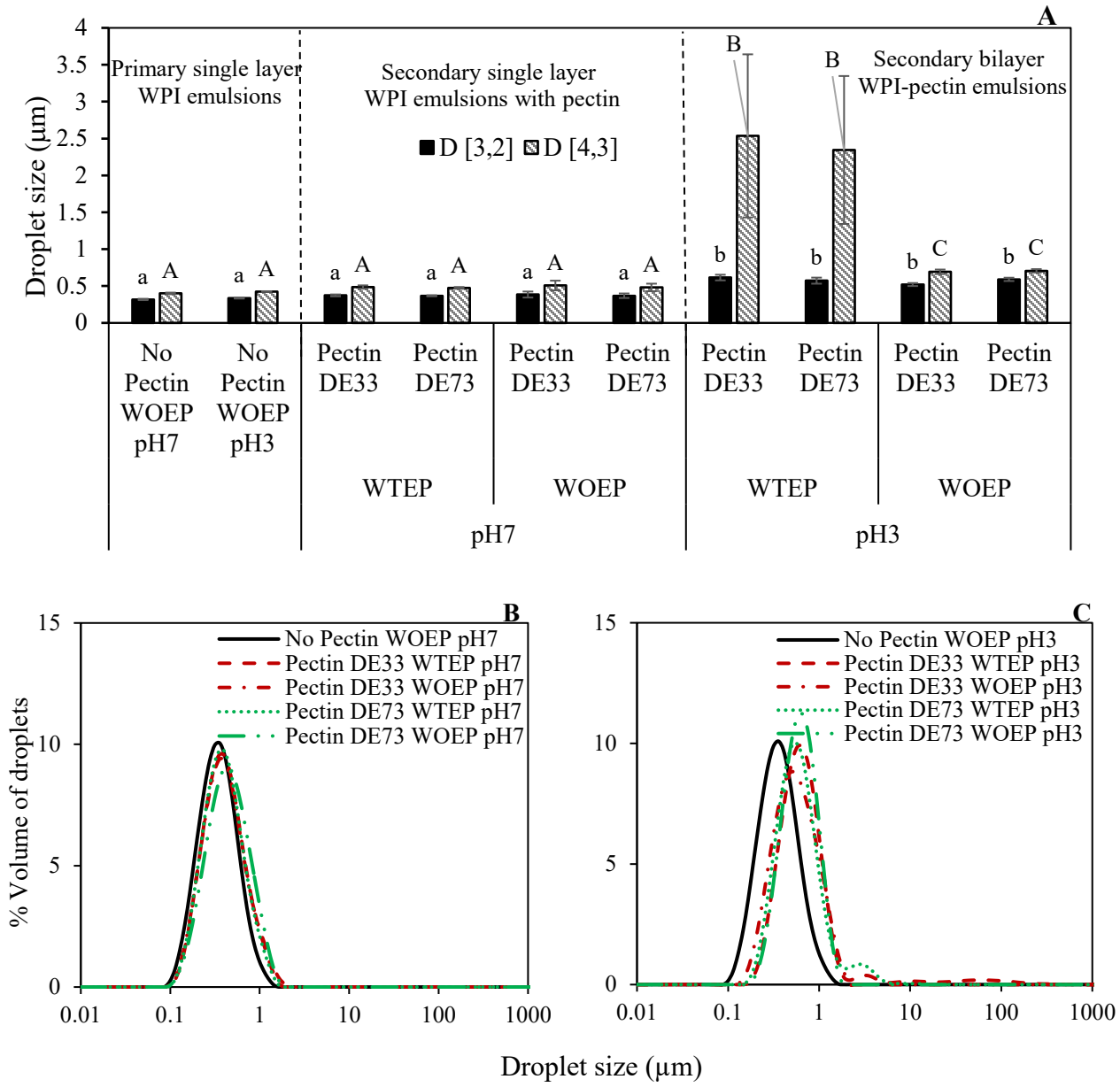

Figure 6.2 Effect of degree of esterification of pectin (DE33 and DE73) on the (A) average droplet size (d_{32} and d_{43}), (B) droplet size distribution at pH 7, and (C) droplet size distribution at pH 3 for primary and secondary emulsions as a function of pH with (WTEP) and without (WOEP) excess protein in the continuous phase of emulsions. Error bars indicate ± standard deviation (n ≥ 3). Different uppercase and lowercase letters denote the statistical significance difference (at 0.05 level) amongst the population means of d_{32} and d_{43} droplet size, respectively.

In contrast, the secondary bilayer emulsions without excess protein (WOEP) at pH 3 also showed a change in the droplet size (d_{43}) from 0.50 to 0.69 for DE33 pectin and 0.48 to 0.70 μm for DE73 pectin, respectively. In the absence of excess protein, there could be greater adsorption of pectin molecules onto the WPI-stabilized droplets at pH 3. Further, more pectin adsorption can contribute to perceiving an increased diameter (core + shell) of the WPI-pectin stabilized bilayer droplets by increasing the interfacial thickness due to increased steric repulsive barrier around the droplets. Such an increase in interfacial thickness of soy β-conglycinin and high methoxy pectin stabilized fish oil-in-water bilayer emulsion droplets was also reported to be in the range of 80 – 170 nm (Xiang et al., 2016). Overall, the changes in pH and excess protein in the continuous phase significantly affected the emulsion droplet size and size distribution.

6.4.2 Droplet charge of emulsions

At first, the zeta-potential of pectin solution was determined to evaluate the effect of pectin DE. The zeta potential values of DE33 and DE73 pectin solutions were – 45.4 and – 30.4 mV at pH 7, which was reduced to – 28.7 and – 14.3 mV at pH 3, respectively (Appendix D, Figure D3A). A significant ($p < 0.05$) decrease in pectin charge was observed with the change in pH from pH 7 to 3 increases the degree of esterification. Pectin with a lower degree of esterification (DE33) has a more significant number of free galacturonic acid for ionization and hence possesses a more negative charge compared to pectin with a higher (DE73) degree of esterification (Surh et al., 2006). Thus, the pectin charge was strongly dependent on its DE and pH of the colloidal dispersion.

Figure 6.3 shows the effect of pectin DE on the zeta potential of the WPI-pectin stabilized bilayer emulsions at pH 3 and pH 7 for WTEP and WOEP in the continuous phase. The zeta potential of WPI-stabilized primary emulsions (no pectin) was – 59.1 and – 58.4 mV at pH 7 for WTEP and WOEP emulsions, respectively. However, the addition of pectin in the primary emulsions significantly reduced the zeta potential of the mixed system in the range of – 49.5 to – 51.5 mV at pH 7. This slight reduction in the overall charge of the mixed system could be attributed to the ability of pectin molecules to make soluble complexes at neutral pH by interacting with the positive patches on the whey proteins (Pillai et al., 2021). This is also evident from the greater reduction in droplet charge (– 49.5 mV) observed for the WTEP emulsions at pH 7 while DE did not show any significant effect. Further, the highly negative charge of the mixed system at pH 7 is signifying a lack of extensive electrostatic complexation between whey proteins and pectin. Simo

et al. (2012) also observed that negatively charged pectin molecules did not adsorb onto the surfaces of negatively charged β-lactoglobulin-stabilized oil droplets at neutral pH due to strong electrostatic repulsion between them. Thus, at pH 7, pectin and whey protein interactions did not show any major effect on the droplet charge, which is also in accordance with the droplet size, which remained unchanged in the secondary emulsions (Figure 6.2A).

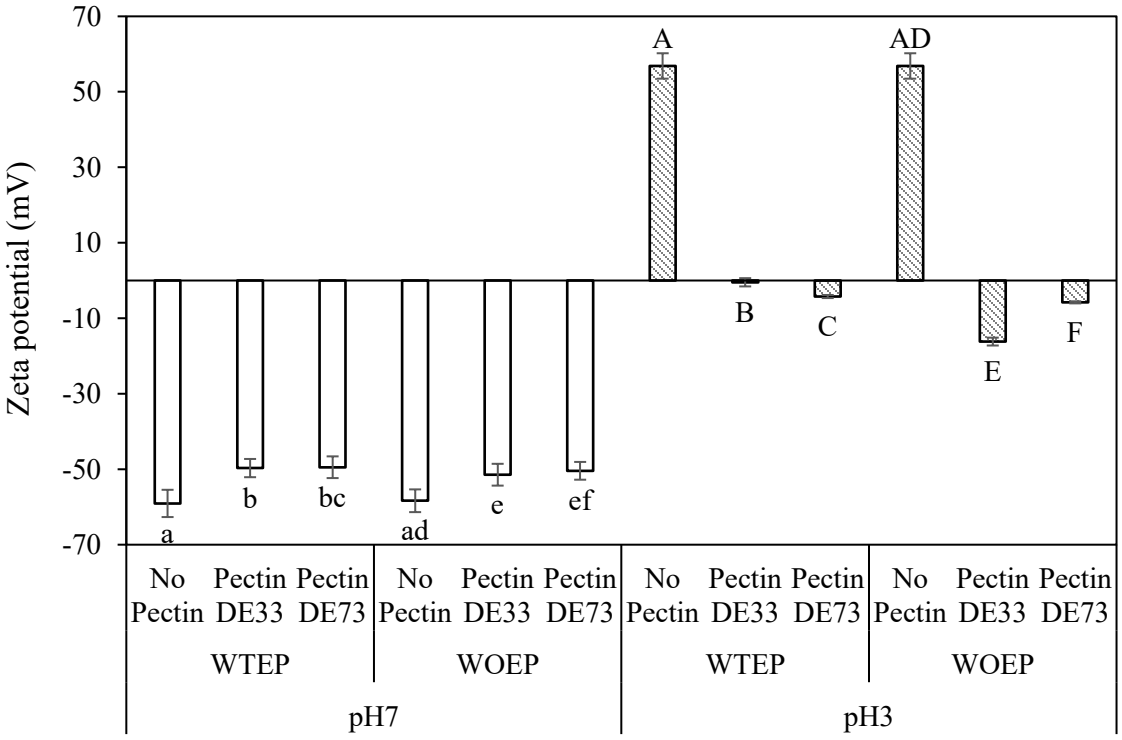

Figure 6.3 Effect of degree of esterification of pectin (DE33 and DE73) on the zeta potential of primary and secondary emulsions at pH 3 and pH 7 with (WTEP) and without (WOEP) excess protein in the continuous phase of emulsions. Error bars indicate ± standard deviation (n ≥ 3). Different uppercase and lowercase letters denote the statistical significance difference (at 0.05 level) amongst the population means at pH 3 and pH 7, respectively.

In the absence of pectin, the droplet charge of the primary WPI-stabilized emulsions was reversed entirely from – 59 mV to + 57 mV upon a change in pH from 7 to 3, respectively (Figure 6.3). This could be attributed to the whey proteins used to stabilize the droplets had a net positive charge below its isoelectric point (pI ~ 5.0) (Cho & McClements, 2009). However, when the secondary emulsions changed to pH 3, the positive charge of WPI-stabilized droplets WOEP

changed to – 16.2 mV for pectin DE33 compared to – 5.8 mV for pectin DE73. This change in the zeta potential suggests the electrostatic deposition of negatively charged pectin molecules onto the positively charged WPI-coated oil droplets (Muhoza et al., 2016). A decrease in the DE had a significant ($p < 0.05$) effect on the negative charge of the pectin-WPI coated droplets. In a similar finding, Verkempinck et al. (2018) also reported an increase in the negative charge of the citrus pectin-stabilized emulsions from – 10 mV to – 30 mV with a decrease in the degree of methylation of pectin. For the WPI-emulsions with excess protein (WTEP) in the continuous phase, the highly negative charge of the droplets was further reduced to – 0.5 mV and – 4.2 mV for DE33 and DE73 stabilized emulsions, respectively (Figure 6.3). This could be attributed to the interaction of highly positive charged excess protein with negatively charged pectin in the continuous phase of the emulsions, leading to a more considerable reduction in the overall negative charge of the secondary emulsions at pH 3. The effect of excess protein on the reduction of charge was also supported by the increase in the droplet aggregate size (d_{43}) of the WTEP secondary emulsions at pH 3 (Figure 6.2A). This is ascribed to the formation of more protein-pectin insoluble complexes in the bulk phase when excess protein was present, and hence less pectin would be accessible to go to the interface to impart the negative charge to the droplets. Similarly, it has been shown that the higher whey protein to pectin ratio (5:1), i.e. more amount of free protein in the bulk phase, was responsible for the reduction of negative charge of WPI-pectin stabilized droplets (Neirynck et al., 2007). We postulated that the adsorption of pectin molecules onto the interface at pH 3 either neutralized or reversed the positive charge of protein-stabilized droplets for WTEP or WOEP in the continuous phase, respectively. Thus, at pH 3, the magnitude of the negative charge of droplets was affected by the pectin charge (DE33 and DE73) and the amount of excess protein present in the continuous phase of the emulsions.

6.4.3 Rheological behaviour of bilayer emulsions

6.4.3.1 Flow behaviour of bilayer emulsions

Figures 6.4A and 6.4B show the effect of pectin DE on the viscosity profiles of WTEP and WOEP emulsions, respectively. The primary emulsions without pectin showed non-Newtonian shear thinning behaviour at a lower shear rate ($< 2\ s^{-1}$) which became shear independent (Newtonian) at a higher shear rate, indicating a complete loss of emulsion structure.

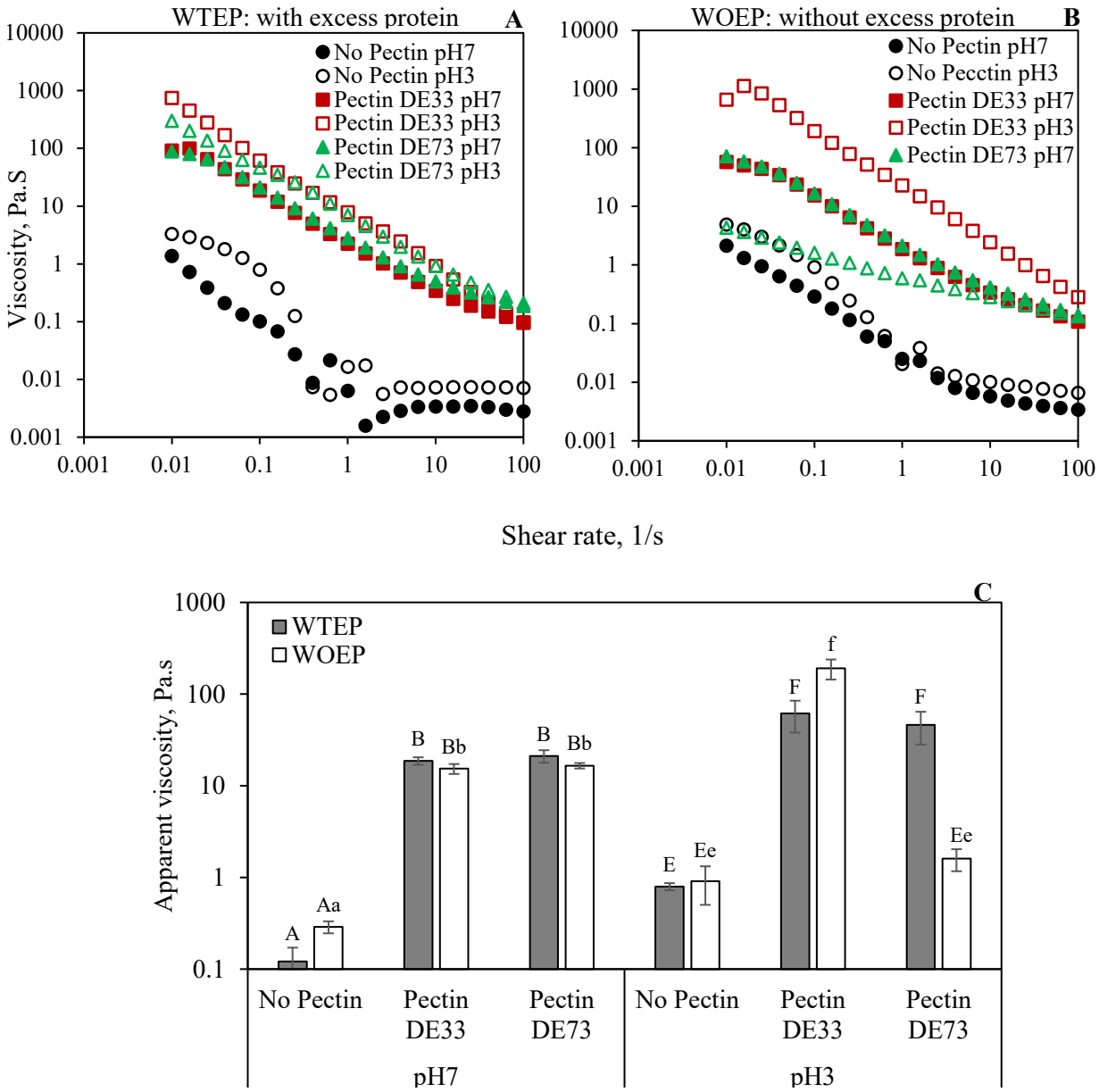

Figure 6.4 Effect of degree of esterification of pectin (DE33 and DE73) on the viscosity-shear rate profiles of primary (no pectin) and secondary emulsions at pH 7 and pH 3 (A) with excess protein (WTEP), (B) without excess protein (WOEP) in the continuous phase. (C) Apparent viscosity at 0.1 s^{-1} shear rate. Error bars indicate ± standard deviation (n ≥ 3). Different uppercase (WTEP) and lowercase (WOEP) letters denote the statistical significance difference (at 0.05 level) amongst the population means.

On the other hand, all the secondary emulsions prepared at pH 3 and pH 7 exhibited pseudoplastic (non-Newtonian) behaviour even at a high shear rate (>10 s^{-1}), indicating some structure still remains at this high shear rate. All the secondary emulsions demonstrated a plateau

at the lowest shear rate, irrespective of the pectin DE and the presence of excess protein in the continuous phase. At pH 7, all the secondary emulsions demonstrated similar pseudoelasticity. In contrast, at pH 3, the secondary emulsions WOEP and pectin DE33 showed the strongest pseudoplastic behaviour while the weakest pseudoplastic behaviour was observed for WOEP with pectin DE73. Concentrated food emulsions are well known to exhibit the pseudoplastic flow in the different types of non-Newtonian behaviour (Anvari & Joyner, 2017a). Interestingly, an initial increase (peak) in viscosity at a lower shear rate indicates yield stress required for the flow of pectin DE33 coated secondary emulsions WOEP at pH 3. This kind of shear thickening (peak in the viscosity) behaviour at a low shear rate is a tendency of the concentrated jammed emulsions where repulsively stabilized droplets rearrange in the direction of the applied shear and then start to flow (Wolf et al., 2007). In this study, shear-thinning of secondary emulsions could be attributed to the shear-induced alignment of close-packed droplets (WOEP) or a breakdown of aggregated oil droplets (WTEP) as a function of shear rate (Pal, 1997).

To better compare the viscosity of primary and secondary emulsions at pH 3 and pH 7, the apparent viscosity (at 0.1 s^{-1} shear rate) was plotted as a function of pectin DE for WTEP and WOEP emulsions (Figure 6.4C). At pH 7, the apparent viscosities of primary emulsions (no pectin) were 0.12 and 0.29 Pa.s for WTEP and WOEP emulsions, respectively. Addition of pectin significantly ($p < 0.05$) increased the apparent viscosity of the secondary emulsions at pH 7 in the range 15.3 – 21.1 Pa.s. However, the pectin charge (DE33 and DE73) and the presence of excess protein in the continuous phase did not show a significant effect ($p > 0.05$) on the viscosity of secondary emulsions at pH 7. An increase in the viscosity of secondary emulsions compared to primary emulsions (at pH 7) might be attributed to free unabsorbed pectin molecules between WPI-stabilized droplets, which can (i) led to the depletion flocculation, and (ii) increase the viscosity of the continuous phase. However, we observed that all the secondary emulsions at pH 7 were flowable liquid-like in the presence of free pectin molecules without any sign of aggregation or depletion flocculation (Figure 6.2). Moreover, the depletion flocculation in the emulsion is very much affected by the structure and viscosity enhancement ability of a biopolymer (McClements, 2015). It has been depicted that if the addition of polymer increases the viscosity of emulsions at a concentration below their critical flocculation concentration, then the mixed system (emulsions + polymer) would be stable and will not show any creaming due to depletion flocculation (McClements, 2000). Many researchers have observed the depletion flocculation phenomenon in

protein-pectin stabilized emulsions; however, all studied dilute emulsions had a larger droplet size (Gharsallaoui, Yamauchi, et al., 2010; Qiu et al., 2015; Surh et al., 2006). To evaluate the effect of biopolymer addition on the overall viscosity of the emulsion system, we have measured the apparent viscosity of aqueous pectin (DE33 and DE73) solutions at pH 7 and pH 3 (Appendix D, Figure D3B). Although the contribution from biopolymer viscosity (0.15 – 0.57 Pa.s) was very small at pH 7, the emulsion viscosity was increased by almost two orders of magnitude with the addition of pectin (DE33 and DE73). Such a high increase in viscosity of emulsions could be attributed to the immobilization of a greater number of protein-coated small droplets due to the unabsorbed polymer network present in the continuous phase (Dickinson, 1993; McClements, 2000). This is also in accordance with the smaller droplet size (Figure 6.2A) of secondary emulsions, which remained similar to the primary emulsions at pH 7. Similarly, an increase in the viscosity of sodium caseinate-stabilized emulsions was also reported when a high concentration (0.75 and 1 wt%) of κ-carrageenan was added at neutral pH (Perrechil & Cunha, 2013). The authors attributed this to the increase in viscosity of the continuous phase by unabsorbed κ-carrageenan molecules, which slowed down the flocculation or droplet movement (Perrechil & Cunha, 2013). Therefore, it can be postulated that the unabsorbed pectin molecules in emulsions could significantly contribute to the viscosity enhancement in the presence of smaller droplets compared to the bulk phase alone; hence overall viscosity of the emulsions increased at pH 7.

At pH 3, the apparent viscosity of primary WPI-stabilized emulsions was 0.8 and 0.9 Pa.s for WTEP and WOEP emulsions, respectively ($p > 0.05$) (Figure 6.4C). The addition of pectin increased the viscosity of secondary WTEP emulsions to 46.1 – 61.4 Pa.s at pH 3. In this case, the electrostatic complexation between protein-pectin was mainly driven by the excess protein in the continuous phase, as discussed earlier, limiting the adsorption of pectin at the droplet surface. Lack of enough pectin can induce droplet aggregation (Figure 6.2A) at charge neutralization (Figure 6.3) due to electrostatic bridging, which could be a reason for the increase in the viscosity of secondary emulsions. Note that the pectin DE did not significantly impact the viscosity of secondary emulsions WTEP ($p > 0.05$). However, the secondary emulsions WOEP showed an enormous increase in the viscosity (191.1 Pa.s) for DE33 compared to 1.6 Pa.s for DE73 emulsions (Figure 6.4C). Thus, in the absence of excess protein, the negative charge provided by the pectin (DE33 versus DE73, Figure 6.3) coated droplets at pH 3 had a significant effect on the viscosity of secondary emulsions ($p < 0.05$). Moreover, the apparent viscosities of primary WPI-stabilized

emulsions and secondary emulsions coated with pectin DE73 were similar but much lower than the pectin DE33 coated emulsions. The higher viscosity of the latter could be explained by the higher magnitude of the negative charge of DE33 pectin (Figure 6.3), which was responsible for the strong electrostatic repulsion in addition to steric repulsion between DE33 coated droplets leading to a near close packing structure. Wijaya et al. (2017) also reported an increase in the viscosity of concentrated emulsions, stabilized by a thick interfacial layer of WPI-pectin complexation at pH 4.5, due to close packing of the droplets. This shows that the interfacial composition (charge of DE33 versus DE73 pectin) affected by the protein-pectin interaction (pH 7 versus pH 3) and the presence of excess protein in the continuous phase are the governing factors for the difference in the viscosity of WPI-stabilized primary versus WPI-pectin stabilized bilayer emulsions.

6.4.3.2 Viscoelastic behaviour of bilayer emulsions

The viscoelastic properties of the emulsions were studied by analyzing the strain and frequency-dependent storage (G′) and loss (G″) moduli. At pH 7, the viscosity profiles of all secondary emulsions were essentially over-lapping without significant effect of pectin DE and excess protein in the continuous phase (Figures 6.4A and 6.4B). Therefore, the viscoelastic behaviour of emulsions was studied only at pH 3, where protein-pectin interactions exhibited a drastic change in the rheology of the secondary multilayer emulsions. Figures 6.5A and 6.5B show the strain-dependent G′ and G″ of primary and secondary emulsions as a function of pectin DE for emulsions WTEP and WOEP, respectively. At a lower strain, the primary emulsions WTEP and WOEP could barely display any linear viscoelastic region (LVR) before crossover, although G′ remained higher than G″ below 1% strain. Similar viscoelastic behaviour was also observed for the WOEP secondary emulsions coated with pectin DE72, indicating weak emulsion gels (Figure 6.5B). All other emulsions showed G′ higher than G″ with a strong LVR before the crossover, indicating dominating elastic behaviour and strong gel formation. For the emulsion WTEP (Figure 6.5A), the plateau G′ within the LVR was higher for pectin with a higher charge (DE33), followed by pectin DE72 and the primary emulsion. This behaviour was attributed to the formation of a strong viscoelastic gel-like structure in the secondary emulsions in contrast to the primary emulsions. Interestingly, the secondary emulsions WOEP showed stronger and longer LVR and considerably higher strain at G′ and G″ crossover when coated with the pectin DE33 than the weak gel behaviour for DE73, likely due to increased rigidity of the system with an increased charge of

the pectin. Stronger LVR is an indicator of increased resistance of the system to permanent deformation, whereas large crossover strain exhibits the resistance to structural breakdown due to dominating elastic component of the system (Anvari & Joyner, 2017b; Preziosi et al., 2017).

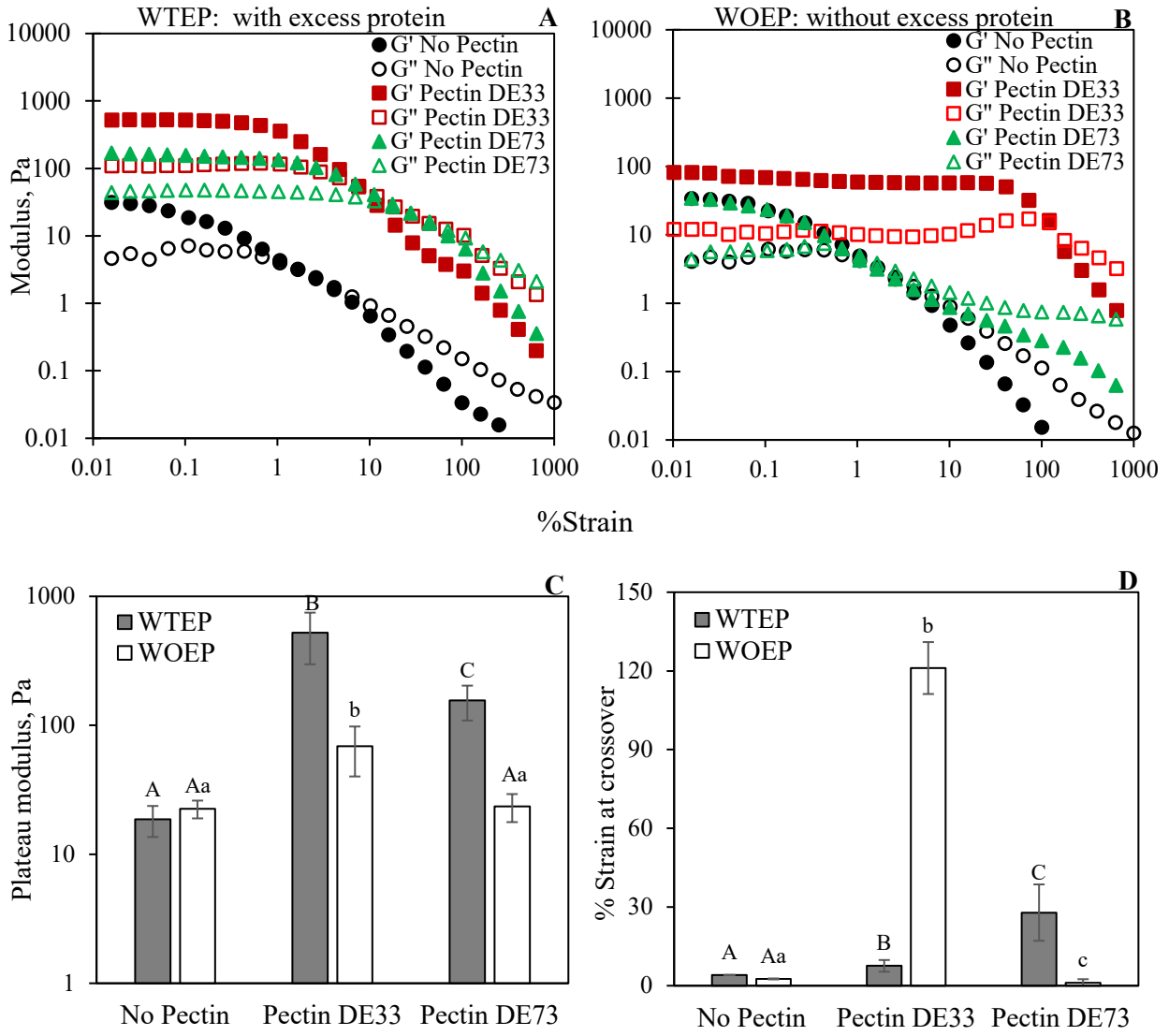

Figure 6.5 Viscoelastic behaviour of primary (no pectin) and secondary emulsions at pH 3 as a function of pectin charge (DE33 and DE73). Strain dependent storage and loss moduli of emulsions (A) with excess protein (WTEP), and (B) without excess protein (WOEP) in the continuous phase, (C) Plateau modulus at 0.1% strain, and (D) %strain at cross-over of G′ and G″. Error bars indicate ± standard deviation (n ≥ 3). Different uppercase (WTEP) and lowercase (WOEP) letters denote the statistical significance difference (at 0.05 level) amongst the population means.

G′ and G″ crossover, beyond the LVR and yield point, suggesting structural reordering or flow of the emulsion droplets induced by the applied stress and an increase in the dominating viscous behaviour. At a strain > 1%, as the emulsions enter the large amplitude oscillatory shear (LAOS) region, the shape of the curves in the non-linear viscoelastic region (NLVR) changed significantly, which could indicate important information about emulsion structure as well as the strength of droplet-droplet interactions (Anvari & Joyner, 2017a; Hyun et al., 2011). For example, at an intermediate strain (1 to 10%), the shape of G″ was similar to G′ curves in the secondary emulsions WTEP, indicating LAOS type I (strain thinning) behaviour. This type of LAOS behaviour is attributed to the re-orientation of the structure in the direction of the applied strain, which, in the case of polymer-based network, results in loss of junction zones due to the polymer chain's inability to rejoin the network structure (Hyun et al., 2011).

In this study, the secondary emulsions WTEP showed two-step yielding, indicating the inter-cluster bond first broken down into individual flocs at a lower strain at around 1% (first yield point) followed by cluster breakdown into individual particles at a higher strain (second yield point, at around 100%) (Koumakis & Petekidis, 2011). The strain thinning and two-step yielding behaviour is typical in the flocculated emulsions with attractive inter-droplet interaction (Datta et al., 2011; Qian et al., 2020). In contrast to this behaviour, pectin DE33-coated secondary emulsions WOEP showed a distinctive peak in the G″ curve at the crossover strain, indicating LAOS type III (weak strain overshoot) behaviour. This behaviour is very common in soft glassy material, i.e., repulsive concentration emulsions, where the shear-induced relaxation and rearrangement of near-close packed droplets is typically observed after escaping from the cage structure. Datta et al. (2011) also observed a similar overshoot of G″ in the strain-dependent viscoelasticity of repulsive emulsions at oil volume fraction ($\phi = 0.65$) above random close packing of droplets. In another study, fish gelatin and gum Arabic stabilized bilayer concentrated emulsions ($\phi = 0.7$) also showed weak strain overshoot at pH 3.6 due to the close-packed structure of emulsions droplets (Anvari & Joyner, 2017a). Overall, it can be said that the secondary emulsions behaved like attractive gel WTEP (Figure 6.5A) and repulsive gel WOEP. The protein-pectin interaction, either occurring in the continuous phase WTEP or at the interface WOEP, is the controlling factor in deciding the emulsions rheology.

For better comparison of the viscoelastic behaviour of all emulsions, the changes in the plateau modulus (G'_p) at 0.1% strain and the crossover strain were plotted in Figures 6.5C and

6.5D. Note that the primary emulsions (no pectin) did not show a plateau at this strain, but it was used for comparison purposes. The primary emulsions did not show any significant difference in the G'_p ($p > 0.05$) value for WTEP and WOEP systems. The G'_p significantly increased for all secondary emulsions WTEP and WOEP ($p < 0.05$), except for the DE73-coated secondary emulsions WOEP which had a similar G'_p (~ 23 Pa) ($p > 0.05$) as the primary emulsions. The G'_p of DE33-coated secondary emulsions WOEP was increased to 69.1 Pa. The G'_p WTEP was further increased to 522.7 Pa and 156.1 Pa for pectin DE33 and DE73-coated secondary emulsions, respectively. However, tan δ value (ratio of G″/ G′ at 0.1% strain) for pectin DE33-coated emulsions WOEP was the lowest (0.15) compared to emulsions WTEP (0.21), indicating comparatively stronger gel structure. This is also in accordance with the higher viscosity of pectin DE33 coated emulsions WOEP compared to emulsions WTEP.

From Figure 6.5D, the crossover strain was also significantly increased with the addition of pectin in the emulsions except for the DE73-coated secondary emulsions. Higher G'_p (522.7 Pa and 156.1 Pa) and tan δ (0.21 and 0.3), but lower crossover strain (7.6% and 27.9%) of DE33 and DE73-coated emulsions WTEP, respectively, was an indication of viscoelastic gels with more brittle structure. The DE33-coated secondary emulsions WTEP showed a more brittle gel-like structure due to its lower crossover strain than DE73-coated emulsions. Oppositely, the much higher crossover strain (121.1%) with much lower tan δ (0.15) and G'_p (69.05 Pa) still being comparatively higher for pectin DE33 coated secondary emulsions WOEP was an indication of stronger viscoelastic gels with more ductile structure.

The gelation behaviour of the emulsions was also studied from the frequency-dependent storage and loss moduli as a function of pectin DE for emulsions WTEP and WOEP (Figures 6.6A and 6.6B). All the emulsions showed G′ greater than G″ with a different degree of frequency dependence. The primary emulsions WTEP and WOEP showed a decrease in G′ and increased in G″ beyond 10 rad/s, leading to an early stage of structural breakdown. Similar behaviour was also observed for the pectin DE73 coated secondary emulsions WOEP (Figure 6.6B), indicating a weak gel-like structure. The addition of pectin increased G′ of secondary emulsions WTEP, indicating an increase in the stiffness (Figure 6.6A). However, the pectin DE73 coated emulsions WTEP showed a decrease in the gap between G′ and G″ with higher dependence on frequency, suggesting the gel-like network consisted of non-covalent physical crosslinks (Tang & Liu, 2013). Only pectin DE33 coated secondary emulsions WOEP (Figure 6.6B) showed a greater difference between G′

and G″ compared to all other emulsions with lesser dependence on frequency, indicating strong gel-like behaviour.

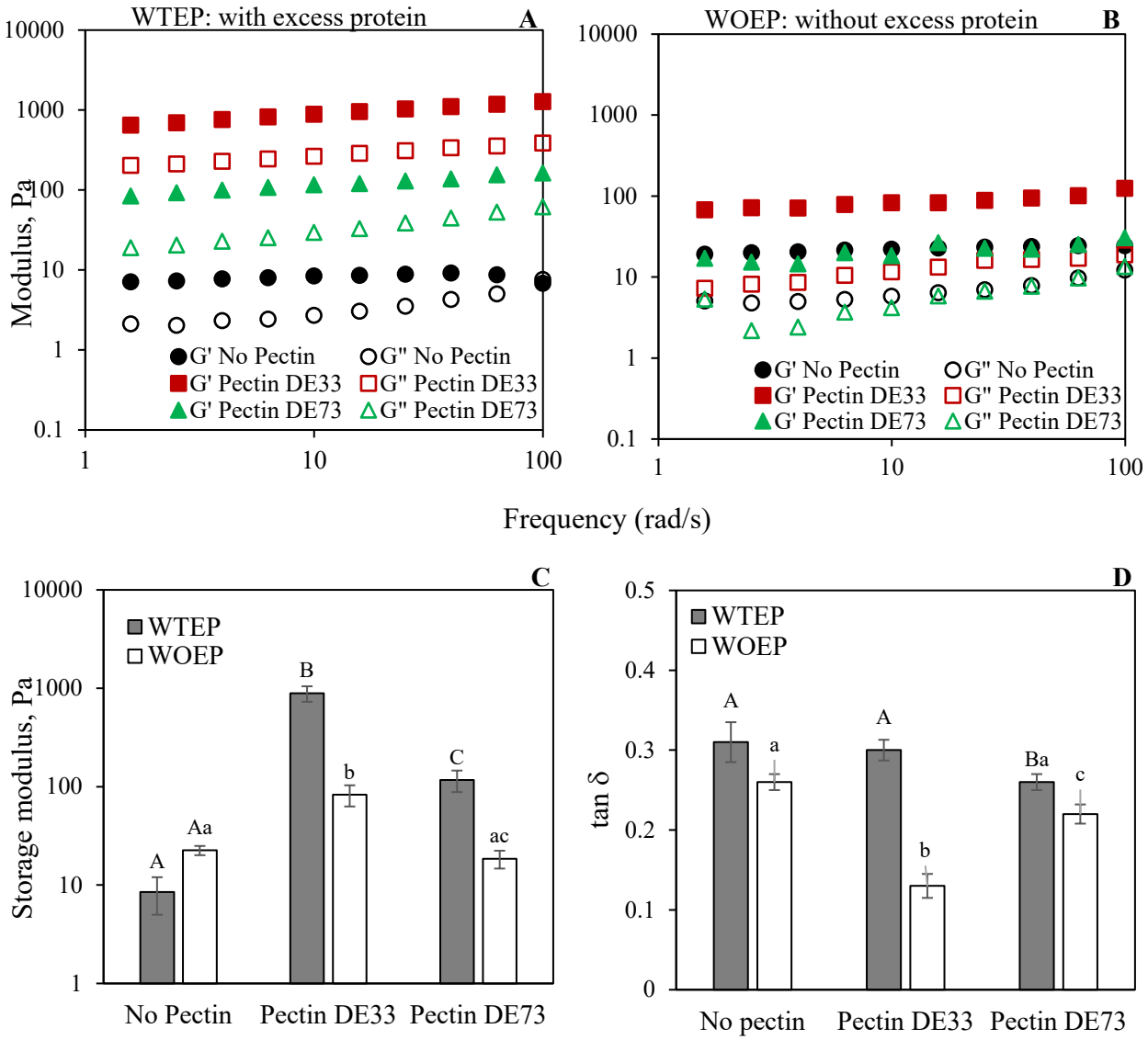

Figure 6.6 Frequency-dependent viscoelastic behaviour of primary (no pectin) and secondary emulsions as a function of pectin charge (DE 33 and DE 73) with (WTEP) and without (WOEP) excess protein in the continuous phase. (A, B) Frequency-sweep storage and loss moduli, (C) Storage moduli, and (D) tan δ (loss tangent) plotted at 10 rad/s. Error bars indicate ± standard deviation (n ≥ 3). Different uppercase (WTEP) and lowercase (WOEP) letters denote the statistical significance (at 0.05 level) amongst the population means.

To directly compare the frequency-dependent viscoelastic behaviour of emulsions, the G′ of the primary and secondary emulsions at 10 rad/s was plotted in Figure 6.6C. The nature of G′ of all emulsions was similar to strain-dependent plateau modulus (G'_p) (Figure 6.5C). The frequency-dependent G′ of primary WPI-stabilized emulsion WTEP was 8.5 Pa, increased to 888.2 Pa, and 116.9 Pa for pectin DE33 and pectin DE73 coated secondary emulsions WTEP, respectively. For the emulsions WOEP, G′ increased from 22.5 Pa for primary emulsions to 83.1 Pa and 18.5 Pa, for pectin DE33 and pectin DE73-coated secondary emulsions WOEP, respectively. The similar gel strength of primary and secondary emulsions with pectin DE73 could be ascribed to the lower charge density of the adsorbed pectin at the interface, which did not significantly contribute to the effective volume fraction of droplets. To differentiate the gel strength, tan δ (G″/ G′) was also calculated for secondary emulsions (Figure 6.6D). The tan δ values of emulsions WTEP were higher, 0.3 (DE33) and 0.26 (DE73), compared to emulsions WOEP, 0.13 (DE33) and 0.22 (DE73). Although G′ was lower for DE33 coated secondary emulsions WOEP, tan δ (G′ >> G″) was significantly lower than emulsions WTEP (G′ > G″), indicating stronger elastic-dominated structure. This is also supported by the highest apparent viscosity (Figure 6.4C) and highest crossover strain (Figure 6.5D) for the DE33 coated secondary emulsions WOEP compared to emulsions WTEP.

6.4.3.3 Creep-recovery compliance of bilayer emulsions

The structural deformation (creep compliance) and the structural recovery of the primary and secondary emulsions were studied by applying and removing the constant stress chosen within the LVR. The creep compliance (J_E) of viscoelastic material under the applied stress denotes the degree of deformation, i.e., higher J_E indicates more deformation or weaker structural material or vice versa (Huang et al., 2016). The recoverable strain (γ_{RE}) represents the elastic properties of colloidal material, i.e., higher γ_{RE} is interpreted as the higher elastic strength of the emulsion network whereas lower γ_{RE} is an indication of more viscous nature of the emulsion structure with irreversible network deformation (Haj-shafiei et al., 2013). Creep-recovery curves of the primary and secondary emulsions are shown in Figure 6.7A. The creep compliance J_E or deformation was remarkably higher for primary emulsions (no pectin) and the secondary emulsions WOEP coated with the pectin DE73. However, the addition of pectin DE33 significantly reduced the J_E of both the secondary emulsions WTEP and WOEP. For example, without pectin, peak compliance (J_{max})

was 8.16 × 10^6 Pa^{-1} for both the emulsions WTEP and WOEP, which was reduced to < 4.0 Pa^{-1} for all the secondary emulsions except for the secondary emulsion WOEP with pectin DE73 (J_{max} = 1.9 × 10^4 Pa^{-1}) (Figure 6.7B).

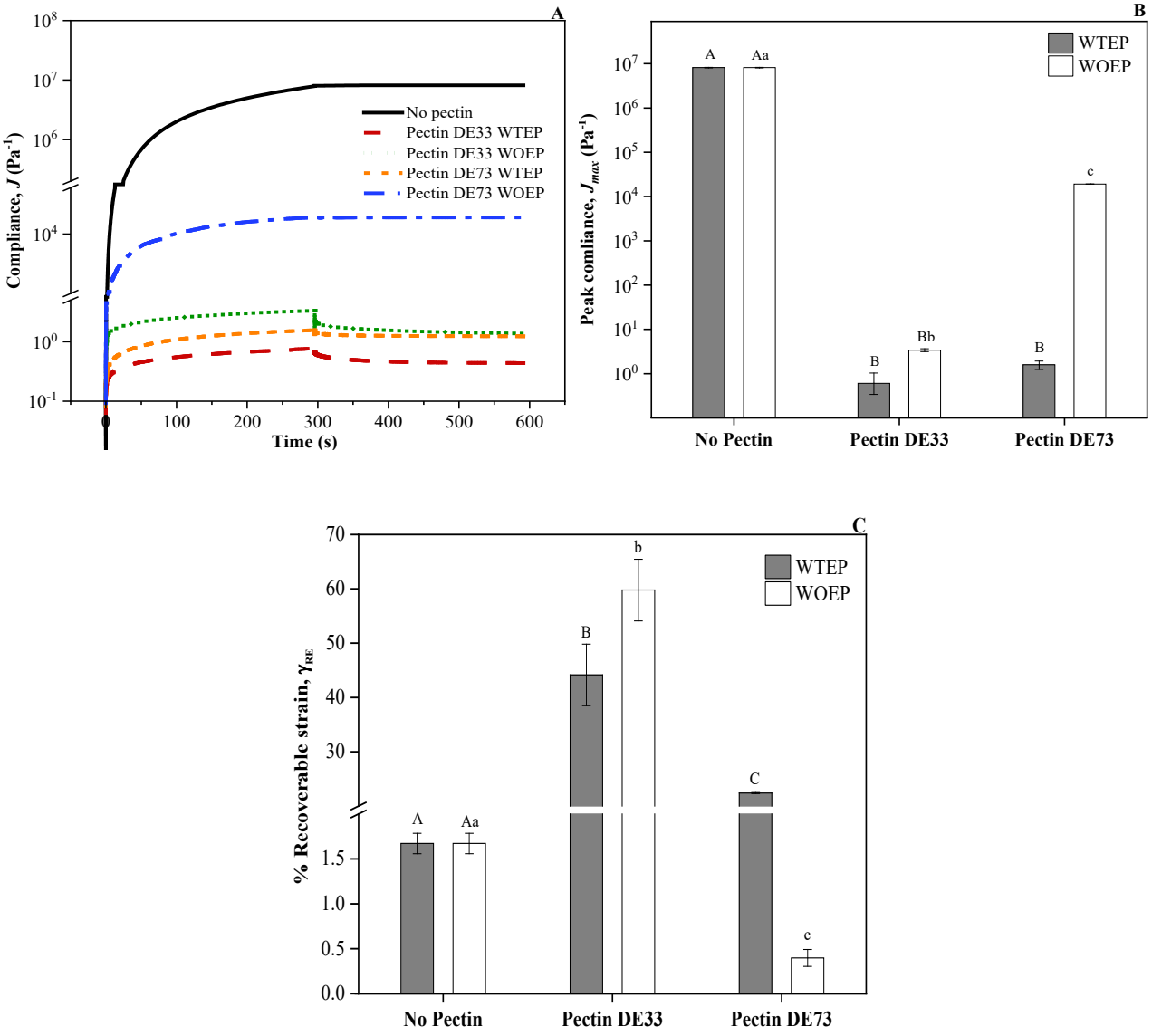

Figure 6.7 Structural recovery of primary (no pectin) and secondary emulsions as a function of pectin charge (DE 33 and DE 73) with (WTEP) and without (WOEP) excess protein in the continuous phase. (A) creep-recovery curves were recorded by applying the constant stress within the LVR limit. (B) peak compliance (J_{max}); and (C) calculated values of % recoverable strain (γ_{RE}) using Equation 6.1 Error bars indicate ± standard deviation (n ≥ 3). Different uppercase (WTEP) and lowercase (WOEP) letters denote the statistical significance difference (at 0.05 level) amongst the population means.

The structural recovery of the primary and secondary emulsions, expressed in terms of %recoverable strain (γ_{RE}), was plotted in Figure 6.7C. The primary emulsions WTEP and WOEP (no pectin) and the secondary emulsion WOEP with pectin DE73 showed very low structural recovery ($\gamma_{RE} < 2\%$). However, the structural recovery was increased to 44.1% and 22.4% for the secondary emulsions WTEP stabilized by DE33 and DE73 pectin, respectively. The highest structural recovery ($\gamma_{RE} = 59.8\%$) after deformation was observed for the pectin DE33 stabilized secondary emulsions WOEP. More deformation and less structural recovery are an indicator of the more viscous nature of these emulsions. On the other hand, reduced deformation and increased structural recovery of secondary emulsions are closely related to a stronger viscoelastic nature attained through the close packing of droplets for the emulsion WOEP or due to droplet aggregation for the emulsions WTEP as discussed earlier.

6.4.4 Visual observation of bilayer emulsions

To better understand the viscoelastic nature of the structure, visual observations of the emulsions were recorded after placing them on the rheometer Peltier plate before and after the oscillatory measurements. The primary emulsion showed a flowable liquid-like behaviour (Figure 6.8A). Both the secondary emulsions WTEP and WOEP with pectin DE33 showed a self-supporting strong viscoelastic gel-like structure before deformation, either due to attractive aggregation (Figure 6.8B) or repulsive close packing (Figure 6.8C) of droplets. For the emulsion WTEP, the excess protein promoted more protein-pectin interaction in the continuous phase; hence less pectin was available to interact with the protein at the droplet surface, which could favour bridging interaction among the droplets due to charge neutralization (Figure 6.3), leading to larger aggregate size (d_{43} in Figure 6.2A). These large aggregates were clearly visible after the oscillatory rheology experiment of the same sample (Figure 6.8B and 6.8D bottom row, for pectin DE33 and DE73, respectively).

In contrast, the absence of any excess protein (WOEP) in the continuous phase favoured more protein-pectin electrostatic interactions at the droplet surface, also supported by the increase in droplet charge with an increase in pectin DE (Figure 6.3) and a smaller droplet size (d_{43} *in* Figure 6.2A). The absorption of pectin DE33 at the interface helped to repulsively stabilize the droplets through a stronger electrostatic and steric repulsions barrier. The increased interfacial shell layer thickness of WPI-pectin DE33 bilayer contributed to an increase in the effective volume fraction

of the oil droplets such that repulsive gelation of the emulsion was possible even with 20 wt% oil. This is further supported by the absence of any aggregated flocs and a smooth texture of the emulsions WOEP post-oscillatory shear in Figure 6.8C and 6.8E bottom row. The lower charge density of pectin DE73 compared to DE33 could have a lower impact on the shell-layer thickness due to a shorter range of repulsive charge cloud around the oil droplets leading to a weakly flowable gel-like structure (Figure 6.8E top row). Thus, in this study, higher gel strength of secondary emulsions compared to primary emulsions could be attributed to the gelation due to bridging flocculation of droplets in the presence of excess protein (WTEP) or due to jamming of repulsively stabilized droplets at a higher charge of pectin without excess protein (WOEP).

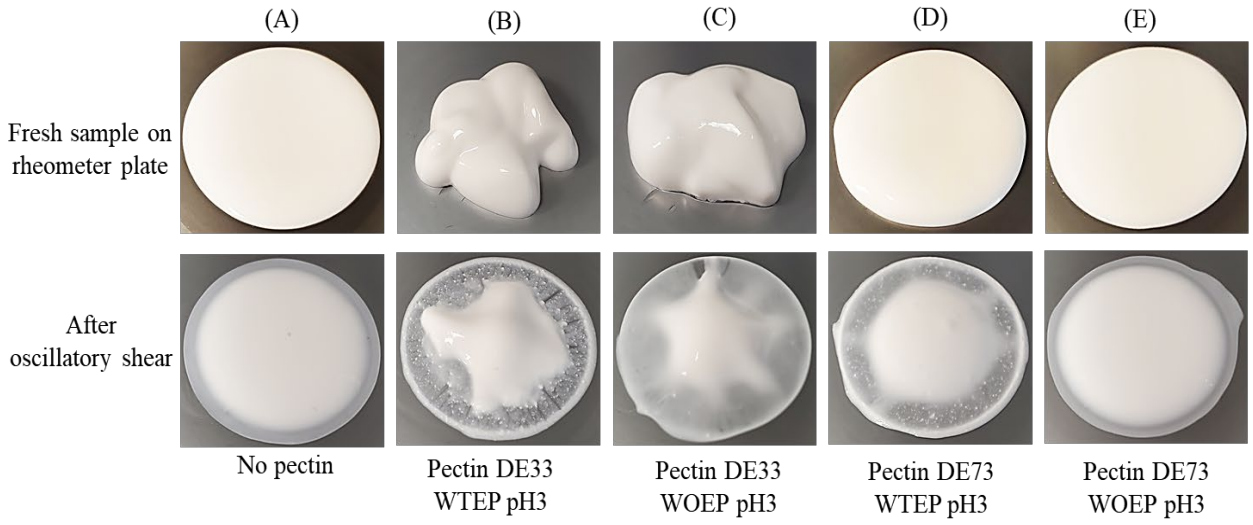

Figure 6.8 Visual appearance of primary (single layer) and secondary (bilayer) emulsions observed before (top) and after (bottom) performing oscillatory rheological measurements. Samples were placed on the Peltier plate of the rheometer.

6.4.5 Microstructure of bilayer emulsions

Figure 6.9 shows typical CLSM images for the primary and secondary emulsions. Here, red oil droplets (core) were stained with Nile red and green WPI or WPI-pectin complexes at the interface (shell) or in the continuous phase were stained with fast green.

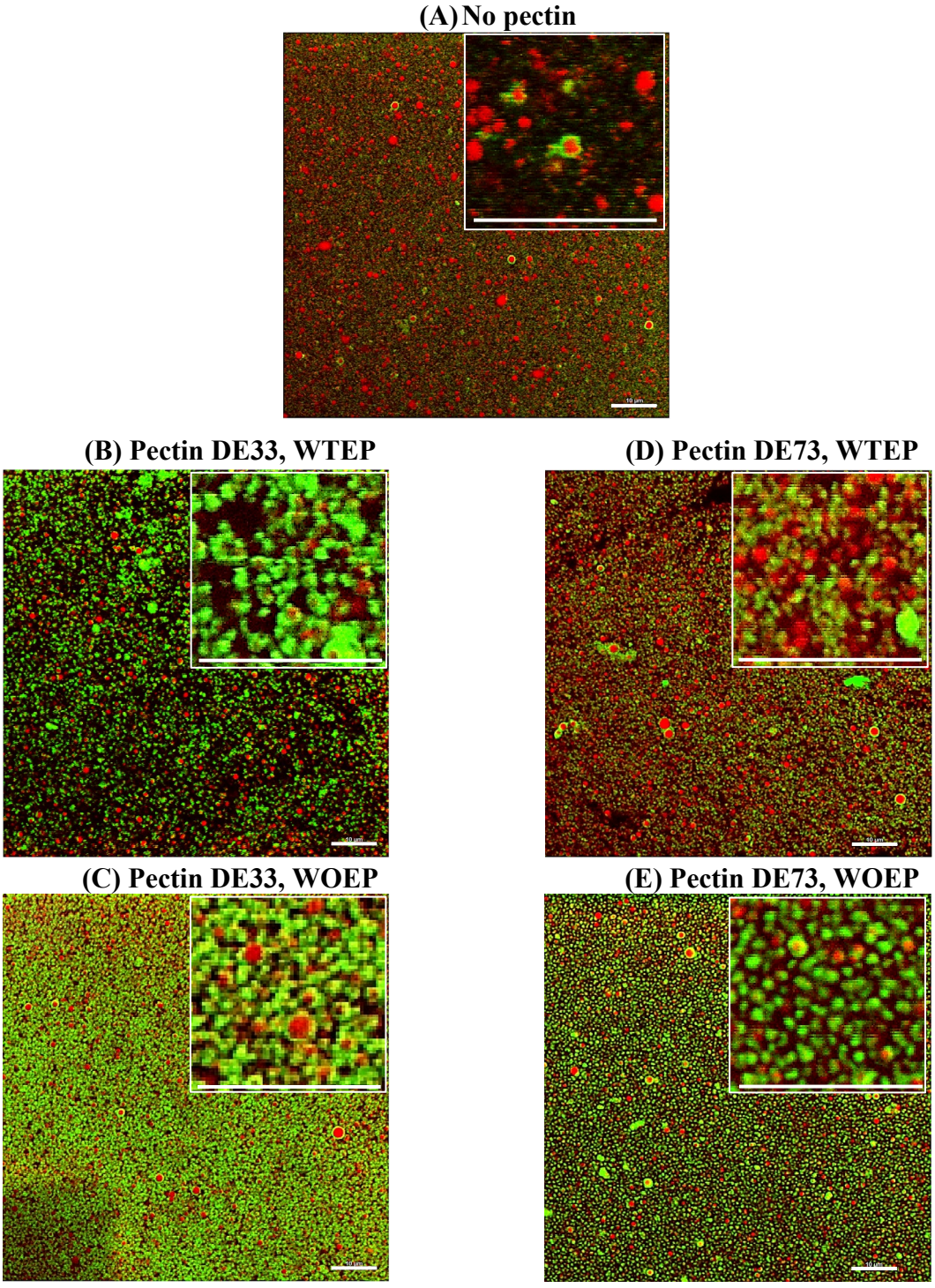

Figure 6.9 Microstructure of 20 wt% canola oil-in-water WPI-stabilized monolayer and WPI-Pectin stabilized bilayer emulsions collected using a confocal microscope. Oil droplets are indicated with the red colour and WPI or WPI-pectin complexes either at the interface or in the continuous phase are indicated with green colour. Insets are 4 times zoomed view of the original images. White scale bar is 10 μm in the original and zoomed images.

Without pectin, the droplets were uniformly distributed, and they were repulsively stabilized by the positive charge of whey protein at pH 3 (Figure 6.9A). However, with the addition of 1 wt% pectin of two different charges (DE33 and DE73), the secondary emulsions showed a drastic change in the microstructure depending on the presence and absence of the excess protein in the continuous phase. The secondary emulsions prepared with the excess protein in the continuous phase (WETP) resulted in droplet flocculation (Figures 6.9B and 6.9D). This is in accordance with the larger aggregates observed during visual observation (post-shear, Figures 6.8B and 6.8D) and larger droplet size reported in Figure 6.2A for the WPI-pectin emulsions WETP. The excess protein (positively charged) sitting in the continuous phase favoured the electrostatic interaction with negatively charged pectin. Due to this interaction, the lack of enough pectin available to cover the oil droplets resulted in the larger flocs and hence stronger attractive gel formed in the presence of excess protein and higher charge of the pectin (DE33). Without the excess protein in the continuous phase (WOEP), the electrostatic interaction between whey protein and pectin exclusively happened at the interface. That is why in Figures 6.9C and 6.9E, the nanodroplets were uniformly covered by the WPI-pectin bilayer without any sign of droplet flocculation. As discussed earlier, the deposition of the second layer of pectin on the WPI-stabilized droplets increased the interfacial shell layer thickness (δ) through the contribution of the steric barrier and charge cloud around them. This increase in δ was quite significant when droplets are covered by the highly negatively charged pectin DE33 compared to less negatively charged pectin DE73. These unique differences between two different pectins (DE33 versus DE73) favoured the strong repulsive gel formation due to the close-packing of droplets stabilized by pectin DE33 as shown in Figure 6.9C. Oppositely, a less negative charge of pectin DE73 failed to create a similar close-packing of the droplets (Figure 6.9E), leading to a weakly flowable gel-like behaviour. Thus, the differences observed in the microstructure and rheology could also reflect the kind of protein-pectin interaction involved in the formation of bilayer emulsions.

6.4.6 Mechanism of gelation in bilayer emulsions as a function of pectin charge

From rheology analysis, we observed that the electrostatic deposition of pectin with higher charge (DE33) increased the viscosity, gel strength, tan δ and structural recovery (%γ_{RE}) of WPI-pectin-stabilized bilayer emulsions compared to pectin with lower charge (DE73) in the absence of excess protein (WOEP). Further, the latter exhibited an almost similar rheological behaviour as

the WPI-stabilized monolayer. This was also supported by the visual observations (Figure 6.8) and confocal microstructure (Figure 6.9) of these mono and bilayer emulsions. We proposed that the gelation of bilayer emulsions with high pectin charge could be mainly due to increased interfacial thickness (δ) of bilayer stabilized droplets compared to monolayer droplets contributed by the repulsive charge cloud and steric layer around the droplets. The increase in thickness of the second layer (due to the steric layer) can also be predicted (from Figure 6.2), 94 nm for DE33 and 129 nm for DE73 pectin coated emulsions WOEP, from the increase in WPI-stabilized droplet size after deposition of pectin layer at pH 3. Patel, Mohanan, et al. (2019) reported the gelation of canola-in-water nanoemulsions at $\phi_{oil} = 0.42$ when stabilized with the sodium caseinate compared to whey protein due to more contribution of repulsive forces (electrostatic and steric) from the previous one in elevating the shell-layer thickness and the effective oil volume fraction (ϕ_{eff}). Similarly, in this study, the pectin with higher charge (DE33) imparted electrostatic and steric stabilization of droplets compared to only steric stabilization by lower charged pectin (DE73). Ettelaie and Akinshina (2014) also calculated theoretically using Self Consistent Field (SCF) theory that the strong electrostatic repulsive forces generated by the electrostatically and sterically (highly charged polysaccharide)-stabilized droplets persists for slightly longer distances than the steric forces alone. This is also applicable to our study wherein the higher charge of pectin DE33 might be a more contributing factor in increasing the δ. This indicates that the steric barrier could increase the interfacial shell-layer thickness and ϕ_{eff}, but more significantly when sterically stabilized droplets are also stabilized by a higher negative charge (electrostatic repulsive force). The higher interfacial shell-layer thickness and hence higher ϕ_{eff} of DE33 pectin-coated droplets could be responsible for their higher viscosity and gel strength of bilayer emulsions compared to DE73-coated bilayer emulsions at $\phi_{oil} = 0.21$. Due to the complexity of estimating the actual contribution of electrostatic repulsive forces (or electric double layer) in interfacial thickness, it is not possible to calculate the ϕ_{eff} of DE33 and DE73-coated bilayer emulsions. However, the close-packed microstructure of droplets observed in confocal (Figure 6.9C) and cryo-SEM (Appendix D, Figure D4) for DE33-coated emulsions are evident to support our hypothesis of an increase in ϕ_{eff} due to increasing in δ.

6.4.7 *In-vitro* lipid digestibility of emulsions

Figure 6.10A shows the FFA release profiles at the different stages of emulsion digestion. Surprisingly, the presence of rabbit gastric lipase (RGL) did not show the release of FFA from the emulsions during the gastric phase of digestion. This could be attributed to very limited hydrolysis by the gastric lipase and the lower amount of the ionized FFA available to react with NaOH at the upper gastric pH (5.5). The consideration of limited ionization of FFA is important while working with pH-STAT protocol due to the high pKa values (~10) of fatty acids present in canola oil (Chatzidaki et al., 2016; Mat et al., 2016). Further, the electrostatic deposition of the pectin layer could also block the site for the pepsin to act on the protein present at the droplet surface. That means WPI-stabilized primary emulsions with no pectin layer are more susceptible to protein hydrolysis, and hence RGL would have easy success to triglycerides molecules during the gastric phase of digestion. However, even that was not detectable using our pH-STAT protocol because the gastric phase has a 10 to 25% contribution to lipid digestibility (Mat et al., 2016). But, any degree of lipid hydrolysis by RGL during gastric digestion could significantly affect the subsequent digestion of emulsions during the intestinal phase (Sassene et al., 2016). Roy et al. (1979) also demonstrated the similar role of RGL in enhancing lipid digestibility during the intestinal phase. This advantage of including RGL in the digestion study is extensively discussed in Chapter 5.4.7 of this thesis. All the emulsions initially showed a rapid release of FFA (at ~ 0.60 % FFA per min) with ~ 6.0 % lipolysis in the initial 10 min of digestion. The rapid rate (at ~ 0.60 % FFA per min) of lipid hydrolysis by the pancreatin lipase was further continued for the WPI-stabilized monolayer emulsions (no pectin) till ~27.0 % of total FFA was released in the first 45 min of intestinal digestion. After that, a sudden reduction in the lipid hydrolysis rate was observed, and the remaining FFA was released gradually at 0.14 %FFA per min for the rest of the intestinal digestion. The inflection points in the rate of digestion showed up at an early stage of digestion for the WPI-pectin bilayer emulsions WOEP. For example, the pectin DE33 coated bilayer emulsions showed a rapid rate (at ~ 0.60 % FFA per min) of lipid hydrolysis till ~ 5.7 % of total FFA released in the initial 10 min whereas the pectin DE73 coated bilayer emulsions showed the rapid rate (at ~ 0.60 %FFA per min) of lipolysis till ~ 10 % of total FFA released in the initial 15 min. Both the bilayer emulsions coated by pectin DE33 and DE73 showed a sudden decrease in the FFA release rate from 0.60 to 0.07 and from 0.60 to 0.13 after the inflection point, respectively. The higher suppressing effect on lipid hydrolysis for pectin DE33 could be attributed to its higher negative

charge compared to DE73 (Appendix D, Figure D3A), which promoted more electrostatic deposition of pectin molecules onto the WPI-stabilized droplets.

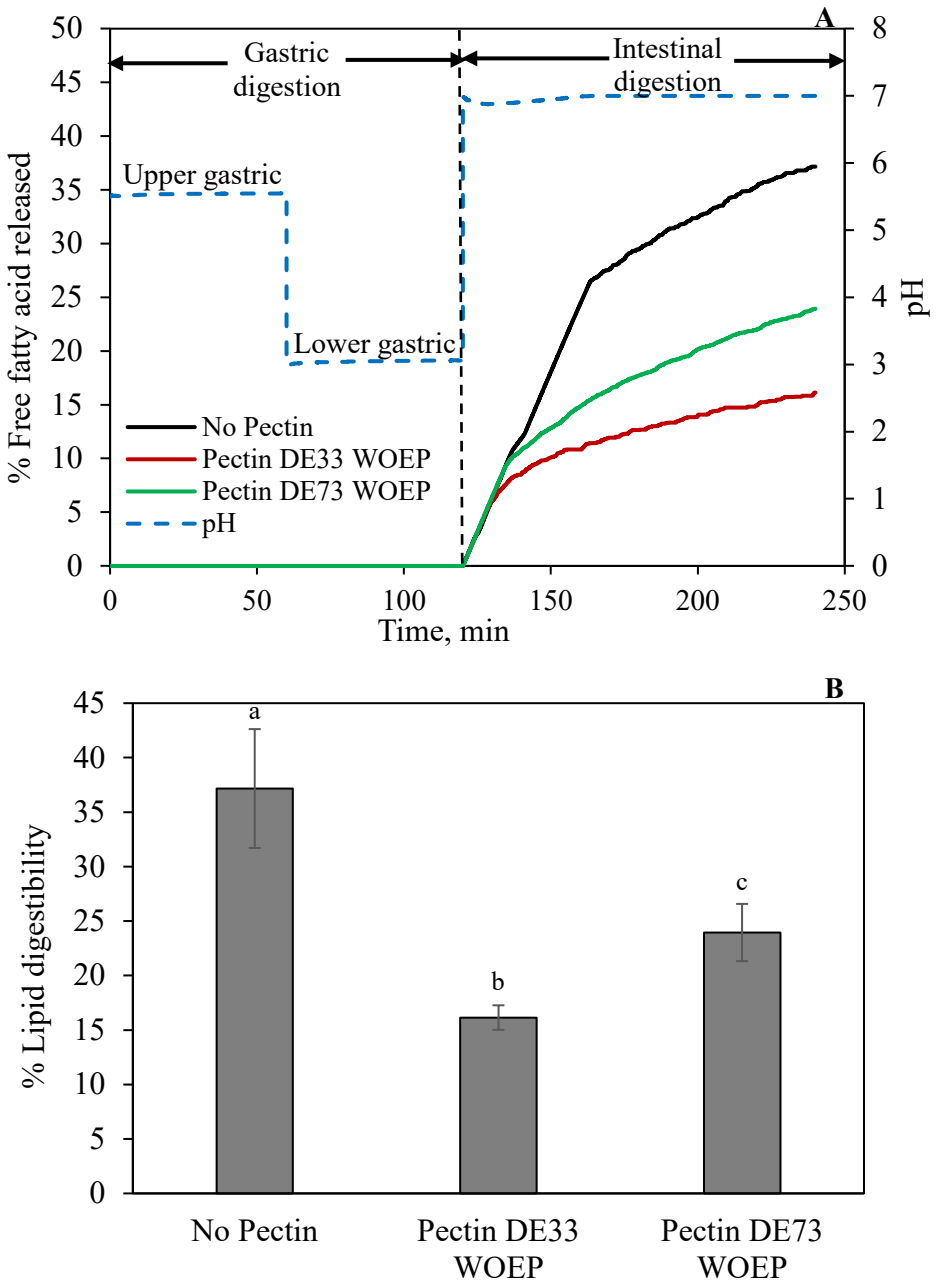

Figure 6.10 Effect of interfacial composition on the *in vitro* lipid digestibility. (A) Free fatty acid release profiles for monolayer and bilayer emulsions, (B) %lipid digestibility with and without pectin and as a function of pectin charge. Error bars indicate ± standard deviation (n ≥ 3). Different lowercase letters denote the statistical significance difference (at 0.05 level) amongst the population means.

The % overall lipid digestibility of all the emulsions after 4 h of *in vitro* digestion is plotted in Figure 6.10B. The overall lipid digestibility of WPI-stabilized monolayer emulsions was 37.2% which was further reduced to 24% and 16% for the bilayer emulsions stabilized by the pectin DE73 and pectin DE33, respectively. Such a significant effect of bilayer on lipid digestibility could be attributed to improvement in the interfacial barrier property in the presence of pectin. An additional layer of pectin might delay either the pepsin action on the protein or the gastric lipase (RGL) action on the lipid during the gastric phase. Malinauskytė et al. (2018) also observed a reduction in lipid digestibility from 28% to 21% for monolayer (whey protein) and bilayer (whey protein and carboxyl methyl cellulose), respectively. The authors also confirmed slower lipid digestion for the bilayer emulsions compared to monolayer emulsions through *in vivo* animals.

In a similar study, the emulsions droplets coated by whey protein – flaxseed gum (FG) (bilayer) showed a reduction in FFA release than those coated by whey protein monolayer alone (Wang et al., 2019). There are different explanations for such behaviour observed in emulsions digestion in the presence of pectin. It has also been shown that the presence of pectin can also affect the activity of enzymes by sequestering the calcium ions (coming from calcium chloride present in the SGF and SIF) that promote enzyme activity in the digestive fluids (Espinal-Ruiz et al., 2016). Calcium has multiple roles to play in the digestion process, and one of them is to act as an enzyme activator by complexing with the surface-active long-chain fatty acids and removing them from the droplet surface (Wilde & Chu, 2011). A higher degree of pectin esterification (less negative charge) lowers the affinity to bind or sequester calcium ions (Willats et al., 2006). Hence, it can be postulated that pectin DE33 has a more suppressive effect on the enzyme activity by binding more calcium compared to pectin DE73 leading to lower overall lipid digestion. Calcium-binding by pectin also promotes junction zone formation by dimerizing galacturonic acid chains (Assifaoui et al., 2015). The dimerization is highly dependent on the pectin charge; with low DE, pectin binds more calcium ions due to greater carboxylic acid moieties in their structure (Persson et al., 1987). The stronger network formation due to more pectin-calcium complexes in the case of DE33 could reduce the lipid digestibility by protecting the droplet surface from lipase action. Hence, the reduction in lipid digestibility in the presence of pectin could be ascribed to the effect of restricted enzyme access to the lipid, the inhibition of enzyme activity by binding the available calcium ions, and the increased strength of the interfacial network for the pectin with a higher

charge. Further research is required to establish the importance of different types of bilayers in controlling the lipid digestion of emulsions.

6.5 Conclusion

The present study has shown that the electrostatic deposition of pectin of different charges on WPI-stabilized emulsion affected their droplet characteristics, rheological properties, microstructure, and lipid digestibility. The addition of pectin with different charges and its interaction with excess protein in the continuous phase (WTEP) was shown to induce droplet aggregation, whereas the absence of excess protein in the continuous phase (WOEP) favoured the protein-pectin interaction at the oil droplet interface. Aggregation of droplets due to the excess protein in the continuous phase led to the transformation of a liquid monolayer emulsion into an attractive viscoelastic gel, evidenced by many folds increase in viscosity and storage moduli of the secondary emulsions. Similarly, the absence of excess protein and higher pectin charge (DE33) resulted in the formation of WPI-pectin stabilized bilayer emulsion, which behaved as a strong repulsive viscoelastic gel. However, the bilayer emulsion WOEP and with a lower pectin charge (DE73) behaved as a flowable weak gel. The interfacial coating of pectin DE33 on WPI-stabilized droplets increased the interfacial shell layer thickness due to the charge cloud, and the steric barrier led to an increased effective volume of droplets resulting in a significant increase in the gel strength of the bilayer emulsions compared to the monolayer emulsions. The change in phase behaviour of the primary emulsion from liquid to gel-like structure as a function of pectin charge was also depicted by the lower creep compliance and higher structural recovery. Monolayer emulsions in the absence of pectin coating showed the highest lipid digestibility. The amount of FFA released decreased as the pectin charge increased in the formation of bilayer emulsions which was attributed to the restricted enzyme access to the lipid due to thicker interfacial layer, the inhibition of enzyme activity by calcium-binding and increased strength of the interfacial pectin layer, which enhanced with increase in pectin charge. These results have an important implication in tailoring the structural and rheological properties of bilayer emulsion gels with controlled lipid digestion, which can be further applied in the food and pharmaceutical industries for calorie reduction and encapsulating bio-active components for controlled delivery.

7. GENERAL DISCUSSION

7.1 Overview

The present project is envisaged with the objective to develop the food-grade nanoemulsion gels at a lower oil volume fraction (ϕ) with controlled *in-vitro* digestibility. The overall goal was to induce gelation in emulsions by increasing the effective oil volume fraction (ϕ_{eff}), which could be possible first by reducing the droplet size (r) to nanoscale and second by increasing the interfacial thickness (δ). To achieve this goal, the research was divided into three different phases: (i) formation of food-grade concentrated nanoemulsions, (ii) removal of excess emulsifiers from the continuous phase of emulsions, and (iii) increase the interfacial thickness by layer-by-layer (LbL) electrostatic deposition technique. In the first phase, the surface-active food-grade LMWE (i.e., Citrem) was chosen and used at different concentrations to prepare concentrated nanoemulsions. The change in droplet size and viscosity of the nanoemulsions as a function of Citrem concentration were examined and correlated with the change in the ϕ_{eff} of the system. This also helped us establish the kind of droplet-droplet interactions responsible for the rheology of nanoemulsions which was significantly influenced by the presence of excess emulsifiers. The understanding from the first phase of the research gave an incite to study the rheology of nanoemulsion as a function of excess emulsifier removal from the continuous phase in the second phase. Any changes in the emulsion's stability were also examined, in the same phase of the research, using an accelerated photo-centrifuge in the presence and absence of excess emulsifier micelles. Next, a novel predicting tool, such as droplet packing behaviour, was used to establish the instability phenomena happening in the nanoemulsion under accelerated gravitation. The removal of excess emulsifiers from the bulk phase of the emulsions is also envisioned to improve the electrostatic deposition of the second layer of biopolymer in the third phase of the research.

In the third phase, the rheology and *in vitro* digestibility of emulsions were studied as a function of interfacial thickness and composition. We hypothesized that the deposition of the second layer of polysaccharide at the interface would help achieve gelation in bilayer-stabilized emulsions at a much lower oil volume fraction due to strong steric and repulsive forces. To

increase the interfacial thickness, the electrostatic complexation of polysaccharides, such as chitosan and pectin, with Citrem and WPI at the droplet surface, respectively, was carried out using two different LbL deposition methods, such as one-step versus two-step mixing (discussed in Chapter 2.4.1). The formation of viscoelastic emulsions gel was studied as a function of polysaccharide concentration and charge. The effect on the rheology and *in-vitro* digestibility of mono- and bilayer emulsions were compared, and the contribution of the interfacial thickness in creating a gel-like emulsion structure was established. The proposed structured emulsions with controlled digestibility can become a new avenue to replace or reduce the unhealthy saturated fat in the food formulation, which will have an added advantage of controlled lipid digestibility.

7.2 Formation and rheology of concentrated food food-grade nanoemulsions

In Chapter 3, an anionic food-grade emulsifier, Citrem, was used to reduce the droplet size to the nanoscale. The droplet size (d_{32}) was reduced with an increase in Citrem concentration and reached less than 250 nm at 3 wt% and 5 wt% Citrem. Interestingly, at this nanoscale droplet size, 3 wt% and 5 wt% Citrem nanoemulsions had a very low apparent viscosity with a liquid like flowable consistency. This was not aligned with the original hypothesis of this work, where it was thought that the nanoscale droplets with thicker interfacial charge cloud layer would lead to ϕ_{eff} beyond maximum random jamming (MRJ), and the nanoemulsions would form a gel-like structure. We found that the higher concentration of emulsifier (3 wt% and 5 wt% Citrem) required to reduce the droplet size to nanoscale, but at these concentrations, excess unabsorbed emulsifier molecules tend to form micelles between the nanodroplets. A very high micelle concentration (much beyond the micelle concentration required for the depletion attraction) induces the formation of structured layers of micelles around the droplet surface (Wasan et al., 2004). Two approaching droplets face a repulsive barrier from negatively charged micelles, and the interdroplet potential reaches a repulsive maximum. On further approach, a micelle layer is squeezed out because of the volume exclusion effect, and the interdroplet potential reaches an attractive minimum. Due to the stepwise thinning of these micelle layers, the inter-droplet interactions oscillate from repulsive to attractive between two approaching droplets; hence they are called oscillatory structural forces (OSF) (Wasan et al., 2004). We hypothesized that a higher magnitude of OSF observed in the presence of excess micelles was responsible for preventing the nanoemulsion from reaching the RCP. The OSF-dominated inter-droplet behaviour in concentrated nanoemulsion reduced the electric double layer (EDL) thickness, attributed to charge

screening by excess ionic emulsifier present in the aqueous phase (Erramreddy & Ghosh, 2014). Because of that, the ϕ_{eff} was also decreased well below the value required for the MRJ (0.64 for monodisperse and > 0.7 for polydisperse systems) of droplets; hence the nanoemulsion exhibited liquid-like behaviour in the presence of excess micelles. In another study, Erramreddy and Ghosh (2014) observed the transformation of the physical state of SDS-stabilized nanoemulsion from strong gel to liquid-like behaviour due to the change in the nature of inter-droplet interactions from repulsive to attractive depletion regime to oscillatory structural forces (OSF)-dominated regime as a function of SDS concentration. From this, we hypothesized that the removal of excess emulsifier micelles from the aqueous phase would have a significant effect on inter-droplet interactions and hence on the rheology of the nanoemulsion.

7.3 Effect of removal of excess emulsifier on the rheology and stability of concentrated nanoemulsion

Based on our hypothesis from the first part of Chapter 3, the excess emulsifier micelles were removed from the aqueous phase of the Citrem-stabilized nanoemulsions using multiple cycles of ultracentrifugation. The removal of excess micelles from 3 wt% and 5 wt% Citrem-stabilized nanoemulsions did not show a significant effect on the droplet size and droplet charge. The same droplet size and charge of nanoemulsions with and without excess Citrem in the continuous phase allowed us to compare rheology, stability, and inter-droplet interactions as a function of Citrem removal. Moreover, the effect of droplet size, ~250 nm for 3 wt% Citrem nanoemulsions and ~150 nm for 5 wt% Citrem nanoemulsions, on the rheological and stability of the nanoemulsions were also compared. There was a 4-to-5-fold increase in the viscosity of nanoemulsions with increased yield stress after removing excess Citrem from the aqueous phase. Similarly, strain-sweep and frequency-sweep analyzed plateau moduli of the nanoemulsions were also increased about 4-to-5 times after removing excess emulsifiers. These observations were also supported by the decrease in the tan δ values towards zero in the absence of excess emulsifier, indicating strong gel-like behaviour. The increase in viscosity and gel strength was more noticeable with a smaller droplet size of 5 wt% nanoemulsions without excess Citrem in their aqueous phase. It indicates that the gelation in nanoemulsions was favoured by reducing droplet size and removing excess emulsifiers.

Overall, all rheological measurements were in support of the transformation of weak gel to a strong gel with the removal of excess emulsifier from the nanoemulsions. This was explained by

the changes in the inter-droplet interactions and corresponding increase in the ϕ_{eff} as a function of excess Citrem removal. As discussed in Chapter 3, nanoemulsions with excess Citrem showed OSF-dominated inter-droplet interaction. However, the magnitude of non-DLVO OSF decreased as we removed the excess emulsifier from the aqueous phase of the nanoemulsions, and it has appeared to transform into DLVO repulsive regime with strong electrostatic interaction between droplets. In the absence of excess Citrem, the droplet-droplet separation distance was determined through the DLVO calculations and using that shell layer thickness (δ) was obtained around 2.7 to 2.9 times κ^{-1} (Debye screening length) from the droplet surface. This helped us to calculate the ϕ_{eff} of the nanoemulsions. With ϕ_{eff} = 0.61 below RCP, 3 wt% Citrem nanoemulsions exhibited a colloidal glassy state with a weak-gel structure due to their larger droplet size. Oppositely, the ϕ_{eff} of 5wt% Citrem nanoemulsions was increased to 0.66 due to their smaller droplet size, which led to a near-MRJ state and a significant increase in the gel strength. The accelerated stability analysis of nanoemulsions also showed a (64%) reduction in the creaming velocity from 0.96 to 0.35 mm h^{-1} with a reduction in droplet size and removing excess Citrem from nanoemulsions. This improved stability could be due to an increase in the gel strength of nanoemulsions in the absence of excess emulsifier, which effectively arrested the droplet movement under accelerated gravitation.

7.4 Packing behaviour of droplets under accelerated gravitation: a tool to predict the droplet-droplet interactions in the presence and absence of excess emulsifier micelles

The previous two phases of research demonstrated the importance of emulsifier concentration in the formation of nanoemulsions and the profound effect of excess unabsorbed emulsifiers on the rheological behaviour and stability of nanoemulsions. We have shown that the gel strength was increased, and the stability of the nanoemulsions was improved by the alteration in the inter-droplet interactions as a function of Citrem removal. The droplet dynamics or droplet-droplet interaction responsible for such an improvement in the stability and rheology can be understood by studying the droplet packing behaviour under accelerated gravitation (Brujić et al., 2003; Krebs et al., 2013). As such, nanodroplets are very stable to gravitational separation; therefore, a novel photo-centrifuge-based accelerated gravitation system (LUMiSizer®) was used to characterize the dynamics of the nanodroplets (Erramreddy & Ghosh, 2014).

In this study, the droplet packing behaviour, expressed in terms of the packing density (ϕ_p), was examined under increased (compression) and decreased (decompression) relative centrifugation force (RCF) in the presence and absence of excess Citrem micelles in nanoemulsions. The presence of excess micelles led to more compression of droplets or higher ϕ_p, attributed to the attractive depletion forces generated by the exclusion effect of excess micelles between the droplets. Oppositely, a strong electrostatic repulsion between the droplets, in the absence of excess micelles, reduced the overall compression of droplets in nanoemulsions, indicated by a decrease in the ϕ_p. In addition to that, ϕ_p was decreased with a reduction in droplet size and an increase in ϕ_{eff}. The inverse relationship between ϕ_p and ϕ_{eff} established through this study was also found to support the rheological changes observed in Chapter 3. Moreover, it was also discovered that the droplet size has more influence on the creaming stability of emulsions compared to the presence or absence of excess micelles. However, the combined factors, reduction in droplet size with the removal of an excess micelles, showed much drastic improvement in the emulsion's stability against accelerated gravitation.

The shelf-life of nanoemulsions was predicted by knowing the velocity of droplets as a function of RCF. Only nanoemulsions with a larger droplet size (stabilized by 3 wt% Citrem) and with excess micelles showed a linear relation between creaming velocity and RCF which was used to predict the shelf-life of 3.5 mm per year at earth's gravitation. Contrary to that, nanoemulsions with smaller droplet sizes (stabilized by 5 wt% Citrem) and without excess micelles exhibited a non-linear relation between creaming velocity and RCF, indicating their shelf-life was infinite or below the instrument detection limit. This non-linear relationship was also observed with the requirement of critical RCF for the flow of the nanoemulsions, which resembled the increase in the yield stress observed in Chapter 3. Thus, the accelerated gravitation study was beneficial in predicting the emulsion's stability and shelf-life with concomitant changes in inter-droplet interaction and rheological behaviour as a function of excess emulsifier in the aqueous phase.

7.5 Improving gelation in emulsions by increasing shell layer thickness using LbL deposition technique

We have demonstrated that the dispersed phase-induced gelation in emulsions can be achieved by reducing the droplet size and increasing the electrostatic repulsion between droplets (Chapter 3). In another study, the gelation in sodium caseinate-stabilized (more flexible protein)

nanoemulsion was observed due to a much higher contribution in interfacial thickness (δ) from both the electrostatic and steric repulsive forces between droplets compared to whey protein-stabilized (globular protein) nanoemulsions (Patel, Mohanan, et al., 2019). Considering this, we hypothesized that it is possible to increase the interfacial thickness by LbL deposition technique with different polysaccharides. This would help us achieve the gelation in emulsions at a much lower oil volume fraction (ϕ) which was the fundamental goal of this research. For this, 3 wt% Citrem-stabilized and 4 wt% WPI-stabilized primary nanoemulsions were chosen to induce gelation by increasing the δ, as they were failed to exhibit the strong gelation in the previously studied nanoemulsions by Kadiya and Ghosh (2019) and Patel, Mohanan, et al. (2019). Before this, less importance was given to the excess unabsorbed emulsifier present in the continuous phase of primary emulsions, which can have a detrimental effect on the deposition of the second layer by the LbL method (Bertsch et al., 2019; Guzey & McClements, 2006; Li, Wu, et al., 2021; McClements et al., 2007; Xiang et al., 2016). We found that 3 wt% Citrem-stabilized and 4 wt% WPI-stabilized nanoemulsions had 1.43 wt% and 1.21 wt% excess emulsifier in their aqueous phase, respectively (Kadiya & Ghosh, 2019; Patel, Mohanan, et al., 2019). The excess emulsifier from the bulk phase of nanoemulsions was removed by the multiple cycles of ultracentrifugation, as discussed in Chapter 3.

The LbL deposition technique was widely used in many dilute emulsions (with low ϕ) systems with an objective to improve the emulsion's stability against various environmental stresses (Berendsen et al., 2014; Bouyer et al., 2011; Gharsallaoui, Saurel, et al., 2010; Roudsari et al., 2006; Wei & Gao, 2016). However, this is the first study where we used two different LbL deposition methods to increase the interfacial thickness in concentrated nanoemulsions (with high ϕ) with the aim to induce gelation. The LbL method can be divided into one-step versus two-step mixing depending on the interfacial composition and pH condition of the primary emulsions (discussed in Chapter 2.4.1) (Guzey & McClements, 2006). For this study, negatively charged Citrem-stabilized droplets were coated with the positively charged chitosan using a one-step mixing method at pH 4. For the two-step mixing method, WPI-stabilized droplets were coated by the pectin molecules. In the first step, WPI-stabilized droplets and pectin are mixed at pH 7 (> pI of WPI), where both WPI and pectin have negative charges. After that, in the second step, the pH was changed to 3, where electrostatic deposition happened due to the opposite charge of both the biopolymers. Based on these methods, the effect of two different interfacial compositions (Citrem-

chitosan and WPI-pectin) on emulsions' rheology and digestion behaviour are discussed in the next phase of the research.

7.6 Impact of one-step mixing (LbL) method on the rheology and digestion behaviour of mono- and bilayer emulsions

An instantaneous electrostatic deposition of the oppositely charged biopolymer occurred after adding Citrem-stabilized negative-charged droplets at the desired pH in the one-step mixing method. The kinetic of droplets dispersion in chitosan solution versus chitosan adsorption process decides the structure and function relationship in the final bilayer coated emulsions. The effect of one-step mixing is further studied by considering two factors, such as chitosan concentration and charge (degree of deacetylation (DDA) 50% and 93%), in the preparation of Citrem-chitosan-stabilized bilayer emulsions. The chitosan with lower DDA (DDA 50%) was obtained by the reacetylation of the original DDA 93 chitosan. The reduction in DDA from 93% to 50% significantly reduced the positive charge of chitosan polymer, attributed to a decrease in the free amino group on the polymer chain due to reacetylation. We hypothesized that such a difference in chitosan charge would significantly affect the electrostatic complexation of polymer with Citrem at the interface and hence the rheological properties of the bilayer emulsions.

At lower to an intermediate concentration of chitosan (0.05 – 0.15 wt%), lack of enough chitosan induced the polymer bridging among the multiple droplets, followed by a complete saturation of droplet surface at higher concentration (> 0.2 wt%), where droplets were repulsively stabilized. This was in accordance with the increase in positive charge of the droplets and concomitant reduction in an aggregate size as a function of chitosan concentration. The lower positive charge with lower DDA of chitosan was found to increase the aggregate size of droplets at an even higher concentration. This was attributed to lower zeta potential still favoured bridging amongst droplets at higher concentrations of DDA 50 chitosan than DDA 93 chitosan. The interaction between the droplets observed at different concentrations and the DDA of chitosan also affected the rheology of mono- and bilayer emulsions. For instance, the apparent viscosity and gel strength (plateau modulus) of emulsions were initially increased at lower to intermediate chitosan concentrations due to bridging flocculation and started to reduce at higher concentrations of chitosan due to strong repulsive interaction between the droplets. At higher concentrations, the viscosity and gel strength of DDA 50 chitosan-coated emulsions were higher than DDA 93 coated emulsions. We hypothesized that a heterogeneous distribution and lower positive charge along

DDA 50 polymer chain could promote more hydrophobic interaction between the droplets. The rheological observations were very well supported by the changes in visual observations and microstructure of emulsions as a function of chitosan concentration and charge. Thus, by increasing the chitosan concentration, the flowable liquid monolayer emulsions were transformed into a strong elastic gel at intermediate concentrations due to bridging flocculation and finally into a repulsive viscoelastic gel at a higher concentration. The bilayer emulsions obtained at a higher chitosan concentration showed higher gel strength than monolayer emulsions due to increased shell layer thickness contributed by an additional steric barrier of chitosan around Citrem-stabilized droplets. The increase in the calculated volume fraction of the shell layer (ϕ_s) from 0.09 to 0.28 due to the bilayer coating of droplets and related increase in ϕ_{eff} from 0.47 to 0.66 observed in this study helped achieve gelation in the bilayer emulsions at a lower oil volume fraction (ϕ = 0.36) and lower Citrem concentration (hence larger droplet size) than that was observed in Chapter 3).

This study also focused on lipid digestibility as a function of chitosan concentration. The inclusion of gastric lipase (rabbit gastric lipase, RGL) during the gastric phase significantly affected the total lipid digestibility of emulsions after the gastric and intestinal phase. The lipid digestibility of the bilayer emulsions decreased with an increase in chitosan concentration. The deposition of chitosan second layer restricted the action of gastric and pancreatic lipase on Citrem and lipid molecules during gastric and intestinal digestion. Further, an increase in shell layer thickness could reduce lipid digestion of the bilayer emulsions compared to the monolayer emulsions. Thus, this study established that two different kinds of emulsions gel structures were obtained with controlled lipid digestibility as a function of chitosan concentration. However, the control over the deposition of the second layer on individual droplets was very limited using the one-step LbL method due to instantaneous complexation of positively charged chitosan with negatively charged Citrem at the droplet surface. The complexation was so rapid that Citrem-stabilized multiple droplets were coated by chitosan before the droplets dispersed uniformly in chitosan solution at high mixing speed. This is also evident from the microstructure of bilayer emulsions depicted in the cryo-SEM image (Appendix C, Figure C6) where multiple nanodroplets coated by chitosan can be seen. The larger or aggregated droplet size (r) was comparatively less effective in a drastic increase in effective oil volume fraction of bilayer emulsions, although interfacial contribution (δ) was still effective. Hence, in the next phase of research, the target was

to individually coat the nanodroplet by polysaccharide to further boost the effective oil volume fraction by increasing the δ/r ratio, where nanodroplets with a thick interfacial layer would further reduce the actual volume fraction of oil required to induce gelation in bilayer nanoemulsion.

7.7 Impact of two-step mixing LbL method on the rheology and digestion behaviour of mono- and bilayer emulsions with and without removal of excess emulsifier

Opposite to the one-step mixing method, the similar charge of polysaccharide and emulsifier molecules at the mixing pH allows the uniform distribution of droplets in the polysaccharide solution using a two-step mixing method. The little or no interactions between similarly charged polysaccharide and emulsifier molecules at the mixing pH ensure that the polysaccharide molecules are evenly distributed around the droplets before reversing their charge for electrostatic deposition at the interface. To increase the interfacial thickness, the two-step mixing method was accompanied by two other factors, such as (i) with excess protein (WTEP) and without excess protein (WOEP) in the aqueous phase of the emulsions, and (ii) magnitude of biopolymer charge. Two different WPI-stabilized 30 wt% canola oil-in-water primary emulsions were obtained WTEP and WOEP by removing the excess protein from an aqueous phase using the ultracentrifugation method as discussed in Chapter 3. The removal of excess protein from the aqueous phase did not affect the droplet size of WPI-stabilized primary emulsions at pH 7. It was found that 1 wt% pectin was required to completely coat the WPI-stabilized droplets, which was optimized using zeta potential measurement of bilayer emulsions as a function of pectin concentration (Appendix D, Figure D2). The primary emulsions WTEP and WOEP were then mixed with 1 wt% pectin solution at pH 7, and thus the secondary emulsions with 20 wt% Canola oil were obtained.

Pectin charge was significantly increased with a decrease in the degree of esterification (DE) from 73% to 33%. Therefore, we hypothesized that the use of pectin DE 33% (DE33) and 73% (DE73) could significantly affect the rheology and digestibility of bilayer secondary emulsions. At pH 7, the addition of the pectin of the different magnitude of charge (DE33 and DE73) did not show any significant effect on the droplet size of the secondary emulsions, but the negative charge of droplets was reduced due to some interaction between negatively charged pectin with the positive patches on WPI-stabilized droplets. The free pectin molecules were also found to increase the viscosity of secondary emulsions by almost two orders of magnitude than monolayer emulsions at pH 7 either by the depletion flocculation or by increasing the viscosity of the continuous phase. Therefore, it was postulated that the presence of free biopolymer molecules and any depletion-

induced attractive interaction between the droplets has a significant role in enhancing the viscosity of the whole system (emulsion + pectin) at pH 7.

The primary WPI-stabilized emulsions showed complete reversal of droplet charge from negative to positive when pH was changed from pH 7 to pH 3. However, the excess protein in primary emulsions (WTEP versus WOEP) did not significantly affect droplet charge and droplet size upon a change in pH to 3. In the secondary emulsions, the electrostatic complexation between protein and polysaccharide occurred at pH 3 due to charge reversal. The aggregated droplet size was increased WTEP in emulsions due to the complexation of excess protein with pectin molecules. This reduced the availability of pectin molecules to make complexes with protein at the interface, which was evident from the reduction in droplet charge (almost neutral charge). The droplets were smaller in size and uniformly distributed in secondary emulsions WOEP, and their charge was highly negative when coated with DE33 pectin compared to DE73. The pectin charge (DE33 versus DE73) was found to affect the droplet charge at pH 3, but the droplet size was unaffected. Overall, the droplets with narrow size distribution were repulsively stabilized (with a highly positive charge) in primary WPI-stabilized emulsions, but with the addition of pectin, either they were aggregated (WTEP, almost neutral charge) or again repulsively stabilized (WOEP, with a highly negative charge and narrow size distribution) in the secondary emulsions. Thus, the droplet characteristics were very much affected by the bulk complexation (WTEP) versus interfacial complexation (WOEP) at pH 3 as a function of the pectin charge.

The kind of protein-pectin complexation that appeared in this study also affected the flow behaviour (viscosity) of emulsions. Just like droplet characteristics, the aggregated (WTEP) or repulsively stabilized droplets (WOEP) in protein-pectin-stabilized secondary emulsions showed a significant increase in viscosity compared to WPI-stabilized primary emulsions at pH 3. The increase in viscosity of secondary emulsions was also higher at pH 3 (due to protein-pectin complexation) compared to pH 7 (pectin in the continuous phase only). A higher viscosity was obtained for DE33 coated emulsions WOEP compared to WTEP. However, the reduction in pectin charge (increase in DE to 73) reduced the viscosity of the bilayer emulsions. The highest viscosity of DE33 coated secondary emulsions was attributed to strong steric and electrostatic repulsion between the droplets compared to DE73 coated droplets in the absence of excess protein (WOEP). Similar trends were observed for the viscoelastic behaviour of secondary emulsions, which was increased WOEP compared to WTEP and with an increase in pectin charge, indicated by an

increase in gel strength (plateau modulus, G'_p), %crossover strain, %recovery in structure and by the reduction in tan δ (towards zero), and creep compliance. The visual observations also showed self-standing strong gel-like behaviour of DE33 coated emulsions WTEP and WOEP compared to flowable liquid like the behaviour of primary emulsions due to aggregation and close packing of droplets, respectively. The higher charge of pectin DE33 was able to show the more close packing of droplets at 20 wt% oil volume fraction in emulsions due to higher contribution in interfacial thickness from steric and repulsive forces. Wijaya et al. (2017) also observed higher viscosity and gel strength of concentrated emulsions stabilized by the WPI-pectin complexation than emulsions stabilized by only the WPI layer at pH 4.5, and they have attributed this behaviour to the close packing of the droplets. Thus, the interfacial composition and hence the viscosity and gel strength of secondary emulsions were very much affected by the change in pectin charge and the excess protein present in the bulk aqueous phase of emulsions.

The digestion behaviour of primary and secondary emulsions WOEP was also studied as a function of the pectin charge. The pectin coating in the secondary emulsions was showed about 40 to 50% less digestibility than overall lipid digestibility observed in the primary emulsions (37%). This could be ascribed to the restricted pepsin or RGL action during gastric digestion in the presence of pectin second layer, which could significantly impact the emulsion's digestion during the intestinal phase. A higher charge of pectin DE33 was more effective in reducing the overall lipid digestibility to 16% than 24% in the case of pectin DE73 which could be explained by the higher affinity of DE33 pectin to bind the available calcium from digestive fluids due to its higher charge compared to DE73 pectin (Willats et al., 2006). The less availability of calcium can have a more suppressive effect on enzyme activity and lipid digestion during intestinal digestion. Apart from that, calcium complexation with a carboxylic group can promote the flocculation of droplets by cross-linking pectin molecules (Persson et al., 1987). The flocculated droplets in simulated gastric fluid, with less surface area available for lipase, could also delay lipid digestion. Thus, the emulsion digestibility of bilayer emulsions was reduced by the many physicochemical and structural changes happening during digestion.

7.8 Summary

This research emphasized the gelation property of emulsions as a function of droplet size, interfacial thickness, and an excess emulsifier in the continuous phase. We have shown that the interfacial shell layer thickness can be increased by changing the droplet-droplet interaction to

strongly repulsive by removing excess ionic emulsifiers or by electrostatic deposition of a second layer onto the droplets. The removal of excess ionic micelles increased the repulsive barrier between droplets, whereas the deposition of charge polysaccharide increased the electrostatic plus steric forces between droplets. Further, removing excess emulsifiers from the continuous phase improved the interfacial adsorption of the highly charged polysaccharide, evident from their zeta potential. As discussed, the individual coating of droplets by the second layer of polysaccharide is also affected by the type of LbL method (one-step versus two-step) used to prepare the secondary emulsions. In one step mixing method, it was not easy to coat the individual droplets at mixing pH because the adsorption of chitosan molecules occurred instantly before droplets were yet dispersed uniformly in chitosan solution. The primary Citrem-stabilized emulsions exhibited liquid-like behaviour at $\phi = 0.4$, which was transformed into a gel-like structure at $\phi = 0.36$ upon deposition of the second layer of chitosan using the one-step method. However, the nature of gel structure, i.e., flocculated gel versus repulsive gel, was controlled by chitosan concentration and charge. The shell layer contribution (ϕ_s) was supportive to our hypothesis to increase ϕ_{eff}, but the multiple droplets coated by the chitosan in one-step mixing method were still limiting to elevate the ϕ_{eff}. This limitation was overcome using a two-step mixing method to elevate further the ϕ_{eff} by individually coat the nanoscale droplets using different interfacial compositions. We observed that the deposition of second layer of pectin on WPI-stabilized droplets transformed the liquid emulsions (at $\phi = 0.3$) into a gel-like structure at an even lower oil volume fraction ($\phi = 0.2$). Here, removing excess protein from the continuous phase and a higher charge of pectin (DE33) helped to achieve gelation in secondary emulsions. We found that the interfacial thickness significantly increased the droplet effective volume fraction as the droplet size approaches the sub-micron size. The increase in effective volume fraction of bilayer droplets was discovered to achieve the gelation in emulsions at a much lower oil volume fraction ($\phi < 0.4$) depending on the biopolymer concentration, charge, and type of LbL method used to deposit the second layer.

Finally, we have also shown that the lipolysis by gastric lipase during the gastric phase significantly affects the overall lipid digestibility. The overall digestibility of emulsions was reduced from 26% to 17% (34.6% decrease) and from 37% to 16% (56.8% decrease) when droplets were coated by bilayer using one-step and two-step mixing methods, respectively. The complete coating of the second layer of polysaccharide (chitosan or pectin) on primary (Citrem or WPI-

stabilized) emulsions droplets delayed the lipolytic action of gastric and the pancreatic lipase on triacylglycerol molecules during *in vitro* digestion study. The more controlled digestion observed in the two-step LbL method could be attributed to a more uniform coating of individual oil droplets by pectin, in contrast to multiple droplets coating by chitosan in the one-step LbL method. The calcium chelating power of pectin could also be detrimental to the enzyme (lipase) activity during hydrolysis of lipids leading to lower lipid digestibility. Thus, the interfacial composition and thickness were found to be controlling factors for the rheology and digestibility of emulsions. This research established that the challenges remain in a complete coating of nanodroplets by polysaccharides, which was affected by the LbL method used and an excess emulsifier in the continuous phase of emulsions. This can be further affected by the droplet concentration and polydispersity of droplets in the formation of bilayer emulsions. Especially, the polydispersity has a big effect in predicting the physical state (glassy and jammed) of emulsions at $\phi_{eff} > \phi_{MRJ}$. Research on predicting ϕ_{MRJ} for polydisperse systems is still very limited (Clusel et al., 2009). Also, the polysaccharide molecules used in this study change their conformation and hence interfacial thickness depending on the charge distribution (block-wise versus random); therefore, they should be studied for the distribution of functional group responsible for the electrical property of the polymer chain. Further work is also required to characterize the nanoscale interfacial thickness of the bilayer system studied in this research to better understand its role in emulsion's rheology and digestibility.

8. OVERALL CONCLUSIONS

The overall goal of this research was to achieve the gelation in nanoemulsion at a much lower oil volume fraction by reducing the droplet size to nanoscale and forming a thicker interfacial layer (δ) with various food-grade emulsifiers and biopolymers layers. We hypothesized that by increasing the ratio of shell layer thickness (δ) to droplet radius (r) in emulsions, it would be possible to increase the effective volume fraction (ϕ_{eff}) of the droplets beyond the random close packing state ($\phi_{MRJ} \sim 0.64$ for monodisperse emulsions) where the droplets cannot move, and emulsions would behave like a gel. Such a transformation in the physical state of emulsions from liquid to gel was characterized by different rheological properties as a function of droplet size, excess emulsifier removal, and interfacial composition. Additionally, the effect of the interfacial composition on lipid digestibility was assessed by *in vitro* digestion study.

As a part of the first objective, in Chapter 3, we have demonstrated the formation of Citrem-stabilized food grade nanoemulsion gel by removing the excess emulsifier from the aqueous phase. We observed that a higher quantity of emulsifiers (Citrem) was required to reduce the droplet size to the nanoscale (~ 200 nm) during high-pressure homogenization. An excess unabsorbed anionic emulsifier (Citrem) tends to form micelles in the aqueous phase of emulsions. Higher micellar concentration, > 15% fraction of aqueous phase, led to long-range non-DLVO oscillatory structural forces (OSF) between the approaching droplets in nanoemulsion, leading to a decrease in interfacial repulsive layer and ϕ_{eff}. The counterions from excess anionic micelles reduced the Debye screening length (repulsive barrier) due to the charge screening effect at the droplet surface, which decreased the ϕ_{eff} well below random jamming (ϕ_{MRJ}). Because of that, the nanoemulsions behaved like a flowable liquid with very low viscosity and gel strength ($G' > G''$) in the presence of excess micelles. The magnitude of OSF reduced with the removal of excess micelles and inter-droplet interactions dominated by the DLVO repulsive forces with increased contribution of the charge cloud thickness (DSL), acted as an interfacial shell layer. An increase in shell layer thickness (δ) with the corresponding rise in ϕ_{eff} below (0.61) or near (0.67) random jamming increased the gel strength ($G' >> G''$) of nanoemulsions. An increase in ϕ_{eff} and hence the gel

strength was also much higher (G′ >> G″) with the reduction in droplet size of nanoemulsions. Thus, we had shown that the gelation in nanoemulsion occurred due to jamming of nanodroplets at 40 wt% canola oil with increased contribution of electrostatic repulsive forces between two approaching droplets when excess emulsifier was removed. The increase in gel strength of monolayer nanoemulsion (Chapter 3) with a reduction in droplet size and increase in interfacial thickness or repulsive barrier as a function of excess micelles removal supports the first hypothesis of the thesis. From this study, we established that the gelation in emulsions is not only initiated by the reduction in droplet size but can also be induced by changing the droplet-droplet interactions as a function of excess micelles removal.

An extension of the first objective is discussed in Chapter 4, where we studied the mechanism responsible for the changes in the stability of nanoemulsion in the presence and absence of excess micelles using an analytical photo-centrifuge. The reduction in droplet size and the removal of excess emulsifier from the aqueous phase increased the gel strength of Citrem-stabilized nanoemulsion with an associated increase in the long-term stability (indicated by a decrease in creaming velocity) and shelf-life of nanoemulsion. We suggested that the reduction in droplet size (~220 nm to ~150 nm) significantly lowered the creaming velocity, followed by an increase in the gel strength (almost five times) with removing the excess micelles. However, when both the factors were combined, droplet size and gel strength, the creaming velocity was reduced significantly. The predicted creaming velocity of the flowable nanoemulsions with larger droplet size was found to be 3.5 mm per year at earth gravitation (or at 1 RCF, relative centrifugal force). All other nanoemulsions showed a critical RCF requirement (beyond 1 RCF) to induce the flow under centrifugal force followed by a non-linear (power-law) relationship between creaming velocity versus RCF, indicating an increase in shelf-life by restricting the droplet movement at earth gravitation. The power-law exponents (n) and critical RCF obtained in this study coincided with the flow behaviours of nanoemulsions observed in Chapter 3. Thus, the accelerated stability technique also helped us to predict the changes in the rheological behaviour of nanoemulsions as a function of excess micelles removal. Such a change in the stability and shelf-life of nanoemulsions in the presence and absence of excess micelles was also supported by a change in their droplet packing behaviour (packing density, ϕ_p) under compression (increasing RCF) and expansion (decreasing RCF). The ϕ_p was decreased with a reduction in droplet size and removal of the excess micelles. It was found that the ϕ_p (under compressed state) and ϕ_{eff} (gel strength) were

inversely correlated to each other. As an alternative, the changes in ϕ_p can be very well correlated with the changes in the inter-droplet interactions in the presence and absence of excess micelles. An increased ϕ_p (more compressed emulsion) in the presence of excess micelles indicated the depletion-induced attractive forces between droplets. In contrast, removing excess micelles reduced the ϕ_p (less compressed emulsion), indicated by the strong repulsive forces between the nanodroplets. Thus, the investigation into the colloidal forces responsible for the stability or instability mechanisms in nanoemulsions can be described by studying the packing behaviour (ϕ_p) of nanodroplets using a real-time advanced photo-centrifuge which proves the second hypothesis of the thesis.

The last three objectives of this research were to study the effect of interfacial thickness (as influenced by the interfacial composition) and layer-by-layer (LbL) electrostatic deposition methods (one-step versus two-step) on the rheology and digestibility of emulsions presented in Chapters 5 and 6. The removal of excess emulsifier (studied in Chapters 3 and 4) from the continuous phase was beneficial for the next phase of research in promoting the electrostatic deposition of biopolymer onto the interface and thereby achieving bilayer formation around the oil droplets. To test the third hypothesis of this research, the rheological and digestion behaviour of monolayer versus bilayer emulsions (prepared using one-step mixing method) was systematically studied as a function of chitosan concentration and DDA (charge). The primary Citrem-stabilized 36 wt% oil-in-water emulsion was liquid with negatively charged smaller droplets. With the addition of chitosan, the aggregated droplet size increased at a lower chitosan concentration due to bridging flocculation amongst the Citrem-stabilized droplets. At an intermediate concentration, droplets were fully saturated with chitosan, indicated by an increase in the positive charge of droplets. With a further increase in chitosan concentration, aggregated droplet size was reduced as the charge reached a maximum. The emulsions coated with higher DDA chitosan found the smallest droplet size at a higher concentration compared to emulsions coated with lower DDA chitosan. It was suggested that the chitosan with a lower charge and more hydrophobicity could promote the interactions among the droplets even beyond the surface saturation. Aggregated droplets behaved like a strong flocculated gel at a lower concentration and charge, which transformed into repulsive viscoelastic gel at higher chitosan concentration and charge. The increase in interfacial thickness contributed by the steric and repulsive forces between highly positively charged (Citrem-chitosan-stabilized) bilayer droplets led to an increase in the

effective volume fraction of emulsions from 0.47 (monolayer) to 0.66 (bilayer), which corresponded to an increase in gel strength, thereby proving the third hypothesis.

To test the fourth hypothesis, two-step LbL method was used to optimize the electrostatic deposition of biopolymer molecules (pectin) at the interface of WPI-stabilized primary emulsion droplets to increase the interfacial thickness. To coat individual oil droplets with pectin, excess WPI was removed from the primary emulsion continuous phase. The droplet size of WPI-stabilized monolayer emulsions remained the same after the removal of excess protein from the continuous phase. Similarly, the size and negative charge of WPI-stabilized droplets remained the same after pectin addition in secondary emulsions at pH 7 (first step of the LbL method), indicating pectin molecules essentially remain dispersed in the continuous phase. The WPI-pectin complexation occurred with the change of pH 7 to pH 3 (second step of the LbL method), which was evident from the change in the positive charge of WPI-stabilized droplets (in the absence of pectin) to the negative charge of the WPI-pectin-stabilized droplets (in the presence of pectin). The negative charge of pectin-coated droplets was increased with the removal of excess protein (WOEP) from emulsions, and it was further increased when droplets were coated by a higher magnitude of pectin charge (lower DE). Thus, it was recognized that the excess protein in the continuous phase hampered the pectin complexation with whey protein at the interface. Oppositely, the removal of excess protein favoured the maximum complexation of pectin with whey protein at the interface, which helped to achieve the goal of this study to increase the interfacial thickness by bilayer formation. The primary emulsions stabilized by a single monolayer (WPI) showed liquid-like behaviour with very low viscosity and gel strength. The excess protein in the continuous phase (WTEP) increased the viscosity and gel strength of bilayer emulsions due to aggregation of droplets where pectin complexed predominantly with excess protein in the continuous phase. This validates our hypothesis discussed in Chapter 6, which talks about the effect of excess protein in creating the aggregated gel-like emulsion structure. Oppositely, the removal of excess protein (WOEP) increased the viscosity and gel strength of emulsions due to close packing of droplets aided by an increase in interfacial thickness where pectin complexed mainly with the protein at the interface. With a higher pectin charge (DE33), the aggregated gel and close-packed emulsions gel became stronger. Thus, two different kinds of structural emulsion gels were obtained in this study, whose rheology was controlled by the pectin charge and amount of excess protein in the aqueous phase.

Comparing the effect of interfacial composition and the LbL method (one-step versus two-step) on the gelation of bilayer emulsions (Chapters 5 and 6), it was established that the actual nanoscale droplet size was obtained using the two-step mixing method compared to the one-step mixing method for the bilayer nanoemulsion. Further, the nanoscale droplet size with thick interfacial thickness obtained using the two-step mixing method significantly contributed to forming a self-standing bilayer nanoemulsion gel at such a low oil volume fraction ($\phi = 0.2$) that satisfied the fourth hypothesis of this research. The Citrem-chitosan-stabilized bilayer droplets were still beyond the critical limit of nanoscale range due to multiple droplets coated by chitosan, indicating that the choice of LbL method could have a big impact on whether individual coating of droplets would be possible.

The fifth hypothesis was tested in both Chapter 5 and 6. In Chapter 3, lipid digestion was the highest in primary Citrem-stabilized emulsions. The lipid digestibility of emulsions coated with chitosan reduced with an increase in chitosan concentration, which was attributed to an increase in interfacial thickness supported by bilayer formation on emulsions droplets thereby delaying the lipase action on the triacylglycerol molecules. In Chapter 6, It was also observed that the lipid digestibility was reduced for the secondary emulsions coated with different pectin charges compared to the primary emulsions. The higher charge of the pectin was more effective in controlling or delaying the lipase action on triglyceride molecules; hence lipid digestibility was further reduced. Therefore, the fifth hypothesis was also proved.

Overall, it can be concluded that it is possible to increase the gel strength of emulsions by reducing the droplet size to nanoscale and increasing the interfacial thickness via electrostatic and static interracial barrier. The fundamental knowledge gained from this research can be used to study the different systems with different compositions to further validate the hypotheses of the research.

9. FUTURE STUDIES

In this research project, the transformation of the physical state of emulsions from liquid to repulsive gel has occurred at oil volume fractions (ϕ) less than 0.4. This was attributed to an increase in the effective volume fraction (ϕ_{eff}) of oil droplets beyond maximum random jamming ($\phi_{MRJ} = 0.64$) achieved by: (i) reducing the droplet size (r) (ii) increasing the interfacial thickness (δ) either through the removal of excess emulsifier from the aqueous phase or (iii) through the deposition of thick steric and charged layer of polysaccharide on emulsifier-stabilized droplets. We have shown that a higher amount of emulsifier (Citrem or whey protein) is required to reduce the droplet size to the nanoscale ($r \sim 100$ to 150 nm). The removal of excess emulsifiers from the continuous phase of emulsions required additional steps of ultracentrifugation and homogenization before deposition of the second layer of polysaccharide by the layer-by-layer (LbL) electrostatic deposition technique. Alternatively, emulsions can be prepared at a relatively lower concentration of emulsifiers, and the use of solvent evaporation technique can be explored to reduce the droplet size to nanoscale before deposition of the second layer (Lee & McClements, 2010). In this technique, the oil-soluble solvent (ethyl acetate) is mixed with the oil in a certain proportion before homogenization to prepare the emulsions. The solvent entrapped droplets are stabilized by the emulsifier (Citrem or whey protein), and any excess emulsifier will stay in the aqueous phase. In the next step, the solvent can be evaporated under vacuum by controlled heating (using Rotavapor), making the droplets shrink to form the nanoscale droplets (Lee & McClements, 2010; McClements, 2011). We hypothesize that the increase in the surface area during this process will lead to adsorption of excess emulsifier from the aqueous phase, which can exclude the extra step of removing the excess emulsifier by ultracentrifugation. Thus, it would be possible to perform two functions, i.e., reduction in droplet size and removal of excess emulsifier, together with solvent evaporation technique.

For the third and fourth objectives, we achieved the gelation in emulsions by increasing the interfacial thickness using LbL deposition of two different kinds of polysaccharides such as chitosan and pectin with different magnitudes of polymer charge, i.e., positive charge (chitosan)

or negative charge (pectin). In the multilayer formation, the composition of adsorbed films and the thickness is affected by the type of polysaccharides and their molecular structure. Further, the configuration of the polysaccharides species and the distribution of charge within the layers are also essential characteristics that are mainly influenced by the blockiness and the charge density carried by polysaccharide molecules (Ettelaie & Akinshina, 2014). It is mentioned that compared to the magnitude of polymer charge, the distribution of functional groups (uniform versus non-uniform) along the polymer chains decides the electrical and configurational property of polysaccharide at the interface (random versus block-wise) (Ettelaie et al., 2008; Ettelaie et al., 2012). In this study, we used chitosan and pectin of different degrees of deacetylation and esterification, respectively, but it was not clear how uniformly the charge was distributed along the polysaccharide chain. The polysaccharide type, random versus block polymer, can also influence its conformation (flat versus extended) at the interface and hence the interfacial thickness while making the electrostatic complexation with an oppositely charged emulsifier or biopolymer (Dickinson, 2011; Ettelaie et al., 2008; Ettelaie et al., 2012). However, the distribution of charge on polysaccharide chains and its effect on forming multilayer or bilayer concentrated emulsions is unknown. Therefore, a more in-depth look at the impact of such a change in polysaccharide conformation at the interface due to its charge distribution on the rheology and structure of bilayer concentrated emulsions should be studied.

Apart from that, different interfacial compositions comprised of monolayer-stabilized of LMWE (Datem (diacetyl tartaric acid ester of mono- and diglycerides), SSL (sodium stearoyl lactylate)) or flexible protein (sodium caseinate, gelatin) and deposited with oppositely charged polysaccharides (chitosan, carrageenan, xanthan gum) needs to be explored in forming a bilayer concentrated emulsions to validate our hypothesis of increasing the effective oil volume fraction (ϕ_{eff}) of droplets by increasing the interfacial thickness (δ). In recent years, plant proteins have been a new avenue to explore for the many foods system. Therefore, the plant proteins such as lentil, pea and canola proteins also need to be investigated in combination with different polysaccharides to form the bilayer emulsions gels.

In this research, the repulsive gelation of emulsions was considered when the effective oil volume fraction (ϕ_{eff}) reached above $\phi_{MRJ} = 0.64$, considering monodisperse system. It should be noted that our emulsions were polydisperse; therefore, it is expected that the random jamming volume fraction (ϕ_{MRJ}) of oil droplets would be even higher than 0.64. It is challenging to predict

the exact physical state (glassy or jammed) of such a polydisperse emulsion gel. For monodisperse emulsions, an empirical model has been developed to predict the state (glassy or jamming) of emulsions at particular ϕ_{eff} (Mason & Scheffold, 2014). In the future, the applicability of the polydisperse model should be considered in predicting the jamming state of polydisperse emulsions.

The next component of this research, which requires equal importance, is analyzing the interfacial thickness (δ) of monolayer versus bilayer using different experimental techniques. The thickness (δ) of the interfacial layer is an essential parameter in predicting the effective oil volume fraction (ϕ_{eff}) of emulsions and its effect on emulsion gelation. The simplest method to characterize the thickness of an adsorbed layer is by considering the core-shell structure formation. In this method, the monodisperse solid particles, such as silica and polystyrene sulphate latex (PSL), can be used as a core, and the biopolymer of interest can be deposited as a shell-layer over these particles. The interfacial thickness can be calculated by subtracting the core diameter from the core plus shell layer diameter measured using dynamic light scattering or small-angle X-ray scattering (SAXS) (Akpinar et al., 2016; Dalgleish, 1990). This research used the DLS technique to measure the average size of the monolayer-stabilized droplets with and without a second layer of polysaccharide, and the interfacial thickness was calculated from an average droplet size. One should be careful while measuring the interfacial thickness using polydisperse oil droplets compared to the monodisperse silica particles. The SAXS technique shall be explored to accurately measure the interfacial thickness by analyzing the radius of gyration (R_g) of the real mono and bilayer-stabilized oil-in-water emulsions system. Other advanced methods such as small-angle neutron scattering (SANS) (Marichal et al., 2019), atomic force microscopy combined with Langmuir-Blodgett film deposition (Cai & Ikeda, 2016), ellipsometry (Hinrichs & Eichhorn, 2014; Malmsten, 1994) can be studied in measurements of the interfacial thickness. For example, the SANS method can be used with the contrast matching principle to measure the interfacial thickness by optimizing the neutron scattering contrast between the solvent (aqueous phase), and shell layer (Marichal et al., 2019). The challenges remain in getting the different neutron scattering patterns of the interfacial layer from the solvent (H_2O) because the organic molecules at the interface adsorb water molecules which ultimately gives a quite similar scattering pattern as solvent (H_2O). For that, the layer of interest can be deposited on silica particles, and the aqueous phase (H_2O) can be proportionately replaced with the D_2O. The change in D_2O/H_2O ratio of solvent will change the

neutron scattering length density (SLD) of interfacial layer (for example, protein) while silica particles have a constant SLD at a different ratio of D_2O/H_2O. In the contrast matching principle, the maximum contrast is considered at a point where the maximum difference in SLD values of interfacial layer and solvent is achieved at the corresponding ratio of D_2O/H_2O. Different models can be fitted to get the radius of gyration of silica particles with and without interfacial layer from the scattering data, which can be further used to calculate the interfacial thickness (Marichal et al., 2019). The interfacial thickness studied by any of these techniques would help to calculate the effective oil volume fraction, which can further explain changes in the rheological properties of the bilayer emulsions in comparison to monolayer emulsions.

Understanding the structure of the mono and bilayer emulsions is essential for predicting their stability and rheology. To understand the structure-function relationship in the formation of bilayer emulsions, we examined the confocal microstructure of mono and bilayer emulsions. However, the confocal resolution was a limiting factor in getting all the details of the structure, especially calculating the interfacial thickness and visualizing a large number of small droplets. We did some preliminary work analyzing the microstructure of the mono and bilayer emulsions using cryo-scanning electron microscopy (SEM), but further optimization of freeze fracturing would be required with minimal destruction of the original structure of emulsions. In the future, non-destructive synchrotron-based bright light scattering techniques in the X-ray region can be used to characterize any small (high resolution) structural details of mono and bilayer emulsions. For example, synchrotron-based techniques such as SAXS and Ultra-SAXS should be studied compared to cryo-SEM to explain the structural information of the bilayer emulsions gel. Mason and colleagues have extensively used SANS and SAXS techniques to investigate nanoemulsion structures and proposed that complete structural information would involve specifying the size and the distance between the nanodroplets in a random jammed state and finding the characteristic length of the structure that forms the basic unit of the entire 3D network (Fryd & Mason, 2012; Wilking et al., 2006). Similarly, SAXS should be used to investigate the droplet size and inter-droplet distance, and interfacial structure of the mono and bilayer emulsions.

Apart from the fundamental knowledge gains for the formation of bilayer emulsions gels, the possibility of actual practical use of these emulsion gels should be explored in the food and pharmaceutical industry. The food-grade emulsion gels developed in this research provide a novel structure that can be used as an alternative to many foods, i.e., table spread, mayonnaise, baking

fat and dairy products such as yogurt and cheese. The gelation at much lower oil volume fractions and controlled lipid digestion makes the bilayer emulsion gels a healthier alternative to replace traditional high-fat foods. In future, this kind of bilayer emulsion structure can also be employed in the pharmaceutical industry to deliver the micronutrients, bioactive, and drugs at targeted sites with controlled release. Moreover, the slow or delayed lipid hydrolysis in the presence of bilayer led to controlled digestion of indigested lipid at the end of (2 hours) *in vitro* digestion which further needs to be tested by considering the gastric emptying rate and satiety. The gastric emptying rate (kcal/min), which was not considered in this study, also has an impact on the overall lipid digestibility (Mulet-Cabero et al., 2020). Therefore, in future, the findings of this *in vitro* digestion study should be further validated by conducting *in vivo* study of bilayer emulsions gel where all the ideal conditions will nearly meet for mimicking the real human digestion system.

10. REFERENCES

Abbasian Chaleshtari, Z., Salimi-Kenari, H., & Foudazi, R. (2020). Interdroplet interactions and rheology of concentrated nanoemulsions for templating porous polymers. *Langmuir, 37*(1), 76-89.

Acosta, E. (2009). Bioavailability of nanoparticles in nutrient and nutraceutical delivery. *Current Opinion in Colloid & Interface Science, 14*(1), 3-15.

Ahmed, J., Ptaszek, P., & Basu, S. (2016). *Advances in food rheology and its applications*: Woodhead Publishing.

Akpinar, B., Fielding, L. A., Cunningham, V. J., Ning, Y., Mykhaylyk, O. O., Fowler, P. W., & Armes, S. P. (2016). Determining the effective density and stabilizer layer thickness of sterically stabilized nanoparticles. *Macromolecules, 49*(14), 5160-5171.

Alemán, J. V., Chadwick, A. V., He, J., Hess, M., Horie, K., Jones, R. G., . . . Moad, G. (2007). Definitions of terms relating to the structure and processing of sols, gels, networks, and inorganic-organic hybrid materials (IUPAC Recommendations 2007). *Pure and Applied Chemistry, 79*(10), 1801-1829.

Anton, N., & Vandamme, T. F. (2011). Nano-emulsions and micro-emulsions: clarifications of the critical differences. *Pharmaceutical research, 28*(5), 978-985.

Antonopoulou, E., Rohmann-Shaw, C. F., Sykes, T. C., Cayre, O. J., Hunter, T. N., & Jimack, P. K. (2018). Numerical and experimental analysis of the sedimentation of spherical colloidal suspensions under centrifugal force. *Physics of Fluids, 30*(3), 030702.

Anvari, M., & Joyner, H. S. (2017a). Effect of fish gelatin-gum arabic interactions on structural and functional properties of concentrated emulsions. *Food Research International, 102*, 1-7.

Anvari, M., & Joyner, H. S. (2017b). Effect of formulation on structure-function relationships of concentrated emulsions: Rheological, tribological, and microstructural characterization. *Food Hydrocolloids, 72*, 11-26. doi:https://doi.org/10.1016/j.foodhyd.2017.04.034

Aoki, T., Decker, E. A., & McClements, D. J. (2005). Influence of environmental stresses on stability of O/W emulsions containing droplets stabilized by multilayered membranes

produced by a layer-by-layer electrostatic deposition technique. *Food Hydrocolloids, 19*(2), 209-220.

Asakura, S., & Oosawa, F. (1954). On Interaction between Two Bodies Immersed in a Solution of Macromolecules. *The Journal of Chemical Physics, 22*(7), 1255-1256. doi:10.1063/1.1740347

Assifaoui, A., Lerbret, A., Uyen, H. T., Neiers, F., Chambin, O., Loupiac, C., & Cousin, F. (2015). Structural behaviour differences in low methoxy pectin solutions in the presence of divalent cations (Ca 2+ and Zn 2+): a process driven by the binding mechanism of the cation with the galacturonate unit. *Soft Matter, 11*(3), 551-560.

Basheva, E. S., Kralchevsky, P. A., Danov, K. D., Ananthapadmanabhan, K. P., & Lips, A. (2007). The colloid structural forces as a tool for particle characterization and control of dispersion stability. *Physical Chemistry Chemical Physics, 9*(38), 5183-5198.

Berendsen, R., Güell, C., Henry, O., & Ferrando, M. (2014). Premix membrane emulsification to produce oil-in-water emulsions stabilized with various interfacial structures of whey protein and carboxymethyl cellulose. *Food Hydrocolloids, 38*, 1-10.

Bergeron, V., Langevin, D., & Asnacios, A. (1996). Thin-film forces in foam films containing anionic polyelectrolyte and charged surfactants. *Langmuir, 12*(6), 1550-1556.

Berli, C. L., Quemada, D., & Parker, A. (2002). Modelling the viscosity of depletion flocculated emulsions. *Colloids and Surfaces A: Physicochemical and Engineering Aspects, 203*(1-3), 11-20.

Berton, C., Genot, C., & Ropers, M.-H. (2011). Quantification of unadsorbed protein and surfactant emulsifiers in oil-in-water emulsions. *Journal of colloid and interface science, 354*(2), 739-748.

Bertsch, P., Thoma, A., Bergfreund, J., Geue, T., & Fischer, P. (2019). Transient measurement and structure analysis of protein–polysaccharide multilayers at fluid interfaces. *Soft Matter, 15*(31), 6362-6368.

Bharti, B., Meissner, J., Klapp, S. H., & Findenegg, G. H. (2014). Bridging interactions of proteins with silica nanoparticles: The influence of pH, ionic strength and protein concentration. *Soft Matter, 10*(5), 718-728.

Bibette, J., Morse, D. C., Witten, T., & Weitz, D. (1992). Stability criteria for emulsions. *Physical review letters, 69*(16), 2439.

Bortnowska, G. (2008). The effect of competitive adsorption between proteins of dried egg yolk and Tween 65 on the stability and microstructure of oil-in-water emulsions. *Electronic Journal of Polish Agricultural Universities, 11*(3), 01.

Bortnowska, G. (2015). Multilayer Oil-in-Water Emulsions: Formation, Characteristics and Application as the Carriers for Lipophilic Bioactive Food Components – a Review. *Polish Journal of Food and Nutrition Sciences, 65*(3), 157. doi:10.2478/v10222-012-0094-0

Bouyer, E., Mekhloufi, G., Le Potier, I., De Kerdaniel, T. d. F., Grossiord, J.-L., Rosilio, V., & Agnely, F. (2011). Stabilization mechanism of oil-in-water emulsions by β-lactoglobulin and gum arabic. *Journal of Colloid and interface science, 354*(2), 467-477.

Bouyer, E., Mekhloufi, G., Rosilio, V., Grossiord, J.-L., & Agnely, F. (2012). Proteins, polysaccharides, and their complexes used as stabilizers for emulsions: alternatives to synthetic surfactants in the pharmaceutical field? *Int J Pharm, 436*(1-2), 359-378.

Briscoe, W. H. (2015). Depletion forces between particles immersed in nanofluids. *Current Opinion in Colloid & Interface Science, 20*(1), 46-53.

Brodkorb, A., Egger, L., Alminger, M., Alvito, P., Assunção, R., Ballance, S., . . . Carrière, F. (2019). INFOGEST static *in vitro* simulation of gastrointestinal food digestion. *Nature protocols, 14*(4), 991-1014.

Bruinsmann, F. A., Pigana, S., Aguirre, T., Dadalt Souto, G., Garrastazu Pereira, G., Bianchera, A., . . . Raffin Pohlmann, A. (2019). Chitosan-coated nanoparticles: Effect of chitosan molecular weight on nasal transmucosal delivery. *Pharmaceutics, 11*(2), 86.

Brujić, J., Edwards, S. F., Grinev, D. V., Hopkinson, I., Brujić, D., & Makse, H. A. (2003). 3D bulk measurements of the force distribution in a compressed emulsion system. *Faraday discussions, 123*, 207-220.

Cai, B., & Ikeda, S. (2016). Effects of the conjugation of whey proteins with gellan polysaccharides on surfactant-induced competitive displacement from the air-water interface. *Journal of Dairy Science, 99*(8), 6026-6035.

Capek, I. (2004). Degradation of kinetically-stable o/w emulsions. *Advances in colloid and interface science, 107*(2), 125-155.

Casandra, A., Chung, M.-C., Noskov, B. A., & Lin, S.-Y. (2017). Adsorption kinetics of sodium dodecyl sulfate on perturbed air-water interfaces. *Colloids and Surfaces A: Physicochemical and Engineering Aspects, 518*, 241-248.

Chanamai, R., & McClements, D. (2002). Comparison of gum arabic, modified starch, and whey protein isolate as emulsifiers: influence of pH, $CaCl_2$ and temperature. *Journal of food science, 67*(1), 120-125.

Chang, Y., & McClements, D. J. (2015). Interfacial deposition of an anionic polysaccharide (fucoidan) on protein-coated lipid droplets: Impact on the stability of fish oil-in-water emulsions. *Food Hydrocolloids, 51*, 252-260.

Chang, Y. H., McLandsborough, L., & McClements, D. J. (2012). Physical Properties and Antimicrobial Efficacy of Thyme Oil Nanoemulsions: Influence of Ripening Inhibitors. *Journal of agricultural and food chemistry, 60*(48), 12056-12063. doi:10.1021/jf304045a

Charalambous, G., & Doxastakis, G. (1989). *Food Emulsifiers: Chemistry, Technology, Functional Properties and Applications*: Elsevier.

Chatzidaki, M. D., Mateos-Diaz, E., Leal-Calderon, F., Xenakis, A., & Carrière, F. (2016). Water-in-oil microemulsions versus emulsions as carriers of hydroxytyrosol: An *in vitro* gastrointestinal lipolysis study using the pHstat technique. *Food & function, 7*(5), 2258-2269.

Chen, B., Li, H., Ding, Y., & Rao, J. (2011). Improvement of physicochemical stabilities of emulsions containing oil droplets coated by non-globular protein–beet pectin complex membranes. *Food Research International, 44*(5), 1468-1475.

Chen, H., Jin, X., Li, Y., & Tian, J. (2016). Investigation into the physical stability of a eugenol nanoemulsion in the presence of a high content of triglyceride. *RSC advances, 6*(93), 91060-91067.

Chen, J., & Dickinson, E. (1999). Effect of surface character of filler particles on rheology of heat-set whey protein emulsion gels. *Colloids and Surfaces B: Biointerfaces, 12*(3), 373-381.

Chen, J., Dickinson, E., Lee, H., & Lee, W. P. (2001). Protein-based emulsion gel: Effects of interfacial properties and temperature. In E. Dickinson & R. Miller (Eds.), *Food Colloids: Fundamentals of Formulation* (pp. 384-391). Cambridge, UK: The Royal Society of Chemistry.

Cho, Y.-H., & McClements, D. J. (2009). Theoretical stability maps for guiding preparation of emulsions stabilized by protein− polysaccharide interfacial complexes. *Langmuir, 25*(12), 6649-6657.

Chu, B.-S., Ichikawa, S., Kanafusa, S., & Nakajima, M. (2007). Preparation of Protein-Stabilized β-Carotene Nanodispersions by Emulsification–Evaporation Method. *Journal of the American Oil Chemists' Society, 84*(11), 1053-1062. doi:10.1007/s11746-007-1132-7

Chun, J.-Y., Choi, M.-J., Min, S.-G., & Weiss, J. (2013). Formation and stability of multiple-layered liposomes by layer-by-layer electrostatic deposition of biopolymers. *Food Hydrocolloids, 30*(1), 249-257.

Clusel, M., Corwin, E. I., Siemens, A. O., & Brujić, J. (2009). A 'granocentric'model for random packing of jammed emulsions. *Nature, 460*(7255), 611-615.

Cooper, C. L., Dubin, P. L., Kayitmazer, A. B., & Turksen, S. (2005). Polyelectrolyte–protein complexes. *Current Opinion in Colloid & Interface Science, 10*(1–2), 52-78. doi:http://doi.org/10.1016/j.cocis.2005.05.007

Coppock, J. D., Krishan, K., Dennin, M., & Moore, B. G. (2009). Fluorescence microscopy imaging of giant folding in a catanionic monolayer. *Langmuir, 25*(9), 5006-5011.

Corstens, M. N., Berton-Carabin, C. C., Kester, A., Fokkink, R., van den Broek, J. M., de Vries, R., . . . Schroën, K. (2017). Destabilization of multilayered interfaces in digestive conditions limits their ability to prevent lipolysis in emulsions. *Food structure, 12*, 54-63.

Crofton, A. R., Hudson, S. M., Howard, K., Pender, T., Abdelgawad, A., Wolski, D., & Kirsch, W. M. (2016). Formulation and characterization of a plasma sterilized, pharmaceutical grade chitosan powder. *Carbohydrate polymers, 146*, 420-426.

Dalgleish, D. G. (1990). The conformations of proteins on solid/water interfaces—caseins and phosvitin on polystyrene latices. *Colloids and surfaces, 46*(2), 141-155.

Danov, K. D., Basheva, E. S., Kralchevsky, P. A., Ananthapadmanabhan, K. P., & Lips, A. (2011). The metastable states of foam films containing electrically charged micelles or particles: experiment and quantitative interpretation. *Advances in colloid and interface science, 168*(1-2), 50-70.

Datta, S. S., Gerrard, D. D., Rhodes, T. S., Mason, T. G., & Weitz, D. A. (2011). Rheology of attractive emulsions. *Physical Review E, 84*(4), 041404.

Deen, G. R., Skovgaard, J., & Pedersen, J. S. (2016). Formation and properties of nanoemulsions. In M. G. Alexandru (Ed.), *Emulsions: Nanotechnology in the Agri-Food Industry* (Vol. 3, pp. 193). Cambridge, United States: Academic press.

Dickinson, E. (1992). Interfacial interactions and the stability of oil-in-water emulsions. *Pure and Applied Chemistry, 64*(11), 1721-1724. doi:10.1351/pac199264111721

Dickinson, E. (1993). Protein-polysaccharide interactions in food colloids. Food Colloids and Polymers Stability and Mechanical Properties. *ElsevierScience LTD, Inglaterra*, 77-83.

Dickinson, E. (1994). Protein-stabilized emulsions. *Journal of Food Engineering, 22*(1), 59-74. doi:https://doi.org/10.1016/0260-8774(94)90025-6

Dickinson, E. (2003). Hydrocolloids at interfaces and the influence on the properties of dispersed systems. *Food Hydrocolloids, 17*(1), 25-39.

Dickinson, E. (2009). Hydrocolloids as emulsifiers and emulsion stabilizers. *Food Hydrocolloids, 23*(6), 1473-1482.

Dickinson, E. (2010). Flocculation of protein-stabilized oil-in-water emulsions. *Colloids and Surfaces B: Biointerfaces, 81*(1), 130-140.

Dickinson, E. (2011). Mixed biopolymers at interfaces: Competitive adsorption and multilayer structures. *Food Hydrocolloids, 25*(8), 1966-1983.

Dickinson, E. (2012). Emulsion gels: The structuring of soft solids with protein-stabilized oil droplets. *Food Hydrocolloids, 28*(1), 224-241.

Dickinson, E. (2013). Stabilising emulsion-based colloidal structures with mixed food ingredients. *Journal of the Science of Food and Agriculture, 93*(4), 710-721. doi:10.1002/jsfa.6013

Dickinson, E. (2019). Strategies to control and inhibit the flocculation of protein-stabilized oil-in-water emulsions. *Food Hydrocolloids, 96*, 209-223.

Dickinson, E., & Chen, J. (1999). Heat-set whey protein emulsion gels: role of active and inactive filler particles. *Journal of Dispersion Science and Technology, 20*(1-2), 197-213.

Dickinson, E., & Pawlowsky, K. (1997). Effect of ι-carrageenan on flocculation, creaming, and rheology of a protein-stabilized emulsion. *Journal of agricultural and food chemistry, 45*(10), 3799-3806.

Dickinson, E., Semenova, M. G., Antipova, A. S., & Pelan, E. G. (1998). Effect of high-methoxy pectin on properties of casein-stabilized emulsions. *Food Hydrocolloids, 12*(4), 425-432. doi:https://doi.org/10.1016/S0268-005X(98)00057-5

Duvarci, O. C., Yazar, G., & Kokini, J. L. (2017). The comparison of LAOS behavior of structured food materials (suspensions, emulsions and elastic networks). *Trends in food science & technology, 60*, 2-11.

Erramreddy, V. V., & Ghosh, S. (2014). Influence of emulsifier concentration on nanoemulsion gelation. *Langmuir, 30*(37), 11062-11074.

Erramreddy, V. V., & Ghosh, S. (2015). Influence of droplet size on repulsive and attractive nanoemulsion gelation. *Colloids and Surfaces A: Physicochemical and Engineering Aspects, 484*, 144-152.

Erramreddy, V. V., Tu, S., & Ghosh, S. (2017). Rheological reversibility and long-term stability of repulsive and attractive nanoemulsion gels. *RSC advances, 7*(75), 47818-47832.

Espinal-Ruiz, M., Restrepo-Sánchez, L.-P., Narváez-Cuenca, C.-E., & McClements, D. J. (2016). Impact of pectin properties on lipid digestion under simulated gastrointestinal conditions: Comparison of citrus and banana passion fruit (Passiflora tripartita var. mollissima) pectins. *Food Hydrocolloids, 52*, 329-342.

Ettelaie, R., & Akinshina, A. (2014). Colloidal interactions induced by overlap of mixed protein+polysaccharide interfacial layers. *Food Hydrocolloids, 42*, 106-117. doi:https://doi.org/10.1016/j.foodhyd.2014.01.020

Ettelaie, R., Akinshina, A., & Dickinson, E. (2008). Mixed protein–polysaccharide interfacial layers: a self consistent field calculation study. *Faraday discussions, 139*, 161-178.

Ettelaie, R., Akinshina, A., & Maurer, S. (2012). Mixed protein–polysaccharide interfacial layers: effect of polysaccharide charge distribution. *Soft Matter, 8*(29), 7582-7597.

Færgemand, M., Murray, B. S., & Dickinson, E. (1997). Cross-linking of milk proteins with transglutaminase at the oil− water interface. *Journal of agricultural and food chemistry, 45*(7), 2514-2519.

Fang, S., Zhao, X., Liu, Y., Liang, X., & Yang, Y. (2019). Fabricating multilayer emulsions by using OSA starch and chitosan suitable for spray drying: Application in the encapsulation of β-carotene. *Food Hydrocolloids, 93*, 102-110.

Feng, Q., Sun, J., & Jiang, X. (2016). Microfluidics-mediated assembly of functional nanoparticles for cancer-related pharmaceutical applications. *Nanoscale, 8*(25), 12430-12443.

Fernandez, P., André, V., Rieger, J., & Kühnle, A. (2004). Nano-emulsion formation by emulsion phase inversion. *Colloids and Surfaces A: Physicochemical and Engineering Aspects, 251*(1–3), 53-58. doi:http://dx.doi.org/10.1016/j.colsurfa.2004.09.029

Fioramonti, S. A., Martinez, M. J., Pilosof, A. M., Rubiolo, A. C., & Santiago, L. G. (2015). Multilayer emulsions as a strategy for linseed oil microencapsulation: Effect of pH and alginate concentration. *Food Hydrocolloids, 43*, 8-17.

Foegeding, E., & Drake, M. (2007). Invited review: Sensory and mechanical properties of cheese texture. *Journal of Dairy Science, 90*(4), 1611-1624.

Franca, E. F., Freitas, L. C., & Lins, R. D. (2011). Chitosan molecular structure as a function of N‐acetylation. *Biopolymers, 95*(7), 448-460.

Fryd, M. M., & Mason, T. G. (2012). Advanced naoemulsions. *Annual review of physical chemistry, 63*, 493-518.

Furusawa, K., Sato, A., Shirai, J., & Nashima, T. (2002). Depletion flocculation of latex dispersion in ionic micellar systems. *Journal of Colloid and interface science, 253*(2), 273-278.

Gancz, K., Alexander, M., & Corredig, M. (2006). In situ study of flocculation of whey protein-stabilized emulsions caused by addition of high methoxyl pectin. *Food Hydrocolloids, 20*(2-3), 293-298.

Gargouri, Y., Pieroni, G., Rivière, C., Lowe, P. A., Saunière, J.-F., Sarda, L., & Verger, R. (1986). Importance of human gastric lipase for intestinal lipolysis: an *in vitro* study. *Biochimica et Biophysica Acta (BBA)-Lipids and Lipid Metabolism, 879*(3), 419-423.

Gashua, I. B., Williams, P. A., & Baldwin, T. C. (2016). Molecular characteristics, association and interfacial properties of gum Arabic harvested from both Acacia senegal and Acacia seyal. *Food Hydrocolloids, 61*, 514-522. doi:https://doi.org/10.1016/j.foodhyd.2016.06.005

Gatto, M., Ochi, D., Yoshida, C. M. P., & da Silva, C. F. (2019). Study of chitosan with different degrees of acetylation as cardboard paper coating. *Carbohydrate polymers, 210*, 56-63.

Genovese, D., Lozano, J., & Rao, M. (2007). The rheology of colloidal and noncolloidal food dispersions. *Journal of food science, 72*(2), R11-R20.

Geremias-Andrade, I. M., Souki, N. P., Moraes, I. C., & Pinho, S. C. (2016). Rheology of emulsion-filled gels applied to the development of food materials. *Gels, 2*(3), 22.

Gharsallaoui, A., Saurel, R., Chambin, O., Cases, E., Voilley, A., & Cayot, P. (2010). Utilisation of pectin coating to enhance spray-dry stability of pea protein-stabilised oil-in-water emulsions. *Food chemistry, 122*(2), 447-454. doi:https://doi.org/10.1016/j.foodchem.2009.04.017

Gharsallaoui, A., Yamauchi, K., Chambin, O., Cases, E., & Saurel, R. (2010). Effect of high methoxyl pectin on pea protein in aqueous solution and at oil/water interface. *Carbohydrate polymers, 80*(3), 817-827. doi:https://doi.org/10.1016/j.carbpol.2009.12.038

Goindi, S., Kaur, A., Kaur, R., Kalra, A., & Chauhan, P. (2016). 19 - Nanoemulsions: an emerging technology in the food industry. In A. M. Grumezescu (Ed.), *Emulsions:: Nanotechnology*

in the Agri-Food Industry (Vol. 3, pp. 651-688). Cambridge, United States: Academic Press.

Groot, R. D., & Stoyanov, S. D. (2011). Close packing density and fracture strength of adsorbed polydisperse particle layers. *Soft Matter, 7*(10), 4750-4761.

Gu, Y. S., Decker, E. A., & McClements, D. J. (2005). Influence of pH and carrageenan type on properties of β-lactoglobulin stabilized oil-in-water emulsions. *Food Hydrocolloids, 19*(1), 83-91. doi:http://doi.org/10.1016/j.foodhyd.2004.04.016

Gudipati, V., Sandra, S., McClements, D. J., & Decker, E. A. (2010). Oxidative stability and *in vitro* digestibility of fish oil-in-water emulsions containing multilayered membranes. *Journal of agricultural and food chemistry, 58*(13), 8093-8099.

Gunasekaran, S., & Ak, M. M. (2000). Dynamic oscillatory shear testing of foods — selected applications. *Trends in food science & technology, 11*(3), 115-127. doi:https://doi.org/10.1016/S0924-2244(00)00058-3

Guo, Q., Bellissimo, N., & Rousseau, D. (2017). Role of gel structure in controlling *in vitro* intestinal lipid digestion in whey protein emulsion gels. *Food Hydrocolloids, 69*, 264-272.

Gupta, A., Eral, H. B., Hatton, T. A., & Doyle, P. S. (2016). Nanoemulsions: formation, properties and applications. *Soft Matter, 12*(11), 2826-2841.

Gutierrez, J. M., Gonzalez, C., Maestro, A., Sole, I., Pey, C. M., & Nolla, J. (2008). Nano-emulsions: New applications and optimization of their preparation. *Current Opinion in Colloid & Interface Science, 13*(4), 245-251. doi:10.1016/j.cocis.2008.01.005

Guzey, D., Kim, H. J., & McClements, D. J. (2004). Factors influencing the production of o/w emulsions stabilized by β-lactoglobulin–pectin membranes. *Food Hydrocolloids, 18*(6), 967-975. doi:https://doi.org/10.1016/j.foodhyd.2004.04.001

Guzey, D., & McClements, D. J. (2006). Formation, stability and properties of multilayer emulsions for application in the food industry. *Advances in colloid and interface science, 128-130*, 227-248. doi:https://doi.org/10.1016/j.cis.2006.11.021

Güzey, D., & McClements, D. J. (2006). Influence of Environmental Stresses on O/W Emulsions Stabilized by β-Lactoglobulin–Pectin and β-Lactoglobulin–Pectin–Chitosan Membranes Produced by the Electrostatic Layer-by-Layer Deposition Technique. *Food Biophysics, 1*(1), 30-40. doi:10.1007/s11483-005-9002-z

Haj-shafiei, S., Ghosh, S., & Rousseau, D. (2013). Kinetic stability and rheology of wax-stabilized water-in-oil emulsions at different water cuts. *Journal of Colloid and interface science, 410*, 11-20.

Hedegaard, S. F., Nilsson, C., Laurinmäki, P., Butcher, S., Urtti, A., & Yaghmur, A. (2013). Nanostructured aqueous dispersions of citrem interacting with lipids and PEGylated lipids. *Rsc Advances, 3*(46), 24576-24585.

Helgeson, M. E. (2016). Colloidal behavior of nanoemulsions: Interactions, structure, and rheology. *Current Opinion in Colloid & Interface Science, 25*, 39-50.

Hespeler, D., Knoth, D., Keck, C. M., Müller, R. H., & Pyo, S. M. (2019). smartPearls(®) for dermal bioavailability enhancement - Long-term stabilization of suspensions by viscoelasticity. *Int J Pharm, 562*, 293-302. doi:10.1016/j.ijpharm.2019.03.016

Hinrichs, K., & Eichhorn, K.-J. (2014). *Ellipsometry of functional organic surfaces and films* (Vol. 52): Springer.

Hong, Y.-H., & McClements, D. J. (2007). Modulation of pH sensitivity of surface charge and aggregation stability of protein-coated lipid droplets by chitosan addition. *Food Biophysics, 2*(1), 46-55.

Hou, Z., Gao, Y., Yuan, F., Liu, Y., Li, C., & Xu, D. (2010). Investigation into the physicochemical stability and rheological properties of β-carotene emulsion stabilized by soybean soluble polysaccharides and chitosan. *Journal of agricultural and food chemistry, 58*(15), 8604-8611.

Hu, M., Li, Y., Decker, E. A., Xiao, H., & McClements, D. J. (2011). Impact of layer structure on physical stability and lipase digestibility of lipid droplets coated by biopolymer nanolaminated coatings. *Food Biophysics, 6*(1), 37-48.

Huang, J., Zeng, S., Xiong, S., & Huang, Q. (2016). Steady, dynamic, and creep-recovery rheological properties of myofibrillar protein from grass carp muscle. *Food Hydrocolloids, 61*, 48-56.

Huang, L., Cai, Y., Liu, T., Zhao, X., Chen, B., Long, Z., . . . Zhao, Q. (2019). Stability of emulsion stabilized by low-concentration soybean protein isolate: Effects of insoluble soybean fiber. *Food Hydrocolloids, 97*, 105232.

Humblet-Hua, N.-P. K., van der Linden, E., & Sagis, L. M. (2012). Microcapsules with protein fibril reinforced shells: effect of fibril properties on mechanical strength of the shell. *Journal of agricultural and food chemistry, 60*(37), 9502-9511.

Hyun, K., Wilhelm, M., Klein, C. O., Cho, K. S., Nam, J. G., Ahn, K. H., . . . McKinley, G. H. (2011). A review of nonlinear oscillatory shear tests: Analysis and application of large amplitude oscillatory shear (LAOS). *Progress in polymer science, 36*(12), 1697-1753.

Iracki, T. D., Beltran-Villegas, D. J., Eichmann, S. L., & Bevan, M. A. (2010). Charged micelle depletion attraction and interfacial colloidal phase behavior. *Langmuir, 26*(24), 18710-18717.

Israelachivili. (2011). *Intermolecular and Surface Forces*.

Ivanov, I. B., & Kralchevsky, P. A. (1997). Stability of emulsions under equilibrium and dynamic conditions. *Colloids and Surfaces A: Physicochemical and engineering aspects, 128*(1-3), 155-175.

Jafari, S. M., Assadpoor, E., He, Y. H., & Bhandari, B. (2008). Re-coalescence of emulsion droplets during high-energy emulsification. *Food Hydrocolloids, 22*(7), 1191-1202. doi:10.1016/j.foodhyd.2007.09.006

James, G., & Walz, J. (2014). Experimental and theoretical investigation of the depletion and structural forces produced by ionic micelles. *Colloids and Surfaces A: Physicochemical and Engineering Aspects, 441*, 406-419.

Jin, W., Xu, W., Liang, H., Li, Y., Liu, S., & Li, B. (2016). Nanoemulsions for food: properties, production, characterization, and applications. In A. M. Grumezescu (Ed.), *Emulsions: Nanotechnology in the Agri-Food Industry* (Vol. 3, pp. 1-36). Cambridge, United States: Academic Press.

Jo, M., Ban, C., Goh, K. K., & Choi, Y. J. (2019). Influence of chitosan-coating on the stability and digestion of emulsions stabilized by waxy maize starch crystals. *Food Hydrocolloids, 94*, 603-612.

Jones, O. G., & McClements, D. J. (2010). Functional biopolymer particles: design, fabrication, and applications. *Comprehensive Reviews in Food Science and Food Safety, 9*(4), 374-397.

Jönsson, B., Lindman, B., Holmberg, K., & Kronberg, B. (1998). Surfactant micellization. *Surfactants and Polymers in Aqueous Solution. John Wiley and Sons, Chichester, UK*, 3-60.

Kaasgaard, T., & Keller, D. (2010). Chitosan coating improves retention and redispersibility of freeze-dried flavor oil emulsions. *Journal of agricultural and food chemistry, 58*(4), 2446-2454.

Kabalnov, A. (2001). Ostwald ripening and related phenomena. *Journal of Dispersion Science and Technology, 22*(1), 1-12.

Kadiya, K., & Ghosh, S. (2019). Conversion of Viscous Oil-in-Water Nanoemulsions to Viscoelastic Gels upon Removal of Excess Ionic Emulsifier. *Langmuir, 35*(52), 17061-17074.

Kartal, C., Unal, M. K., & Otles, S. (2017). Production and stabilization of a flaxseed oil multi-layer emulsion containing sodium caseinate and pectin. *International Journal of Food Properties, 20*(4), 833-844.

Kawada, H., Kume, T., Matsunaga, T., Iwai, H., Sano, T., & Shibayama, M. (2010). Structure and rheology of a self-standing nanoemulsion. *Langmuir, 26*(4), 2430-2437.

Kim, H. S., & Mason, T. G. (2017). Advances and challenges in the rheology of concentrated emulsions and nanoemulsions. *Advances in colloid and interface science, 247*, 397-412.

Klinkesorn, U., & McClements, D. J. (2009). Influence of chitosan on stability and lipase digestibility of lecithin-stabilized tuna oil-in-water emulsions. *Food chemistry, 114*(4), 1308-1315.

Klinkesorn, U., & McClements, D. J. (2010). Impact of lipase, bile salts, and polysaccharides on properties and digestibility of tuna oil multilayer emulsions stabilized by lecithin–chitosan. *Food Biophysics, 5*(2), 73-81.

Klongdee, S., Thongngam, M., & Klinkesorn, U. (2012). Rheology and microstructure of lecithin-stabilized tuna oil emulsions containing chitosan of varying concentration and molecular size. *Food Biophysics, 7*(2), 155-162.

Knudsen, J. C., Øgendal, L. H., & Skibsted, L. H. (2008). Droplet surface properties and rheology of concentrated oil in water emulsions stabilized by heat-modified β-lactoglobulin B. *Langmuir, 24*(6), 2603-2610.

Koroleva, M. Y., & Yurtov, E. V. (2012). Nanoemulsions: the properties, methods of preparation and promising applications. *Russian Chemical Reviews, 81*(1), 21.

Koumakis, N., & Petekidis, G. (2011). Two step yielding in attractive colloids: transition from gels to attractive glasses. *Soft Matter, 7*(6), 2456-2470.

Kralova, I., & Sjöblom, J. (2009). Surfactants used in food industry: a review. *Journal of Dispersion Science and Technology, 30*(9), 1363-1383.

Krebs, T., Ershov, D., Schroen, C., & Boom, R. (2013). Coalescence and compression in centrifuged emulsions studied with in situ optical microscopy. *Soft Matter, 9*(15), 4026-4035.

Krog, N. J., & Sparso, F. V. (2004). Food emulsifiers: their chemical and physical properties. *Food emulsions, 12*.

Kuentz, M., & Rothlisberger, D. (2002). Sedimentation analysis of aqueous microsuspensions based on near infrared transmission measurements during centrifugation Determination of a suitable amount of gelling agent to minimise settling in the gravitational field. *STP pharma sciences, 12*(6), 391-396.

Kuentz, M., & Röthlisberger, D. (2003). Rapid assessment of sedimentation stability in dispersions using near infrared transmission measurements during centrifugation and oscillatory rheology. *Eur J Pharm Biopharm, 56*(3), 355-361. doi:10.1016/s0939-6411(03)00108-5

Kumar, N., & Mandal, A. (2018a). Surfactant stabilized oil-in-water nanoemulsion: stability, interfacial tension, and rheology study for enhanced oil recovery application. *Energy & fuels, 32*(6), 6452-6466.

Kumar, N., & Mandal, A. (2018b). Thermodynamic and physicochemical properties evaluation for formation and characterization of oil-in-water nanoemulsion. *Journal of Molecular Liquids, 266*, 147-159.

Lapasin, R., Grassi, M., & Coceani, N. (2001). Effects of polymer addition on the rheology of o/w microemulsions. *Rheologica acta, 40*(2), 185-192.

Leal, L. (2004). Flow induced coalescence of drops in a viscous fluid. *Physics of fluids, 16*(6), 1833-1851.

Lee, L., & Norton, I. T. (2013). Comparing droplet breakup for a high-pressure valve homogeniser and a Microfluidizer for the potential production of food-grade nanoemulsions. *Journal of Food Engineering, 114*(2), 158-163. doi:10.1016/j.jfoodeng.2012.08.009

Lee, S. J., & McClements, D. J. (2010). Fabrication of protein-stabilized nanoemulsions using a combined homogenization and amphiphilic solvent dissolution/evaporation approach. *Food Hydrocolloids, 24*(6-7), 560-569.

Lerche, D. (2019). Comprehensive Characterization of Nano-and Microparticles by In-Situ Visualization of Particle Movement Using Advanced Sedimentation Techniques. *KONA Powder and Particle Journal, 36*, 156-186.

Lerche, D., & Sobisch, T. (2011). Direct and accelerated characterization of formulation stability. *Journal of Dispersion Science and Technology, 32*(12), 1799-1811.

Lesmes, U., Sandra, S., Decker, E. A., & McClements, D. J. (2010). Impact of surface deposition of lactoferrin on physical and chemical stability of omega-3 rich lipid droplets stabilised by caseinate. *Food chemistry, 123*(1), 99-106.

Létang, C., Piau, M., & Verdier, C. (1999). Characterization of wheat flour–water doughs. Part I: Rheometry and microstructure. *Journal of Food Engineering, 41*(2), 121-132. doi:https://doi.org/10.1016/S0260-8774(99)00082-5

Li, H., Wu, J., Doost, A. S., Su, J., & Van der Meeren, P. (2021). Electrostatic interaction between whey proteins and low methoxy pectin studied by quartz crystal microbalance with dissipation monitoring. *Food Hydrocolloids, 113*, 106489. doi:https://doi.org/10.1016/j.foodhyd.2020.106489

Li, J. L., Cheng, Y. Q., Wang, P., Zhao, W. T., Yin, L. J., & Saito, M. (2012). A novel improvement in whey protein isolate emulsion stability: Generation of an enzymatically cross-linked beet pectin layer using horseradish peroxidase. *Food Hydrocolloids, 26*(2), 448-455.

Li, M., McClements, D. J., Liu, X., & Liu, F. (2020). Design principles of oil‐in‐water emulsions with functionalized interfaces: Mixed, multilayer, and covalent complex structures. *Comprehensive Reviews in Food Science and Food Safety, 19*(6), 3159-3190.

Li, Q., Wang, Z., Dai, C., Wang, Y., Chen, W., Ju, X., . . . He, R. (2019). Physical stability and microstructure of rapeseed protein isolate/gum Arabic stabilized emulsions at alkaline pH. *Food Hydrocolloids, 88*, 50-57.

Li, Q., Xu, M., Xie, J., Su, E., Wan, Z., Sagis, L. M., & Yang, X. (2021). Large amplitude oscillatory shear (LAOS) for nonlinear rheological behavior of heterogeneous emulsion gels made from natural supramolecular gelators. *Food Research International, 140*, 110076.

Li, Y., Hu, M., Xiao, H., Du, Y., Decker, E. A., & McClements, D. J. (2010). Controlling the functional performance of emulsion-based delivery systems using multi-component biopolymer coatings. *European Journal of Pharmaceutics and Biopharmaceutics, 76*(1), 38-47.

Li Zhai, J., Day, L., Aguilar, M.-I., & Wooster, T. J. (2013). Protein folding at emulsion oil/water interfaces. *Current Opinion in Colloid & Interface Science, 18*(4), 257-271.

Lianos, P., & Zana, R. (1981). Fluorescence probe studies of the effect of concentration on the state of aggregation of surfactants in aqueous solution. *Journal of Colloid and Interface Science, 84*(1), 100-107.

Lin, M., Lindsay, H., Weitz, D., Klein, R., Ball, R., & Meakin, P. (1990). Universal diffusion-limited colloid aggregation. *Journal of Physics: Condensed Matter, 2*(13), 3093.

Liu, C., Tan, Y., Xu, Y., McCleiments, D. J., & Wang, D. (2019). Formation, characterization, and application of chitosan/pectin-stabilized multilayer emulsions as astaxanthin delivery systems. *International journal of biological macromolecules, 140*, 985-997.

Liu, Y., Yadav, M. P., & Yin, L. (2018). Enzymatic catalyzed corn fiber gum-bovine serum albumin conjugates: Their interfacial adsorption behaviors in oil-in-water emulsions. *Food Hydrocolloids, 77*, 986-994. doi:https://doi.org/10.1016/j.foodhyd.2017.11.048

Lucey, J., Johnson, M., & Horne, D. (2003). Invited review: Perspectives on the basis of the rheology and texture properties of cheese. *Journal of Dairy Science, 86*(9), 2725-2743.

Lutz, R., Aserin, A., Wicker, L., & Garti, N. (2009). Structure and physical properties of pectins with block-wise distribution of carboxylic acid groups. *Food Hydrocolloids, 23*(3), 786-794.

Ma, P., Zeng, Q., Tai, K., He, X., Yao, Y., Hong, X., & Yuan, F. (2018). Development of stable curcumin nanoemulsions: effects of emulsifier type and surfactant-to-oil ratios. *Journal of food science and technology, 55*(9), 3485-3497.

Ma, P. L., Lavertu, M., Winnik, F. M., & Buschmann, M. D. (2009). New Insights into chitosan− DNA interactions using isothermal titration microcalorimetry. *Biomacromolecules, 10*(6), 1490-1499.

Malinauskytė, E., Ramanauskaitė, J., Keršienė, M., Jasutienė, I., Leskauskaitė, D., Devold, T. G., & Vegarud, G. E. (2018). Impact of Interfacial Composition on Emulsion Digestion Using *in vitro* and *in vivo* Models. *Journal of food science, 83*(11), 2850-2857.

Malmsten, M. (1994). Ellipsometry studies of protein layers adsorbed at hydrophobic surfaces. *Journal of Colloid and interface science, 166*(2), 333-342.

Mao, Y., & McClements, D. J. (2012). Modulation of emulsion rheology through electrostatic heteroaggregation of oppositely charged lipid droplets: Influence of particle size and emulsifier content. *Journal of Colloid and interface science, 380*(1), 60-66. doi:https://doi.org/10.1016/j.jcis.2012.05.007

Marangoni, A. G. (2000). Elasticity of high-volume-fraction fractal aggregate networks: A thermodynamic approach. *Physical Review B, 62*(21), 13951.

Marichal, L., Giraudon--Colas, G. l., Cousin, F., Thill, A., Labarre, J., Boulard, Y., . . . Renault, J. P. (2019). Protein–nanoparticle interactions: what are the protein–corona thickness and organization? *Langmuir, 35*(33), 10831-10837.

Marinova, K., Gurkov, T., Dimitrova, T., Alargova, R., & Smith, D. (1998). Role of oscillatory structural forces for interactions in thin emulsion films containing micelles. *Langmuir, 14*(8), 2011-2019.

Mason, T. (1999). New fundamental concepts in emulsion rheology. *Current Opinion in Colloid & Interface Science, 4*(3), 231-238.

Mason, T., Bibette, J., & Weitz, D. (1995). Elasticity of compressed emulsions. *Physical review letters, 75*(10), 2051.

Mason, T., Lacasse, M.-D., Grest, G. S., Levine, D., Bibette, J., & Weitz, D. (1997). Osmotic pressure and viscoelastic shear moduli of concentrated emulsions. *Physical Review E, 56*(3), 3150.

Mason, T., Wilking, J., Meleson, K., Chang, C., & Graves, S. (2006). Nanoemulsions: formation, structure, and physical properties. *Journal of Physics: Condensed Matter, 18*(41), R635.

Mason, T. G., Bibette, J., & Weitz, D. A. (1996). Yielding and flow of monodisperse emulsions. *Journal of Colloid and interface science, 179*(2), 439-448.

Mason, T. G., & Scheffold, F. (2014). Crossover between entropic and interfacial elasticity and osmotic pressure in uniform disordered emulsions. *Soft Matter, 10*(36), 7109-7116.

Mason, T. G., Wilking, J. N., Meleson, K., Chang, C. B., & Graves, S. M. (2007). Nanoemulsions: formation, structure, and physical properties. *Journal of Physics-Condensed Matter, 19*(7). doi:10.1088/0953-8984/19/7/079001

Mat, D. J., Le Feunteun, S., Michon, C., & Souchon, I. (2016). *In vitro* digestion of foods using pH-stat and the INFOGEST protocol: Impact of matrix structure on digestion kinetics of macronutrients, proteins and lipids. *Food Research International, 88*, 226-233.

Matalanis, A., Jones, O. G., & McClements, D. J. (2011). Structured biopolymer-based delivery systems for encapsulation, protection, and release of lipophilic compounds. *Food Hydrocolloids, 25*(8), 1865-1880.

McClements, D. (2000). Comments on viscosity enhancement and depletion flocculation by polysaccharides. *Food Hydrocolloids, 14*(2), 173-177.

McClements, D. J. (2006). Non-covalent interactions between proteins and polysaccharides. *Biotechnology advances, 24*(6), 621-625.

McClements, D. J. (2010). Emulsion design to improve the delivery of functional lipophilic components. *Annual review of food science and technology, 1*, 241-269.

McClements, D. J. (2011). Edible nanoemulsions: fabrication, properties, and functional performance. *Soft Matter, 7*(6), 2297-2316. doi:10.1039/c0sm00549e

McClements, D. J. (2012a). Advances in fabrication of emulsions with enhanced functionality using structural design principles. *Current Opinion in Colloid & Interface Science, 17*(5), 235-245.

McClements, D. J. (2012b). Nanoemulsions versus microemulsions: terminology, differences, and similarities. *Soft Matter, 8*(6), 1719-1729. doi:10.1039/c2sm06903b

McClements, D. J. (2015). *Food emulsions: principles, practices, and techniques*: CRC press.

McClements, D. J., & Chanamai, R. (2002). Physicochemical properties of mono disperse oil-in-water emulsions. *Journal of dispersion science and technology, 23*(1-3), 125-134.

McClements, D. J., Decker, E. A., & Weiss, J. (2007). Emulsion‐based delivery systems for lipophilic bioactive components. *Journal of food science, 72*(8), R109-R124.

McClements, D. J., & Demetriades, K. (1998). An integrated approach to the development of reduced-fat food emulsions. *Critical reviews in food science and nutrition, 38*(6), 511-536.

McClements, D. J., & Li, Y. (2010). Structured emulsion-based delivery systems: Controlling the digestion and release of lipophilic food components. *Advances in colloid and interface science, 159*(2), 213-228.

McClements, D. J., & Rao, J. (2011). Food-grade nanoemulsions: formulation, fabrication, properties, performance, biological fate, and potential toxicity. *Critical reviews in food science and nutrition, 51*(4), 285-330.

McClements, D. J., & Xiao, H. (2012). Potential biological fate of ingested nanoemulsions: influence of particle characteristics. *Food & function, 3*(3), 202-220.

McKenna, B., & Lyng, J. (2003). Introduction to food rheology and its measurement. *Texture in food, 1*, 130-160.

Meinders, M. B., & van Vliet, T. (2004). The role of interfacial rheological properties on Ostwald ripening in emulsions. *Advances in colloid and interface science, 108*, 119-126.

Meleson, K., Graves, S., & Mason, T. G. (2004). Formation of concentrated nanoemulsions by extreme shear. *Soft Materials, 2*(2-3), 109-123. doi:10.1081/smts-200056102

Missel, P. J., Mazer, N., Benedek, G., Young, C., & Carey, M. C. (1980). Thermodynamic analysis of the growth of sodium dodecyl sulfate micelles. *The Journal of Physical Chemistry, 84*(9), 1044-1057.

Mondain-Monval, O., Leal-Calderon, F., & Bibette, J. (1996). Forces between emulsion droplets: role of surface charges and excess surfactant. *Journal de Physique II, 6*(9), 1313-1329.

Mrokowska, M. M., & Krztoń-Maziopa, A. (2019). Viscoelastic and shear-thinning effects of aqueous exopolymer solution on disk and sphere settling. *Scientific reports, 9*(1), 1-13.

Muhoza, B., Karangwa, E., Duhoranimana, E., Zhang, X., & Xia, S. (2016). Influence of Pectin on the Stability of Whey Protein Isolate Stabilized Emulsion for Encapsulating Lutein. *Advance Journal of Food Science and Technology, 12*(11), 617-626.

Mulet-Cabero, A.-I., Egger, L., Portmann, R., Ménard, O., Marze, S., Minekus, M., . . . Carrière, F. (2020). A standardised semi-dynamic *in vitro* digestion method suitable for food–an international consensus. *Food & function, 11*(2), 1702-1720.

Mun, S., Decker, E. A., & McClements, D. J. (2005). Influence of droplet characteristics on the formation of oil-in-water emulsions stabilized by surfactant− chitosan layers. *Langmuir, 21*(14), 6228-6234.

Mun, S., Decker, E. A., & McClements, D. J. (2006). Effect of molecular weight and degree of deacetylation of chitosan on the formation of oil-in-water emulsions stabilized by surfactant–chitosan membranes. *Journal of Colloid and interface science, 296*(2), 581-590.

Mun, S., Decker, E. A., Park, Y., Weiss, J., & McClements, D. J. (2006). Influence of interfacial composition on *in vitro* digestibility of emulsified lipids: potential mechanism for chitosan's ability to inhibit fat digestion. *Food Biophysics, 1*(1), 21-29.

Mun, S., & McClements, D. J. (2006). Influence of Interfacial Characteristics on Ostwald Ripening in Hydrocarbon Oil-in-Water Emulsions. *Langmuir, 22*(4), 1551-1554. doi:10.1021/la0525751

Mundo, J. L. M., Zhou, H., Tan, Y., Liu, J., & McClements, D. J. (2020). Enhancing emulsion functionality using multilayer technology: Coating lipid droplets with saponin-polypeptide-polysaccharide layers by electrostatic deposition. *Food Research International*, 109864.

Nagarajan, R., & Ruckenstein, E. (1991). Theory of surfactant self-assembly: a predictive molecular thermodynamic approach. *Langmuir, 7*(12), 2934-2969.

Neirynck, N., Van der Meeren, P., Lukaszewicz-Lausecker, M., Cocquyt, J., Verbeken, D., & Dewettinck, K. (2007). Influence of pH and biopolymer ratio on whey protein–pectin interactions in aqueous solutions and in O/W emulsions. *Colloids and Surfaces A: Physicochemical and Engineering Aspects, 298*(1), 99-107. doi:https://doi.org/10.1016/j.colsurfa.2006.12.001

Nejatian, M., & Abbasi, S. (2019). Formation of concentrated triglyceride nanoemulsions and nanogels: natural emulsifiers and high power ultrasound. *RSC advances, 9*(49), 28330-28344.

Nejatian, M., Abbasi, S., & Kadkhodaee, R. (2018). Ultrasonic-assisted fabrication of concentrated triglyceride nanoemulsions and nanogels. *Langmuir, 34*(38), 11433-11441.

Ngouémazong, E. D., Christiaens, S., Shpigelman, A., Van Loey, A., & Hendrickx, M. (2015). The emulsifying and emulsion‐stabilizing properties of pectin: A review. *Comprehensive Reviews in Food Science and Food Safety, 14*(6), 705-718.

Norton, I. T., Spyropoulos, F., & Cox, P. (2010). *Practical food rheology: an interpretive approach*: John Wiley & Sons.

Noshad, M., Mohebbi, M., Koocheki, A., & Shahidi, F. (2016). Influence of interfacial engineering on stability of emulsions stabilized with soy protein isolate. *Journal of Dispersion Science and Technology, 37*(1), 56-65.

Noshad, M., Mohebbi, M., Shahidi, F., & Koocheki, A. (2015). Freeze–thaw stability of emulsions with soy protein isolate through interfacial engineering. *International Journal of Refrigeration, 58*, 253-260.

Ogawa, S., Decker, E. A., & McClements, D. J. (2003a). Influence of environmental conditions on the stability of oil in water emulsions containing droplets stabilized by lecithin− chitosan membranes. *Journal of agricultural and food chemistry, 51*(18), 5522-5527.

Ogawa, S., Decker, E. A., & McClements, D. J. (2003b). Production and characterization of O/W emulsions containing cationic droplets stabilized by lecithin− chitosan membranes. *Journal of agricultural and food chemistry, 51*(9), 2806-2812.

Osorio, P., & Urbina-Villalba, G. (2011). Influence of drop deformability on the stability of decane-in-water emulsions. *Journal of Surfactants and Detergents, 14*(2), 281-300.

Pal, R. (1996a). Effect of droplet size on the rheology of emulsions. *AIChE Journal, 42*(11), 3181-3190.

Pal, R. (1996b). Rheology of emulsions containing polymeric liquids. *Encyclopedia of emulsion technology, 4*, 93.

Pal, R. (1997). Dynamics of flocculated emulsions. *Chemical engineering science, 52*(7), 1177-1187.

Pallandre, S., Decker, E. A., & McClements, D. (2007). Improvement of Stability of Oil‐in‐Water Emulsions Containing Caseinate‐Coated Droplets by Addition of Sodium Alginate. *Journal of food science, 72*(9), E518-E524.

Patel, A., Kadiya, K., & Ghosh, S. (2017). The effect of emulsifier type on the formation and stability of nanoemulsion gels. *Lipid Technology, 29*(11-12), 111-114.

Patel, A., Longmore, N., Mohanan, A., & Ghosh, S. (2019). Salt and pH-induced attractive interactions on the rheology of food protein-stabilized nanoemulsions. *ACS omega, 4*(7), 11791-11800.

Patel, A., Mohanan, A., & Ghosh, S. (2019). Effect of protein type, concentration and oil droplet size on the formation of repulsively jammed elastic nanoemulsion gels. *Soft Matter, 15*(47), 9762-9775.

Perrechil, F., & Cunha, R. (2013). Stabilization of multilayered emulsions by sodium caseinate and κ-carrageenan. *Food Hydrocolloids, 30*(2), 606-613.

Persson, H., Nair, B. M., Frølich, W., Nyman, M., & Asp, N.-G. (1987). Binding of mineral elements by some dietary fibre components—*in vitro* (II). *Food chemistry, 26*(2), 139-148.

Petsev, D., & Bibette, J. (1995). Stability of osmotically compressed emulsions in the presence of ionic surfactants. *Langmuir, 11*(4), 1075-1077.

Petsev, D. N., Denkov, N. D., & Kralchevsky, P. A. (1995). Flocculation of deformable emulsion droplets: II. interaction energy. *Journal of Colloid and interface science, 176*(1), 201-213.

Pillai, P. K., Ouyang, Y., Stone, A. K., & Nickerson, M. T. (2021). Effect of different levels of esterification and blockiness of pectin on the functional behaviour of pea protein isolate–pectin complexes. *Food Science and Technology International, 27*(1), 3-12.

Preziosi, V., Perazzo, A., Tomaiuolo, G., Pipich, V., Danino, D., Paduano, L., & Guido, S. (2017). Flow-induced nanostructuring of gelled emulsions. *Soft Matter, 13*(34), 5696-5703.

Primozic, M., Duchek, A., Nickerson, M., & Ghosh, S. (2017). Effect of lentil proteins isolate concentration on the formation, stability and rheological behavior of oil-in-water nanoemulsions. *Food chemistry, 237*, 65-74.

Qian, C., & McClements, D. J. (2011). Formation of nanoemulsions stabilized by model food-grade emulsifiers using high-pressure homogenization: Factors affecting particle size. *Food Hydrocolloids, 25*(5), 1000-1008. doi:10.1016/j.foodhyd.2010.09.017

Qian, X., Lu, Y., Xie, W., & Wu, D. (2020). Viscoelasticity of olive oil/water Pickering emulsions stabilized with starch nanocrystals. *Carbohydrate polymers, 230*, 115575.

Qiu, C., Zhao, M., & McClements, D. J. (2015). Improving the stability of wheat protein-stabilized emulsions: Effect of pectin and xanthan gum addition. *Food Hydrocolloids, 43*, 377-387. doi:https://doi.org/10.1016/j.foodhyd.2014.06.013

Quemada, D., & Berli, C. (2002). Energy of interaction in colloids and its implications in rheological modeling. *Advances in colloid and interface science, 98*(1), 51-85. doi:http://doi.org/10.1016/S0001-8686(01)00093-8

Quina, F. H., Nassar, P. M., Bonilha, J. B., & Bales, B. L. (1995). Growth of sodium dodecyl sulfate micelles with detergent concentration. *The Journal of Physical Chemistry, 99*(46), 17028-17031.

Rao, J., & McClements, D. J. (2012). Food-grade microemulsions and nanoemulsions: Role of oil phase composition on formation and stability. *Food Hydrocolloids, 29*(2), 326-334. doi:10.1016/j.foodhyd.2012.04.008

Rinaudo, M. (2006). Chitin and chitosan: Properties and applications. *Progress in polymer science, 31*(7), 603-632.

Roudsari, M., Nakamura, A., Smith, A., & Corredig, M. (2006). Stabilizing Behavior of Soy Soluble Polysaccharide or High Methoxyl Pectin in Soy Protein Isolate Emulsions at Low pH. *Journal of agricultural and food chemistry, 54*(4), 1434-1441. doi:10.1021/jf051369g

Roy, C., Roulet, M., Lefebvre, D., Chartrand, L., Lepage, G., & Fournier, L. (1979). The role of gastric lipolysis on fat absorption and bile acid metabolism in the rat. *Lipids, 14*(9), 811-815.

Saccani, J., Castano, S., Beaurain, F., Laguerre, M., & Desbat, B. (2004). Stabilization of phospholipid multilayers at the air− water interface by compression beyond the collapse: A BAM, PM-IRRAS, and molecular dynamics study. *Langmuir, 20*(21), 9190-9197.

Saifullah, M., Ahsan, A., Rezaul, M., & Shishir, I. (2016). Production, stability and application of micro-and nanoemulsion in food production and the food processing industry. *Emulsions, 3*, 405.

Sala, G., van de Velde, F., Stuart, M. A. C., & van Aken, G. A. (2007). Oil droplet release from emulsion-filled gels in relation to sensory perception. *Food Hydrocolloids, 21*(5), 977-985.

Salhi, A., Amara, S., Mansuelle, P., Puppo, R., Lebrun, R., Gontero, B., . . . Carrière, F. (2020). Characterization of all the lipolytic activities in pancreatin and comparison with porcine and human pancreatic juices. *Biochimie, 169*, 106-120.

Salminen, H., & Weiss, J. (2014). Electrostatic adsorption and stability of whey protein–pectin complexes on emulsion interfaces. *Food Hydrocolloids, 35*, 410-419.

Salvia-Trujillo, L., Soliva-Fortuny, R. C., Rojas-Graü, M. A., Martín-Belloso, O., & McClements, D. J. (2017). Edible Nanoemulsions as Carriers of Active Ingredients: A Review. *Annual review of food science and technology, 8*(1), 439-466.

Sams, L., Paume, J., Giallo, J., & Carrière, F. (2016). Relevant pH and lipase for *in vitro* models of gastric digestion. *Food & function, 7*(1), 30-45.

Sarles, S. A., & Leo, D. J. (2010). Physical encapsulation of droplet interface bilayers for durable, portable biomolecular networks. *Lab on a Chip, 10*(6), 710-717.

Sassene, P., Fanø, M., Mu, H., Rades, T., Aquistapace, S., Schmitt, B., . . . Müllertz, A. (2016). Comparison of lipases for *in vitro* models of gastric digestion: lipolysis using two infant formulas as model substrates. *Food & function, 7*(9), 3989-3998.

Schmelz, T., Lesmes, U., Weiss, J., & McClements, D. J. (2011). Modulation of physicochemical properties of lipid droplets using β-lactoglobulin and/or lactoferrin interfacial coatings. *Food Hydrocolloids, 25*(5), 1181-1189.

Schmidt, U. S., Pietsch, V., Rentschler, C., Kurz, T., Endreß, H.-U., & Schuchmann, H. (2016). Influence of the degree of esterification on the emulsifying performance of conjugates formed between whey protein isolate and citrus pectin. *Food Hydrocolloids, 56*, 1-8.

Shah, B. R., Zhang, C., Li, Y., & Li, B. (2016). Bioaccessibility and antioxidant activity of curcumin after encapsulated by nano and Pickering emulsion based on chitosan-tripolyphosphate nanoparticles. *Food Research International, 89*, 399-407.

Shahidi, F., Arachchi, J. K. V., & Jeon, Y.-J. (1999). Food applications of chitin and chitosans. *Trends in food science & technology, 10*(2), 37-51.

Sharma, M. (1978). Ultracentrifugal stability of oil-in-oil emulsions *Emulsions* (pp. 75-77): Springer.

Simo, O. K., Mao, Y., Tokle, T., Decker, E. A., & McClements, D. J. (2012). Novel strategies for fabricating reduced fat foods: Heteroaggregation of lipid droplets with polysaccharides. *Food Research International, 48*(2), 337-345. doi:https://doi.org/10.1016/j.foodres.2012.04.018

Sjoblom, J. (2001). *Encyclopedic handbook of emulsion technology*: CRC press.

Sobisch, T., & Lerche, D. (2002). Characterization of nanostructuring effects at solid/liquid interfaces by analytical centrifugation. *Chemistry Preprint Archive, 2002*(9), 170-184.

Solans, C., Izquierdo, P., Nolla, J., Azemar, N., & Garcia-Celma, M. (2005). Nano-emulsions. *Current Opinion in Colloid & Interface Science, 10*(3), 102-110.

Sozer, N. (2009). Rheological properties of rice pasta dough supplemented with proteins and gums. *Food Hydrocolloids, 23*(3), 849-855.

Stauffer, C. E. (1999). *Emulsifiers*.

Stephen, A. M. (1995). *Food polysaccharides and their applications* (Vol. 67): CRC press.

Stubenrauch, C., & Von Klitzing, R. (2003). Disjoining pressure in thin liquid foam and emulsion films—new concepts and perspectives. *Journal of Physics: Condensed Matter, 15*(27), R1197.

Surh, J., Decker, E. A., & McClements, D. J. (2006). Influence of pH and pectin type on properties and stability of sodium-caseinate stabilized oil-in-water emulsions. *Food Hydrocolloids, 20*(5), 607-618. doi:https://doi.org/10.1016/j.foodhyd.2005.07.004

Surh, J., Gu, Y. S., Decker, E. A., & McClements, D. J. (2005). Influence of environmental stresses on stability of O/W emulsions containing cationic droplets stabilized by SDS− fish gelatin membranes. *Journal of agricultural and food chemistry, 53*(10), 4236-4244.

Tabilo-Munizaga, G., & Barbosa-Cánovas, G. V. (2005). Rheology for the food industry. *Journal of Food Engineering, 67*(1), 147-156. doi:https://doi.org/10.1016/j.jfoodeng.2004.05.062

Tadros, T. (2015). Viscoelastic properties of sterically stabilised emulsions and their stability. *Advances in colloid and interface science, 222*, 692-708. doi:https://doi.org/10.1016/j.cis.2015.03.001

Tadros, T., Izquierdo, R., Esquena, J., & Solans, C. (2004). Formation and stability of nano-emulsions. *Advances in colloid and interface science, 108*, 303-318. doi:10.1016/j.cis.2003.10.023

Tadros, T. F. (1994). Fundamental principles of emulsion rheology and their applications. *Colloids and Surfaces A: Physicochemical and Engineering Aspects, 91*, 39-55.

Tadros, T. F. (2011). *Rheology of dispersions: principles and applications*: John Wiley & Sons.

Tah, B., Pal, P., Mahato, M., & Talapatra, G. (2011). Aggregation behavior of SDS/CTAB catanionic surfactant mixture in aqueous solution and at the air/water interface. *The Journal of Physical Chemistry B, 115*(26), 8493-8499.

Tan, C. P., & Nakajima, M. (2005). Effect of polyglycerol esters of fatty acids on physicochemical properties and stability of β‐carotene nanodispersions prepared by emulsification/evaporation method. *Journal of the Science of Food and Agriculture, 85*(1), 121-126.

Tanford, C. (1980). *The hydrophobic effect: formation of micelles and biological membranes 2d ed*: J. Wiley.

Tang, C.-H., & Liu, F. (2013). Cold, gel-like soy protein emulsions by microfluidization: Emulsion characteristics, rheological and microstructural properties, and gelling mechanism. *Food Hydrocolloids, 30*(1), 61-72. doi:https://doi.org/10.1016/j.foodhyd.2012.05.008

Taylor, P. (1998). Ostwald ripening in emulsions. *Advances in colloid and interface science, 75*(2), 107-163.

Thanasukarn, P., Pongsawatmanit, R., & McClements, D. J. (2006). Utilization of layer-by-layer interfacial deposition technique to improve freeze–thaw stability of oil-in-water emulsions. *Food Research International, 39*(6), 721-729.

Thompson, K. L., Derry, M. J., Hatton, F. L., & Armes, S. P. (2018). Long-term stability of n-alkane-in-water pickering nanoemulsions: Effect of aqueous solubility of droplet phase on Ostwald ripening. *Langmuir, 34*(31), 9289-9297.

Tokle, T., Lesmes, U., & McClements, D. J. (2010). Impact of electrostatic deposition of anionic polysaccharides on the stability of oil droplets coated by lactoferrin. *Journal of agricultural and food chemistry, 58*(17), 9825-9832.

Townsend, A. K., & Wilson, H. J. (2018). Small- and large-amplitude oscillatory rheometry with bead–spring dumbbells in Stokesian Dynamics to mimic viscoelasticity. *Journal of Non-Newtonian Fluid Mechanics, 261*, 136-152. doi:https://doi.org/10.1016/j.jnnfm.2018.08.010

Trokhymchuk, A., Henderson, D., Nikolov, A., & Wasan, D. T. (2001). A simple calculation of structural and depletion forces for fluids/suspensions confined in a film. *Langmuir, 17*(16), 4940-4947.

Tuinier, R., Rieger, J., & De Kruif, C. (2003). Depletion-induced phase separation in colloid–polymer mixtures. *Advances in colloid and interface science, 103*(1), 1-31.

Vachoud, L., Zydowicz, N., & Domard, A. (1997). Formation and characterisation of a physical chitin gel. *Carbohydrate research, 302*(3-4), 169-177.

van Stam, J., Depaemelaere, S., & De Schryver, F. C. (1998). Micellar aggregation numbers-A fluorescence study. *Journal of chemical education, 75*(1), 93.

Van Vliet, T. (1988). Rheological properties of filled gels. Influence of filler matrix interaction. *Colloid & Polymer Science, 266*(6), 518-524.

Verkempinck, S. H. E., Kyomugasho, C., Salvia-Trujillo, L., Denis, S., Bourgeois, M., Van Loey, A. M., . . . Grauwet, T. (2018). Emulsion stabilizing properties of citrus pectin and its interactions with conventional emulsifiers in oil-in-water emulsions. *Food Hydrocolloids, 85*, 144-157. doi:https://doi.org/10.1016/j.foodhyd.2018.07.014

Walker, R., Decker, E. A., & McClements, D. J. (2015). Development of food-grade nanoemulsions and emulsions for delivery of omega-3 fatty acids: opportunities and obstacles in the food industry. *Food & function, 6*(1), 41-54.

Walstra, P. (1993). Principles of emulsion formation. *Chemical engineering science, 48*(2), 333-349. doi:10.1016/0009-2509(93)80021-h

Walstra, P. (2003). Physical chemistry of foods. Marcel Decker. *Inc., New York*.

Wang, X., Li, X., Xu, D., Zhu, Y., Cao, Y., Wang, J., & Sun, B. (2019). Comparision of heteroaggregation, layer-by-layer and directly mixing techniques on the physical properties and *in vitro* digestion of emulsions. *Food Hydrocolloids, 95*, 228-237. doi:https://doi.org/10.1016/j.foodhyd.2019.04.034

Warnakulasuriya, S., Pillai, P. K. S., Stone, A. K., & Nickerson, M. T. (2018). Effect of the degree of esterification and blockiness on the complex coacervation of pea protein isolate and

commercial pectic polysaccharides. *Food chemistry, 264*, 180-188. doi:https://doi.org/10.1016/j.foodchem.2018.05.036

Wasan, D., Nikolov, A., & Aimetti, F. (2004). Texture and stability of emulsions and suspensions: role of oscillatory structural forces. *Advances in colloid and interface science, 108*, 187-195.

Wasan, D., Nikolov, A., & Henderson, D. (2003). New vistas in dispersion science and engineering. *AIChE journal, 49*(3), 550-556.

Wei, Z., & Gao, Y. (2016). Physicochemical properties of β-carotene bilayer emulsions coated by milk proteins and chitosan–EGCG conjugates. *Food Hydrocolloids, 52*, 590-599.

Weiss, J., & McClements, D. J. (2000). Influence of Ostwald ripening on rheology of oil-in-water emulsions containing electrostatically stabilized droplets. *Langmuir, 16*(5), 2145-2150.

Welch, C. F., Rose, G. D., Malotky, D., & Eckersley, S. T. (2006). Rheology of high internal phase emulsions. *Langmuir, 22*(4), 1544-1550.

Wijaya, W., Van der Meeren, P., Wijaya, C. H., & Patel, A. R. (2017). High internal phase emulsions stabilized solely by whey protein isolate-low methoxyl pectin complexes: effect of pH and polymer concentration. *Food & function, 8*(2), 584-594.

Wilde, P., & Chu, B. (2011). Interfacial & colloidal aspects of lipid digestion. *Advances in colloid and interface science, 165*(1), 14-22.

Wilde, P., Mackie, A., Husband, F., Gunning, P., & Morris, V. (2004). Proteins and emulsifiers at liquid interfaces. *Advances in colloid and interface science, 108*, 63-71.

Wilking, J., Graves, S., Chang, C., Meleson, K., Lin, M., & Mason, T. (2006). Dense cluster formation during aggregation and gelation of attractive slippery nanoemulsion droplets. *Physical review letters, 96*(1), 015501.

Wilking, J. N., Chang, C. B., Fryd, M. M., Porcar, L., & Mason, T. G. (2011). Shear-induced disruption of dense nanoemulsion gels. *Langmuir, 27*(9), 5204-5210.

Wilking, J. N., & Mason, T. G. (2007). Irreversible shear-induced vitrification of droplets into elastic nanoemulsions by extreme rupture. *Physical Review E, 75*(4), 041407.

Willats, W. G., Knox, J. P., & Mikkelsen, J. D. (2006). Pectin: new insights into an old polymer are starting to gel. *Trends in food science & technology, 17*(3), 97-104.

Wolf, B., Lam, S., Kirkland, M., & Frith, W. J. (2007). Shear thickening of an emulsion stabilized with hydrophilic silica particles. *Journal of Rheology, 51*(3), 465-478.

Wong, B. T., Day, L., & Augustin, M. A. (2011). Deamidated wheat protein–dextran Maillard conjugates: Effect of size and location of polysaccharide conjugated on steric stabilization of emulsions at acidic pH. *Food Hydrocolloids, 25*(6), 1424-1432. doi:https://doi.org/10.1016/j.foodhyd.2011.01.017

Wooster, T. J., Golding, M., & Sanguansri, P. (2008). Impact of Oil Type on Nanoemulsion Formation and Ostwald Ripening Stability. *Langmuir, 24*(22), 12758-12765. doi:10.1021/la801685v

Xiang, N., Lyu, Y., & Narsimhan, G. (2016). Characterization of fish oil in water emulsion produced by layer by layer deposition of soy β-conglycinin and high methoxyl pectin. *Food Hydrocolloids, 52*, 678-689.

Xiong, W., Ren, C., Tian, M., Yang, X., Li, J., & Li, B. (2018). Emulsion stability and dilatational viscoelasticity of ovalbumin/chitosan complexes at the oil-in-water interface. *Food chemistry, 252*, 181-188.

Xu, D., Aihemaiti, Z., Cao, Y., Teng, C., & Li, X. (2016). Physicochemical stability, microrheological properties and microstructure of lutein emulsions stabilized by multilayer membranes consisting of whey protein isolate, flaxseed gum and chitosan. *Food chemistry, 202*, 156-164.

Xu, D., Wang, X., Jiang, J., Yuan, F., & Gao, Y. (2012). Impact of whey protein–Beet pectin conjugation on the physicochemical stability of β-carotene emulsions. *Food Hydrocolloids, 28*(2), 258-266.

Xu, D., Yuan, F., Gao, Y., Panya, A., McClements, D. J., & Decker, E. A. (2014). Influence of whey protein–beet pectin conjugate on the properties and digestibility of β-carotene emulsion during *in vitro* digestion. *Food chemistry, 156*, 374-379.

Xu, X., Luo, L., Liu, C., & McClements, D. J. (2017). Utilization of anionic polysaccharides to improve the stability of rice glutelin emulsions: Impact of polysaccharide type, pH, salt, and temperature. *Food Hydrocolloids, 64*, 112-122. doi:https://doi.org/10.1016/j.foodhyd.2016.11.005

Ye, A., Gilliland, J., & Singh, H. (2011). Thermal treatment to form a complex surface layer of sodium caseinate and gum arabic on oil–water interfaces. *Food Hydrocolloids, 25*(7), 1677-1686.

Yerramilli, M., & Ghosh, S. (2017). Long-term stability of sodium caseinate-stabilized nanoemulsions. *Journal of food science and technology, 54*(1), 82-92.

Zając, A., Hanuza, J., Wandas, M., & Dymińska, L. (2015). Determination of N-acetylation degree in chitosan using Raman spectroscopy. *Spectrochimica Acta Part A: Molecular and Biomolecular Spectroscopy, 134*, 114-120.

Zeeb, B., Fischer, L., & Weiss, J. (2011). Cross-linking of interfacial layers affects the salt and temperature stability of multilayered emulsions consisting of fish gelatin and sugar beet pectin. *Journal of agricultural and food chemistry, 59*(19), 10546-10555.

Zhang, C., Xu, W., Jin, W., Shah, B. R., Li, Y., & Li, B. (2015). Influence of anionic alginate and cationic chitosan on physicochemical stability and carotenoids bioaccessibility of soy protein isolate-stabilized emulsions. *Food Research International, 77*, 419-425.

Zhang, Z., & McClements, D. J. (2018). Chapter 2 - Overview of Nanoemulsion Properties: Stability, Rheology, and Appearance. In S. M. Jafari & D. J. McClements (Eds.), *Nanoemulsions* (pp. 21-49): Academic Press.

Zhu, Y., Gao, H., Liu, W., Zou, L., & McClements, D. J. (2020). A review of the rheological properties of dilute and concentrated food emulsions. *Journal of texture studies, 51*(1), 45-55.

11. APPENDIX A: SUPPLEMENTARY MATERIALS FOR CHAPTER 3

A1. Gas chromatography calibration curve for different Citrem concentration

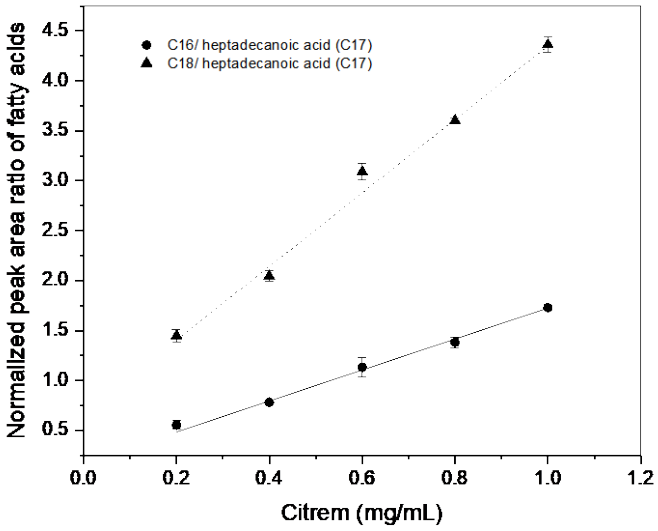

Figure A1 Normalized peak area ratio of major fatty acids (C16 – palmitic acid and C18 – stearic acid) of Citrem and internal standard (C17 – heptadecanoic acid) as a function of known concentration of Citrem. The correlation coefficients (r^2) were more than 0.99 for all observations. A minimum of three measurements were performed to get the mean with error bars showing standard deviation.

A2. Droplet size (d_{32}) as a function of Citrem concentration

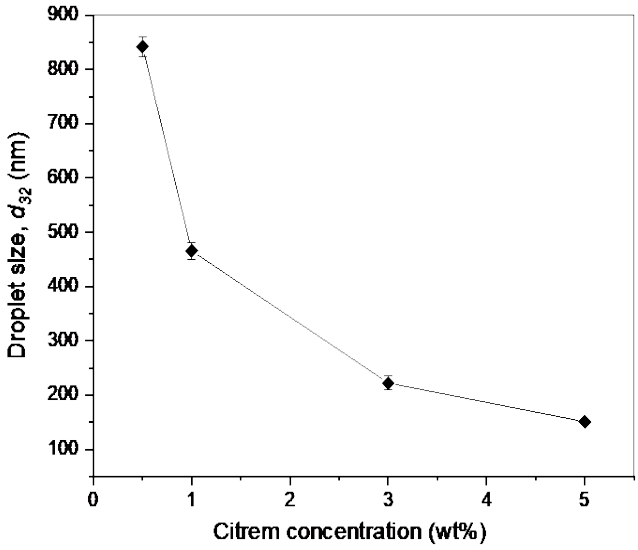

Figure A2 Changes in the average droplet size of emulsions as a function of Citrem concentration. Error bars indicate ± standard deviation (n ≥ 3).

A3. Gibbs surface excess (Γ) and critical micelle concentration (CMC) of Citrem

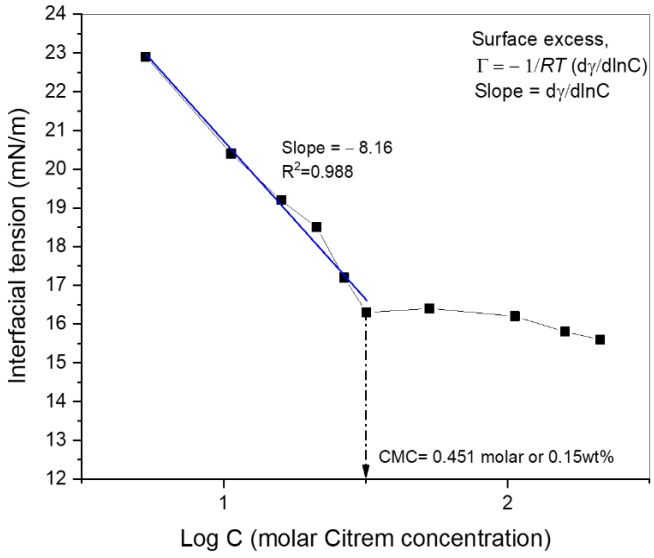

Figure A3 Calculation of Gibbs surface excess (Γ) and critical micelle concentration (CMC) of Citrem, obtained from the measurement of oil-water interfacial tension as a function of Citrem concentration. Gibbs surface excess was calculated from the initial slope of the curve before CMC.

A4. Droplet charge as a function of excess Citrem removal

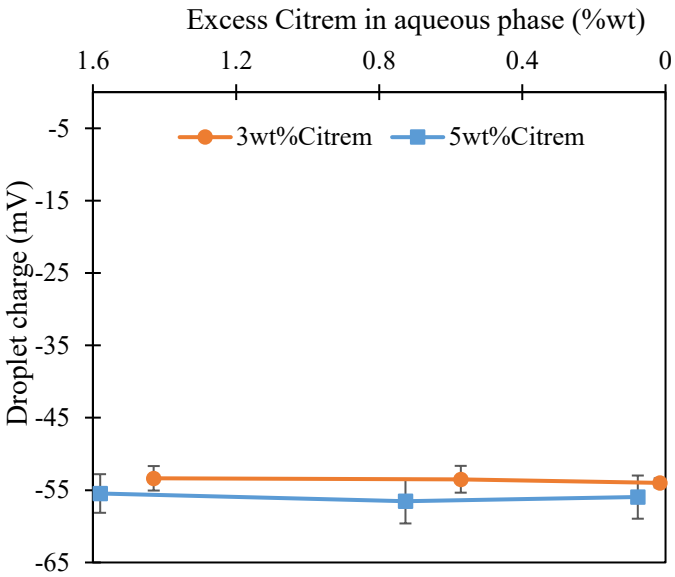

Figure A4 Changes in the droplet charge as a function of excess Citrem removal from the aqueous phase of nanoemulsions. Error bars indicate ± standard deviation (n ≥ 3).

12. APPENDIX B: SUPPLEMENTARY MATERIALS FOR CHAPTER 4

B1. Working principle of a photocentrifuge - LUMiSizer®

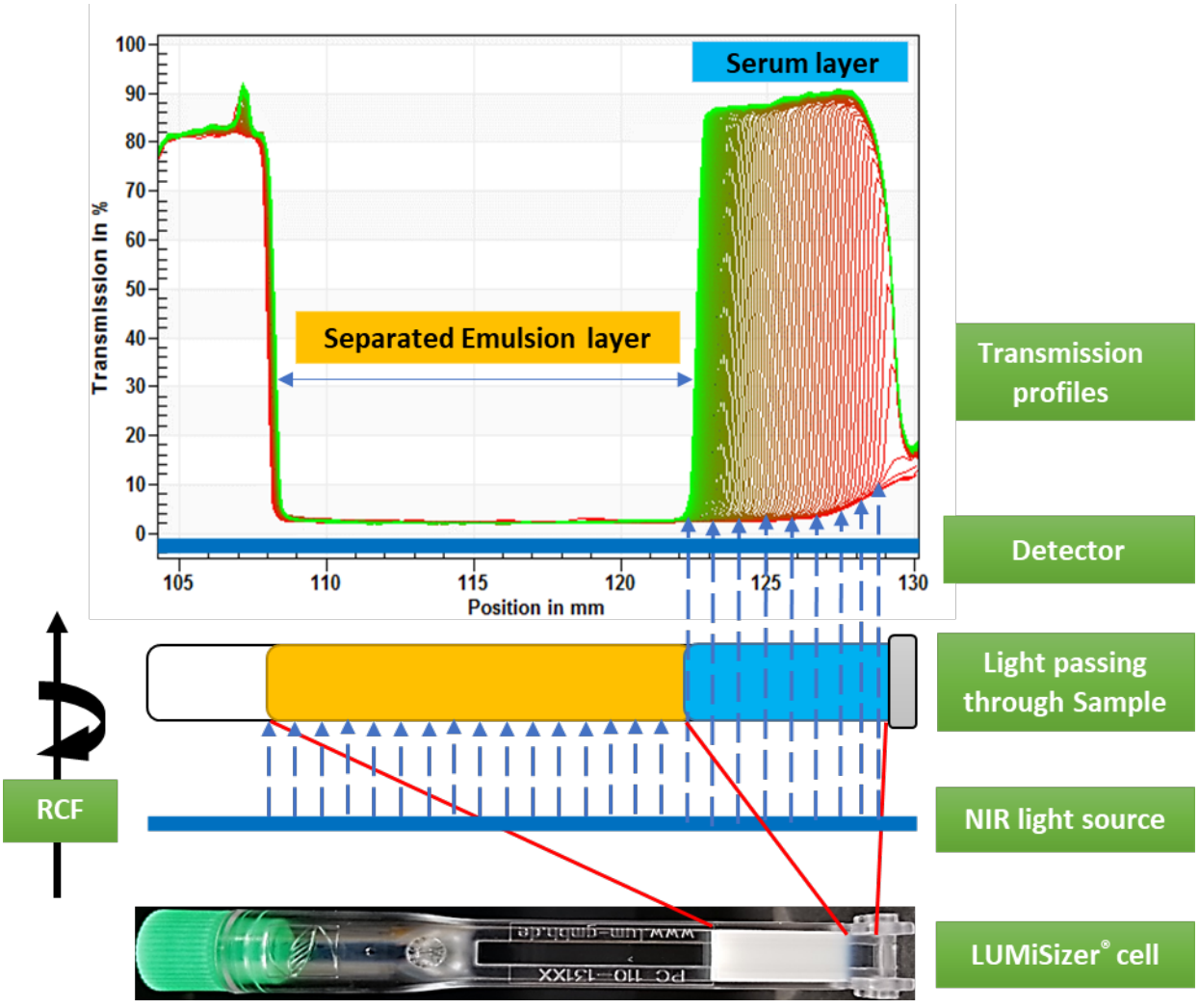

Figure B1 Schematic diagram explaining the working principle of a photocentrifuge - LUMiSizer® based on the STEP (Space and Time-resolved Extinction Profiles) technology and a case of creaming of nanoemulsion droplets under applied relative centrifugation force (RCF).

B2. Repulsive shell-layer thickness with and without excess Citrem micelles

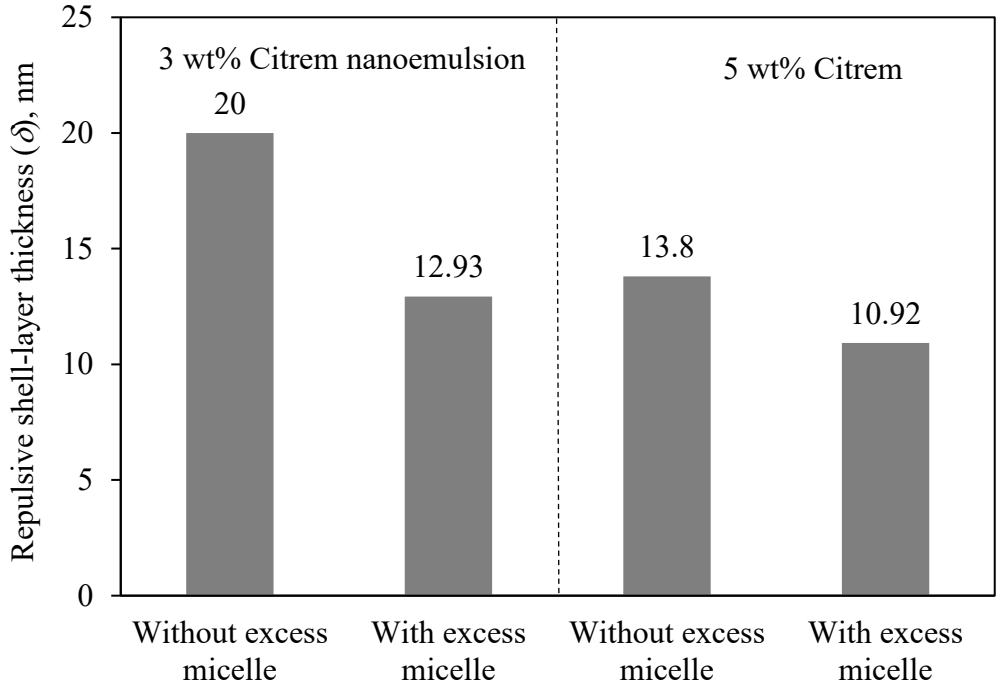

Figure B2 Changes in thickness of repulsive shell-layer (δ) of nanodroplets with and without excess micelles in the continuous phase of nanoemulsions calculated according to Kadiya and Ghosh (2019).

B3. Transmission profiles of 3 wt% Citrem nanoemulsions

3wt% Citrem nanoemulsion	With excess micelles	Without excess micelles
RPM: 1000 RCF ~ 145	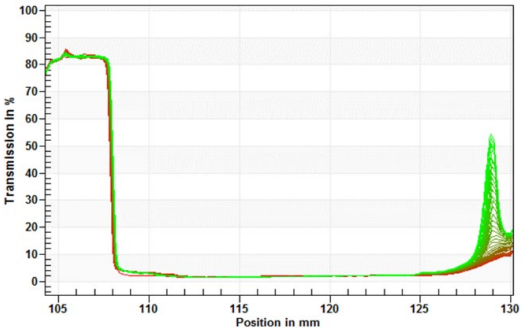	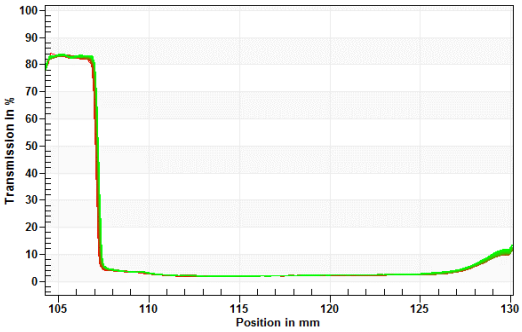
RPM: 2000 RCF ~ 582	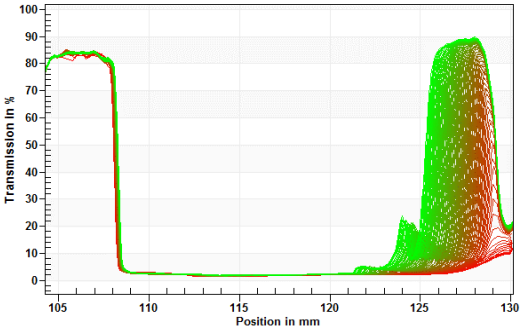	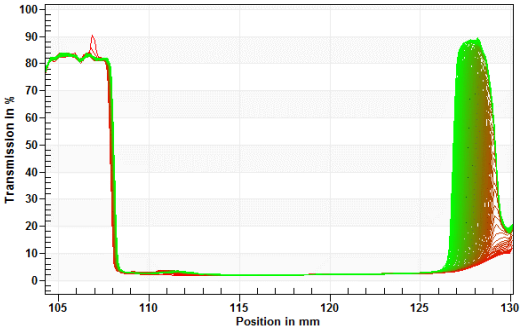
RPM: 3000 RCF ~1308	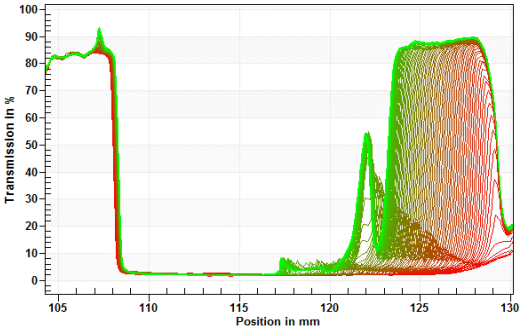	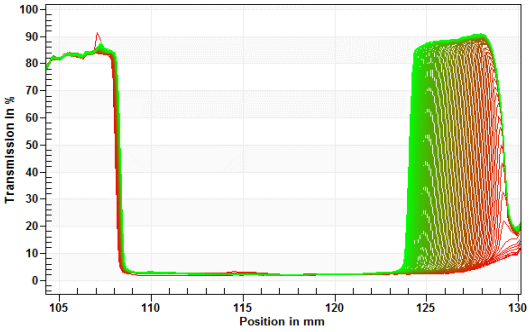
RPM: 4000 RCF ~2325	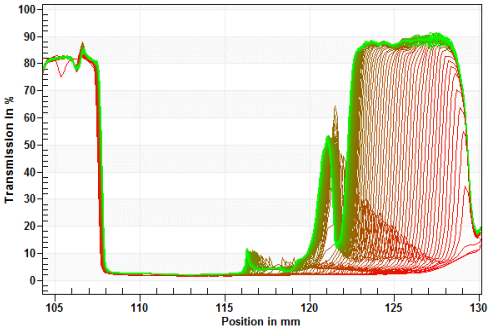	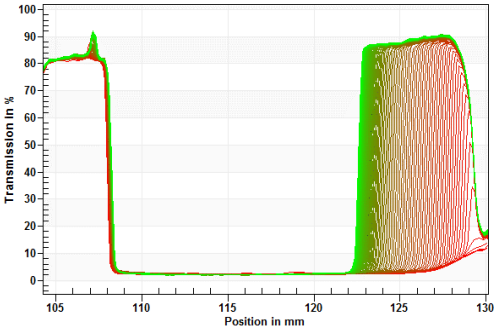

Figure B3 Transmission profiles obtained for creaming of 3 wt% Citrem nanoemulsion droplets, subjected to the different magnitude of RCF with and without excess micelles in the continuous phase. Transmission profiles used for the front tracking of the separating droplets and the droplet separation velocity (in mm per hour) at different RCF was calculated from the linear slope of position (in mm) of the cream layer throughout the optical path length versus time.

B4. Transmission profiles of 5 wt% Citrem nanoemulsions

5wt% Citrem nanoemulsion	With excess micelles	Without excess micelles
RPM: 1000 RCF ~ 145	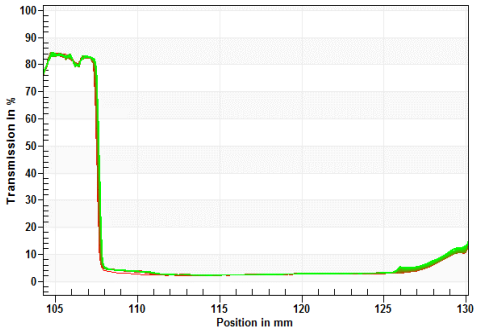	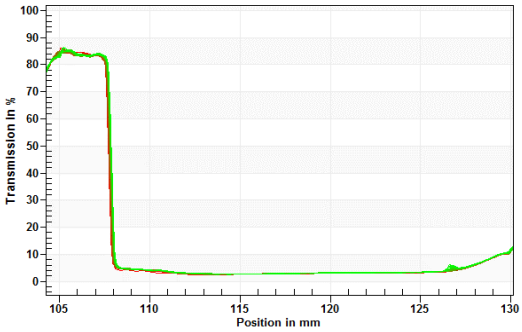
RPM: 2000 RCF ~ 582	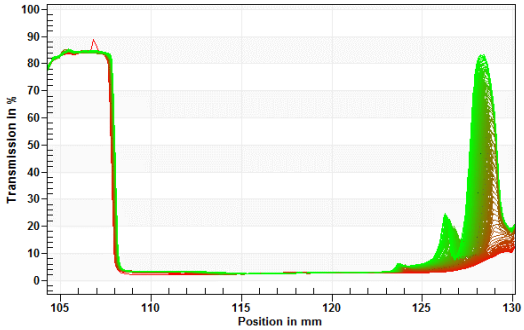	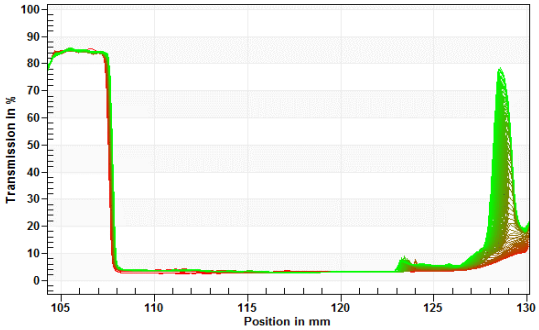
RPM: 3000 RCF ~1308	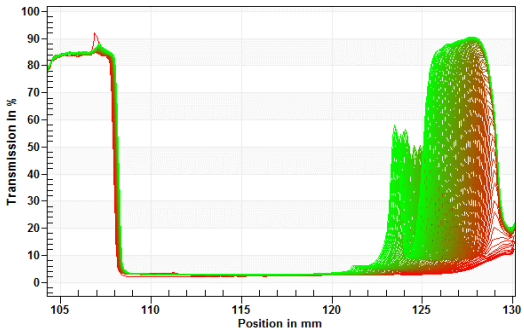	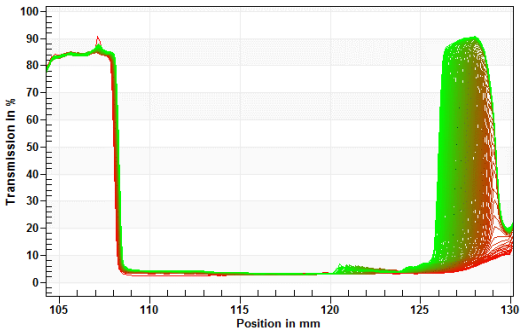
RPM: 4000 RCF ~2325	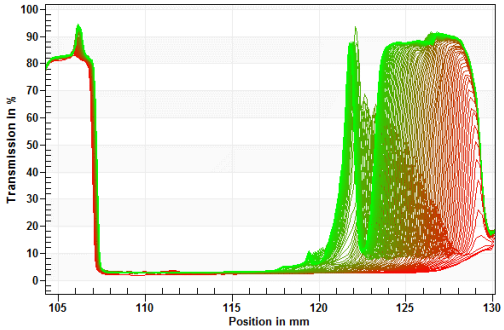	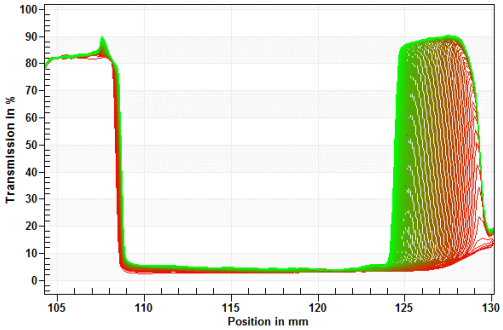

Figure B4 Transmission profiles obtained for creaming of 5 wt% Citrem nanoemulsion droplets, subjected to the different magnitude of RCF with and without excess micelles in the continuous phase. Transmission profiles used for the front tracking of the separating droplets and the droplet separation velocity (in mm per hour) at different RCF was calculated from the linear slope of position (in mm) of the cream layer throughout the optical path length versus time.

B5. Yield stress of Citrem nanoemulsions with and without excess micelles

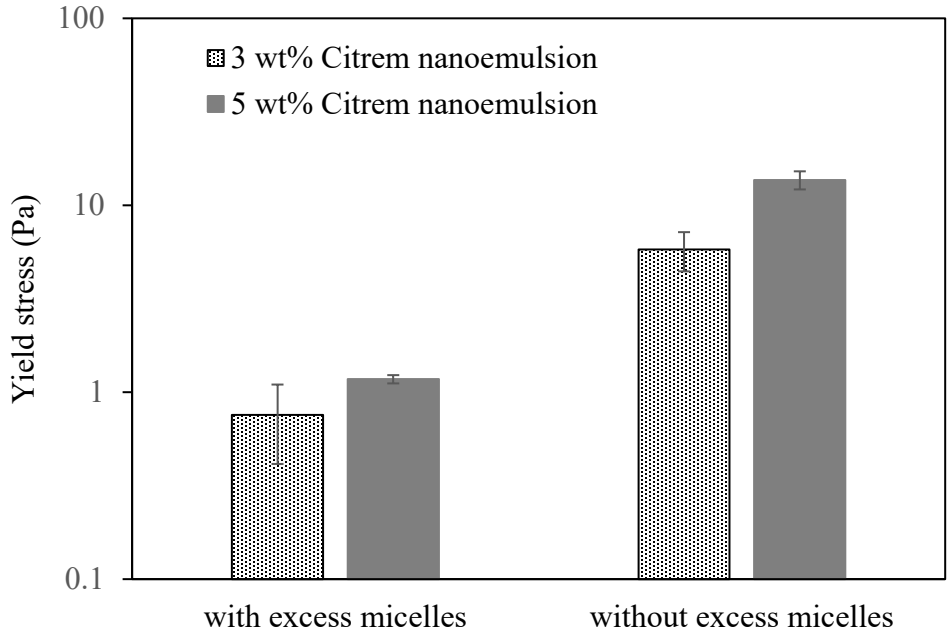

Figure B5 Changes in yield stress of oil-in-water nanoemulsions as a function of Citrem concentration with and without excess micelles in their continuous phase. The yield stress was calculated from the viscosity data using the Herschel-Bulkley model. Error bars indicate ± standard deviation ($n \geq 3$).

13. APPENDIX C: SUPPLEMENTARY MATERIALS FOR CHAPTER 5

C1. Preparation of Citrem-stabilized primary emulsion followed by removal of excess Citrem

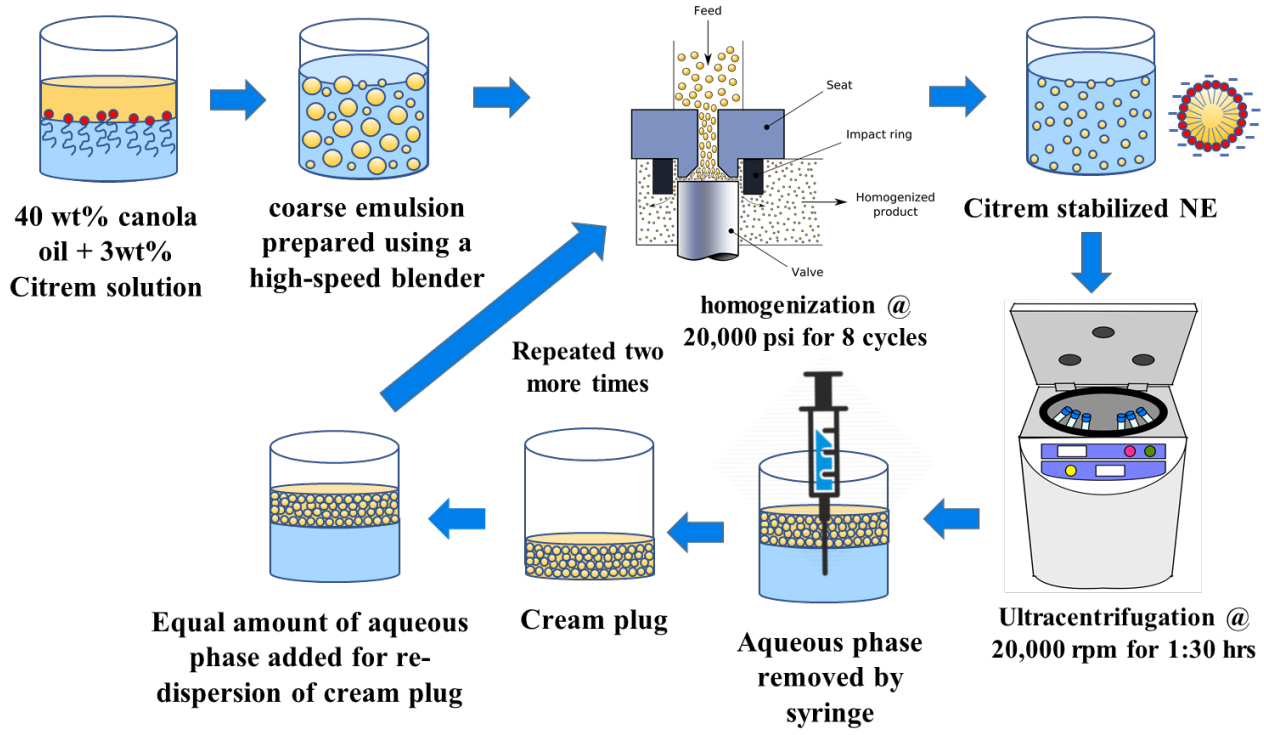

Figure C1 Preparation of Citrem-stabilized primary emulsion followed by removing excess emulsifier from the continuous phase of the emulsion by multiple cycles of ultracentrifugation.

C2. Preparation of 50% DDA chitosan by reacetylation

As shown in Equation C1, the commercial chitosan sample obtained with 93% DDA was chemically transformed into 50% DDA using a reacetylation method described by Vachoud et al. (1997) and Gatto et al. (2019).

$$Chitosan\ (DDA\ 93\%) + Acetic\ anhydride \xrightarrow{Reacetylation} Chitosan\ (DDA\ 50\%) \quad \text{(C1)}$$

First, an aqueous solution of 3 wt% Chitosan DDA 93 was prepared by adding the 3 g chitosan powder (containing [-NH_2] groups) in 97 g of 2wt% aqueous acetic acid [AcA] by considering the stoichiometric proportions of ([AcA] = [-NH_2]) and was stirred overnight. Subsequently, the methanolic solution of chitosan DDA 93 was prepared by mixing an equal amount of chitosan solution and methanol. At first, 90 mL of methanol was added to 100 mL chitosan solution (corresponding to 90% v/v of the chitosan solution) and stirred for 2 h. The other 10 mL methanol (corresponding to 10% v/v of the chitosan solution) was used to prepare the acetic anhydride (AAn) solution for the reacetylation of chitosan DDA 93. The AAn amount (m_{AAn}, g) required to prepare the chitosan with DDA 50 was determined using Equation C2.

$$m_{AAn} = \frac{m_c(DDA_1 - DDA_2)(1 - w_{H_2O})M_{AAn}}{Mw_c} \quad \text{(C2)}$$

Where m_c is the amount of chitosan DDA 93 (g), DDA_1 (0.93) and DDA_2 (0.50) are initial and desired DDAs, respectively, w_{H2O} is moisture content (8 wt%) in the DDA 93 chitosan powder, M_{AAn} is the molecular weight of AAn (102.1 g/mol), and Mw_C is an average molecular weight, calculated using Equation C3, (164.14 g/mol) of the repetitive units of chitosan DDA 93 (Ma et al., 2009):

$$Mw_c = (0.93 \times M_w\ of\ GlcN)\ + (0.07\ \times M_w\ of\ GlcNAc) \quad \text{(C3)}$$

where, M_w of GlcN and M_w of GlcnAc are the molecular weight of glucosamine and glucosamine acetyl units of chitosan, respectively.

A methanolic solution of AAn was prepared by mixing the calculated amount of AAn, from Equation C2, in 10 mL methanol (corresponding to 10% v/v of the chitosan solution) and was mixed at 400 rpm for 45 min. The reacetylation was performed by adding methanolic AAn

dropwise to the Chitosan DDA 93 solution and then stirring overnight. The next day, the re-acetylated chitosan with DDA 50 was precipitated using concentrated NH_4OH and filtered out using Whatman filter paper #1 inserted in the 400 mL Buchner funnel. The resultant wet mass was repeatedly washed with distilled water until the water pH reached around 7. After washing, the wet mass was spread onto an aluminium pan and vacuum dried at 50°C till final moisture content reached 6 - 8 wt% in dried chunks. A fine powder was prepared from dried chunks by grinding using mortar and pestle and stored in a desiccator for further DDA analysis.

C3. Analysis of Degree of Deacetylation of Chitosan

The degree of deacetylation (DDA) of chitosan DDA 50 and DDA 93 was determined by the pH-conductometric titration method adopted from Crofton et al. (2016). The pH-conductometric titration was performed by dissolving 100 mg of chitosan powder in the mixture of 90 mL deionized water and 10 mL of 0.1 N HCl. The chitosan solution in 0.1 N HCl was stirred overnight, and the next day it was titrated with 0.1 N NaOH. During the titration, a fixed amount (200 µL) of 0.1 N NaOH was added at a constant rate, and a simultaneous change in the pH and conductivity of solution was recorded with an Orion star A215 pH-Conductivity meter equipped with an Orion conductivity cell and pH electrode. A typical pH-Conductometric titration curve, shown in Figure C2, was obtained by plotting NaOH volume versus conductivity and pH. The first deflection point appeared in the curve due to an increase in conductivity, indicates the neutralization of excess H^+ ions available in chitosan solution from excess 0.1 N HCl, which is followed by the neutralization of the weak acid, i.e., the ammonium salt in chitosan. The second deflection point indicates the complete neutralization of ammonium, and any further addition of OH^- leads to an increase in conductivity. Hence, the volume of 0.1 N NaOH used between the first and second deflection points correspond to the neutralization of the protonated amino groups of chitosan, which was used to calculate the %DDA of chitosan by following Equation from Crofton et al. (2016):

$$\%DDA = \frac{M_{NaOH} \times (v_2 - v_1) \times 161.16}{W_{ch}(g)} \quad \text{(C4)}$$

Where W_{ch} is the weight of chitosan powder (g), M_{NaOH} is the molarity (mol/L) of standard NaOH solution, v_2 and v_1 are volumes of NaOH (Litre) used till the second and first deflection point, respectively, and 161.16 g/mol is the molar mass of chitosan.(Ma et al., 2009).

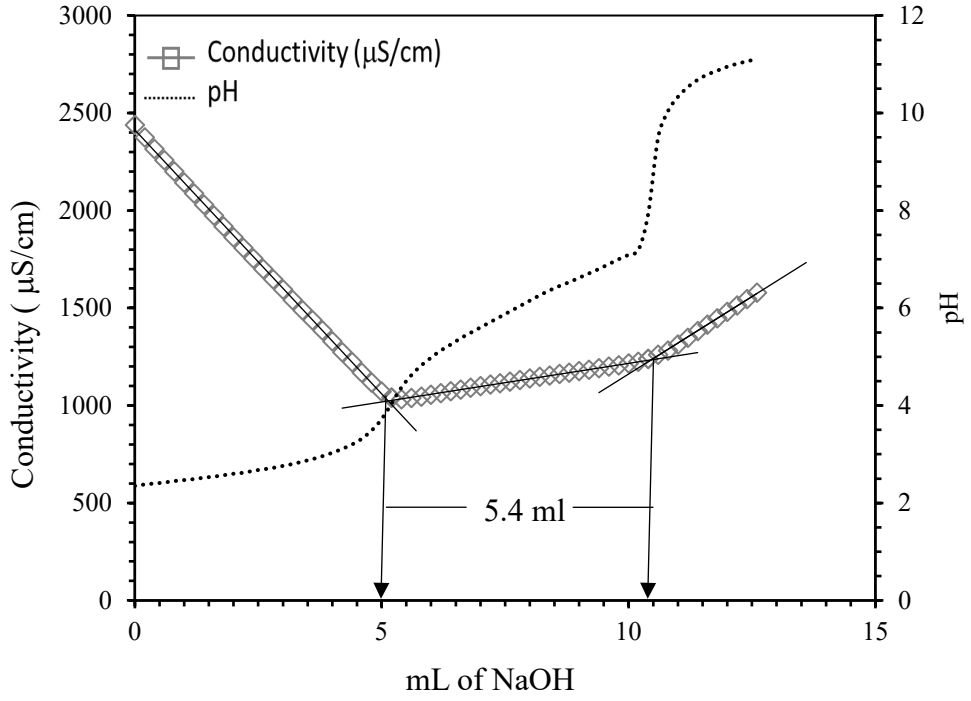

Figure C2 Analysis of the degree of deacetylation (DDA) of chitosan using the pH-conductometric titration as a function of addition of sodium hydroxide (NaOH).

C4. Raman spectra of DDA 50 and DDA 93 chitosan

For the confirmation of DDA in DDA 50 and DDA 93 chitosan samples, the Raman spectra of their functional groups were also collected at room temperature using a Renishaw InVia Reflex Raman microscope in the 500 cm^{-1} to 4000 cm^{-1} spectral range (785 nm solid-state diode laser with a 1200 lines/mm grating system). The instrument wavelength was calibrated at 520 cm^{-1} using an internal Si (110) sample. All the collected spectra were analysed using WiRE 5.3 software (Figure C3).

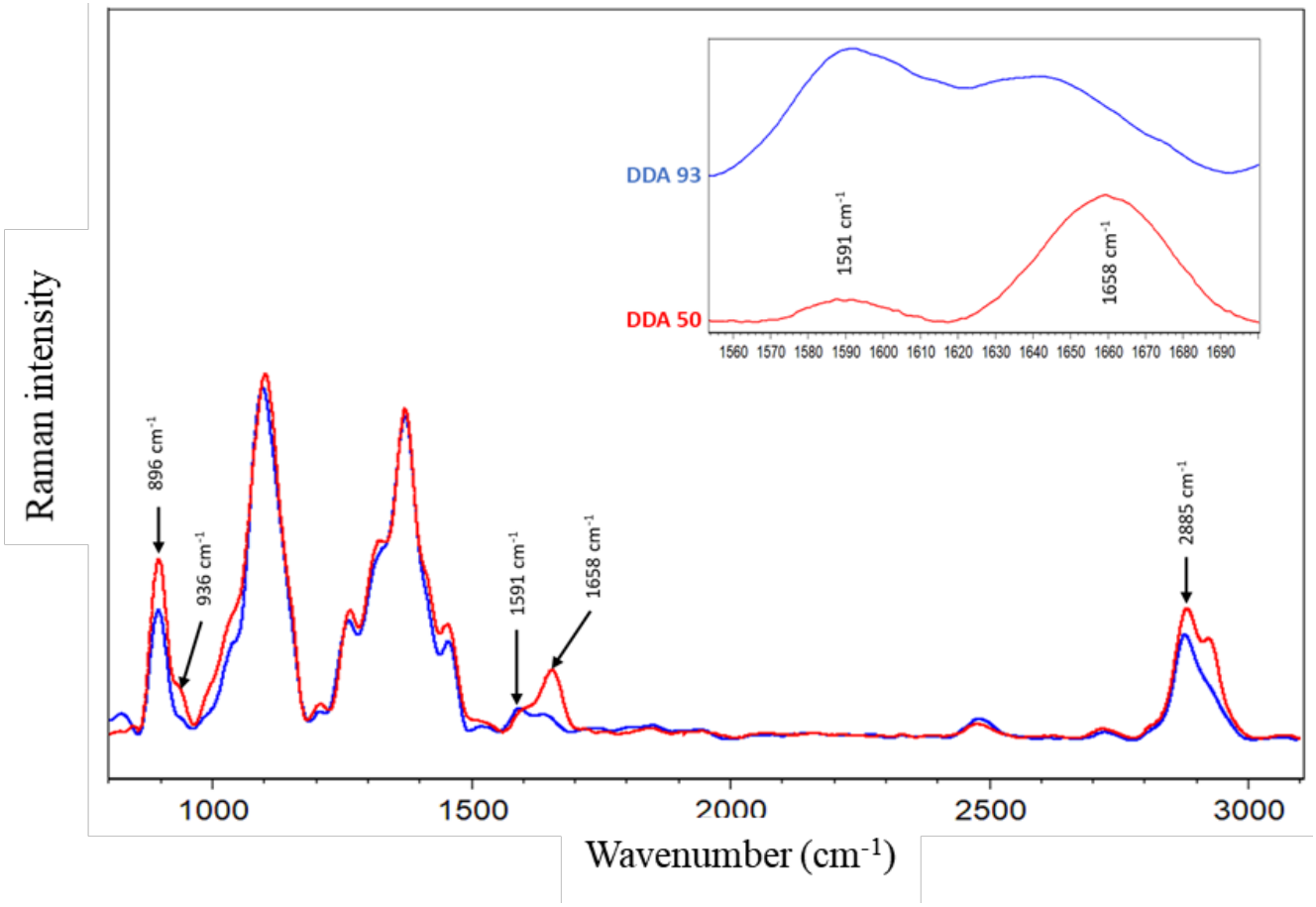

Figure C3 Raman spectra of chitosan DDA 50 (red) and DDA 93 (blue). The inset shows two peaks at 1591 cm^{-1} and 1658 cm^{-1} for functional groups amide II (NH) and carbonyl (CO).

C5. Formulation for preparing Citrem-chitosan bilayer emulsions

Table C1 Formulation for preparing the Citrem-chitosan bilayer emulsions with different concentration of chitosan DDA 50 and DDA 93

Concentration of Chitosan (%wt)	***0***	***0.05***	***0.065***	***0.075***	**0.0825**	***0.1***	***0.15***	***0.2***	***0.25***
Quantity of Citrem emulsion (40% oil) at pH 4 (g)	18	18	18	18	18	18	18	18	18
Quantity of 2.5 wt% Chitosan (g)	0	0.4	0.52	0.6	0.66	0.8	1.2	1.6	2
Quantity of acetate buffer pH4 (g)	2	1.6	1.48	1.4	1.34	1.2	0.8	0.4	0
Total quantity (g)	20	20	20	20	20	20	20	20	20
wt% Canola oil in final emulsion	36	36	36	36	36	36	36	36	36

C6. Static *in vitro* digestion assembly

A

B

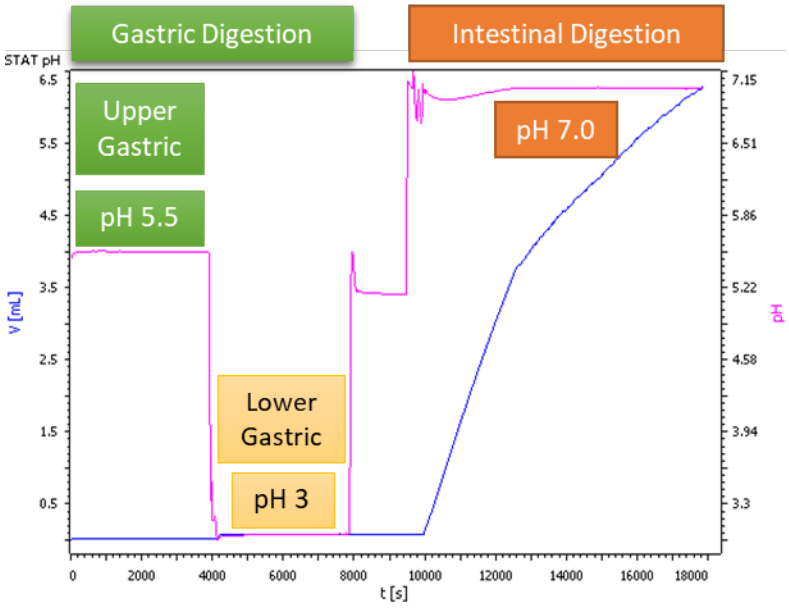

Figure C4 (A) Static *in vitro* digestion assembly attached to pH-STAT auto-titrator assembly (B) Output of the pH-STAT digestion kinetics (volume of NaOH added as a function time, blue line) mentioned with the three phases of digestion monitored at different pH values (pink line).

C7. Analysis of chitosan layer thickness by dynamic light scattering (DLS) and Cryo-scanning electron microscopy (Cryo-SEM)

Dynamic light scattering: The core-shell structure phenomenon and the dynamic light scattering (DLS) technique was used in characterizing the shell-layer thickness of sterically stabilized particles.(Akpinar et al., 2016) In the present study, to measure the thickness of the chitosan (DDA 50 and DDA 93) layer, the core-shell structure was created at pH 4 (as shown in Figure C5), where Citrem-stabilized emulsion droplets were taken as the core (yellow, Figure C5), and their average hydrodynamic diameter was determined using a dynamic light scattering instrument (Litesizer™ 500, Anton Paar, Montreal, QC, Canada). The shell layer (green, Figure C5) was created by adding chitosan solution at pH 4 to promote the electrostatic complexation at the interface between negatively charged Citrem and positively charged chitosan. The hydrodynamic diameter of the bilayer (Citrem + chitosan) droplets was again determined using the DLS instrument. First, the highly diluted dispersion of Citrem-stabilized emulsion was used for core size measurement, followed by the addition of chitosan solution in the same solution. The chitosan shell layer thickness (Δ) was obtained by deducting the Citrem-stabilized droplet (core) size (D_1) from the size of Citrem plus chitosan-stabilized droplets (D_2) (Figure C5). The chitosan layer thickness (Δ) was calculated using Equation C5.

$$\Delta = \frac{D_2 - D_1}{2} \qquad \text{(C5)}$$

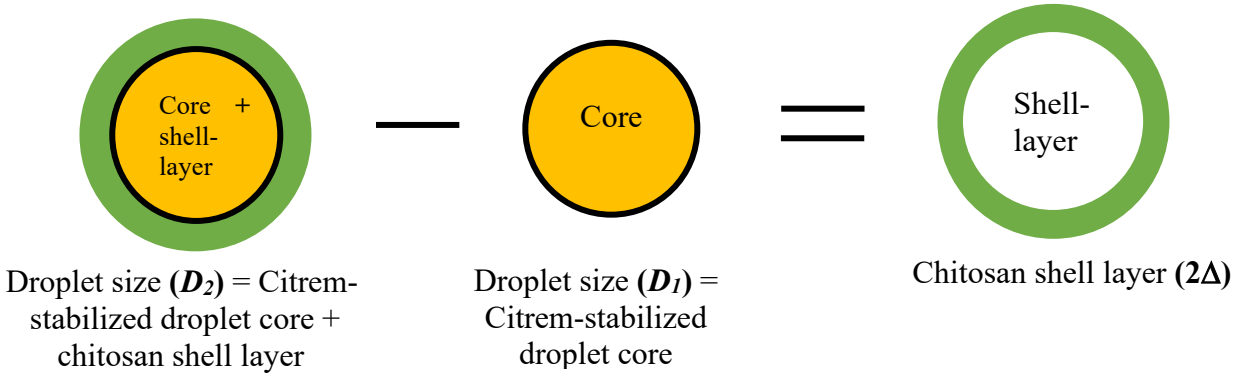

Figure C5 Schematics of chitosan layer thickness measurement from the hydrodynamic diameter of Citrem plus chitosan-stabilized droplets minus the Citrem-stabilized droplets.

Table C2 Estimation of chitosan shell layer thickness using the dynamic light scattering measurements considering the core-shell structure of the bilayer droplets using Equation C5

Chitosan sample	Core + shell, D_2 (nm)	Core, D_1 (nm)	Chitosan shell-layer thickness (Δ) (nm)
DDA 50%	388.9 ± 6.9	216.2 ± 3.8	86.35 ± 3.96
DDA 93%	366.5 ± 2.8	216.2 ± 3.8	75.16 ± 0.62

Cryo-scanning electron microscopy: Freeze-fracture Cryo-SEM was also used to investigate the microstructure of polymer encapsulated droplets, and to get an estimation of the thickness of shell wall.(Humblet-Hua et al., 2012; Xiang et al., 2016) In this study, the microstructure of the emulsion droplets with chitosan shell layer was observed by freeze fracturing a small amount of emulsion sample in the cryo-preparation chamber (PP3010T Cryo-SEM preparation system, Quorum Technologies, UK) using liquid nitrogen at -70°C. Then, the freeze fractured sample was sputter-coated with platinum and imaged using JEOL JSM 7100F SEM (JEOL Ltd., Tokyo, Japan) under high vacuum and at an accelerated voltage of 3 keV. The SEM experiment was performed at the Ghent University, Belgium. From the cryo-SEM image an approximate thickness of chitosan DDA 93 can be sees as 75 nm, which matched quite well with shell-layer thickness from the DLS experiment.

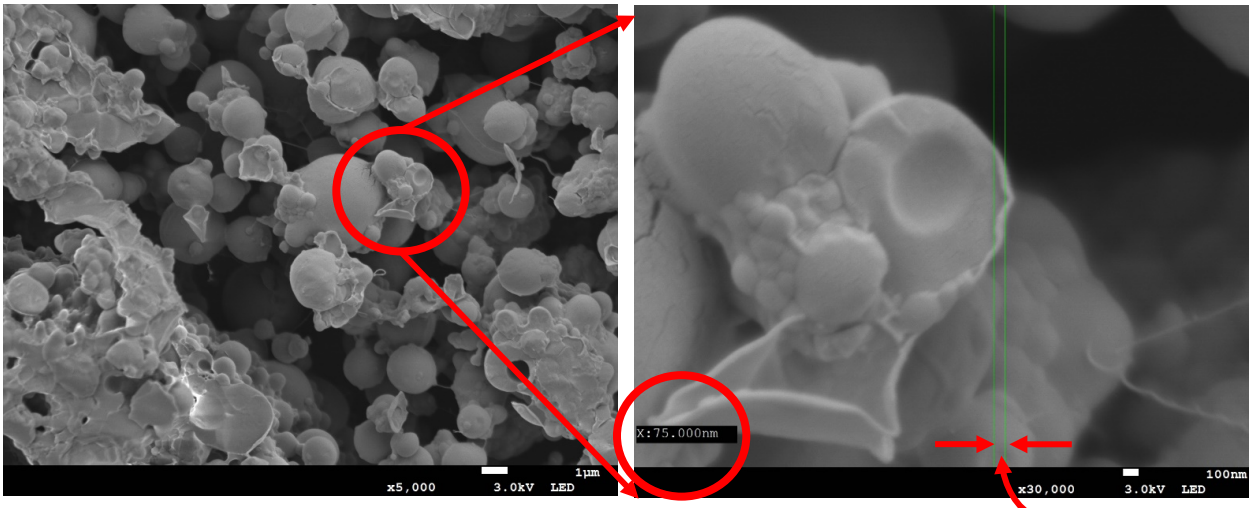

Figure C6 Cryo-SEM analysed microstructure of Citrem plus chitosan-stabilized emulsions for the determination of the chitosan shell-layer thickness

C8. Determination of effective oil volume fraction for mono- and bilayer emulsions

The volume fraction of the shell layer (ϕ_s) as a function of droplet size (r) and shell layer thickness (δ) can be calculated using Equation C6.

$$\phi_s = 1 - \frac{r^3}{(r+\delta)^3} \quad \text{(C6)}$$

Here, δ is the interfacial repulsive shell layer thickness contributed by the charge cloud alone in case of ionic emulsifier (Cirem-stabilized monolayer emulsions) or the charge cloud plus the steric barrier (Cirem-chitosan-stabilized bilayer emulsions) around the droplet in case of the multilayer emulsions. Based on our previous work, the shell layer thickness of Cirem-stabilized monolayer emulsion was calculated using Equations C7 and C8.(Kadiya & Ghosh, 2019)

$$\delta = 2.9\ \kappa^{-1} \quad \text{(C7)}$$

$$\text{Debye length, } \kappa^{-1} = {}^{0.304}/_{\sqrt{C}}\ ; C \text{ is the molar ionic concentration} \quad \text{(C8)}$$

Here, the factor 2.9 was obtained from our previously published data on DLVO calculation for 3 wt% Citrem-stabilized emulsions.(Kadiya & Ghosh, 2019) To calculate the Debye length, the molar ionic concentration of free sodium and chloride ions present in the emulsion continuous phase was determined by using a NaCl conductivity calibration curve following the methodology by Kadiya and Ghosh (2019). Finally, the overall repulsive barrier (δ) around a bilayer droplet was calculated from the combined effect of charge cloud (x) plus the steric barrier (Δ) according to Patel e*t al.*Patel, Mohanan, et al. (2019) The calculated and experimentally determined values of shell layer thickness for both mono- and multi-layer emulsions and the predicted ϕ_s and ϕ_{eff} are reported in Table C3.

Table C3 Predicted values of volume fraction of the shell layer (ϕ_s) and effective oil volume fraction (ϕ_{eff}) for Citrem-stabilized monolayer and Citrem-chitosan-stabilized bilayer droplets calculated from the average droplet size and the values of repulsive charge cloud and steric layer thickness.

Emulsion and chitosan type	**Droplet radius, r(nm)**	**Counterion conc. (mol m^{-3})[§]**	**Debye length, κ^{-1} (nm)**	**Repulsive charge cloud thickness $2.9\kappa^{-1}$ (x nm)**	**Steric layer thickness (Δ nm)**	**Shell layer thickness, $\delta = x + \Delta$ (nm)**	**volume fraction of shell layer (ϕ_s)**	**Effective oil volume fraction[♣] $\phi_{eff} = \phi_{oil} + \phi_s$**
Monolayer emulsion	242.0	14.08	2.56	7.43	-	7.43[#]	0.09	0.47
Bilayer emulsion (DDA 50)	1714.9[⌘]	17.24	2.32	6.71	86.35[**]	93.06[*]	0.15	0.53
Bilayer emulsion (DDA 93)	695.7[⌘]	18.33	2.25	6.52	75.16[**]	81.68[*]	0.28	0.66

[⌘]*Droplet radius (r) of bilayer emulsions considered without steric barrier* (Δ), $r = d_{32} - \Delta$.
[§]Counter ion concentration was calculated from the molar ionic concentration in the emulsion continuous phase
[#]δ *for monolayer emulsion was determined from the repulsive charge cloud using Equation C7.*
[*]δ *for bilayer emulsion is the sum of electrostatic (x) and steric* (Δ) *repulsion between the droplets.*
[**]*The steric layer thickness* (Δ) *is obtained from Table C2 using Method C7.*
[♣]*36 wt% oil used in emulsion preparation is equivalent to 0.38 oil volume fraction* ($\phi_{oil} = 0.38$).

14. APPENDIX D: SUPPLEMENTARY MATERIALS FOR CHAPTER 6

D1. Schematic flow to prepare the WPI-pectin stabilized secondary emulsions

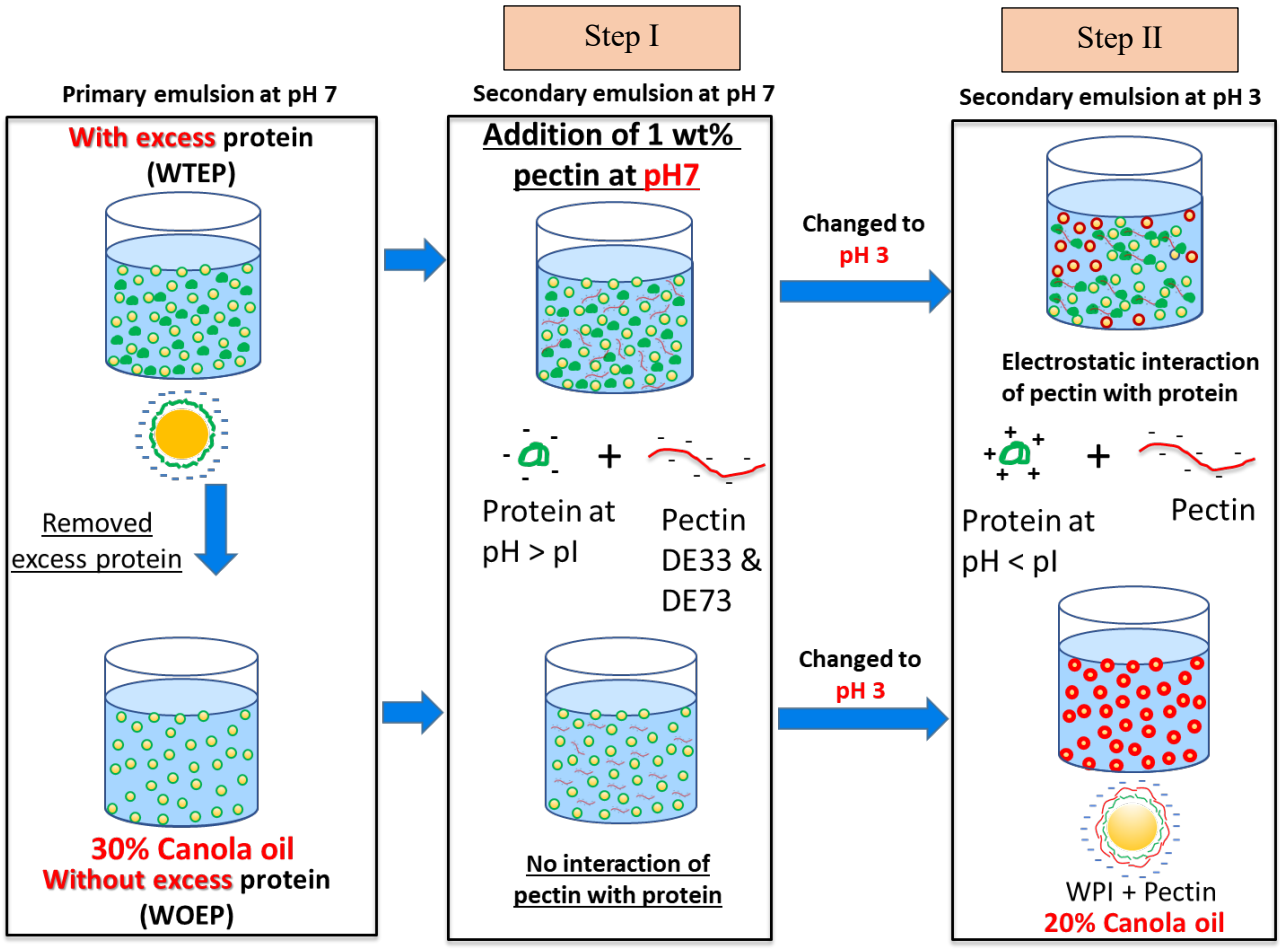

Figure D1 Schematic flow of the two-step process to prepare the WPI-Pectin stabilized secondary emulsions at pH 7 and pH 3 with excess protein (WTEP) and without excess protein (WOEP) in the continuous phase of emulsions.

D2. Droplet charge as a function of pectin DE and concentration

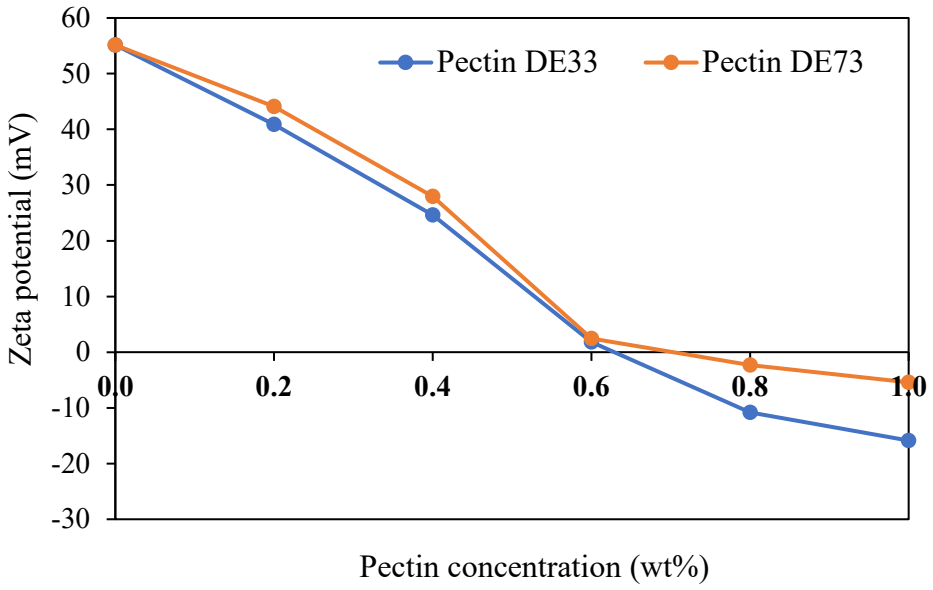

Figure D2 Optimization of pectin concentration for the preparation of secondary WPI-Pectin stabilized emulsions. Effect of pectin concentration and the degree of esterification (DE) on zeta potential of emulsion droplets.

D3. Pectin charge and viscosity at pH 7 and pH 3

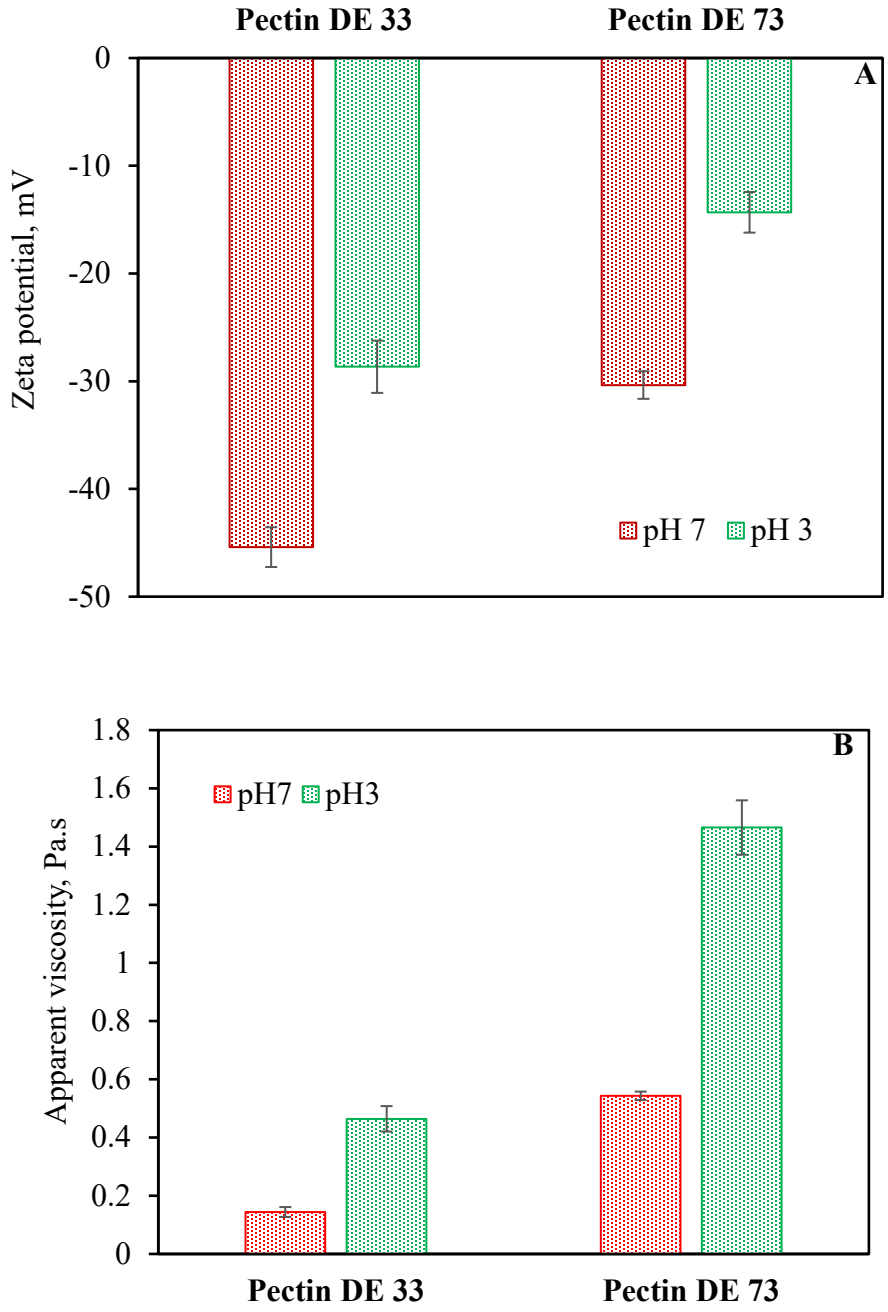

Figure D3 Characterization of the commercial samples of pectin with different degree of esterification (DE) for (A) zeta potential and (B) apparent viscosity at 0.1 s^{-1} shear rate at an aqueous phase concentration of 3 wt%. Error bars indicate ± standard deviation ($n \geq 3$).

D4. Cryo-SEM microstructure of Pectin DE33-coated bilayer emulsions

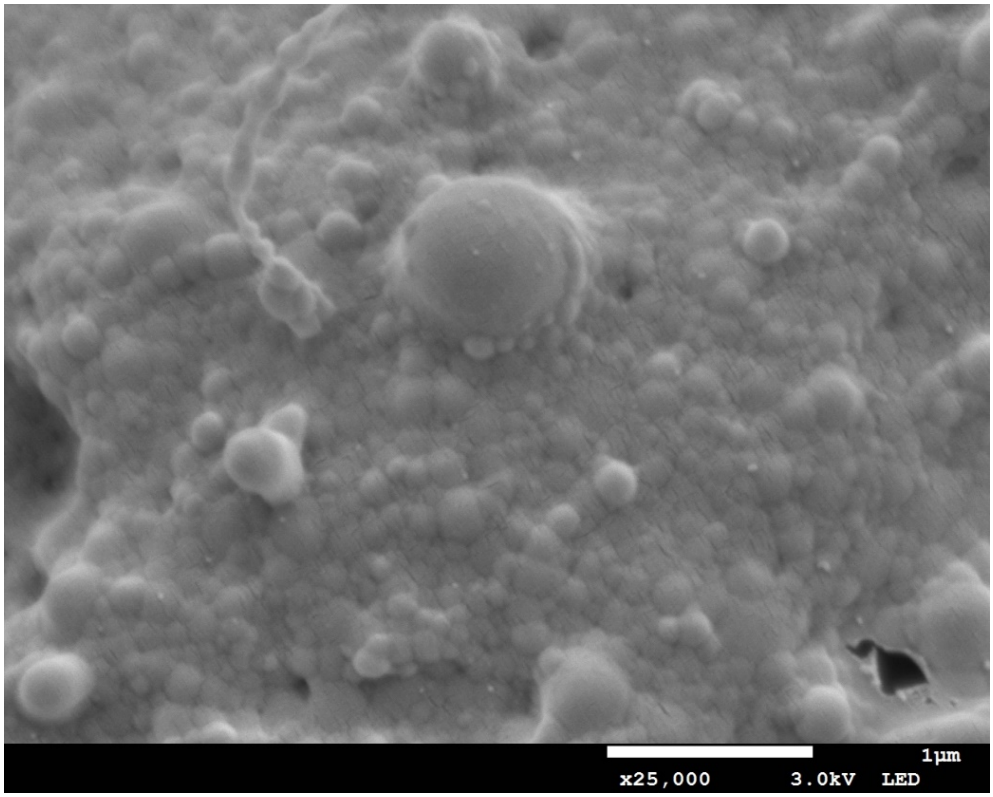

Figure D4 Cryo-SEM analysed microstructure of WPI plus pectin (DE33)-stabilized bilayer emulsions WOEP. Scale bar is 1 µm.

References for Appendices A to D

Akpinar, B., Fielding, L. A., Cunningham, V. J., Ning, Y., Mykhaylyk, O. O., Fowler, P. W., & Armes, S. P. (2016). Determining the effective density and stabilizer layer thickness of sterically stabilized nanoparticles. *Macromolecules, 49*(14), 5160-5171.

Crofton, A. R., Hudson, S. M., Howard, K., Pender, T., Abdelgawad, A., Wolski, D., & Kirsch, W. M. (2016). Formulation and characterization of a plasma sterilized, pharmaceutical grade chitosan powder. *Carbohydrate polymers, 146*, 420-426.

Gatto, M., Ochi, D., Yoshida, C. M. P., & da Silva, C. F. (2019). Study of chitosan with different degrees of acetylation as cardboard paper coating. *Carbohydrate polymers, 210*, 56-63.

Humblet-Hua, N.-P. K., van der Linden, E., & Sagis, L. M. (2012). Microcapsules with protein fibril reinforced shells: effect of fibril properties on mechanical strength of the shell. *Journal of agricultural and food chemistry, 60*(37), 9502-9511.

Kadiya, K., & Ghosh, S. (2019). Conversion of Viscous Oil-in-Water Nanoemulsions to Viscoelastic Gels upon Removal of Excess Ionic Emulsifier. *Langmuir, 35*(52), 17061-17074.

Ma, P. L., Lavertu, M., Winnik, F. M., & Buschmann, M. D. (2009). New Insights into chitosan− DNA interactions using isothermal titration microcalorimetry. *Biomacromolecules, 10*(6), 1490-1499.

Patel, A., Mohanan, A., & Ghosh, S. (2019). Effect of protein type, concentration and oil droplet size on the formation of repulsively jammed elastic nanoemulsion gels. *Soft Matter, 15*(47), 9762-9775.

Vachoud, L., Zydowicz, N., & Domard, A. (1997). Formation and characterisation of a physical chitin gel. *Carbohydrate research, 302*(3-4), 169-177.

Xiang, N., Lyu, Y., & Narsimhan, G. (2016). Characterization of fish oil in water emulsion produced by layer-by-layer deposition of soy β-conglycinin and high methoxyl pectin. *Food Hydrocolloids, 52*, 678-689.

15. APPENDIX E: COPYRIGHT PERMISSION

15.1 Copyright permission for the published paper, used as a chapter 3 in this thesis.

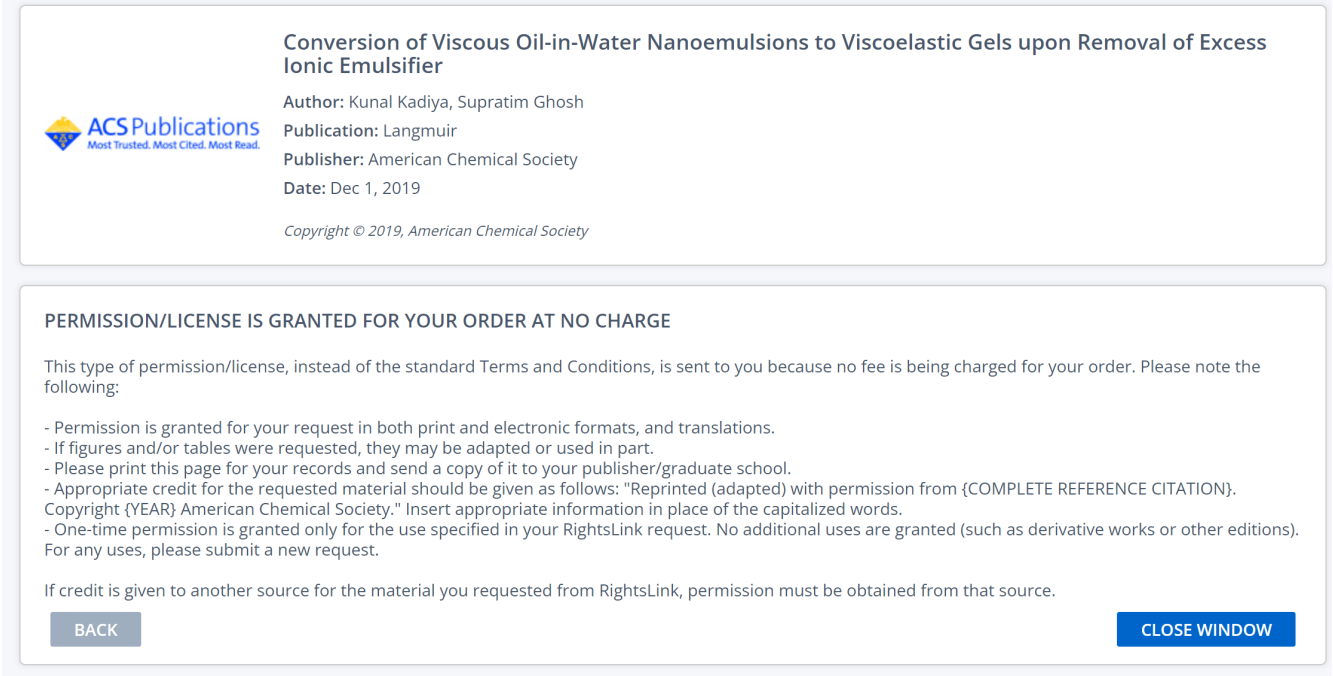

Conversion of Viscous Oil-in-Water Nanoemulsions to Viscoelastic Gels upon Removal of Excess Ionic Emulsifier

Author: Kunal Kadiya, Supratim Ghosh
Publication: Langmuir
Publisher: American Chemical Society
Date: Dec 1, 2019

Copyright © 2019, American Chemical Society

PERMISSION/LICENSE IS GRANTED FOR YOUR ORDER AT NO CHARGE

This type of permission/license, instead of the standard Terms and Conditions, is sent to you because no fee is being charged for your order. Please note the following:

- Permission is granted for your request in both print and electronic formats, and translations.
- If figures and/or tables were requested, they may be adapted or used in part.
- Please print this page for your records and send a copy of it to your publisher/graduate school.
- Appropriate credit for the requested material should be given as follows: "Reprinted (adapted) with permission from {COMPLETE REFERENCE CITATION}. Copyright {YEAR} American Chemical Society." Insert appropriate information in place of the capitalized words.
- One-time permission is granted only for the use specified in your RightsLink request. No additional uses are granted (such as derivative works or other editions). For any uses, please submit a new request.

If credit is given to another source for the material you requested from RightsLink, permission must be obtained from that source.

BACK CLOSE WINDOW

15.2 Copyright permission for the published paper, used as a chapter 4 in this thesis.

Analytical photo-centrifuge-based prediction of shelf-life and droplet packing behaviour of nanoemulsions upon removal of excess micelles

Author: Kunal Kadiya,Supratim Ghosh

Publication: Colloids and Surfaces A: Physicochemical and Engineering Aspects

Publisher: Elsevier

Date: 5 March 2021

Journal Author Rights

Please note that, as the author of this Elsevier article, you retain the right to include it in a thesis or dissertation, provided it is not published commercially. Permission is not required, but please ensure that you reference the journal as the original source. For more information on this and on your other retained rights, please visit: https://www.elsevier.com/about/our-business/policies/copyright#Author-rights

BACK CLOSE WINDOW